Effects of Ozone Loading Rate and Ecotoxicity of Products During Ozonation of Soil Containing Weathered Crude Oil

by

Burcu Manolya Yavuz

A Dissertation Presented in Partial Fulfillment
of the Requirements of the Degree
Doctor of Philosophy

Approved June 2022 by the
Graduate Supervisory Committee:

Bruce E. Rittmann, Chair
Anca Delgado
Paul Westerhoff

ARIZONA STATE UNIVERSITY

August 2022

ABSTRACT

The world currently faces hundreds of millions of cubic meters of soil contaminated with petroleum crude oil residuals. The application of ozone gas (O_3) to contaminated soil is an effective means to oxidize petrogenic compounds and, when used with bioremediation, remove the oxidized byproducts. The overarching goal of this dissertation was to evaluate two areas of potential concern to large-scale O_3 deployment: the capacity of O_3-treated petroleum contaminated soils to support seed germination before bioremediation and the transport characteristics of O_3 in soil columns.

A matched study comparing the germination outcomes of radish (*Raphanus sativus* L.), grass (*Lagurus ovatus*), and lettuce (*Lactuca sativa*) in soils contaminated with three crude oils at various O_3 total-dose levels showed that radish germination was sensitive to the soluble byproducts of oxidized petroleum (assayed as dissolved organic carbon [DOC]), but not sensitive to the unreacted petroleum (total petroleum hydrocarbon [TPH]). A multivariable logistic regression model based on the radish results showed that adverse germination outcomes varied with the DOC concentration and that DOC ecotoxicity decreased with increasing O_3 dose-level and background organic material. The model was used to create a risk management map of conditions that created 10%, 25%, and 50% extra risks of adverse radish germination. Thus, while O_3 effectively lowered TPH in soils, the byproducts exhibited ecotoxicity that inhibited radish germination. On the other hand, the sensitivity of radish germination to oxidized petroleum byproducts could be utilized to assess ecological risk.

The feasibility of gas transport in the soil matrix is also of paramount concern to field-scale utilization of O_3. A matched study comparing TPH removal at three field-relevant loading rates (4, 12, or 36 mg_{ozone}/ g_{soil}/ hr) and various total dose-levels showed an anisotropic pattern along the axial distance favoring the column inlet end. The asymmetry decreased as loading rate decreased and with concurrent improvements in O_3-transport distance, O_3 utilization, and heat balance. Overall, a low O_3 loading rate significantly improved O_3 transport and utilization efficiency, while also better distributing reaction-generated heat along the gas flow path for a depth typically utilized in bioremediation field settings.

ACKNOWLEDGEMENTS

This dissertation represents not only my own work, but the work of those who helped me, challenged me, and, above all, asked me to participate. I thank them from the bottom of my heart; I only ever want to participate in this difficult and beautiful world.

My closest intellectual partner has been my advisor, Professor Bruce E. Rittmann. Bruce is a miracle to those who have the privilege of working with him. It is impossible to overstate his indefatigable work ethic, his abiding optimism, and his unmitigated commitment to science. For eight years I have been guided and aided by a person who is as unfailingly steadfast as any being ever was, real or mythical. Bruce, you are Marcus Aurelius, you are the rock of Gibraltar, you are Ol' Man River, to me. I am forever changed by your exemplar of purpose, and I will refer to the standard you have set for the rest of my life.

I also wish to earnestly thank my other committee members. To Professor Anca Delgado: the foundation she laid for the analysis of total petroleum hydrocarbon (TPH) was the bread and butter of much of my work, and this dissertation would not be possible without it. In addition, I want to thank her for the time and care she took as a committee member on this dissertation, as a manuscript editor, and, especially, for her early friendship. I also want to thank Professor Paul Westerhoff for his honest and timely responses to all my manuscripts, and for his contributions on my committee.

Dr. Tengfei Chen is owed gratitude for his friendship and recognition for his extensive work on this project. Looking back on what we've accomplished, I am exceptionally proud: it will be a secure footing for those who come after us. I also want to thank Tengfei for simply being a wonderful person: at times mysterious and other times

utterly transparent, generous to a fault, and the center of gravity wherever he happened to be. I will cherish the memory of your smile, my dear friend.

It has been my absolute honor to work with some exceptional students on this project. If I have taught them anything, they have taught me so much more. To Garrett Montoya: the respect you so generously bestowed on me, your sense of decorum and deference to my judgement, relieved a burden I didn't know I carried. It changed the way I treat those around me and I owe you a lifelong debt of gratitude for the kind, courteous, and graceful example you set. It gives me indescribable joy to see your life unfold as a physician—your patients are in good hands. To Brielle Januszewski: your work ethic, energy, and enthusiasm were inspiring. You are a shining example of "more is more" when it comes life's ambitious projects, and what can be accomplished with hard work. That you went on to pursue a doctorate in Chemical and Environmental Engineering at Yale University makes my heart glow. To Melanie Hekeu: you are a natural scientist, and I enjoyed your wholly sincere curiosity, the best quality a scientist can have.

This dissertation is one piece of a larger body of research funded and organized by the Chevron Energy Technology (ETC) called the Heavy Hydrocarbon Soil Remediation Group (HHSRG). I wish extend my sincere gratitude to Chevron ETC for funding much of my doctoral education, and everyone involved with the HHSRG. Thank you to Professor Paul Dahlen, who organized our research at ASU and aided construction of the *in situ* Push-Pull device. Paul, you are a man who knows how to do things! From Chevron, I want thank our immediate project managers Roopa Kamath and Yi (Eve) Zuo, Natasha Sihota and Timothy Patterson for manuscript review, Kitty Kong and Sara

McMillen for facilitating at yearly meetings. Kirk O'Reilly was a valuable and interested participant, as was Rob Hinchee who offered encouragement about field applicability.

I also wish to thank all my friends and colleagues at the Swette Center for Environmental Biotechnology (SCEB), but especially my amazing Lab Manager Sarah Arrowsmith and business operations manager Carol Flores, who is goodwill itself.

I save until the end, those remembrances and affections that no mere ink on paper can illuminate, but I must try. First, to one of my oldest friends Leah Rebecca Levinger. I couldn't have survived this year without you—your wisdom and grace carried my exhausted soul so far. I will never forget our chariot ride out of the American Southwest with a very beloved beagle—a testament to our profound and quixotic friendship. I'm so grateful that we still break bread together, and I have the privilege of being by your side as you become a mother. I also owe thanks to Daniel Gnidovic: your light, generous soul brought such happiness to what was the darkest year of my life.

And finally, to my beloved family, I wish to convey my profound esteem and boundless thankfulness. To my sister Beyza Yavuz, the pride I feel for you surpasses anything I can feel for myself. Each year you grow in wisdom, fortitude, and passion for life. To see you excel as teacher, a student (4.0 in your Master's degree!), and a sister is everything I could wish for. The world is your oyster, my darling.

I dedicate this work to my mother, Hatice Yavuz. You embody vim and vigor, limitless love and compassion, and faith in the world and in God that made it. You have inspired me to participate, to hurl myself in headfirst. If I draw deeply from a wellspring of hope and imbibe boldly life's possibilities, those headwaters flow from you.

TABLE OF CONTENTS

Page

LIST OF TABLES ... xii

LIST OF FIGURES ... xiii

LIST OF ABBREVIATIONS ... xvii

CHAPTER

1 INTRODUCTION: CHEMICAL CHARACTER, ENVIRONMENTAL BEHAVIOR, AND REMEDIATION ... 1

1.1 The World's Crude Oil Supply ... 1

1.2 The Chemical Characteristics of Crude Oil ... 4

1.3 Chemical Characterization of Crude Oil ... 9

1.4 The Crude Oil Products ... 11

1.5 Crude Oil Released into the Environment ... 13

1.6 Goals of the Dissertation ... 19

1.7 Dissertation Outline ... 23

2 BACKGROUND: O_3 AND ITS REACTIONS WITH ORGANIC CARBON COMPOUNDS ... 27

2.1 O_3 Discovery and Current Production ... 27

2.2 The Criegee Ozonolysis ... 29

2.3 The Relative Reactivity of O_3 ... 30

CHAPTER Page

2.4 Ozonation of the π- Conjugated Ring 35

2.4.1 Mechanism and Products of Benzene Ozonation 35

2.4.2 Substituent Effects on the π-Conjugated Ring 38

2.4.3 O_3 Attack on Benz-Fused Carbocyclics: Polyaromatic Hydrocarbons.... 40

3 RESEARCH: OZONATION OF THREE DISTINCT CRUDE OILS FOR TOXICOLOGY TESTING 47

3.1 Introduction 47

3.2 Laboratory Methods 51

3.2.1 Test Soil (TS) Classification 51

3.2.2 ICP-MS for Total Metals 52

3.2.3 Crude Oil Analyses 53

3.2.4 Preparation of Test Soil with Crude Oil (TSC) 53

3.2.5 Moisture Determination 54

3.2.6 Preparation of Test Soil with Ozonated Crude Oil (TSOC) 55

3.2.7 Extraction and Quantitation for TPH 57

3.2.8 Extraction and Quantitation for DOC 58

3.3 Results and Discussion 59

3.3.1 Test Soil (TS) Classification 59

3.3.2 ICP-MS for Total Metals 60

3.3.3 Crude Oil Analyses 60

3.3.4 Effluent O_3 63

CHAPTER Page

3.3.5 Quantitation of TPH Removal (C9-C36) 65

3.3.6 Quantitation of DOC 69

3.3.7 Comparison TPH Reduction to DOC Production 71

3.3.8 Residual Material for Toxicity Testing 72

3.3.9 Soil pH, Moisture, and Salinity 73

3.4 Conclusions 73

4 RESEARCH: LETTUCE, GRASS, AND RADISH GERMINATION BY SIMPLE LOGISTIC REGRESSION 75

4.1 Introduction 75

4.2 Laboratory Methods 78

4.2.1 Ozonation of Soils 78

4.2.2 Water Holding Capacity (WHC) 79

4.2.3 pH Adjustment 80

4.2.4 The Dilution Series, Planted Tray, and Crude-Seed Set 80

4.3 Results and Discussion 84

4.3.1 Water Holding Capacity (WHC) 84

4.3.2 Evaluation of the Bin Control for Climate Conditions 85

4.3.3 Effects of Treatment Type on Germination 85

4.3.4 Effects of Crude Oil Type on Germination (Both Untreated Crude and Ozonated Crude) 87

4.3.5 Effects of Dose on Germination 93

CHAPTER Page

4.4 Conclusions 94

5 RESEARCH: USING RADISH (*RAPHANUS LATIVUS* L.) GERMINATION TO ESTABLISH A BENCHMARK DOSE FOR THE TOXICITY OF OZONATED-PETROLEUM BYPRODUCTS IN SOIL 96

5.1 Introduction 96

5.2 Materials and Methods 100

5.2.1 Crude Oil and TPH Analyses 100

5.2.2 Characterization of Test Soil (TS) 100

5.2.3 Preparation of Test Soil with Crude Oil (TSC) 100

5.2.4 Preparation of Test Soil with Ozonated Crude Oil (TSOC) 100

5.2.5 Determination of TPH, DOC, Moisture, pH, and WHC 100

5.2.6 The Planted Tray and the ORGANIC Series 101

5.2.7 The Independent Covariates 101

5.2.8 Purposeful Selection of Covariates 101

5.3 Results and Discussion 106

5.3.1 Quantification of TPH Removal (g C from C9 to C36) and DOC Production 106

5.3.2 NOAEL and LOAEL for TPH and DOC 110

5.3.3 Interpretation of Model Results 113

5.4 Environmental Implications 120

CHAPTER Page

6 RESEARCH: OZONATION OF PETROLEUM HYDROCARBONS IN SOIL COLUMNS: EFFECTS OF OZONE LOADING RATE ALONG THE AXIAL DISTANCE 122

6.1 Introduction 122

6.2 Materials and Methods 126

6.2.1 Crude Oil Source and Characteristics 126

6.2.2 Soil Source and Characteristics 126

6.2.3 Preparation of Petroleum Contaminated Test Soil 126

6.2.4 Soil Column Ozonation Apparatus 127

6.2.5 Quantification for TPH and Moisture 129

6.3 Results and Discussion 129

6.3.1 Extractable TPH Prior to Ozonation of Soil Columns 129

6.3.2 Effluent Ozone Profiles (“Break-through”) Over Time 130

6.3.3 Bulk TPH Removal and O_3-Utilization Efficiency 131

6.3.4 TPH Removal by Distance Through the Length of the Soil Column 133

6.3.5 Temperature at Input, Mid-Point, and Outlet End of the Soil Columns 136

6.3.6 Movement of Moisture Across the Column 139

6.3.7 Heat Gain and Loss Along the Column 142

6.4 Summary and Conclusion 145

7 SUMMARY AND FUTURE WORK 146

CHAPTER Page

7.1 Summary and Implications 146

7.2 Potential for Field Deployment.. 150

7.3 Future Research 153

BIBLIOGRAPHY.. 156

APPENDIX

A SOIL PHYSICAL AND CHEMICAL DATA... 183

B TPH CONCENTRATIONS OF RAW/WEATHERED CRUDE OILS 187

C SUPPLEMENTARY DATA FOR LOGISTIC REGRESSION............................. 189

D THE LOGISTIC REGRESSION METHOD... 194

E COLUMN AND COLUMN BREAKDOWN.. 215

F LATENT HEAT ADJUSTMENT FOR MOISTURE LOSS 217

LIST OF TABLES

Table Page

1.1 Proven Global Oil Reserves in 1999 and 2019 and R/P Ratio. 2

2.1. Relative Reactivity of Alky Radicals with O_3 Gas by the Rate Constant K_1. 33

3.1 Metal Elements in a Standard Soil (San Joaquin), Test Soil (TS) 60

3.2. Summary of Ozone Losses as Effluent Over Time. 64

3.3. Summary of TPH Removal Results 68

3.4 Summary of DOC Production Results 70

3.5 Soil pH for Crude Only Contaminated Soil (TSC) and Crude Oil+O_3 Soils (TSOC) at Three Different Dosages Among 3 Crude Oils 73

4.1 Water Holding Capacity Measurements for Soils Under Study 85

5.1. Results of Fitting the Multivariable Logistic Regression Model with TPHc Variable Removed (N = 840) 113

5.2 List of the 10%, 25%, and 50% Extra-Risk Margins (± Std. Error) ……………......117

6.1. Summary of the 9 Ozonation Experiments, each Using 600 g of TSC. 129

6.2. Summary of Average TPH Values for 9 Ozonation Experiments. 133

7.1 Summary of the Impacts of O_3 Dosage Among the Three Crude Oils, O_3 Dosages, O_3 Concentrations 147

LIST OF FIGURES

Figure Page

1.1 Global Oil Demand By Product 13

2.1 (A) Methane, and a (B) Primary, (C) Secondary, (D) Tertiary, and (E) Quaternary Bonding Arragement 31

2.2 Hydrocarbon Radicals Represented in Order of Increasing Stability. 32

2.3 The Order of Reactivity of O_3 Gas for Various Organic Groupings 34

2.4 The Reaction Rates of O_3 Trend as Follows: Fluorene < Indane < 9,10 Dyhyrdoanthracene << Indene. 36

2.5 Cleavage of the POZ Intermediate 38

2.6 Second-Order Relative Rate Constants for the Ozonation of Benzene and Benzene Homologs Performed in CCl_4 at 20-25°C 39

2.7 Angular PAHs Discussed Include: (A) Naphthalene, (B) Phenanthrene, (C) Chrysene, and (D) Picene 42

2.8 O_3 Reacts with Naphthalene to Produce Phthalic Acid in 48% Yield 42

2.9 O_3 Reacts with Phenanthrene to Produce Diphenic Acid in 50% Yield. 43

2.10 O_3 Reacts with Chrysene to Produce 2-(O-Caroxyphenyl)-1-Napththoic Acid 44

2.11 O_3 Reacts with Picene to Produce Terphenyltetracarboxylic Acid Anhydride 45

3.1. Schematic of the Experimental Set Up for Soil Ozonation 56

3.2 TPH (C8-C38) Profiles of Raw Crude Oils ANS, ARAB, and SJV Before Any Treatment. 61

Figure Page

3.3. Relative Abundance of GRO (C5-C12), DRO (C12-C22), and ORO (C22-C40) for Crude Oils ANS (API Gravity 29-32), ARAB (API Gravity 30-32), and SJV (API Gravity 13-15)...... 62

3.4. Relative Abundances of Aliphatic and Aromatic Hydrocarbons (C10-C35) for Crude Oils ANS (API Gravity 29-32), ARAB (API Gravity 30-32), and SJV (API Gravity 13-15) 62

3.5 TPH (C9-C36) Profiles of Weathered Crude Oils ANS, ARAB, and SJV Before Ozonation 63

3.6. Effluent Losses of O_3 Over Time for the 240-Min (40-g Dose) Group...... 64

3.7 Summary TPH Removal (C9-C36) for ANS, Arab, and SJV Crude Oil...... 65

3.8 (A-C) TPH Decreases Across the Carbon Range (C9-C36) for (A) ANS, (B) ARAB, and (C) SJV Crude Oil. 67

3.9 The DOC Concentration of Soils Contaminated with Either ANS, Arab, and SJV Crude Before (Control, No O_3) and after Treatment with O_3 Gas at Either A 5-g, 10-g, or 40-g Dose. 70

3.10 Comparison of the Total Mass of DOC Produced and TPH Lost...... 71

3.11 The Combined Concentration of TPH (C9-C40) and DOC...... 72

4.1 Dilution Series for a Given Test Condition. 81

4.2 Matrix of Mixtures of the Potting Soil and the Amounts of Each of the Test Soils... 83

4.3 Schematic of the Study Design 84

4.4 Germination of Proportions Between Treatment Groups 86

4.5 Effects of Crude Oil Type on Radish Germination 89

Figure Page

4.6 Crude/Oxidized Crude Comparisons for Radish Germination 89

4.7 Effects of Crude Oil Type on Lettuce Germination.. 91

4.8 Crude/Oxidized Crude Comparisons for Lettuce Germination 91

4.9 Effects of Crude Oil Type On Grass Germination... 92

4.10 Crude/Oxidized Crude Comparisons for Grass Germination 93

4.11 Oxidized Crude Oil Comparisons About Dose.. 94

5.1 (A-C). (A) TPH Decreases Across the Carbon Range (C9-C36) for ANS Crude Oil; (B) Direct Comparison of TPH Loss to DOC Gain; (C) Comparison of TPH and DOC for Absolute Change in Mass of Carbon, Mass of Carbon Change Per Hour (g Δ C/H), and Ozone Utilization (g O_3/g Δ C). 109

5.2 (A-O). Comparison of Germination Rate (%), DOC (ppm), and TPH (ppm), By Dilution Series (*% B-ORGANIC*).. 112

5.3(A-D). Predictive Margins with 95% Confidence Intervals 115

5.4. The 10%, 25%, and 50% Extra-Risk Margins.. 118

6.1. Left-Panel Shows the Schematic of the Experimental Setup for Soil Ozonation; Right-Panel Shows Detail of Column (Figure 1. F/G) with Temperature Indicating Labels in Position. 128

6.2 Arab Medium Crude Oil Before and After Laboratory Weathering Processes 130

6.3 (A-I). The Vertical Axis Represents Distance (cm) from the Inlet End, and the Horizontal Axis Represents % TPH Removal Normalized to Respective Control Experiments.. 135

Figure Page

6.4 (A-I). The Vertical Axis Represents Distance (cm) from the Inlet End, and the Horizontal Axis Represents Time (min) of Each Experimental Condition............. 138

6.5 (A-I). The Vertical Axis Represents Distance (cm) from the Inlet End, and the Horizontal Axis Represents Mass of Moisture.. 141

6.6 (A-I). Spatial Distribution of Specific Heat and Latent Released or Gained Along The Column 144

LIST OF ABBREVIATIONS

AOP, Advanced Oxidation Process

ANS, Alaska North Slope

AUC, Area Under the Curve

BDE, Bond Dissociation Energy

BMD, Benchmark Dose

DOC, Dissolved Organic Carbon

DRO, Diesel-Range Organics (C12-C22)

GJIC, Gap Junctional Intercellular Communication

GRO, Gasoline-Range Organics (C5-C12)

HF, Hydraulic Fracturing

ICP-MS, Inductively Coupled Plasma – Mass Spectrometer

ISCO, *In Situ* Chemical Oxidation

LE, Localization Energy

LL, Liquid Limit

LOAEL, Lowest-Observed-Adverse-Effect-Level

NA, Naphthenic Acids

NOAEL, No-Observed-Adverse-Effect-Level

O_3, Ozone

OR, Odds Ratio

ORO, Oil-Range Organics (C22-C40)

OSPW, Oil-Sands Process Water

PAH, Polyaromatic Hydrocarbon

PL, Plastic Limit

ROC, Receiver Operating Characteristics

SOM, Soil Organic Matter

TPH, Total Petroleum Hydrocarbons

TPHc, Total Petroleum Hydrocarbons by Carbon

TS, Test Soil

TSC, Test Soil Contaminated with Crude Oil

TSOC, Test Soil Contaminated with Ozonated Crude Oil

1 INTRODUCTION: CHEMICAL CHARACTER, ENVIRONMENTAL BEHAVIOR, AND REMEDIATION

1.1 The World's Crude Oil Supply

Global oil demand contracted in 2020 for the first time in a decade because of the social and economic restrictions imposed by the novel Coronavirus (COVID-19).[1] This period and the recession of 2009 are the only anomalies in the last quarter century, in which global oil consumption otherwise steadily rose from just below 70 million barrels per day (mbd) in 1994 to nearly 100 mbd in 2020.[2] Oil consumption grew in Asia, Africa, and the Middle East, and it remained unchanged in the CIS[a], Europe, South and Central America, and North America.[3]

Increasing consumption patterns have been satisfied by expansions in oil exploration and extraction.[3] Table 1.1 shows proven global oil reserves (R) between 1999 and 2019 in the 15 countries that together hold 93% of the world's crude oil supply.[3] The values in Table 1.1 indicate that oil reserves have risen by a remarkable 54% in the last 20 years. Geological and engineering information indicates with reasonable certainty that approximately 245 billion metric tons (~1,800 billion barrels) can be recovered in the future.[3] Even if only 0.1% of the recovered oil is spilled during exploration, extraction, transport, or storage, the world's natural and anthropogenic spheres will have to cope with crude oil contamination on the order of 245 million metric tons—a mass of oil 6,600 times greater than Exxon Valdez and 350 times greater than Deepwater Horizon.[4,5]

---

[a] The Commonwealth of Independent States (CIS) is a regional intergovernmental organization of nine members post-Soviet republics in Eurasia. They include Armenia, Azerbaijan, Belarus, Kazakhstan, Kyrgyzstan, Moldova, Russia, Tajikistan, Uzbekistan.

Table 1.1 Proven Global Oil Reserves in 1999 And 2019 And R/P Ratio.[2]

	1999 (10^9 Barrels)	*2019 (10^9 Barrels)*	*% Δ*	*% Supply*	*R/P (Years)*	*Region*
Venezuela	77	304	300%	17.5%	>500	C/S America
Saudi Arabia	263	298	13%	17.2%	69	Middle East
Canada	182	170	-6.5%	9.8%	82	N America
Iran	93	156	67%	9.0%	121	Middle East
Iraq	113	145	29%	8.4%	83	Middle East
Russian Fed.	112	107	-4.4%	6.2%	26	CIS
Kuwait	97	102	5.2%	5.9%	93	Middle East
UAE	98	98	0.0%	5.6%	67	Middle East
US	30	69	130%	4.0%	11	N America
Libya	30	48	64%	2.8%	110	Africa
Nigeria	29	37	28%	2.1%	48	Africa
Kazakhstan	5	30	460%	1.7%	43	CIS
Qatar	13	25	92%	1.5%	37	Middle East
China	15	26	74%	1.5%	19	Asia
Total Above	1155	1614	40%	93%	93	Regions Above
Total World	1277	1734	54%	100%	50	World

[2] Data adapted from source.[3]

Table 1.1 also shows the R/P ratio: the value, in years, until reserves (R) are depleted at current production rates (P). If worldwide production remains unchanged, the International Energy Agency (IEA) estimates the world to have a roughly a 50-year oil supply: the United States (4% of world supply) has 11 years, Russia (6% of world supply) has 25 years, and Saudi Arabia (17% of world supply) has 69 years.[3] During these final decades of oil production, all the world's remaining reserves will be drilled, pumped, and hydraulically pressurized to release product. As reserves wane, efforts will eventually turn to decommissioning and dismantling oil drills, wells, pipelines, and refineries, and society will face the inevitable task of assessing the residuals left behind after more than a century of manipulating vast volumes of crude oil.[6]

Early oil exploration yielded the lightest[c] crudes first, because of their relative buoyancy and ease of extraction. Since it is unlikely that the world will discover any other significant reserve of light "sweet" (low-sulfur) crude oil, the oil industry will also turn to refractory stocks, like Canada's Athabasca tar sands and the extra heavy crude in Venezuela's Orinoco Belt; if they were to be developed, those reserves would extend the proven world supply by 9.4% and 15.4% (respectively).[3] Thus, the endgame crude oil product that is piped, trucked, and tanked thousands of miles across the globe will be those oils that are heaviest and already degraded of simpler components.[7,8]

---

[c]Light, medium, heavy, and extra heavy are categories are established using the American Petroleum Institute gravity, or simply, the API gravity. The formula to calculate API gravity from Specific Gravity (SG) is:

$$API\ Gravity\ =\ \frac{141.5}{SG} - 131.5$$

Light crude oil has an API gravity higher than 31.1° (i.e., less than 870 kg/m^3), medium oil has an API gravity between 22.3 and 31.1° (i.e., 870 to 920 kg/m^3), heavy crude oil has an API gravity below 22.3° (i.e., 920 to 1000 kg/m^3), and extra heavy oil has an API gravity below 10.0° (i.e., greater than 1000 kg/m^3).

1.2 The Chemical Characteristics of Crude Oil

Petroleum crude is a mineral oil of natural origin consumed at a rate of 98 mbd.[1–3] Accurate information about the composition of crude oil is especially important for the selection of appropriate "downstream" refining processes, which determine the oil's net economic value.[9] The precise characterization of crude oil, however, is difficult due to the manifold structural potential of hydrocarbons.[7,9]

Petroleum crude oil has been described as one of the world's most compositionally complex organic mixtures, containing anywhere from 10,000 to 100,000 chemically distinct constituents.[9] The elemental makeup, by contrast, is fairly small. Roughly 83-87 wt% of crude oil can be attributed to carbon and another 10-14 wt% to hydrogen.[7,9–11] The remaining 3-7 wt% of crude mass results from the presence of the so-called heteroatoms: nitrogen (0.1-1 wt%), sulfur (0.05-6.0 wt%), and oxygen (0.05-2.0 wt%).[11] Small amounts of organometal complexes can be ascribed mostly to vanadium (~1200 ppm) and nickel (120ppm).[7,9–11] Nevertheless, this elemental simplicity belies the vast number of bonding configurations possible from these basic building blocks. The molecules in crude oil have manifold structural possibilities because the carbon backbone can reach C150, bonding configurations can include single as well as double bonds, the molecular structure can be a straight chain, branched, ringed, or a combination of each of these, and, finally, the presence of even one heteroatom can fundamentally change the chemical character.[7]

That petroleum and its derivatives tend to follow a homologous series simplifies the characterization to an extent. The most fundamental series has no rings and no double bonds and begins with methane (CH_4), which has a hydrogen:carbon (H:C) mole ratio of

4:1. Extending methane one carbon at a time forms the molecules ethane (C_2H_6), propane (C_3H_8), and butane (C_4H_{10}), the volatile end of the homolog series of "normal" alkanes (i.e. n-alkanes), which are propagated according to the formula C_nH_{2n+2}.[7] As the chain is lengthened with the addition of methylene ($–CH_2$), the additional hydrogen atoms of the methyl group ($–CH_3$) at either end (the "+2" in the alkane formula) contribute less and less to the H:C ratio, which gradually decreases toward the methylene mole ratio of 2:1.[7] When the alkane structure is branched, however, "isoalkanes" have a methyl cap at the end of each branching chain, adding to the overall hydrogen count and driving the H:C mole ratio above 2.[10] The n-alkanes are sometimes referred to as the "paraffin" group, especially when above C20. A higher H:C ratio signifies greater paraffinic character in a given group or crude-oil fraction. [12] The denomination is derived from the Latin phrase *parum affinis*, describing the "little affinity" paraffins have for other chemicals. In other words, the paraffins are noted for having a low level of reactivity.[13] The n-alkanes and isoalkanes comprise approximately 30-35 wt% of most producible[d] crude oils. [8]

When a singly bonded carbon backbone forms one or more rings (with or without side chains), the resulting molecule is known as a cycloalkane, or a cycloparaffin when greater than 20 carbon atoms are present.[e] These types of molecules are an extremely important constituent of crude oil. A singled-ringed cycloalkane has the formula C_nH_{2n}

[d] Producible crude oil refers to that oil which is free flowing to distinguish it from bitumen source oil.
[e] Cycloalkanes are also sometimes called "naphthenes" in the petrochemical industry. The term "naphthene" must be distinguished from the term "naphthalene," which is the name for a polyaromatic unsaturated hydrocarbon comprised of two fused benzene rings. Naphthenes should also be distinguished from "naphtha" the mixture of n-alkanes and cycloalkanes that distils between 30°C and 220°C in a refining process.

and is named according to its straight-chain homolog (cyclopropane, cyclobutane, cyclopentane, cyclohexane, etc.). Each additional ring creates a hydrogen deficit of -2, and a general chemical formula for the cycloalkanes is $C_cH_{2(c+1-g)}$, where "c" equals the number of carbon atoms and "g" equals the number of rings in the molecule. The carbon atoms in cycloalkanes are singly bonded and, like n-alkanes, are relatively unreactive. They can contain straight-chain projections or form isolated rings, spiro rings, fused rings, or bridged rings. Small rings, containing 3- and 4-carbons, have significant angle strain resulting from the distortion of the sp^3 carbon bond angles from the ideal 109.5° to 60° and 90°, respectively.[14] This angle strain often heightens the chemical reactivity of such compounds relative to the straight-chain homolog. On the other hand, a ring shape also enhances London forces that give cycloalkanes higher boiling points, melting points, and densities than n-alkanes.[15]

The cycloalkanes make up the next 30-35 wt% of crude oil. Like n-alkanes, cycloalkanes also can contain straight-chain branches. Above C10, mono- and di-cycloalkanes comprise between 50 and 55 wt% of all cycloalkanes. Next, the three-ringed tri-cycloalkanes comprise approximately 20 wt% of all cyclic alkanes, while tetra- and penta-cyclics account for about 25 wt% together. Polycyclic molecules can be comprised of up to 6 rings, with 5- and 6-carbon rings appearing in the same molecule.[16] Some of the larger polycyclic alkanes fall into the class tetra-cylic steranes (C27-C30) and penta-cylic triterpanes (C27-C35), important biomarkers that document the provenance of crude oil or its degree of degradation.[16,17] Triterpanes like hopane are sometimes used as an internal standard to describe the degree to which an oil has shifted from its baseline composition.[18,19] Whether straight-chain, branched, or cyclic, a hydrocarbon molecule formed by only C—C single bonds, even when heteroatoms[f] are present, is described as "saturated." Together, the n-alkanes, isoalkanes, and cycloalkanes comprise about 60 wt% of most producible crude oils that have not been degraded by environmental processes.

That the carbon backbone can form double or single bonds greatly amplifies the complexity of the crude mixture. When a straight-chain alkane loses two hydrogens to form a C—C double bond along the chain, the molecule is said to be "unsaturated." This group is referred to as the alkenes, or more often as the "olefins," a corresponding term to "paraffin" and widely used in organic chemistry and the petroleum literature.[1–3,20] The straight-chain olefins are not naturally present in high quantities in petroleum, but are important products formed during the refining process.[8,20] In crude oil, naturally occurring C—C double bonds occur predominantly in the cyclic analogs of olefins, otherwise known as the "aromatic" group.[16] To meet the chemical definition of aromaticity, the unsaturated chemical compounds must be characterized by at least one resonance-stabilized unsaturated ring core; the smallest such unit is the benzene ring.[21]

Crude-oil compounds comprised of 2-6 benzene rings are known as the polyaromatic hydrocarbons (PAHs), or sometimes the polyaromatic compounds (PACs) for those molecules containing heteroatoms. The benzene homolog series is propagated by the addition of subsequent C_6H_6 according to the chemical formula C_cH_{2c-6}, as in naphthalene (2 rings), anthracene (4 rings), pyrene (4 rings), benzo(a)pyrene (5 rings), and benzo(ghi)perylene (6 rings). Of all aromatic compounds, monoaromatics are ~33

[f] Of the heteroatoms, only oxygen appears with any important mass percent in the saturated group, usually due to some degree of degradative acidification.[10]

wt%, diaromatics are ~23 wt%, triaromatics are ~13 wt%, and <tetra polyaromatics are ~7 wt%. A true aromatic molecule will contain only aromatic rings and chains.[8] However, in crude oil characterization, napthenoaromatics also are major constituents of the aromatic group. They are characterized by one five-membered saturated ring in addition to the aromatic rings as in fluorene (3 rings), benzofluorene and fluoranthene (4 rings), and benzofluoranthene (5 rings). In addition, the aromatic group also includes sulfur-containing compounds. Thiophene derivatives are constructed of five- and six-membered rings with at least one of the rings containing a sulfur atom (e.g., benzo- and dibenzothiophenes). The thiophene derivatives comprise up to 24 wt% of all aromatics in crude oil. Taken together, the aromatic, napthenoaromatics, and sulfur aromatic compounds comprise 20-45 wt% of crude oil.[8]

The geologic pressures that form saturated and aromatic compounds also can produce the heaviest and most polar molecules from the covalent bonding of these basic groups: The most complex examples of such molecules are the asphaltenes and resins.[8,8,22] The asphaltenes and resins are typically comprised of 6 to 20 fused rings with finger-like alkyl projections. They can comprise 0-40 wt% of all crude oil, though on average are around 14 wt%.[8] Heavily degraded crudes, like the Athabasca and Orinoco deposits, can have an asphaltene and resin content of 25-60 wt%.[23] Their enrichment usually indicates degradation of the oil. These molecules also have a higher-than-average frequency of heteroatoms and can complex with metals such as nickel and vanadium.[24] The nitrogen in crude oil is primarily found in resins and asphaltenes, although it sometimes appears in PAHs as a six-membered pyridinic ring or five-membered pyrrolic ring.[7] In contrast, sulfur appears with almost equal frequency in aromatics, resins, and asphaltenes.[9,10,24] The increase in heteroatom frequency leads to an increase in polarity, which in turn causes asphaltenes and resins to absorb much more readily to soil and rock.[8]

The molecular size and structure of asphaltenes and resins have been notoriously difficult to characterize, because the molecules form non-covalent complexes and aggregates in the form of dimers and tetramers at high concentrations and even in some solvents.[7,25,26] Low-energy collisions were finally able to separate aggregates without causing fragmentation.[7,25,27] These analyses demonstrated that asphaltenes, in particular, can contain up to 150 carbons and have an average mass between 400 and 800 Da (with distribution extending between 300 and 1400 Da).[25,28] The asphaltenes are typically larger than resins, with a higher degree of aromaticity and heteroatom content. Thus, the two groups are defined operationally based on their differing solubility. Resins show solubility in low molecular mass aliphatic hydrocarbons (n-heptane or n-hexane), as well as aromatic solvents (benzene and toluene). Asphaltenes are insoluble in the former group but soluble in the latter because of their higher aromatic character.[28–31]

1.3 Chemical Characterization of Crude Oil

As molecular weight increases, aliphatic character decreases, while aromaticity correspondingly increases, and heteroatoms appear with higher frequency.[23,24] However, sorting the petroleum hydrocarbons based on mass alone cannot elucidate structure, since the nearest integer mass of groups like —CH_2 vs N, —NH_2 vs. O, and CH_4 vs. O are identical.[32] Instead, a hierarchical characterization of crude has been proposed as more logical and orderly.[7] The field of “petroleomics” has emerged to meet the challenge of complete chemical characterization of crude oil and related substances like bitumen, tar sands, or coal as well as the products of downstream refining processes such as vacuum residuals.[7,9,32,33] This field relies on dimensional characterization of crude oil that includes three levels.[9]

First, hydrocarbons can be sorted by relative abundance according to "class." The term "class" describes the elemental composition of a given hydrocarbon molecule ($C_cH_hN_nO_oS_s$).[23,24,34] Depending on the crude oil type and provenance, 10-60% of the molecules in crude oil will be comprised of hydrogen and carbon atoms only. Other classes with greater than >1% abundance include N_1, O_2, N_1S_1, N_1S_2, N_1O_1, N_1O_2, N_2, O_1, O_1S_1, O_2S_1, O_3S_1, and O_4S_1.[7] This is particularly true in heavy crudes oils (API <10) and sour (sulfur-containing) crude oils. Overall, the classes occurring with the most frequent % abundance (depending on crude and analytical method[g]) are usually N_1, N_1S_1, and O_2.[7,10,24,32]

Second, since the H:C ratio deviates in a predictable manner based on the presence of rings, double bonds, and nitrogen, the integers of $C_cH_hN_nO_oS_s$ can be used as a quantitative descriptor of hydrocarbon "type." This value is called the double-bond equivalent (DBE).[h] The DBE is equal to the number of rings plus double bonds involving carbon (CcHhNnOoSs⍰ $= c - \frac{h}{2} + \frac{n}{2} + 1$ Equation 1.1), and it is a direct measure of aromaticity of petroleum components.[7]

$$(C_cH_hN_nO_oS_s) = c - \frac{h}{2} + \frac{n}{2} + 1 \qquad \text{Equation 1.1}$$

---

[g] Positive and negative modes in electrospray ionization between mass spectrometry methods can yield different relative abundances for the same crude oil.[7,24,32,35]

[h] The petroleum industry sometime uses the measure called "hydrogen deficiency" or "Z" defined as C_cH_{2c+Z} to describe the degree to which the H:C ratio deviates from that of an n-alkane.

where c = the number of carbon atoms, h = the number of hydrogen atoms, and n = the number of nitrogen atoms. Thus, within a given a class, relative abundance can be sorted according to DBE, i.e., according to type.

Finally, for a given heteroatom class and a given DBE type, the third level of characterization depends on carbon number. By first sorting according to class (i.e., number and identity of heteroatoms), then type (bonding configuration quantified by the DBE), and then carbon number, the overlap of functional groups is avoided, and a highly refined identification system of the hydrocarbons in crude oil is possible.[7] This 3-dimensional characterization requires sophisticated techniques with an ultra-high degree of resolution, like the Fourier-transform ion cyclotron resonance mass spectrometry (FT-ICR-MS)[i], such that classes can be recognized by mass differences to the nearest 1000th decimal place.[7,9]

1.4 The Crude Oil Products

At atmospheric pressure and temperature, crude oil usually[j] exists in the liquid phase, though physical liquid characteristics like density and viscosity can vary considerably. These physical differences are exploited in the process of turning most of the recovered crude oil into a wide range of petroleum products.

Fractional distillation recovers the lightest compounds first, consisting of non-condensable gases hydrogen, methane, ethane, and short-chain olefins. The gases

[i] This technique makes use of a mass spectrometer for determining the mass-to-charge ratio (m/z) of ions based on the cyclotron frequency of the ions in an extremely powerful fixed magnetic field. The technique can achieve mass resolution as high as $m/\Delta m_{50\%} \approx 400{,}000$.

[j] Some crude oils with high level of long chain n-alkanes or isoalkanes are characterized as "waxy," may be solid at room temperature, even though they are characterized by "light" API.

condensable under pressure, mainly the light saturated paraffinic hydrocarbons propane (C_3H_8) and butane (C_4H_{10}) (or a combination of the two), come next and are sold as liquefied petroleum gases (LPG). Together, ethane and LPG account for 15% of the crude oil product soil.[1] The next important chemical product is called "naphtha" (7% v/v) and is comprised of "light naphtha," recovered between 30°C and 90°C (C_5-C_6), and "heavy naphtha," recovered between 90°C and 200°C (C_6–C_{12}). Naphtha is an essential feedstock of the petrochemical industry and is the backbone for the manufacture of ethylene plastics. Motor gasoline, perhaps the most important product of modern age, comprises 25% v/v of crude oil. It also distills between 35°C and 215°C; it is the light hydrocarbon (C4-C12) used for internal combustion engines of land-based motor vehicles.

The jet fuel/kerosene group comprises aviation gasoline (30°C -180°C), gasoline type jet fuel (100°C -250°C), kerosene type jet fuel (150°C-300°C), and other kerosene; these account for 8% v/v of crude oil product. Gas/diesel oil includes heavy gas oils. Gas oils and diesel (180°C and 380°C) are obtained from the lowest fraction from atmospheric distillation of crude oil, while heavy gas oils are obtained by vacuum re-distillation of the residual left over from atmospheric distillation. They are used for diesel compression ignition (cars, trucks, marine transport, etc.) as well as light heating oil for industrial and commercial uses. This group also includes heavy gas oils which distill between 380°C and 540°C and which are used as petrochemical feedstocks. Finally, fuel oil, spirits, lubricants, bitumen, paraffin waxes, petroleum coke, tar, and sulfur are the most rigid elements derived from crude oil from vacuum residuals. Figure 1.1 recapitulates the demand of the products derived from crude oil.

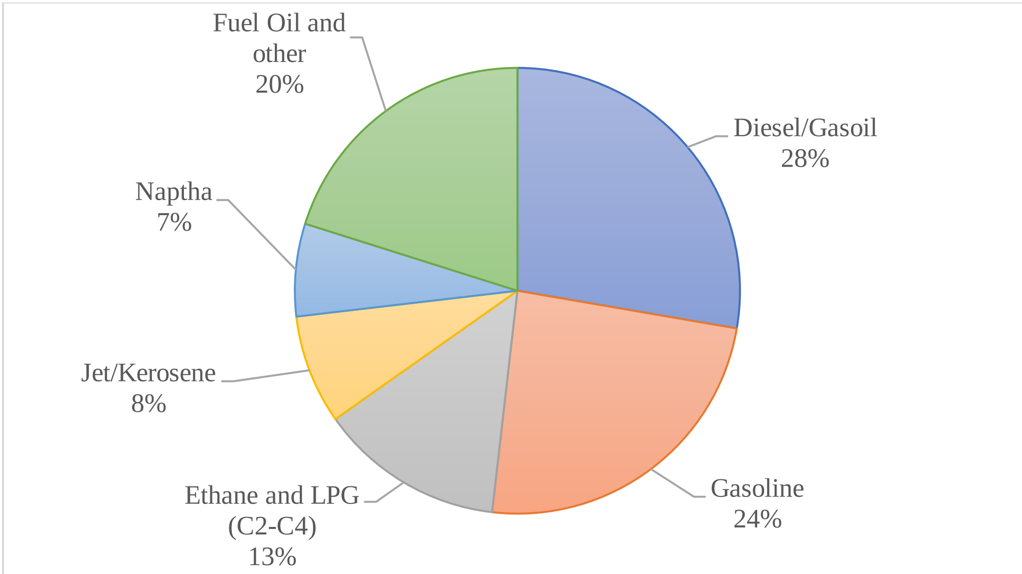

Figure 1.1 Global oil demand by product.[k,1]

1.5 Crude Oil Released into the Environment

The accidental release of petroleum into the environment is an inevitable outcome of a global supply chain that moves up to 100 mbd.[4] Such releases, whether on land or sea, are attenuated and transformed by microbial biodegradation, photooxidation, hydrolysis, and evaporation[l], as well as dispersive and diluting processes of dissolution, spreading, and emulsification.[38] Taken together, these collective "weathering" processes enrich recalcitrant components that often are among the most toxic and, via photo-modification, generate oxidized intermediates which have demonstrable acute toxicity to a variety of species.[39–42] The weathering of crude oil is possible because the individual chemicals that comprise crude oil exhibit strong differences in air diffusion coefficient,

[k] Modified from source.
[l] The literature on petroleum spills often refers to the "evaporation" of labile components, though the term volatilization is more appropriate. The interested reader should use both terms.[36,37]

liquid density, water solubility, pure chemical vapor pressure, boiling point, and Henry's Law constant.[1] In essence, weathering is a process by which natural media (air, water, and soil), physical elements (heat and light), and biological actors (more frequently lower order organisms like bacteria and yeast) can preferentially change or remove specific chemical components thereby selectively enriching the remainder.

Ambient conditions such as temperature and the presence or absence of wind can make profound changes to a spilled crude oil; the extent of those changes is governed by the chemical makeup of the crude itself and the thickness of the spill. A crude oil release first loses those components that are volatile at ambient temperatures (-25°C-45°C). In a few days, light crude oils can be reduced by up to 75% of their initial volume and medium crudes by up 40% of their volume.[37] In contrast, heavy or residual oils only lose about 5% of their volume in the first few days following a spill.[37] Although each individual crude-oil component has a unique loss rate, the differing rates of volatilization among different components give the appearance of a logarithmic loss rate with respect to time.[36] Most oil that is lost to volatilization does so within the first 8 hours of a spill.[43] The presence of wind will sharply advance the volatilization rate since moving air prevents the air-oil interface from becoming saturated; while the presence of wind is important, the intensity of the wind has not been shown to be a significant factor.[37,44] It has also been noted that oil thickness, or the size of the spill, will change the degree to which oil can lose mass to volatilization—thicker spill volatilizes less by allowing waxy crust formation and adhesion forces between oil molecules.[43]

Sunlight is another factor that significantly alters the chemical profile of crude oil and enhances toxic effect.[45] Sunlight causes a substantial decline of the aromatic fraction and the concomitant increase in the resin and asphaltene fractions.[45] The aromaticity of irradiated oil has been found to be significantly lower.[45] The oxygen content in irradiated oil is also found to increase with greater exposure to sunlight, a process called photo-oxidation. The sunlight mediated photo-oxidation significantly increases the water-soluble fraction of crude oil.[45] Maki et al. found that the concentration of dissolved organic carbon (DOC) increased linearly during sunlight irradiation, matched by an increase in ultraviolet absorptive materials in the seawater.[45] Another feature of sunlight is photoactivation of PAHs.[46] The absorption of UV light and even visible light by PAHs causes a molecular excitation that can lead to the formation of reactive oxygen species (ROS) and other reactive intermediates that can damage DNA, protein, and cell membrane.[47–49] Thus, sunlight irradiation of PAHs, while sometimes leading to their removal, also can cause acute toxicity and genotoxicity.[50]

Dissolution, spreading, and emulsification are most salient to open water crude oil spills, where the action of large volumes of moving water separates crude oil constituents. For example, an oft-encountered frothy oil-water emulsion is commonly known as "mousse."[51] Smaller molecules of aromatic hydrocarbons and small polar molecules, such as naphthenic acids, dissolve if sufficient water is present, causing the heavier molecular components to aggregate then precipitate. Other commonly encountered features in water-spill scenarios are tar balls, which are floating aggregations of asphaltenes and resin. In the case of highly dense material, tar balls become tar mats that condense on the ocean floor.[52] The removal of water-soluble components of oil spills is sometimes known as "washing," and it is of real importance when significant volumes of water are present, allowing oil to disperse into the water column.[53] The dramatic increase in the surface area in open water also allows for microbial colonization and biodegradation.

The microbial alteration of crude oil is known as biodegradation, and is well-established fact in the reservoirs of the petroleum industry and in environmental contamination scenarios.[4,51,54,55] Biodegradation of crude oil is a selective utilization of certain types hydrocarbons by microorganisms, usually started under aerobic conditions, but also including anerobic processes.[56] The biodegradation of petroleum is carried out largely by diverse bacterial populations which, even in pristine environments, are ubiquitous though not abundant (< 1% of the total bacterial population).[55] These bacteria presumably utilize hydrocarbons that are naturally produced by plants, algae, and other living organisms, particularly waxy exudates that are themselves geologic progenitors of crude oil.[8] The microorganisms are selectively enriched in contaminant scenarios, where they can exceed 10% of the total bacterial population.[55]

Biodegradation by aerobic and/or anerobic microorganisms results in partial or total removal of n-alkanes first, usually C10 to C26, then slightly branched alkanes (isoprenoid alkanes), and finally some smaller low-molecular-weight aromatics such as benzene, toluene, and xylene, which are among the toxic compounds found in petroleum.[51] Decreasing levels of simpler, smaller carbon chains increase the relative abundance of those molecules with greater complexity. The distribution of cycloalkanes with 1 to 5 rings remains practically unchanged. Larger branched isoprenoids—like pristane and phytane—only decrease in scenarios of extreme oil degradation. Molecules with multiple aromatic rings—the PAHs—are also relatively resistant when intact crude oil is spilled. These also include sulfur-containing compounds like thiophene derivatives.

The loss of light compounds enriches the nitrogen-containing end of the crude oil profile as well, due to the recalcitrance of asphaltenes and resins to biodegradation. Thus, as the simpler biodegradable compounds disappear, the resistance of the residual mixture to further biodegradation steadily increases, and the rate of oil removal takes a steep decline.[57] A residue is nearly always left over and often appears as black tar due to the relative enrichment of asphaltenes and resins.[51] Moreover, slow rates of biodegradation necessarily increase the likelihood of accumulating partially oxidized metabolites.[51]

The microbial pathways that are used in hydrocarbon utilization are well-characterized.[57] Molecular oxygen is required in initial steps that involve enzymatic oxidation of hydrocarbons via oxygenases.[57] Alkanes are converted to carboxylic acids and then biodegraded via β-oxidation, which forms acetate, which then enters the tricarboxylic acid cycle.[57] Aromatic compounds, on the other hand, are oxygenated to form diols, which are then cleaved to catechols.[51] These compounds also ultimately enter the tricarboxylic acid cycle. The biodegradation of aromatic hydrocarbons results in detoxification and does not produce toxic intermediates.[57] For those compounds that can be assimilated by bacteria and fungi, the digestion of hydrocarbons results, like complete combustion, in carbon dioxide and water byproducts, as well as cell biomass.

In surface conditions, molecular oxygen is not normally a rate-limiting factor, and the complete digestion is possible for those compounds that can be mobilized by microbiota. Oil—water emulsions, which are facilitated by the secretion of biosurfactants by bacterial communities on crude oil, can lead to mobilization.[54] Even when mobilized in the presence of excess oxygen, biomass production also requires nitrogen and phosphorus. These nutrients often are limiting in common contamination scenarios.[57] In fact, the simple addition of fertilizers has shown demonstratable efficacy for promoting crude oil biodegradation.[51] After the Exxon Valdez oil spill, the application of oleophilic fertilizer to field test plots stimulated biodegradation so that the surfaces of the oil blackened rocks on the shoreline turned white and appeared to be free of surface oil within 10 days after treatment.[58] The striking visual results strongly supported the idea that oil degradation in Prince William Sound was nutrient limited and that fertilizer application was a useful bioremediation strategy.[58]

A crude oil that penetrates to the subsurface will become a multi-phase, physically sequestered problem, due to limitations in oxygen and nutrients. The distribution of subsurface petroleum hydrocarbons can involve 4 distinct phases: (1) hydrocarbons trapped in the vadose zone as a solid phase sorbed to soil particles; (2) volatile hydrocarbons in the gas phase (in the vadose zone); (3) an immiscible free-phase liquid at the capillary fringe, above the water table; (4) and a dissolved phase of water soluble hydrocarbons.[59–61] The sorbed- and free-phases at the focal point of the spill are often referred to as the "source zone" since they continually release material both in the gas phase and in the aqueous phase. [61] While the heaviest and most polar molecules, such as the asphaltenes, strongly absorb to soil, lighter constituents from the sorbed phase and free phase can be continually released as vapor to the surface above. The problem of "petroleum vapor intrusion" (PVI) from subsurface contamination onto the above-ground surface is heavily researched.[62] Likewise, light non-aqueous phase liquid (LNAPL) at the capillary fringe or otherwise contacting the water table will release water soluble oil components into groundwater, creating plumes that can stretch for miles.[63–65]

In general, the weathering process can be summarized first by the physical process of volatilization and dissolution, which primarily remove lower boiling-point components of oil. Second, oxidative processes, particularly those mediated by UV radiation, promote a loss in saturated and aromatic hydrocarbons with a concomitant increase in asphaltenes. Biodegradation also results in the almost total removal of n-alkanes, smaller isoprenoids, and monoaromatics. Thus, nearly all environmental weathering processes (physical, chemical, and biological) leave behind heavier, more complex materials and oxidize saturated molecules, shifting the crude oil profile to one with a higher proportion of large aromatic molecules and molecules with greater NSO character.

1.6 Goals of the Dissertation

Soils are multicomponent, thermodynamically open systems comprised of solids, liquids, and gases that exchange matter and energy with the surrounding environment. Soils support biomass, promote nutrient cycling, and act as reservoirs for carbon, nitrogen, and biodiversity.[66-4] For example, carbon is 50-fold more concentrated in soil than in the parent material of Earth's crust, and soil nitrogen is 80-fold more concentrated.[67] Soils also purify and store a considerable portion of Earth's fresh water supply, sometimes called "green water" to distinguish it from the open "blue water" of lakes and rivers.[66,68] Thus, soil pollution can harm the soils' capacity to support biomass, thus causing lasting damage, particularly when contamination affects soils in biomes with major impacts on biodiversity, climate regulation, and material cycles (e.g., water, carbon, and nutrients).[69,70]

Petroleum contamination is a ubiquitous soil pollutant that is proven to harm human health and disrupt ecological systems.[48,71–74] Point sources of petroleum release include overflowing, failing, or unlined oil pits; leaking oil pipelines; leaking tanks; leaking well heads; and interaction between ground water and petroleum inside well bores. Diffuse petroleum residuals from large-scale catastrophic releases also remains a prominent concern.[4,52,75–78] After a spill, large volumes of petroleum are lost due to environmental weathering processes leaving behind residual petroleum hydrocarbons that are recalcitrant to further natural attentuation.[75] In practice, the level of petroleum-hydrocarbon contamination is measured as Total Petroleum Hydrocarbons (TPH), which usually varies between 1 wt% and 10 wt%; regulatory maxima range from 0.1%, the upper limit for agricultural use, to 1 wt%, the upper limit for industrial use. [4,69,79–81] Soils targeted for decontamination typically are unsaturated material excavated within 3-8 feet of the surface.

Ozone gas (O_3) has been proposed as a means to enhance the bioremediation of large quantities of soil contaminated with petroleum hydrocarbons.[82] O_3 is advantageous because it decays into non-hazardous O_2 molecules, leaving no residue. On the one hand, Chen et al. showed that O_3 treatment could lower TPH by 40-50%. The loss of total organic carbon, on the other hand, was ≤12%[83,84] The TPH molecules were converted to partly oxidized products, which were readily biodegradable.[83] In particular, the loss of TPH was accompanied by increases in dissolved organic carbon (DOC), soluble chemical oxygen demand, and 5-day biochemical oxygen demand (BOD_5). Thus, treatment with O_3 gas increased the bioavailability of petroleum hydrocarbons, resulting in accelerated bioremediation, enhanced ability to meet regulatory limits, and a decrease in the time that the soil could not support ecosystem or agricultural functions.[45,83,85,86]

Oxidation of petrogenic compounds by O_3 will create a new set of residuals—carboxylic acids, ketones, aldehydes, quinones, alcohols, and esters—which, though not technically classified as "TPH," may persist in the environment, particularly if the soil is not subsequently bioremediated. A means to quantitatively understand the fate and toxicity of these oxidized crude oil byproducts is urgently needed, particularly in the context of a remediation effort that targets returning the soil to productive ecological roles (nutrient recycling, purification of water, and decomposition of biomass) or for managed human use (e.g., provision of food in agriculture, fiber and raw materials in forestry, etc.). One metric that measures the biological production potential of soil is its ability to facilitate the germination of plant seeds; in the context of O_3-treated soils, information about this characteristic is non-existent.

A primary goal of this dissertation is, therefore, to evaluate the capacity of O_3-treated petroleum contaminated soils to support seed germination before bioremediation. Because crude-oil contamination is a global problem, the number of salient terrestrial plant targets for germination studies is vast. This dissertation looks at lettuce (*Lactuca sativa*), a species with dose-response sensitivity to petroleum contamination; radish (*Raphanus sativus* L.), a known accumulator of soil contaminants; and fountain grass (*Lagurus ovatus*), since grass are known to be pioneer organisms in contaminated soils as well as candidates for petroleum phytoremediation efforts.[87–93] Plant diversity is paralleled by crude-oil variability, which can take on different compositional profiles based on the relative proportion of saturates, aromatics, resins, asphaltenes.[94] Thus, a subordinate goal in this work is to test each of the three selected plant species with respect to toxic effect between three distinct crude oils which have been treated with O_3.

A second goal of the dissertation is to evaluate a major operational parameter of the dosing regimen in field settings: O_3 loading rate (mass O_3/ mass soil/ hour). While *in situ* advanced oxidation (ISCO) and *ex situ* treatment (involving soil excavation) are viable treatment means, both require improved knowledge about depth of treatment when contamination exceeds 1 wt% TPH. While O_3 deployment as an ISCO technology is in its nascent stages, landfarming is a mature setting in which to deploy this treatment model.[95] In landfarming, the depth for treatment is typically ~2 ft, the total treatment area is large (1-2 acres), and moisture levels are kept between 30 and 80% field capacity to ensure the survival of hydrocarbon-degrading bacteria.[95,96]

Since industrial O_3 production can be anywhere from 1 wt% to 16 wt%, the relative advantages and disadvantages of the range of production must be substantively evaluated.[97] For instance, a low loading rate will confer a given mass of O_3 in a higher total volume of gas at a longer treatment time; this may be more advantageously utilized with larger soil volumes. On the other hand, high-concentrations of O_3 will necessarily decrease contact time, since a given dose of O_3 is supplied more quickly, potentially decreasing the treatment interval between bioremediation cycles.[98] Thus, a primary goal of this dissertation is to systemically evaluate three fields scale loading rates—4, 12, or 36 mg_{O3}/ g_{soil}/ hr)—for petroleum contaminated soil.

Given the complex chemical and physical structure of soil, as well as the necessary presence of soil water, an auxiliary concern is the dimensional reactivity of O_3 with TPH. While multiple studies have evaluated O_3 break-through, these findings were limited with respect to information about the reaction path of O_3 in highly contaminated soils (i.e., >1 wt% TPH). Therefore, this dissertation evaluates O_3 transport at 5 points along the the axial distance at a depth close to that seen in a landfarm (45 cm) and in conditions of ~2 wt% TPH contamination. Along with visualizing TPH removal in the axial distance, the transport of soil moisture and the movement of heat along the reaction path are also systematically assessed.[99]

The overarching goal of this dissertation was to evaluate two areas of potential concern to large-scale O_3 deployment: the capacity of O_3-treated petroleum contaminated soils to support seed germination before bioremediation and the transport characteristics of O_3 in soil columns. Overall, this work lays a foundation for field-scale deployment of ozonation by evaluating two highly salient to field-scale deployment concerns.

1.7 Dissertation Outline

The chapters that follow lay out the scientific bases for using ozone to remediate soils contaminated with crude-oil residuals. This section provides a "road map" to the following chapter: the topic of each and why it is important to my research.

Chapter 2, Background on the kinetic and thermodynamic principles of O_3 and its reactions with organic carbon compounds. In this chapter, I discuss the basic principles of hyperconjugation and induction that influence the positions of attack of the O_3 molecule on complex hydrocarbons, as they relate to the scope of this work. This chapter describes the stepwise reactions in which O_3 is known to attack electron-rich hydrocarbons. Special attention is paid to ozonation kinetics and thermodynamics in the gas-phase for different classes of hydrocarbons (normal alkanes, branched alkanes, cycloalkanes, aromatics, resins, and hetero-atom containing molecules etc.). These reactions are relevant for gas-based ozonation of crude oil in soil. Chapter 2 also lists potential ozonation products.

Chapter 3, Ozonation among 3 distinct crudes at 3 distinct doses. This chapter summarizes the effects of O_3 gas on three different crude oils at three distinct dose levels. This study serves as the basis for examining toxicity of the oxidized crudes and the ensuing logistic regression analysis in Chapters 4 and 5. Briefly, I evaluated 3 crude oils: ANS (API gravity 29-32), ARAB (API gravity 30-32), and SJV (API gravity 13-15) ozonated at 5 g, 10 g, and 20 g O_3 with continuous monitoring of effluent (unreacted) ozone gas. The control soil and O_3 treated soil were then evaluated for total petroleum hydrocarbon (TPH), dissolved organic carbon (DOC), and pH.

Chapter 4, Lettuce, grass, and radish germination by simple logistic regression. I used simple logistic regression to evaluate germination difference between treatment groups (background soil, crude oil contaminated soil, and soil with crude oil treated with O_3), dose groups (5g O_3, 10g O_3, and 40g O_3), and crude oil groups (ANS, ARAB, and SJV crude oils) for the germination lettuce, grass, and radish seeds. I performed in-depth logistic regression analysis using Stata v. 16.1. The use of a formal logistic regression model allowed me to build confidence intervals and test statistical significance of differences between the groups under study as they relate to crude oil, seed, and dose.

Chapter 5, Using radish (Raphanus lativus L.) germination to establish a benchmark dose for the toxicity of ozonated-petroleum byproducts in soil. The concentration-response relationship between the adverse germination outcome of radish (*Raphanus lativus* L.*)* and ozonated petroleum residuals was determined from Chapter 4. *TREATMENT* categories (control, petroleum, petroleum + 5 g O_3, petroleum + 10 g O_3, and petroleum + 40 g O_3) were used to create a dilution series for radish germination using different proportions of the test soil and a commercially available potting mix (~75% w/w organic matter) to evaluate the effects of background organic matter (*b-ORGANIC*) in conjunction with *TPH* and *DOC*. Multivariable logistic regression was performed on the adverse germination outcome as a function of *TPH*, *DOC*, *TREATMENT*, and *b-ORGANIC*. Results showed that the parameters controlling germination were the continuous variable *DOC,* categorical variables *TREATMENT*, and *b-ORGANIC*. The results were used to tabulate extra-risk levels for adverse germination effects.

Chapter 6, Ozonation of Petroleum Hydrocarbons in Soil Columns: Effects of Ozone Loading Rate along the Axial. Columns containing soils containing petroleum crude oil (~20,000 ppm) were treated with ozone gas (O_3) at 3 loading rates (4, 12, or 36 mg_{ozone}/ g_{soil}/ hr) to achieve 3 total-dose levels (5 g, 10 g, and 20 g O_3). Every experiment was monitored for effluent O_3 ("break-through") and temperature at 10 points along the axial distance (45 cm). After ozonation, soil columns were evaluated in five segments for total petroleum hydrocarbons (TPH) and moisture. TPH changes, moisture flux, temperature, and total heat were described along the axial distance of the column.

Chapter 7, Summary and Future Work. This chapter provides a summary of findings and suggestions for future work.

2 BACKGROUND: O_3 AND ITS REACTIONS WITH ORGANIC CARBON COMPOUNDS

2.1 O_3 Discovery and Current Production

O_3 is as old as lightning, but it was Christian Friedrich Schönbein (1799-1868) who first identified it as a distinctly odorous gas at the University of Basel in 1939 and named it accordingly[m].[100] At the time, Schönbein reported that the electrolysis of water produced, at the cathode, an odor that was identical to the odor produced by an arc between two electrodes and attributed that odor to a new chemical.[100] Since its discovery, O_3 quickly transitioned from a chemical curiosity to an important reagent in analytic and synthetic chemistry, as well as in water treatment. As early as 1910, the city of Paris began using O_3 gas for the disinfection of drinking water and wastewater.[101] Drinking-water disinfection remains an application in which O_3 gas is generated on a large scale.[102] Ozonation also is valuable in bleaching, semiconductor processes, and, increasingly, for neutralizing pathogens on fruits and vegetables and even as a sanitizing oxidant in liquid foods.[103,104] Finally, O_3 also has become an indispensable reagent for organic synthesis and an extremely useful tool for structural determination of natural products.[105]

O_3 is an allotropic modification of O_2 that, unlike O_2, is intensely colored, diamagnetic, poisonous, and explosive at high concentration (>60 wt%).[97,106,107] It is generally produced by a device that employs dielectric barrier discharge, hereafter

[m] From the Greek *ozein*, "to smell", as suggested by Schönbein's colleague, W. Vischer, Professor of Greek in Basel, Switzerland.

referred to as an ozone generator (OG), from either O_2 or air feed gas.[108] In this arrangement, O_2 is separated into O atoms by direct electron impact as in

$$e + O_2 \rightarrow 2O + e \qquad \text{Equation 2.1}^{108}$$

The O_3 molecules are then formed from a three-body collision between the remaining O atom, and a third body denoted M (Equation 2.2).[108]

$$O + O_2 + M \rightarrow O_3 + M \qquad \text{Equation 2.2}$$

When O_3 is generated from a pure-O_2 feed gas, the third body (M) can be O_3, O_2, O, or a surface.[109] Innovation in the efficiency of electron transfer has enabled the production of high concentrations of O_3.[108] This was accomplished first by adopting pure O_2 as a feed gas and second by shortening the discharge gap in the OGs to achieve a high electric field.[108] These improvements have yielded O_3 concentrations exceeding 200 mg/L.[102]

The remarkable physical and chemical properties of O_3 are a result of the large excess of energy of its molecule upon decomposition to O_2.[101]

$$O_3 \rightarrow \frac{3}{2} O_2 + 143\ kJ/mol \qquad \text{Equation 2.3}$$

It is this energy that makes O_3 extremely explosive at a certain critical concentration: Self-sustaining decomposition occurs above 15 wt%, deflagration at ~50 wt%, and explosion at ~60 wt%.[110] Ultra-high-efficiency OGs can reach concentrations of 15 wt% using an O_2 feed gas, which is considered safe to handle.[102] Higher concentrations can only be achieved through some form of separation of O_3 from the feed gas like low temperature liquid[n] distillation or silica-gel absorption/desorption at super-cooled

[n] The liquid or solid pure O_3 product is extremely unstable and explosive.

temperatures (-60 to -80°C).[106,107,111] Thus, gas-based ozonation reactions must occur in the presence of the carrier gas, which will contain O_2 at high concentrations.[111]

2.2 The Criegee Ozonolysis

The exceptional reactivity of O_3 gas was determined very soon after its discovery. From 1840-1845, it was shown qualitatively that O_3 reacted with a host of inorganic compounds (particularly metals).[100] By 1845, the reactivity of O_3 with organic compounds became established when it was demonstrated that the potent odor of O_3 disappeared in the presence of straw, humus, humus containing earth, sawdust, flour, potato starch, egg white, mushrooms, and many more.[100] Even at this early stage, chemists noted that the reactions of O_3 with organic compounds did not convert the organic substrate to the highest oxidation state (CO_2), but instead to aldehydes and carboxylic acids. The vigorous reaction of O_3 with unsaturated organic compounds attracted the attention of organic chemists. The work of C. D. Harries, from 1903 to 1916 in the German towns Berlin and Kiel, established experimental procedures for "ozonolysis," the process by which the unsaturated bonds of alkenes, alkynes, or azo compounds are cleaved using O_3.[105] Harries also initiated investigations into the mechanistic understanding of ozonolysis, which was proposed nearly 40 years later by Rudolf Criegee in Karlsruhe, Germany and confirmed in 2009.[105,112,113] The reaction of O_3 with double bonds, along with the decomposition of the resulting products, is one of the most dependable procedures for oxidative splitting of unsaturated molecules as well as for the determination of the double-bond position.[114]

The Criegee ozonolysis of alkenes (aka olefins) is a classic reaction of organic chemistry and underscores the ability of O_3 to pinpoint the double bond position on an unsaturated straight-chain hydrocarbon.[112] The electrophilic attack by O_3 is described as a 1,3-dipolar cycloaddition[o] and produces a unique molozonide or primary ozonide (1,2,3-trioxolane) that rapidly rearranges to a carbonyl compound and a biradical (or zwitterion),[p] the so-called Criegee intermediate.[112,113,115–118] These, in turn, recombine to form the class of secondary ozonides, the 1,2,4-trioxolanes, that are reactive and thermally unstable (decomposing at 70-80 °C).[113,115] Secondary work-up determines the downstream products. If the work-up is reductive, the ozonide degrades to alcohols or carbonyl compounds, while oxidative work-up leads to smaller carboxylic acids or ketones. For this reason, O_3 was used in the early in the 20th century to “cut” high molecular weight alkenes into smaller molecules that were easier to analyze with the then available organic chemistry techniques. [101]

2.3 The Relative Reactivity of O_3

The remarkable reactivity of O_3 with unsaturated (olefinic) compounds was naturally followed up by the ozonation of other organic groupings. O_3 is like most oxidants in that the nature of the substituents exerts a strong effect on position of attack and rate of the reaction for a given compound.[119] This relative reactivity is noted among hydrocarbon types (alkanes, cycloalkanes, aromatics, heterocycles) and with respect to the attack position of the hydrocarbon itself.[101,120,121] The simplest example can be observed in the

[o] Although this reaction is most accurately described as a pericyclic reaction, chemists have observed that electron-rich alkenes react faster with ozone than electron-poor alkenes.
[p] A molecule containing the oxide of a carbonyl group.

oxidation differences within the alkane group due to substituent pressure around a given carbon position. A carbon atom with only single bonds will form four[q] specific bonding arrangements.[122,123] Aside from the unique structure of methane, a carbon can be in a primary, secondary, tertiary, or quaternary position depending on whether it is bonded to one, two, three, or four other carbon atoms, as illustrated (Figure 2.1). [21]

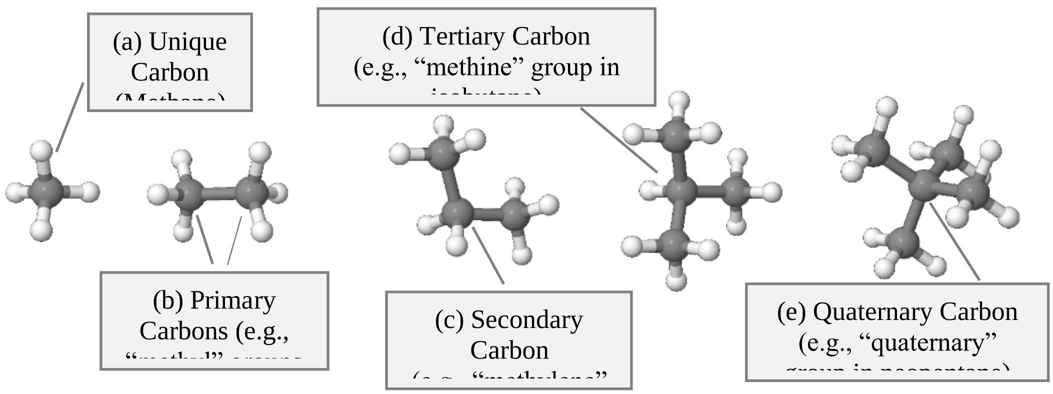

Figure 2.1 Aside from the unique bonding arrangement in (a) methane, a carbon atom can form (b) primary, (c) secondary, (d) tertiary, and (e) quaternary bonding arrangements depending on whether it is bonded to one, two, three, or four other carbon atoms as demonstrated with ethane, propane, isobutane, and neopentane, respectively.

The bonding arrangement within a hydrocarbon molecule determines the electron density proximal to each carbon, which in turn establishes the degree to which a carbon undergoing bond cleavage can delocalize an electron deficiency. This delocalization phenomenon is known as hyperconjugation and is important in hydrocarbon reactions that produce either a carbon radical by homolytic[r] bond cleavage or hydrocarbon ion

[q] Methane is considered "unique" in this series.
[r] Homolytic bond cleavage results in the breaking of a covalent bond in a single molecule such that resulting structures (atoms or molecules) each gain only one electron from a bonding pair.

through heterolytic[s] bond cleavage.[124,125] The relative stability of carbon radicals and carbocation increases with the number of adjacent carbon atoms that can delocalize an unpaired electron.[125] As such, an unpaired electron at a tertiary carbon position is more stable than a secondary carbon, which is more stable than a primary carbon, which, in turn, is more stable than a methyl radical, as shown in Figure 2.2.

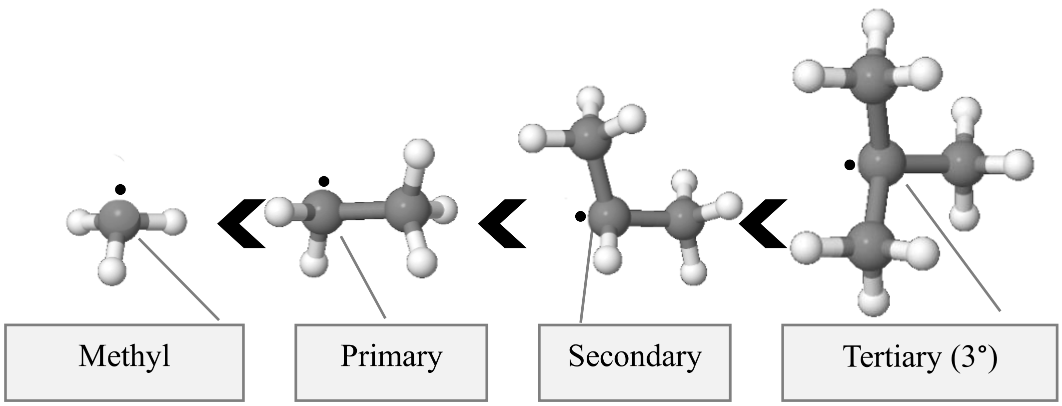

Figure 2.2 Hydrocarbon radicals represented in order of increasing stability; stability improves (from left to right) as an electron deficiency can be dispersed among p-orbitals of adjacent bonding carbons.

Hyperconjugation effects explain differences in C—H bond dissociation energy in alkanes.[119] In a demonstration of this feature in ozonation, Paltenghi and coworkers measured the rates constants of alkyl radicals reacting with O_3 at 298K shown in Table 2.1.[126] The trends were similar to those observed for the reaction of organic reactions with O_2, wherein the rate constant *k* increased with decreasing ionization potential (IP) of the radical.

[s] Heterolytic covalent bond cleavage, otherwise known as ionic fission, results into both electrons in a bonding pair leaving with one molecule (or atom). For a hydrocarbon, a leaving pair creates a carbocation that follows the stability pattern of carbon radicals (tertiary>secondary>primary). On the other hand, if the hydrocarbon keeps both electrons the resultant carbanion will be destabilized by adjacent carbons (tertiary<secondary<primary).

Table 2.1. Relative reactivity of alky radicals with O_3 gas by the rate constant k_1. Data modified from source.[126]

Radical	*k_1 (10^{-12} cm^3/molecule·s)*
Methyl (CH_3)	2.53±0.54
Ethyl (C_2H_5)	25.3±5.80
Propyl (1-C_3H_7)	24.4±5.90
Propyl (2-C_3H_7)	46.5±10.9
Tert-Butyl (t-C_4H_9)	54.5 ± 11.4

The energy for a homolytic bond cleavage between a carbon atom and hydrogen atom is, by definition, exactly equal to bond dissociation energy (BDE) and decreases if the resulting radical species is more stable.[21,119,127] Hence, the BDE of a carbon—hydrogen (C—H) bond is inversely related the to the number of carbons adjacent to the C—H bond being broken. It is then unsurprising that the BDE of C—H bond in methane is 440 kJ/mol, in a primary carbon it is 410 kJ/mol, in a secondary carbon it is 400 kJ/mol, and in a tertiary carbon it is 390 kJ/mol.[123] In other words, BDE can be considered a measure of radical stability, and ease of oxidation.

This order of reactivity is relevant to chemical transformation of a petroleum crude oil, which contains a mix of hydrocarbon structures reacting at different rates. Since any factor that either helps to donate electron density to the half-filled orbital, or to delocalize an unpaired electron will stabilize a radical intermediate and promote the oxidation, some structures will be oxidized more readily than others. Carbon position (methyl < primary < secondary < tertiary) is one example. However, several other factors are important to stabilizing free-radicals: e.g., an adjacent aromatic core, such as benzene or adjacent atoms with lone-pair electrons, like nitrogen.

The relative importance of each kind of substituent (alkyl group, aromatic group, lone pair) has been observed in the various types of O_3 attack on organic molecules. While O_3 behaves with a 1,3-dipolar addition to carbon—carbon double bonds, O_3 also reacts as an electrophile and, in some cases, as a nucleophile. O_3 can react with carbon triple bonds (acetylenic compounds), aromatic rings, nucleophilic groups (like amines and sulfides), carbon—nitrogen and carbon—sulfur double bonds, carbonyl groups, carbon—hydrogen bonds, and organometals.[120] These reactions occur at different rates, with some to the exclusion of others when more than one group is present in the system at the same time. Figure 2.3 describes the general trends observed for the functional groups.

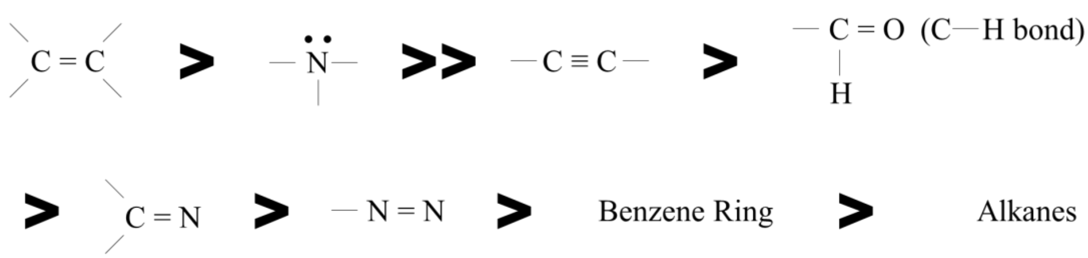

Figure 2.3 The order of reactivity of O_3 gas for various organic groupings.[120]

The great difference in reaction order indicates that ozonation, at least in non-participating aprotic solvents, may proceed in series. Indeed, certain organic materials are known to “shield” other organic substituents from a reaction with ozone. Cataldo and

Ori experimented with buckminsterfullerene (C60) dissolved in CCl_4 to determine whether it could shield a dienic rubber (*cis*-1,4-polyisoprene, an olefinic polymer) from oxidation.[128] Instead, the authors found the opposite: While fullerene alone began to oxidize in O_3 gas in 3 minutes, the presence of dissolved *cis*-1,4-polyisoprene acted as an O_3 scavenger and protected buckminsterfullerene for additional 40 minutes. Similarly, Bailey notes that, while O_3 can react vigorously with alcohols, alcohol can still be used as a solvent when it contains organic compounds that are more reactive toward O_3.[120] These results suggest that O_3 oxidations tend to happen in series, not in parallel, particularly when the reactants are in excess.

2.4 Ozonation of the π- Conjugated Ring

Detailed knowledge of the mechanism of the reactions of O_3 with aromatic hydrocarbons is of great importance for a complete understanding of the chemistry of the petroleum hydrocarbon oxidation because of their typical prevalence (~30-60 wt %) in petroleum crude and their ease of oxidation relative to the other major group, the saturates. A mechanistic understanding informs O_3 utilization and expected products. The precise mechanism of the reaction of ozone and has been most studied with respect to the benzene ring. This model is used here, although benzene is typically not present in weathered crude oils.

2.4.1 Mechanism and Products of Benzene Ozonation

It became obvious early on that the aromatic compounds reacted much more slowly than alkenes. Indeed, a phenyl substituted alkene would be attacked at the double bond only, even if the alkene were in ring conformation.[120] Confirmation comes from Atkinson et al., who found the following rate constants for the reaction of O_3 (cm^3/molecule•s) with the following napthenoaromatics[t]: fluorene, $<2x10^{-19}$; indane, $<3x10^{-19}$; 9,10-dihydroanthracene, $(9.0\pm2.0)x10^{-19}$; and, indene, $(1.7\pm0.5)x10^{-16}$; reactions were executed in tropospheric conditions, Figure 2.4.[129]

a. 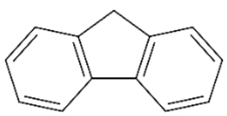 b. 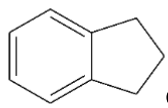 c. 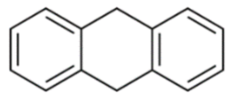 d. 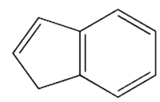

Figure 2.4 The reaction rates of O_3 trend as follows: a. fluorene < b. indane < c. 9,10 dyhyrdoanthracene << d. indene.

It is generally acknowledged that the O_3 attack on a benzene ring is like that of the Criegee ozonolysis: The O_3 molecule attacks two adjacent (ortho) carbons in what is described as a 1,3-dipolar cycloaddition. This nomenclature indicates that the terminal (1,3) O atoms are oppositely charged and simultaneously attack a double bond forming a primary ozonide with a 1,2,3 trioxolane conformation.[130,131] However, the reaction is slower than the alkene ozonolysis by 6 orders of magnitude.[132,133] The thermodynamic differences naturally recapitulate the preferential order of the kinetics, though not with the same scale differences. Hendrickx and Vinckier found that the following theoretical activation barriers for benzene, phenol, and ethylene, respectively: +15.8, +9.5, and +3.3, kcal/mol, which agreed with experimental values. [130,133] The theoretical differences in exothermicity also corresponded to experimental values, though the differences between

[t] Napthenoaromatics include one or several condensed aromatic rings, fused with naphthenic rings and chains.[8]

hydrocarbon classes were smaller in magnitude: –18.9, –29.0, –52.5 kcal/mol, for benzene, phenol, and ethylene, respectively.[130] Though reactions with an aromatic ring are orders of magnitude slower than alkenes, the energy released from a delocalized double bond in benzene is half as much as that released from normal alkene.

The activation energy of the first reaction (for the preferred -endo geometry) is noted by Wen et al. to be close to 16.6. kcal/mol (very close to the 15.8 kcal/mol found by Hendrickx and Vinckier).[130,134] The initial release of energy from the first-step of the reaction of benzene is thought to be 18.9 kcal/mol from Wen et al. and 21.8 kcal/mol from Hendrickx and Vinckier.[130,134] The formation of the primary ozonide (POZ) intermediate is the rate-limiting step which cleaves the first C—C double bond to single bond and disrupts the aromatic core. The two ortho carbons are bound to the 3 oxygen atoms in a ring conformation exactly like the 1,2,3-trioxalane POZ in the ozonolysis of an alkene. The two remaining C—C double bonds are no longer aromatic but olefinic, though still probably linked in ring conformation.

The second O_3 molecule disrupts a π-bond, not a conjugated π-system. Therefore, the reaction is predicted to be faster, more exothermic (-40 to -50 kcal/mol), and with a negative activation energy of -5 kcal/mol, meaning that it has nearly no energy barrier. The second addition of O_3 can proceed by several paths. The most thermodynamically favored is the addition of a second O_3 molecule, which causes the 1,2,3-trioxalane bridge of the first O_3 to collapse to a carbonyl oxide and a biradical (just like in a Criegee mechanism) and open the ring of carbons into a chain conformation. Unlike the Criegee ozonolysis of an alkene, the benzene reaction produces a carbonyl and biradical that are linked by the remaining double bond, which is illustrated in Figure 2.5.

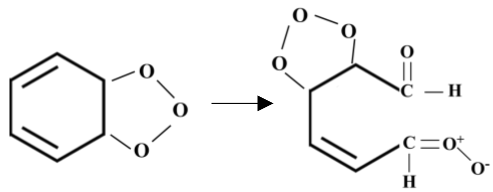

Figure 2.5 Cleavage of the POZ intermediate on the addition of a second O_3 molecule.[120]

The final C—C double bond also is vulnerable to ozonolysis. Like the second addition, the third addition has little energy barrier and is exothermic (-40 to -50 kcal/mol).[134] Also like the second addition, the third molecule O_3 appears to cause the bridge of the second O_3 to collapse. Unlike the second addition, however, the third addition causes molecular cleavage, which releases several products, such as CO_2 and glyoxal, major non-peroxidic products. The remainder of the carbon chain, containing carbonyl oxides, can form peroxidic depending on the reaction environment.

2.4.2 Substituent Effects on the π-Conjugated Ring

The presence of substituent groups enhances the reaction rates of O_3 with benzene or its homologs. Figure 2.6 summarizes some of these findings normalized to the ozonation of benzene in CCl_4 at 25°C and clustered for polyaromatic hydrocarbons, methyl-substituted benzene rings, and ethyl-substituted benzene rings. Compared to benzene, phenanthrene and pyrene react over 1000 times faster. Similarly, methylated benzene homologs show remarkable increases in reactivity. Compared to benzene, toluene reacts 3 times faster; an additional methyl group to form xylene increases that rate another 3- to 5-fold. The rate constant for mesitylene (3-methyl groups) is 70 times greater than benzene, and for durene (4 methyl groups) 400 times greater.

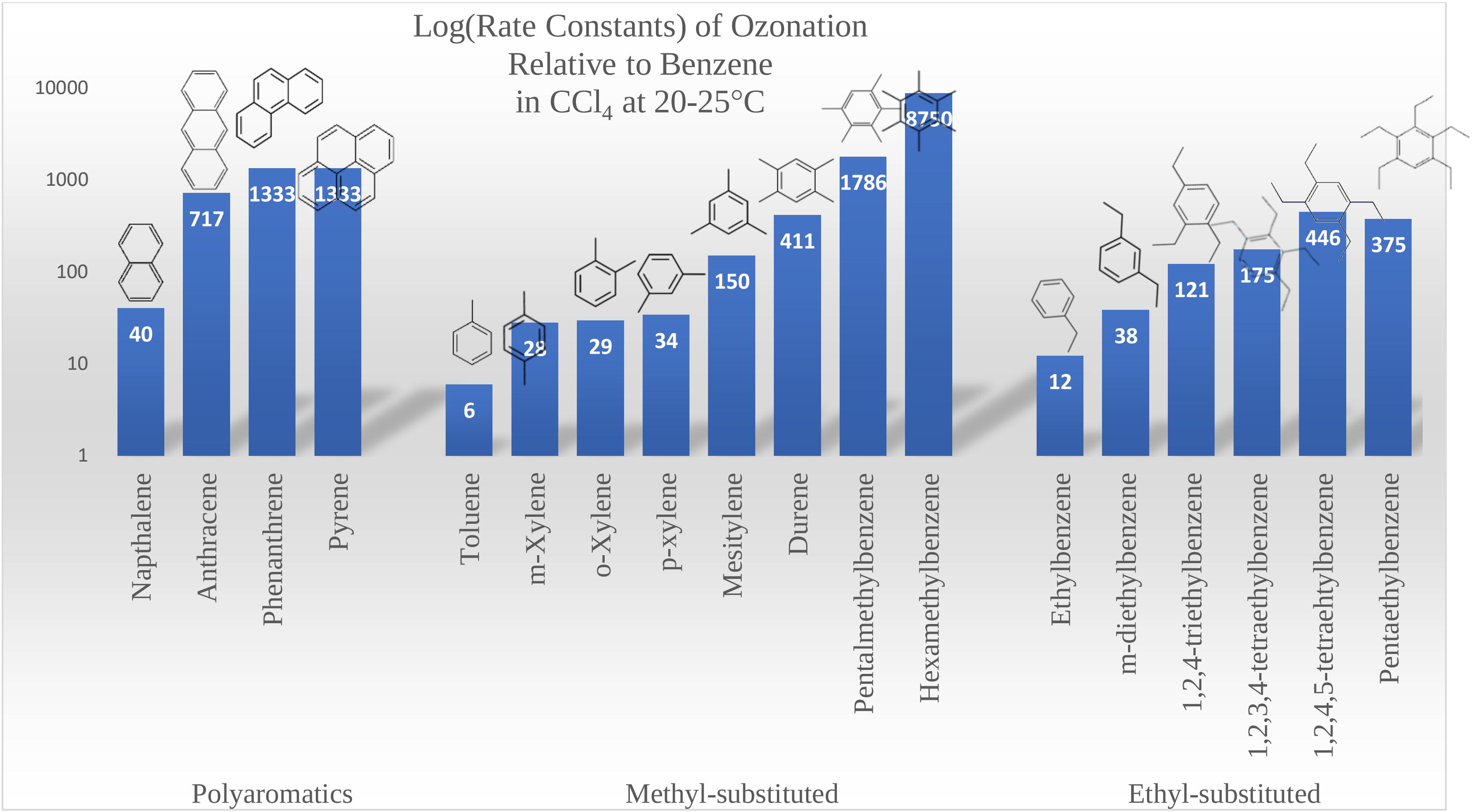

Figure 2.6 Second-order relative rate constants for the ozonation of benzene and benzene homologs performed in CCl_4 at 20-25°C. Values on Y-axis are normalized to benzene and on a log-scale. Data are adapted from Bailey.[120]

Substituents to the benzene ring increase the reaction rate considerably, but the increase in rate constant appears to maximize and level-off at some point. In addition, certain types of moieties create steric hindrance (as in hexaethylbenzene, not shown) and slow the rate of oxidation. Nevertheless, the trends appear to indicate that larger, more substituted aromatic rings and polyaromatic rings react more readily than less substituted ones. In a complex hydrocarbon mixture like crude oil, reactivity is likely to vary over many orders of magnitude. This feature is sometimes called "activation." Electron-donating groups enhance (i.e., "activate") the rate of oxidation by O_3, and electron-withdrawing groups "deactivate" the ring to which they are attached. The principles underpinning "activation" or "de-activation" of the aromatic core might be considered an extension of the delocalization concepts discussed in Section 2.3.

2.4.3 O_3 Attack on Benz-Fused Carbocyclics: Polyaromatic Hydrocarbons

The reaction on polyaromatic hydrocarbons, or benz-fused carboxylics, like naphthalene and phenanthrene, are indeed activated by the adjacent aromatic cores. As noted, the reaction rates for PAHs can be orders of magnitude higher than that of benzene because of the electron-donating effects of adjacent aromatic rings. On the other hand, a primary ozonide that has decomposed on a fused aromatic ring does not usually open a chain of olefinic bonds (naphthalene is the exception). The following discusses 2 homolog conformations, angular and linear, and their pattern of reactivity with O_3. Angular PAH homologs are shown in Figure 2.7.

In Figure 2.7, the primary reacting bond is shown in red and is the bond of lowest localization energy (LE_b)[u]. The unique placement of the LE_b means that a 1,3-dipolar cyclo-addition by O_3 at the LE_b disrupts aromaticity for some, but not all, the carbons on the reacting ring, as happens in benzene. O_3 attack on naphthalene (Figure 2.7a), for example, disrupts the aromaticity of 4 of the 6 carbons on the reacting ring. The remaining 2 carbon atoms on the breached aromatic ring are still bond to a conjugated π-centers on the adjacent ring. For phenanthrene (Figure 2.7b) and chrysene (Figure 2.7c), only the 2 carbons directly involved at the reacting bond are affected; the remaining 4 carbons are still in a π-conjugated system on adjacent rings. The following section discusses the 2-ringed naphthalene, 3-ringed phenanthrene, 4-ringed chrysene, and 5-ringed picene in more detail.

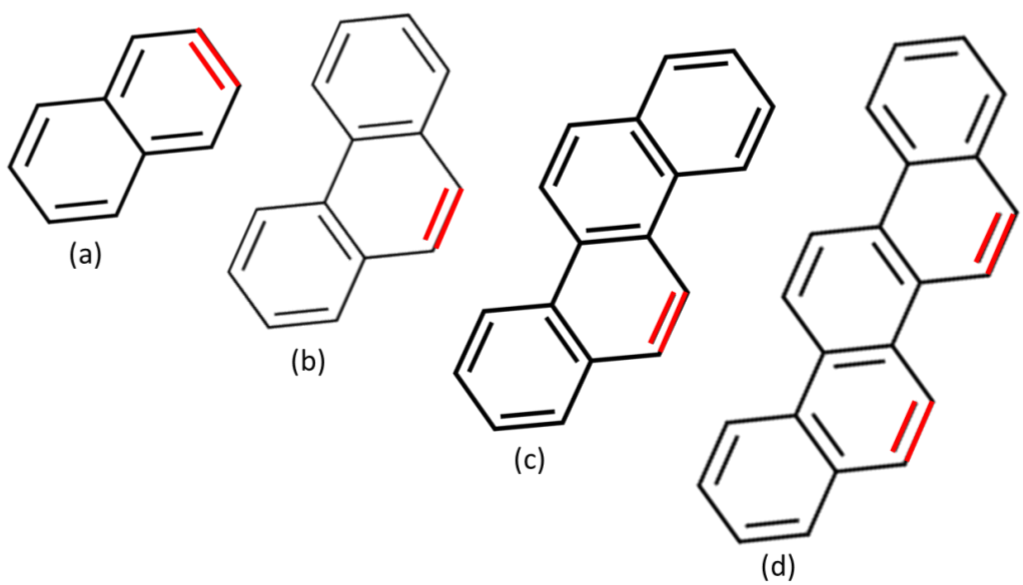

[u] Defined as the π-binding energy required to attach a proton or a hydride ion to a given π-electronic system.[135]

Figure 2.7 Angular PAHs discussed include: (a) Naphthalene, (b) phenanthrene, (C) chrysene, and (d) picene. Bond with lowest localization energy (LE_b) noted in red.

Wibaut and coworkers found that naphthalene reacted much more readily than benzene with two moles of O_3, whereas a third mole of O_3 reacted much more slowly.[136] The reaction product was primarily phthalic acid (Figure 2.8). Rindone et al. also ozonated naphthalene and found that the primary products were phthalic aldehyde, 2-formyl benzoic acid, and phthalic anhydride. Each of the structures found by Wibaut and Rindone shows that only one of the aromatic rings was cleaved by 2 moles of O_3, while the other ring remained intact. As an analogy to benzene, the first mole of O_3 attacks an aromatic core activated by the adjacent core. This first addition also exposes a single olefinic bond on the breached ring, making a second molar addition of O_3 to that ring thermodynamically favorable and faster.[120] However, carbonyl groups from the cleavage of the first core deactivate the addition of a third mole of O_3 to the unreacted aromatic ring.[120,136,137]

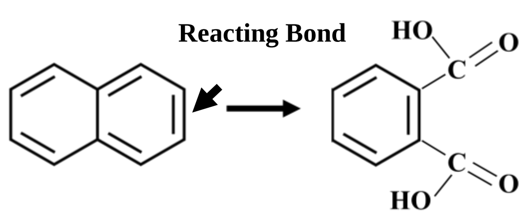

Figure 2.8 O_3 reacts with naphthalene to produce phthalic acid in 48% yield.[120]

Wibaut and coworkers also ozonated methylated naphthalene, finding the activation of substituents groups for oxidation noted above.[136] The products of methylated naphthalene (2,3 and 1,4-dimethylnaphthalene) produced small yields of glyoxal, methylglyoxal, biacetyl (in reducing conditions), and a major product of acetic acid (in oxidizing conditions). These results suggest that activating methyl groups, particularly in oxidizing reaction conditions, cause a complete degradation of both aromatic rings in naphthalene. As in the discussion for benzene, polymeric intermediate may also be formed, but decompose on further reduction or oxidation. Though unstable, the suggested structure of the polymer nearly always contains a repeating benzene core.[120]

Phenanthrene is considerably more reactive to O_3 than naphthalene because the central benzene ring is highly stabilized by two adjacent aromatic cores. Nevertheless, the opening of the core aromatic ring does not expose C—C double bonds, as in benzene or naphthalene. Instead, the ozonide and biradical intermediate degrade to a variety of products depending on secondary work-up. In oxidizing conditions, like with additional O_2/O_3, the cleavage produces diphenic acid in 50% yield, though as many as six other products are possible (Figure 2.9).[120,138] Researchers have found the products of ozonation of phenanthrene to be less biodegradable and more toxic.[138] It also is clear that the reaction product has not lost carbon atoms.

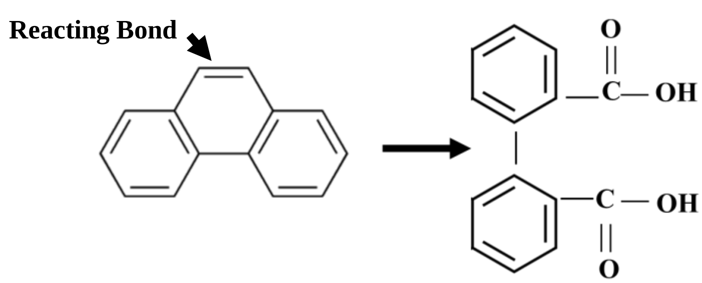

Figure 2.9 O_3 reacts with phenanthrene to produce diphenic acid in 50% yield.

Chrysene has four aromatic cores and, like phenanthrene, easily absorbs 1 mole of O_3 at the bond of lowest localization energy (5,6 position). The resulting primary ozonide is peroxidic, which likely is polymeric in a non-participating solvent.[120] In an oxidizing environment, however, these primary products decompose to 2-(*o*-carboxyphenyl)-1-naphthoic acid in 48% yield (Figure 2.10) according to Bailey.[120,139] Luster-Teaseley et al. found also found this product as well as additional products 2-(2'-formyl) phenyl-1 naphthaldehyde and 2-(2'formyl) phenyl-1-naphthoic acid, which were more toxic than chrysene itself. In particular, 2-(2'-Formyl) phenyl-1-naphthaldehyde inhibited *in vitro* gap-junctional intercellular communication (GJIC) and caused irreversible damage that lead to cell death.[139] Each of the three reaction products listed above retain 3 of the 4 aromatic cores on chrysene. The 2 carbon positions (the 5,6 carbons on chrysene) where the initial O_3 molecule attacked lead to some combination of carbonyl and carboxylic acid, though there is not loss of carbon from the molecule.

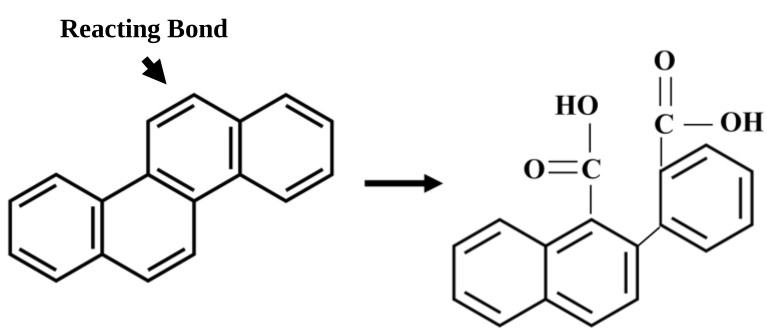

Figure 2.10 O_3 reacts with chrysene to produce 2-(o-caroxyphenyl)-1-napththoic acid in 48% Yield.

The 5-ringed picene molecule readily absorbs 2 moles of O_3 gas, attacking the 5,6 and 7,8 positions, both which are bonds of lowest LE_b. Like chrysene and phenanthrene, the primary products are peroxidic polymeric ozonides in a non-participating solvent, which are oxidatively decomposed to a 35% yield of terphenyltetracarboxylic acid anhydride (Figure 2.11). It is worth noting that the C—O—C bridge in the center position represents the "anhydride," which is formed by the loss of H_2O from two –OH groups of the central carboxylic acids. The loss of H_2O, and often H_2O_2 as well, is a frequent decomposition products of work-up (both oxidative and reductive) of the primary reaction products of O_3 and PAHs.[120]

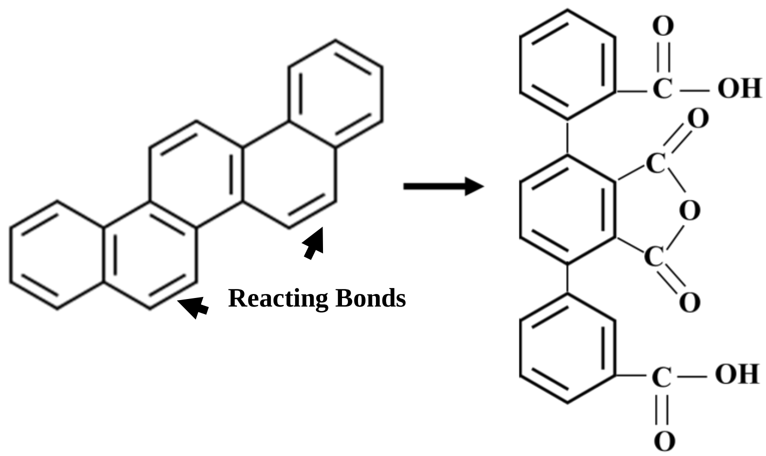

Figure 2.11 O_3 reacts with picene to produce terphenyltetracarboxylic acid anhydride in 35% yield.

The reactions of PAHs are activated by fused aromatic rings and are, therefore, considerably more reactive than the unsubstituted benzene ring. The positions of attack are usually the bond of lowest localization energy; that is, the bond that can most approximate double-bond character in the overall ring structure. For the angular PAHs, the attack on this position does not typically expose olefinic bonds, as in benzene. Hence, although angular PAHs are more reactive, they also only absorb between 1 and 2 moles O_3. The overriding feature of the above reactions is the residue of some of the aromatic rings, deactivated by adjacent electron withdrawing groups. Because of the residual aromatic cores, additional ozonation can occur, although it is much slower and more exhaustive.

The linearly fused PAHs (sometimes called polyacenes), represent a different combination of the straight-chain aromatics, which are also highly reactive.[135] They include naphthalene (2 rings) as well as anthracene (3-rings), tetracene[v] (4 rings), pentacene (5 rings), hexacene (6 rings), and heptacene[w] (7 rings). Anthracene is more reactive than naphthalene; it is easily oxidized in the middle ring to anthraquinone. Tetracene, pentacene, and hexacene (6) also are readily photo-oxidized. Except for anthracene, the polyacenes are not prevalent in crude oil. Nevertheless, the ozonation of these compounds shows an entirely different kind of O_3 attack on a fused aromatic structure, the electrophilic substitution at atom of lowest localization energy (LE_a). That is, the most reactive site in these molecules is the innermost solo carbon atom.

[v] Tetracene is also known as naphthacene.[120]
[w] 6 Heptacene is so unstable that it has never been obtained in a pure state.[135]

3 RESEARCH: OZONATION OF THREE DISTINCT CRUDE OILS FOR TOXICOLOGY TESTING[x]

3.1 Introduction

Over the last 50 years, the exploration, extraction, transport, and storage of 70-100 million barrels per day (mbd) of crude oil have resulted in stockpiles of contaminated soil and water from continual small releases and vast catastrophic ones.[1,4,38,52,76,77] The spilled oil, though susceptible to chemical, physical, and biological degradation, can still leave residuals that persist for decades and present environmental hazards to native ecology and human health.[38,48,78,140] This widespread contamination has necessitated research into petroleum fate and transport in environmental matrices, interaction with microbial consortia, and standards for risk assessment.[55,86,140,141]

Exposure to crude oil and weathered residuals of crude oil spills have been extensively studied in plants and animals.[5,47,72,74,91,140,142–147] Few studies, however, have looked at the effect of multiple intact crude oils simultaneously. Many studies have focused on the environmental releases of a single crude oil in an accidental release scenario. For example, Cowell examined large oil spills in Pembrokeshire, Wales; de Jong looked at crude oil contamination from a fractured pipeline in Saskatchewan, Canada; Han et al. used samples from the Chennai oil spill in India; Venosa et al. examined the Exxon Valdez oil spill in Alaska's Prince William Sound; Klinger et al. assessed the toxicity of the Deepwater Horizon disaster in the Gulf of Mexico; and

[x] This Chapter and the next will be incorporated into a manuscript.

Incardona et al. looked at Cosco Busan bunker oil spill in San Francisco Bay, etc.[4,79,148–150]

Other scientists simply obtain oils from a single site or sources without being able to control for background conditions: e.g., Chaîneau and colleagues used oil obtained in Marne, France; Besalatpour et al. obtained oil-contaminated soils from a field in Tehran, Iran; Tang et al. used soil from Shengli Oilfield in Shandong Province of China; and Zhu et al. used samples from a field of the Beijing Agriculture and Forest Science, etc.[79,144,146,151] At times, diesel, gasoline, motor oil, lubricating oil, or even vegetable oil were used to characterize the toxicity of hydrocarbon contaminants.[91,152–155] A study by Ogboghodo et al. looked at two crude oils simultaneously, but they were closely related: Forcados and Escravos were light crude oils received from Nigerian National Petroleum Corporation (NNPC) in Warri, Nigeria.[156]

Crude oil differences can be vast, however. On the one hand, the elemental composition is relatively simple: 83-87 wt% carbon and 10-14 wt% to hydrogen, and the remaining 3-7 wt% from the heteroatoms nitrogen (0.1-0.2 wt%), sulfur (0.05-6.0 wt%), and oxygen (0.05-2.0 wt%), with trace metals due mostly to vanadium (~1200 ppm) and nickel (120ppm).[7,9–11] On the other hand, the vast bonding configurations of those simple ingredients can create between 10,000 to 100,000 unique chemical constituents.[8] The molecular differences of these constituents contribute greatly to differences in behavior in the environment and the potential for toxic affect.

The lighter compounds components of crude oil have increased motility in the gas phase through volatilization, aqueous phase via a higher partition coefficient in water, and sometimes even the solid phase through thermodynamic flexibility and adsorption to native organic content.[157–160] Lighter (<C20) saturated compounds are not usually implicated with serious ecological or human health risks and are highly susceptible to aerobic and anaerobic biodegradation. Aromatic compounds, on the other hand, can include some of the most notoriously toxic and carcinogenic compounds in our environment. Benzene, for example, has no safe level of exposure according to the American Petroleum Institute (API).[161] While benzene is attenuated through volatilization in weathered crude oil, fused benzene homologs are not. Most PAHs are mutagenic in cell experiments and carcinogenic to animals and humans.[133] The large molecular size and increase in heteroatom frequency of asphaltenes and resins leads to an increase in polarity and van der Waals forces.[160] Both features allow these molecules to resist volatilization, dissolution, and transport through the solid matrix, since they adsorb much more readily to inorganic substrates such as the soil mineral backbone.[8,160] The recalcitrance and immobility of resins and asphaltenes often mean they are discounted from hazard assessments, though that view is changing.[160,162,163]

The toxicity of these basic groups is mediated through exposure to weathering conditions and, in some cases, can increase toxicity dramatically.[41,48,73,74,164,165] Exposure to sunlight, in particular, creates oxidized weathered petroleum products that show acute toxic effect in a variety of ecological settings.[45,47,48,53,150,164,166] For example, Maki et al. found that photo irradiation increased oxygenation, decreased aromaticity, increased the relative fraction of asphaltenes and resins, and increased dissolved organic carbon (DOC) thereby increasing bioavailability of oil. The oxidized water-soluble fraction, however, showed acute toxicity to crustaceans.[45] Barron et al. found that Alaskan North Slope Crude oil (ANS) was phototoxic and that UV could be a causative factor in the mortality of early life stages of herring.[48] In a later study, Barron et al. find that phototoxicity can create a 2- to 1000-fold increase in chemical toxicity to aquatic organisms.[47] Incardona et al. found that Cosco Busan oil and UV co-exposure were necessary and sufficient to induce an acutely lethal necrotic syndrome in hatching herring embryos.[150]

Natural oxidative processes play a critical role in destroying petroleum hydrocarbons and removing them from the biosphere.[53] Owing to their efficacy, artificial oxidation has been proposed as a means to accelerate environmental remediation of crude oil spills. Advanced oxidation processes (AOPs) for removing weathered crude oil, and indeed many types of hydrocarbon contamination, are an important environmental tool. AOPs include Fenton oxidation, photocatalysis, plasma oxidation, and ozonation.[85] Yet, direct evidence is minimal about changes to toxicity when crude oil residuals are transformed into oxidized products in a remediation setting. Research demonstrating these technologies with reference only to decreased TPH or PAH levels neglects the fact that, outside the specific case of complete mineralization, the oxidation of petrogenic compounds will create a new set of residuals—carboxylic acids, ketones, and esters—which, though not technically classified as “PAH” or “TPH”, persist in the environment. While it is true that oxidization byproducts will have increased solubility and biodegradability, it is also the case that these compounds will have new routes of environmental exposure for toxic affect.

While ozone (O_3) gas has been proposed as an effective oxidant to accelerate the bioremediation of petroleum hydrocarbons, of urgent need is assessing the toxicity of the oxidized residuals in a terrestrial setting, in which O_3 gas would be deployed. This assessment must (1) control background soil condition, (2) assess the effect of different types of crude (both untreated and O_3-treated), and (3) determine the effect of increasing O_3 dose. This chapter serves as a foundation for the following two chapters, which assess terrestrial toxicity of ozonated crude oil in three plant species. In this chapter, I create synthetically contaminated soils using three distinct crude oils: ANS (API gravity 29-32), ARAB (API gravity 30-32), and SJV (API gravity 13-15). I evaluate how each soil responds to ozonation at three doses by evaluating the loss of TPH, the gain of DOC, and pH change. The use of a standard background controls for the potential effects of the mineral background, the simultaneous comparison of three crude oils allows me to examine whether ozonation can create important differences in amount and carbon number of oxidized products, and the dosing sequence allows me to observe whether the degree of ozonation can affect toxicity as examined in later chapters.

3.2 Laboratory Methods

3.2.1 Test Soil (TS) Classification

The base *Test Soil (TS)* used in all experiments was locally sourced topsoil (*All Star Materials*, Guadalupe, AZ) that was free of organics that would interfere with the quantitation of hydrocarbons or their oxidized byproducts (<2%). Before use, the soil was sieved through a No. 10 mesh to remove material that larger than 2 mm in diameter.

After sieving, particle-size distribution was determined using ASTM Method D422-63 "Standard Test Method for Particle-Size Analysis of Soils" (Appendix A).[167] Liquid limit (LL) and plastic limits (PL) were determined using ASTM Method D4318-10 "Standard Test Methods for Liquid Limit, Plastic Limit, and Plasticity Index of Soils" (Appendix A).[168] The particle-size analysis, LL, and PL were used to determine the soil classification using ASTM Method D2487 – 11 "Standard Practice for Classification of Soils for Engineering Purposes (Unified Soil Classification System) (Appendix A)."[169]

Soil conductivity and organic matter content by the loss-on-ignition method (360°C) were determined at the University of Connecticut Soil Nutrient Analysis Laboratory (Storrs, CT).[170,171] Conductivity was 1.73 ± 0.2 dS/mm and organic matter was 0.5 ± 0.05% w/w. The pH, before and after ozonation, was measured in 1:2 (w/w) soil/water mixture with a Thermo Scientific Orion 2 Star pH probe (Thermo Fisher Scientific Inc.).

3.2.2 ICP-MS for Total Metals

Total metal content was tested at ASU facilities using a Thermo Scientific Quadrupole Inductively Coupled Plasma – Mass Spectrometer (ICP-MS). Soils preparation for ICP-MS followed EPA method 3051a.[172] Briefly, soils for analysis were air-dried, ground with a mortar and pestle, and weighed to a sample size of approximately 0.1 grams. The soil sample was then added to a clean Teflon microwave tube; to this, 9 mL of concentrated nitric acid, 1 mL of concentrated hydrochloric acid, and 1 mL of concentrated hydrofluoric acid were added. The Teflon sample tubes were microwave heated for 1 hour and 30 minutes in a heat sequence to 150°C to aid in the digestion of all organic material. The samples were then cooled for 30 minutes. Samples were digested for over 72 hours in a chemical hood. After digestion, samples were moved to clean heat-resistant polypropylene tubes. The samples were heated on a hotplate to 240°C in a chemical hood to evaporate HF and other acids for approximately 4 hours. The samples were then re-suspended in nitric acid and run on ICP-MS for the following metal elements: iron, manganese, copper, chromium, zinc, and nickel.

3.2.3 Crude Oil Analyses

Chevron Energy Technology Company (ETC) (Richmond, CA) provided three distinct crude oils coded *ANS* (API gravity 29-32), *ARAB* (API gravity 30-32), and *SJV* (API gravity 13-15); they are categorized as medium, medium, and heavy crude oil, respectively. Crude-oil samples were sent to Eurofins Lancaster Laboratories Environmental (Lancaster, PA) for analysis of total petroleum hydrocarbon (TPH) using MA DEP EPH and polyaromatic hydrocarbons (PAHs) using EPA Method SW-846 8270C.[173,174] From these analyses, I determined gasoline-range (GRO, C5-C12), diesel-range (DRO, C12-C22), and oil-range (ORO, C22-C40) organics, as well as aliphatic and aromatic fractions.

3.2.4 Preparation of Test Soil with Crude Oil (TSC)

I created three batches of Test Soil with Crude (TSC) by mixing ANS, ARAB, or SJV into the *TS*. In a fume hood, a 15-kg batch of TS (initial moisture <1-2% w/w) was spiked with a crude oil at 10% w/w. The mixture was vigorously mixed by hand with a trowel until an even consistency was achieved and transferred to clean heat-resistant (up to 60°C) to 57-L polypropylene containers. The containers were placed on a heated platform to raise the soil temperature to ~40-50°C and kept at this temperature for up to 1 week with intermittent trowel mixing to allow off-gassing of volatile components. Then, the soils were lightly sprayed with water and mixed every 2-3 days for a period of 4-6 weeks to stimulate the natural attenuation of the most biodegradable and volatile compounds. The soils for testing are identified as *TSC-ANS*, *TSC-ARAB*, or *TSC-SJV* according to the crude with which they were contaminated. After contamination and artificial weathering, soil was analyzed for TPH.

3.2.5 Moisture Determination

Moisture content was determined before ozonation, to bring samples up to 10 wt% moisture, and after ozonation to make TPH and DOC determination normal to dry mass of soil. Each measurement was an average of 3 independent samples taken from the homogenized soil and weighting exactly 2.00 g each ($Soil\ Mass_{Wet}$ (g)). The soil samples were then dried in an oven (105°C) until constant weight was achieved ($Soil\ Mass_{Dry}$ (g)). The moisture content (moisture %, w/w) of a soil was determined by difference:

$$\mathbf{Moisture}\ \%\ (\mathbf{w/w}) = \frac{\mathbf{Soil\ Mass_{Wet} - Soil\ Mass_{Dry}}}{\mathbf{Final\ Mass_{Wet}}} \times \mathbf{100} \qquad \text{Equation 3.1}$$

Untreated *TSC* had a native moisture content of <2% w/w. I increased the soil moisture % to ~10% w/w moisture (confirmed by measurement) to simulate field conditions for ozonation experiments. After ozonation, moisture % (w/w) was measured determined again.

3.2.6 Preparation of Test Soil with Ozonated Crude Oil (TSOC)

TSC, at a mass of 600-g and 10% w/w moisture, was loaded into the main chamber of the reaction vessel, which was gently tapped to allow the soil to settle to a height of 45 cm. The final volume of the soil was approximately 500 cm^3, giving estimated density of 1.2 g/cm^3 and pore space of 0.50 based on soil classification. For the 60- and 240-min doses, I interrupted the ozone gas flow every 30 min, removed the soil from the chamber, mixed the soil thoroughly, and returned the soil to the chamber; this method prevented uneven treatment from gas-channeling.[84] A 600-g batch of one of the crude-oil contaminated soils (*TSC-ANS*, *TSC-ARAB*, or *TSC-SJV*) was ozonated at one of three ozone-doses (5 g, 10 g, and 40 g), which corresponded to treatment times of 30, 60, and 240 min at 5 L/min flow rate. A portion of each of the *TSC* soils were reserved as the no-ozone control.

The ozonation apparatus is shown in Figure 3.1. Briefly, O_3 was generated with an Ozonia (Trevose, PA) Triogen LAB2B laboratory ozone generator. The feed gas was ultra-high purity (UHP) oxygen delivered at 5 L/min via a dual-stage pressure regulator. At the maximum power setting and at 5 L/min feed-gas flow rate, the production concentration was 17,000 ppmv O_3, giving a mass output of approximately 10 g O_3/h. The O_3-bearing gas (1.70% O_3, 98.30% O_2 by volume) was directed through a 500-mL gas-washing bottle to add humidity and then connected to the antechamber of the reaction vessel via the ¼" threaded glass inlet. A 10-min stabilization period was allowed for the ozone generator before it was connected to the apparatus. After this, the influent ozone was connected to the washing-bottle, which was connected into the antechamber of the reaction vessel. The O_3 gas advected through the course frit diffusion plate in up-flow mode into the chamber containing the soil. Effluent gas was released out of the top of the chamber by the other ¼" hose connection and directed into desiccation vessel to remove water vapor. The gas leaving the desiccation chamber was directed into a Model 465M Ozone Monitor (Teledyne Advanced Pollution Instrumentation, San Diego, CA). The concentration of O_3 in the effluent was measured every 5 minutes during treatment.

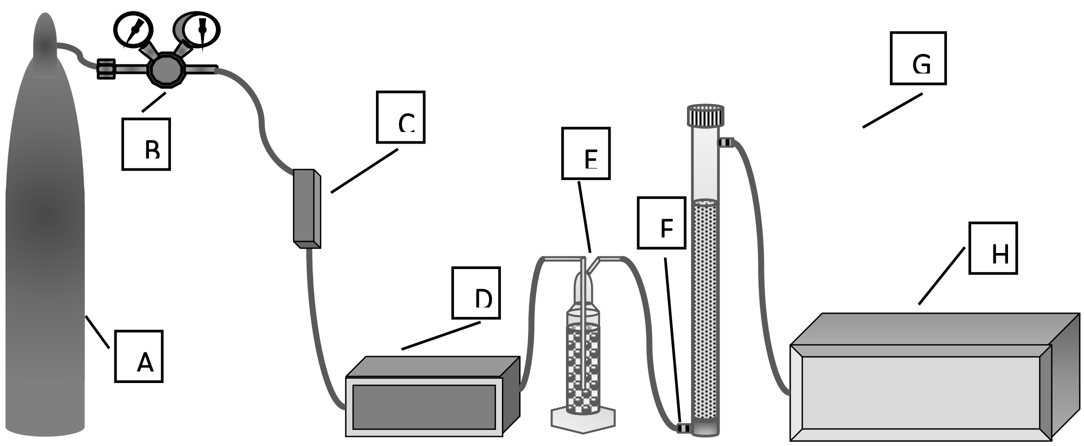

Figure 3.1. Schematic of the experimental set up for soil ozonation directed gas as follows: (A) ultra-high purity (UHP) compressed tank provided O_2 to a (B) dual stage pressure regulator, then to a (C) flowmeter, (D) Ozonia Triogen LAB2B laboratory O_3 generator for low and medium loading experiments, or Ozonia Model CFS-1 2G O_3 generator for high loading experiments, (E) gas-washing bottle containing 500mL of 18MΩ water for humidification, the (F) ¼"-influent connection to reaction vessel antechamber, the (G) ¼"-effluent connection, and (H) Model 465M Ozone Monitor.

3.2.7 Extraction and Quantitation for TPH

Extraction and quantitation of TPH closely followed the methods of Chen et al.[83] Triplicate independent measurements of 2-g soil samples were performed. Each independent measurement was placed in a 40-mL VOA glass vial (Scientific Specialty Services, Hanover, MD), vigorously mixed with 12 g of sodium sulfate, and then transferred to a clean cellulose extraction thimble (Advantec, Ottawa, IL) supported in a 54 mm x 130 mm glass extraction beaker (Gerhardt, Königswinter, Germany). To the glass extraction beaker, I added 130 mL of reagent-grade dichloromethane in a chemical fume hood. The beaker was placed in a Gerhardt automated Soxhlet extraction mechanism (Soxhlet Basic Unit 2-place; Gerhardt, Königswinter, Germany) for 2 cycles. The final extract (<30 mL) was concentrated under a stream of ultra-high purity (UHP) N_2 gas to <2 mL and transferred to a Target® 2-mL clear glass GC vial. The volume was then brought back up to exactly 2 mL using clean DCM. The 2-mL extract was measured for TPH by Gas Chromatography-Flame Ionization Detection (GC-FID) according to the methods established by the Method for the Determination of Extractable Petroleum Hydrocarbons (EPH) as established by the Massachusetts Department of Environmental Protection (referred to as the MA EPH Method).[174]

The resulting GC-FID chromatogram demonstrated the classic unresolved complex matrix (UCM) containing aliphatic and aromatic hydrocarbons in approximately the range C9-C40. The instrument's output (area) was converted to concentration using a calibration factor (CF) specific for each compound. For the hydrocarbons, CF differed slightly with carbon content, differences of 5-10% across the carbon range. I chose 15 representative hydrocarbon carbons from C9-C40 to determine the CF for any given carbon range using a standard mix (System Performance Standard of n-alkanes (50 μg/mL) in Hexane, provided by AccuStandard® (New Haven, CT)). The areas of the 15 individual segments (C9, C10-C12, C13-C14, C15-C16, C17-C18, C19-C20, C21-C22, C23-C24, C25-C26, C27-C28, C29-C30, C31-C32, C33-C34, C35-C40) was converted into a raw concentration using the CF of the respective aliphatic hydrocarbon for each subgroup. The relationship of the calibration factor, response area, and concentration of a compound is:

$$Raw\ Concentration_{\ Carbon\ Subgroup}\left(\frac{\mu g}{mL}\right)=$$

$$\frac{Area\ Under\ the\ Curve_{\ Carbon\ Subgroup}(dimensionless)}{Calibration\ Factor_{Representative\ Hydrocarbon}\left(\frac{\mu g}{mL}\right)^{-1}} \qquad \text{Equation 3.2}$$

The raw concentration was converted to a final concentration for each section using the soil moisture content, sample soil mass (g), and final DCM volume (mL). The calibration procedure allowed me to customize the computed carbon range from C_a to C_b:

$$Total\ Petoleum\ Hydrocarbon_{C_a-C_b}\ \left(\frac{\mu g}{g}\ or\ ppm\right)=$$

$$\sum_{C_a}^{C_b}\frac{\left[Raw\ Concentration_{C_a-C_b}\left(\frac{\mu g}{mL}\right)\times Final\ Volume\ DCM(mL)\right]}{[Soil\ mass\ (g)-(Soil\ Mass(g)\times Moisture\ Fraction)]} \qquad \text{Equation 3.3}$$

TPH is reported as the average mass (g) of TPH extractable carbon per mass of dry soil (kg), or $g/kg_{dry\ soil}$. For total TPH, the carbon range is C9-C40.

3.2.8 Extraction and Quantitation for DOC

Extraction and quantitation of dissolved organic carbon (DOC) followed the methods of Chen et al.[83] Triplicate independent measurements of 2-g soil samples were performed. Each 2-g soil sample was retrieved from a batch of well-mixed control or ozonated soil and placed in a 15-mL centrifuge tube containing exactly 10 mL of 0.5 M K_2SO_4 aqueous solution. The soil-K_2SO_4 slurry was vortexed for 45 min at 2000 rpm and centrifuged for 5 min at 10,000 rpm. I withdraw supernatant and filtered exactly 2 mL through a 25-mm acrylic syringe filter with a 0.2-µM pore-size cellulose acetate membrane (VWR™, Radnor, PA) into a 40-mL glass VOA vial (Scientific Specialty Services, Hanover, MD) containing exactly 28 mL of water acidified with H_2SO_4 to pH 2-3. The final volume of the analyte was 30 mL. The diluted and acidified extract was analyzed for DOC using a Shimadzu TOC analyzer (Shimadzu, Kyoto, Japan). The raw DOC concentration was adjusted for blanks, total sample volume, extract fraction, and soil dry mass of soil as shown in Equation 3.4. Soil DOC is reported as the average mass (g) of water-soluble carbon (C) per mass of dry soil (kg), or $g/kg_{dry\ soil}$.

$$Dissolved\ Organic\ Carbon\ \left(\frac{mg}{g}\right) = \frac{\left[Raw\ DOC\left(\frac{mg}{L}\right) - Blank_{Average}\left(\frac{mg}{L}\right)\right] \times 0.030L\ analyte}{\frac{1}{5}supernatant \times Dry\ Soil\ Mass\ (g)} \qquad \text{Equation 3.4}$$

For comparisons of TPH reduction and DOC production, g TPH was converted to g C by multiplying by 85% (according to the mass percentage of carbon in petroleum hydrocarbons). [8]

3.3 Results and Discussion

3.3.1 Test Soil (TS) Classification

The particle-size distribution of the sieved soil (Appendix A) revealed that the TS was primarily sand (71.2%) and silt/clay (28.6%). Data from the particle size distribution, along with LL and PL data (Appendix A), were used to classify the TS as a silty-clayey sand (SC-SM), or a "course-grained soil with fines according to Unified Soil Classification System" (Appendix A)[175]

3.3.2 ICP-MS for Total Metals

Total metals analysis by ICP-MS showed Table 3.1. Values for a typical topsoil are shown in parentheses.

Table 3.1 Metal elements in a standard soil (San Joaquin), test soil (TS)

Metal (Typical Quantity)	*Test Soil Content (ppm)*
Chromium (100 PPM)	17.2
Manganese (600 PPM)	251.0
Iron (38000 PPM)	13138.4
Nickel (50 PPM)	11.0
Copper (30 PPM)	16.5
Zinc (50 PPM)	33.4

3.3.3 Crude Oil Analyses

The TPH profiles across the carbon range of the raw crude oils are shown in Figure 3.2. The total TPH values for ANS, ARAB, and SJV oils were 510,000 ppm, 440,000 ppm, 520,000 ppm, respectively. ANS and ARAB were comparatively enriched in the C12 to C26 carbon range. On the other hand, the SJV's carbon range was more uniform, with closer agreement between the carbons from C12 to C36, although the lighter end was slightly higher.

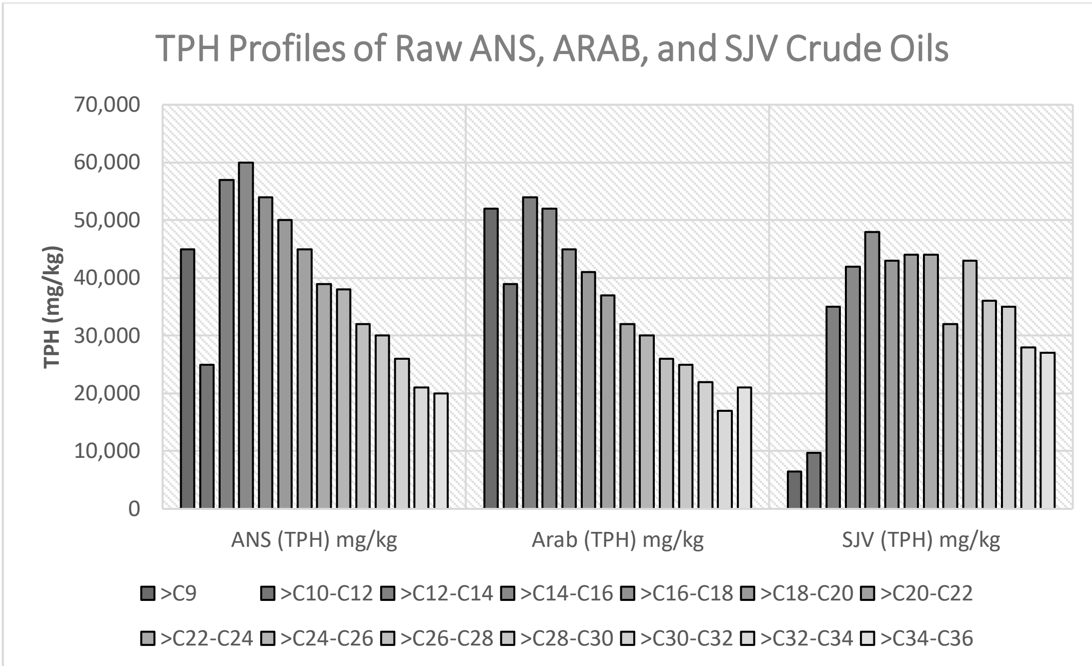

Figure 3.2 TPH (C8-C38) profiles of raw crude oils ANS, ARAB, and SJV before any treatment.

The analyses included gasoline range organics (GRO, C5-C12), diesel range organics (DRO, C12-C22), and oil-range organics (ORO, C22-C40). Those results are shown in Figure 3.3. Although the GRO range was considerably different for SJV, the weathering process likely volatilized the lighter end, and the oil compositions among ANS, ARAB, and SJV were similar in the testing phase. Finally, the analyses distinguished between aliphatic and aromatic hydrocarbons from C10 to C25. Those results, in Figure 3.4, show general agreement of those proportions among the three crude oils.

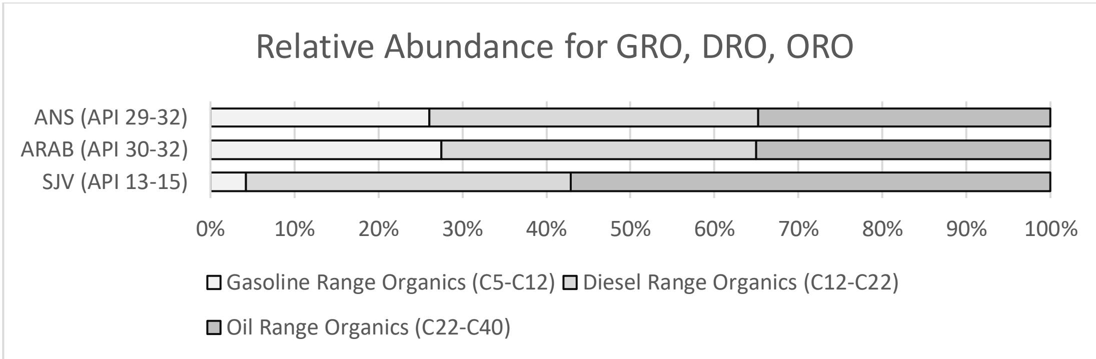

Figure 3.3. Relative abundance of GRO (C5-C12), DRO (C12-C22), and ORO (C22-C40) for crude oils ANS (API gravity 29-32), ARAB (API gravity 30-32), and SJV (API gravity 13-15).

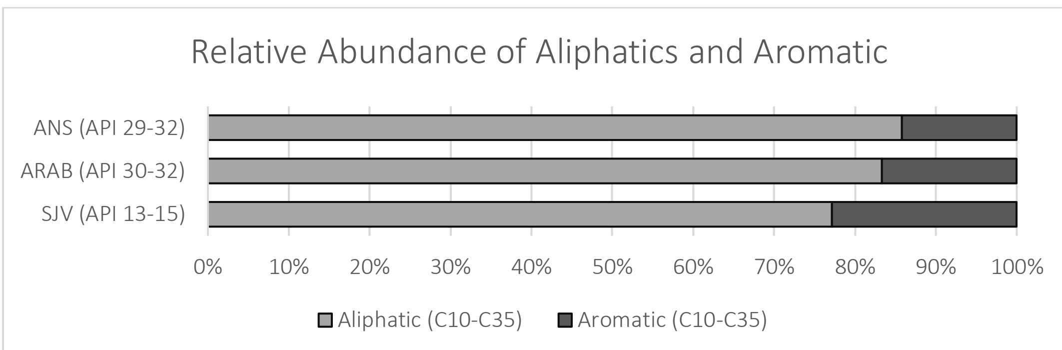

Figure 3.4. Relative abundances of aliphatic and aromatic hydrocarbons (C10-C35) for crude oils ANS (API gravity 29-32), ARAB (API gravity 30-32), and SJV (API gravity 13-15).

After addition to soil (10% w/w) and artificial weathering, petroleum hydrocarbons C6-C36 were extracted and measured as mg TPH per kg dry soil. These concentrations were 33,400±2,440 ppm (7% CV), 45,400±2,280 ppm (5% CV), and 38,100±1,990 ppm (CV 5%) for ANS, ARAB, and SJV contaminated soil, respectively. The results in Figure 3.5 indicate that, as expected, the C9 hydrocarbons (and presumably lighter hydrocarbons) were volatilized. The C10-C12 range also was reduced substantially for TSC-ARAB and TSC-SJV soils. TSC-ANS soil had a higher relative decrease of C12-C26 hydrocarbons compared to TSC-ARAB and TSC-SJV. The latter soil was relatively unchanged for carbons >C12. For comparisons of raw and weathered crude oil normalized to total TPH see Figure D, APPENDIX .

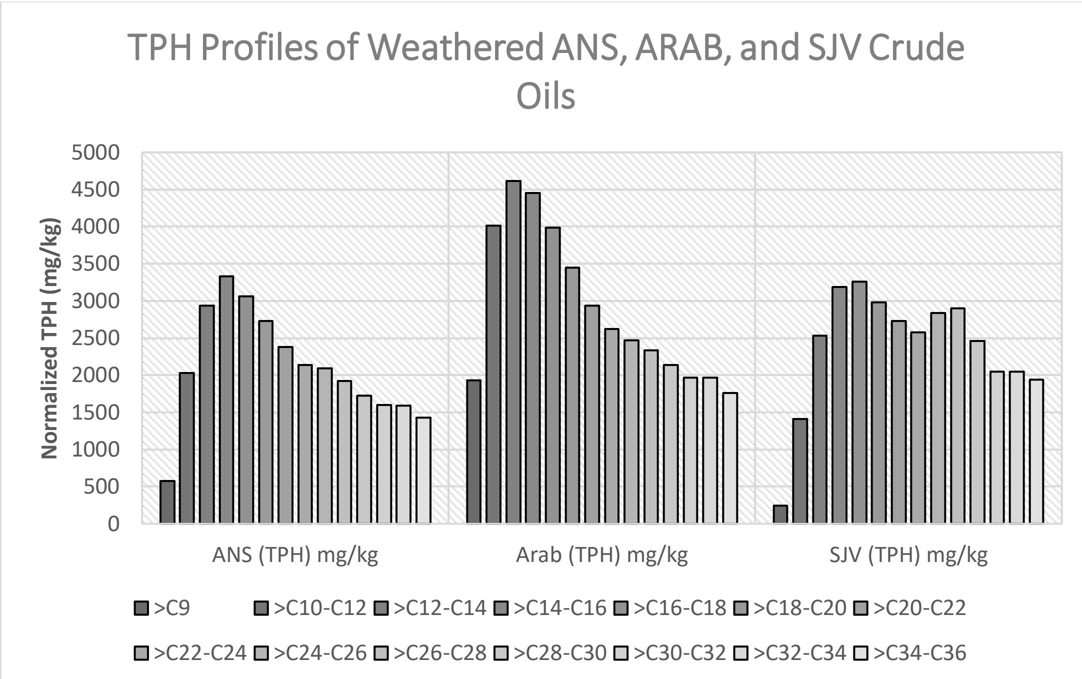

Figure 3.5 TPH (C9-C36) profiles of weathered crude oils ANS, ARAB, and SJV before ozonation, but after addition to soil

3.3.4 Effluent O_3

Effluent O_3 was measured every five minutes for each of three contaminated soils—TSC-ANS, TSC-ARAB, TSC-SJV—at each of the three ozone doses (5 g, 10 g, and 40 g). No O_3 was detected (<0.1%) in the effluent in the first 30 minutes for each of the three contaminated soils. From 0 to 60 minutes, TSC-ANS and -ARAB still showed negligible O_3 breakthrough, while TSC-SJV showed a total discharge of 1-2% of applied

O_3. When O_3 application was extended to 240 minutes (i.e., a 40-g dose), the concentration of O_3 in the effluent continued to rise for TCS-SJV and became detectable for TSC-ANS and -ARAB. The results for this high dose are shown in Figure 3.6. Each line represents an average of the triplicate experiments for each crude. Dips in effluent O_3 occurred at 30-min intervals, when treatment was paused to mix soil. Integrated over time, the losses of O_3 in the effluent account for <1% for TSC-ARAB and TSC-ANS. The losses for TSC-SJV, on the other hand, amounted to a loss of 7% of the total dose O_3 administered. In other words, at the highest dose for SJV contaminated soil, 3 g of O_3 were lost in the effluent for a total absorbed dose of 37 g O_3. A summary of doses and discharges in the effluent are shown in Table 3.2.

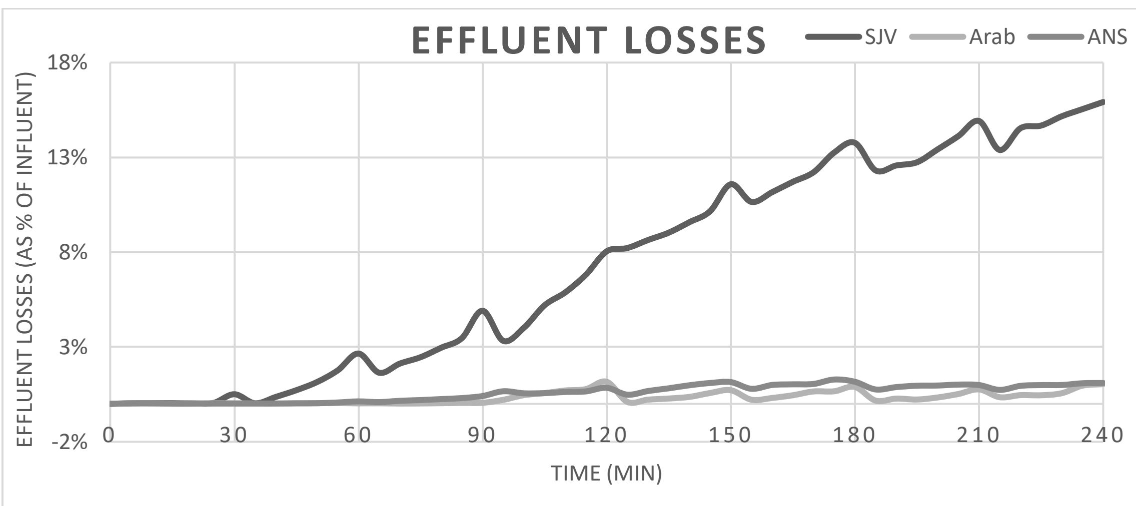

Figure 3.6. Effluent losses of O_3 over time for the 240-min (40-g dose) group. Lines represent the average of triplicate experiments.

Table 3.2. Summary of ozone losses as effluent over time. The most meaningful loss of ozone gas as effluent occurred in the during the 240min ozonation of SJV contaminated soil. Values represent the average of triplicate experiments.

Dose (min)	*Ozone Dose (g)*	*ANS*	*Arab*	*SJV*
30	5	n/a	n/a	n/a
60	10	n/a	n/a	<1%
240	40	<1%	<1%	7.30%

3.3.5 Quantitation of TPH Removal (C9-C36)

The TPH levels of untreated soil (control) and soils treated at 5 g, 10 g, and 40 g O_3 for ANS, Arab, and SJV contaminated soils are summarized in Figure 3.7.

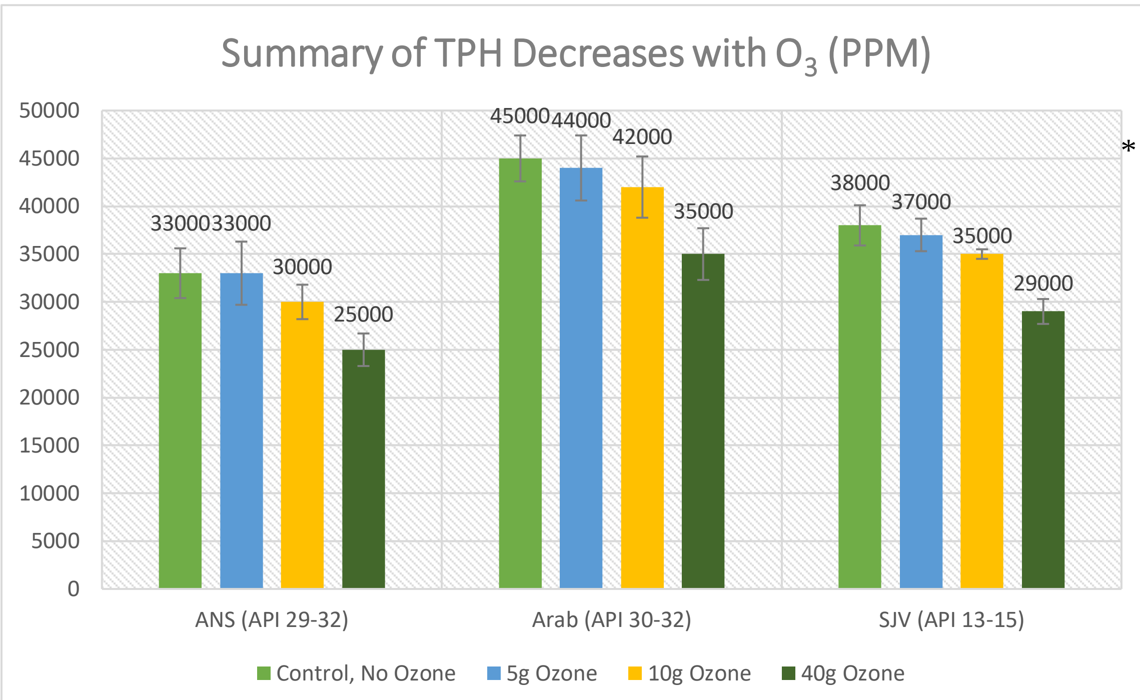

Figure 3.7 Summary TPH removal (C9-C36) for ANS, Arab, and SJV crude oil: control (light green), 5 g O_3 (light blue), 10 g O_3 (yellow), and 40 g O_3 (dark green). *Soil contaminated with SJV at the highest dose level absorbed only 37g of O_3, with 3 g O_3 lost in the effluent.

The measurable TPH from C9-C36 is shown in Figure 3.8 for (a) TSC-ANS, (b) TSC-ARAB, and (c) TSC-SJV. TSC-ARAB tended to have even removals across the carbon range, but TSC-ANS and TSC-SJV showed a slight tapering at the lighter and heavier ends, with the bulk of treatment happening from C13-C30.

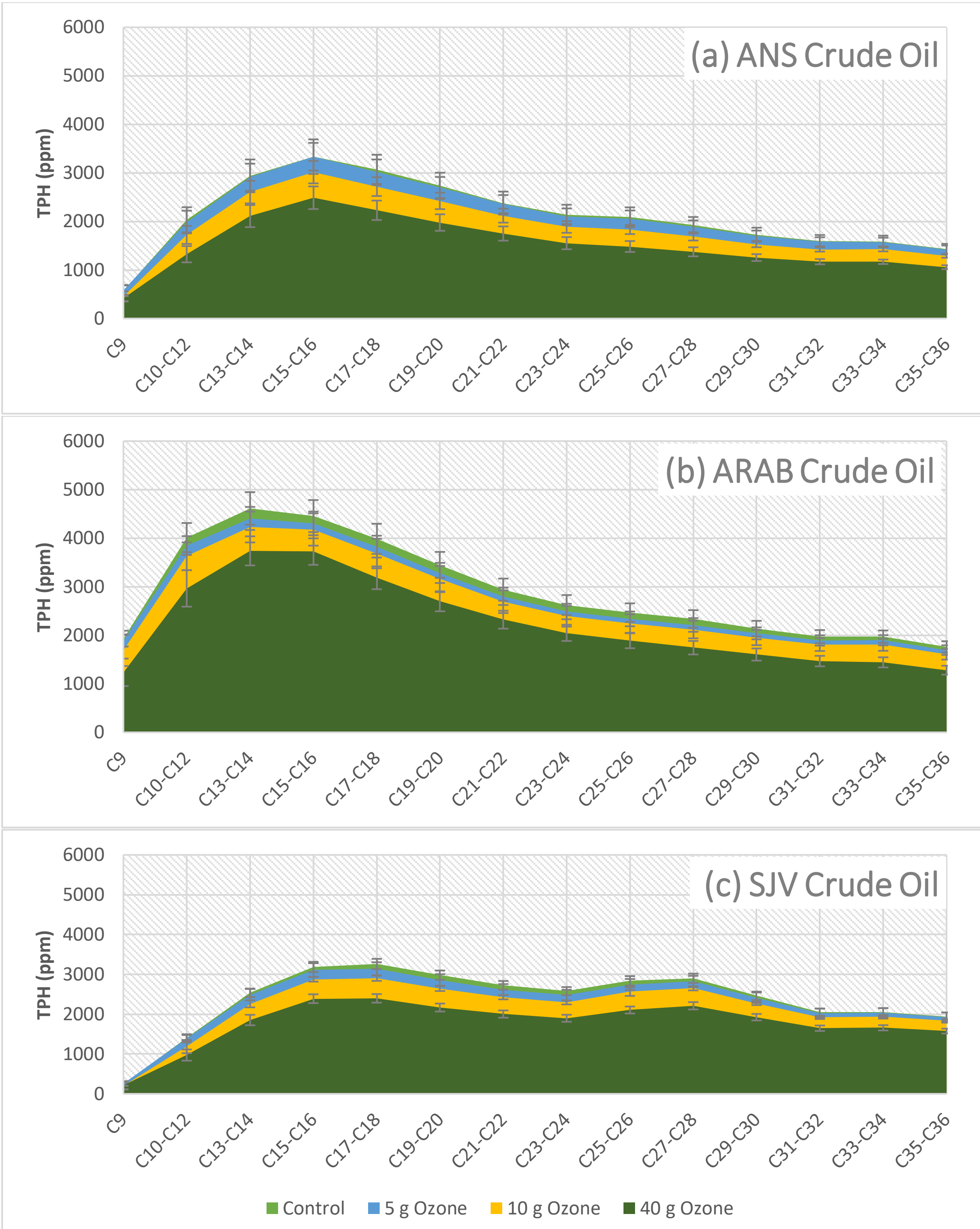

Figure 3.8 (a-c) TPH decreases across the carbon range (C9-C36) for (a) ANS, (b) ARAB, and (c) SJV crude oil: control (light green), 5 g O_3 (light blue), 10 g O_3 (yellow), and 40 g O_3 (dark green).

Table 3.3 summarizes important average values for the 9 experimental conditions (all run in triplicate). The control values for the mass of quantifiable TPH for the 600 g soil experiments are listed in the first row, followed by soil loading (g O_3/kg Soil/h) and TPH loading (g O_3/g Initial TPH/h). TPH removal, TPH removal rate, and O_3 utilized per mass of TPH removed are also listed. O_3 utilization per mass of TPH removed represents the lowest value of g O_3 applied/g TPH removed, which I call the "O_3 utilization ratio."

Table 3.3. Summary of TPH removal results from 600 g of soil using 5 g, 10 g, or 40g O_3 for 3 distinct crude contaminated soils. Data are average of 9 measurements; boldface is peak O_3 utilization.

Group	*Units*	*ANS*	*ARAB*	*SJV*
Soil Loading	g Ozone/g Soil/h	0.017	0.017	0.017
TPH Loading	g Ozone/g TPH/h	0.55	0.41	0.49
Control TPH	g TPH (C9-C40)	18	25	21
5 g Ozone	g TPH removed	0.2 (1%)	1 (4%)	0.5 (2%)
1 0g Ozone		2 (11%)	2 (8%)	2 (9%)
40 g Ozone		5 (27%)	6 (23%)	5 (23%)
5 g Ozone	g TPH removed/h	0.4	2.0	0.9
10 g Ozone		2.0	2.1	1.8
40 g Ozone		1.2	1.4	1.2
5 g Ozone	g Ozone/g TPH removed	25.7	5.0	10.9
10 g Ozone		**4.9**	**4.8**	**5.6**
40 g Ozone		8.3	7.1	7.9*

*The O_3 utilization (g O_3/g TPH removed) for the 40g dose of the SJV group is adjusted for the 7.3% loss of O_3 as effluent.

The masses of measurable TPH (C9-C40) before treatment with O_3 were 18 g, 25 g, and 21 g for ANS-, ARAB-, and SJV-contaminated soils (600-g batch), respectively. O_3 gas was administered at 17 g O_3/kg Soil/h, while loading rate normalized to mass of TPH depended on the differences in initial TPH. Removal rates varied from a minimum of 0.40 g TPH removed/h (TSOC-ANS 5g O_3) to a maximum of 2.1 g TPH removed/h

(TSOC-ANS 10g O_3 and TSOC-ARAB 10g O_3). The O_3 utilization ratio is highlighted in **boldface** in Table 3.3, and the minimum values occurred for the 10 g dose for all three crude oils (4.8 – 5.6 g O_3/g TPH removed), with TCS-ARAB having the lowest ratio of O_3 needed for TPH removed. The largest ratios occurred for the smallest dose (ozonation for 30 minutes), which indicates that the TPH-oxidation process was delayed. The highest O_3 doses (240-minutes of ozonation) also had increased ratios, which suggests that the most readily oxidizable TPH may have been consumed in the first 60 minutes.

3.3.6 Quantitation of DOC

The DOC levels of untreated soil (control) and soils treated at 5 g, 10 g, and 40 g O_3 for ANS-, ARAB-, and SJV-contaminated soils are summarized in Figure 3.9. Table 3.4 summarizes key findings for DOC production (given in g-C) during ozonation. The measurements of DOC before ozonation, noted in the first row, were 0.14 g, 0.09 g, and 0.15 g for ANS-, ARAB-, and SJV-contaminated soils, respectively. The DOC level of background soil only (*TS*, no crude), measured before and after a 4-h ozonation, were below the detection limit. The production rates of DOC varied from a minimum of 0.2 g DOC produced/h to a maximum of 2.0 g DOC produced/h. Like TPH reduction, DOC production rates plateaued. However, the lowest utilization ratio of O_3 consumed per DOC produced (i.e., the most efficient ratio) was with the 5-g O_3 dose, different than the minimum at a 10-g dose for O_3 consumer per TPH removed.

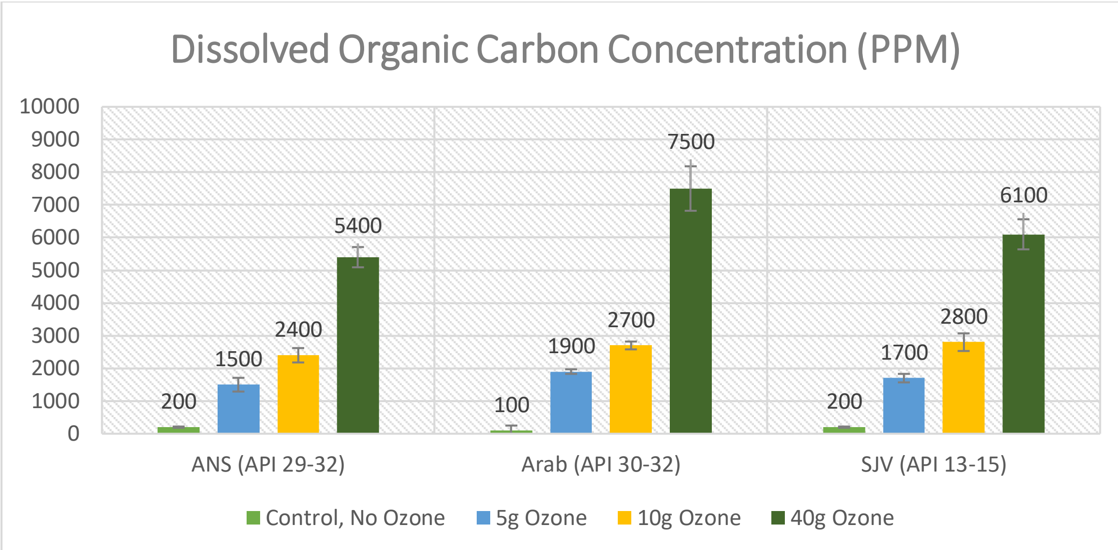

Figure 3.9 The DOC concentration of soils contaminated with either ANS, Arab, and SJV crude before (Control, No O_3) and after treatment with O3 gas at either a 5-g, 10-g, or 40-g dose.

Table 3.4 Summary of DOC production results from 600g of soil using 5 g, 10 g, or 40 g O_3 for 3 distinct crude contaminated soils. Data are average of 9 measurements; boldface is peak O_3 utilization.

	Units	*ANS*	*Arab*	*SJV*
Soil Loading	g Ozone/g Soil/h	0.017	0.017	0.017
Initial DOC	g Initial DOC	0.12	0.08	0.13
5 g Ozone	g DOC Produced (%)	0.8 (640%)	1.0 (1300%)	0.9 (700%)
10 g Ozone		1.3 (1100%)	1.4 (1800%)	1.5 (1100%)
40 g Ozone		2.9 (2300%)	4.1 (5200%)	3.3 (2500%)
5 g Ozone	g DOC Produced/h	1.6	2.0	1.9
10 g Ozone		1.3	1.3	1.3
40 g Ozone		0.2	0.2	0.2
5 g Ozone	g Ozone/g DOC Produced	6.3	5.0	5.4
10 g Ozone		**7.7**	**6.9**	**6.6**
40 g Ozone		13.8	9.9	11.5

3.3.7 Comparison TPH Reduction to DOC Production

Figure 3.10 directly compares the production of DOC (in g C) to the loss TPH (in g C).[y] The ratio of DOC loss to TPH gain (in g DOC/g TPH-C) for ANS, ARAB, and SJV were, respectively: 4.8, 1.2, and 2.4 at the 5-g O_3 dose; 0.7, 0.8, and 1.0 at the 10-g dose; and 0.7, 0.8, and 0.8 at the 40-g dose. At a 5-g O_3 dose, all ratios are > 1 for all three crude oils, reinforcing that a small amount of oxidation was needed to make the partially oxidized TPH soluble.[84] The ratio of DOC gain/TPH loss was < 1 g DOC/g TPH-C at the 10-g and 40-g doses.

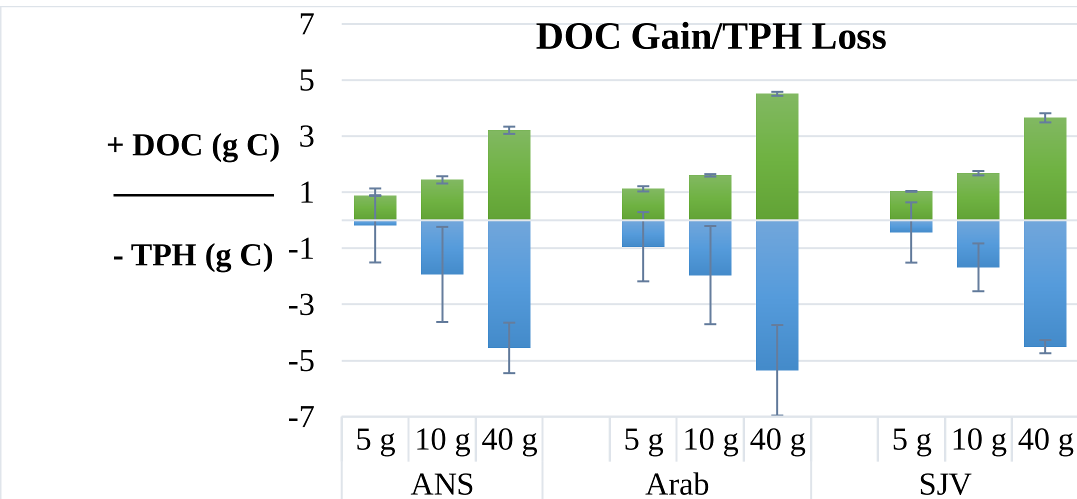

	ANS 5 g	ANS 10 g	ANS 40 g	Arab 5 g	Arab 10 g	Arab 40 g	SJV 5 g	SJV 10 g	SJV 40 g
(+) DOC (g C)	0.9	1.4	3.2	1.1	1.6	4.5	1.0	1.7	3.7
(-) TPH (g C)	-0.2	-1.9	-4.6	-0.9	-2.0	-5.3	-0.4	-1.7	-4.5
Ratio (g DOC Lost/g TPHc Gain)	4.8	0.7	0.7	1.2	0.8	0.8	2.4	1.0	0.8

Figure 3.10 Comparison of the total mass of DOC produced and TPH lost in 600-g batches of soil. TPH has been normalized to it g C for direct comparison to DOC.

[y] I assume that carbon comprises 85% of all TPH measured.[8]

3.3.8 Residual Material for Toxicity Testing

Much of the TPH reductions can be accounted for in the DOC gains. Hence, depending on O_3 dose, between 1% and 27% of the measurable TPH and other organic material was not mineralized, but was transformed into a new organic material. The ozonation of TPH, therefore, leaves two types of residuals: (1) un-oxidized TPH and (2) DOC (the transformed TPH). Figure 3.11 recapitulates the amount of residual (i.e., remaining) material in the soil. The clear trend is a net loss of carbon among all crude oils, suggesting some degree of mineralization. The important result is that soils submitted for toxicity testing will have considerable amounts of carbon from remaining TPH and carbon from DOC production. The toxicity of those combinations will be tested against crude oil alone and background soil for three plant species in Chapter 4.

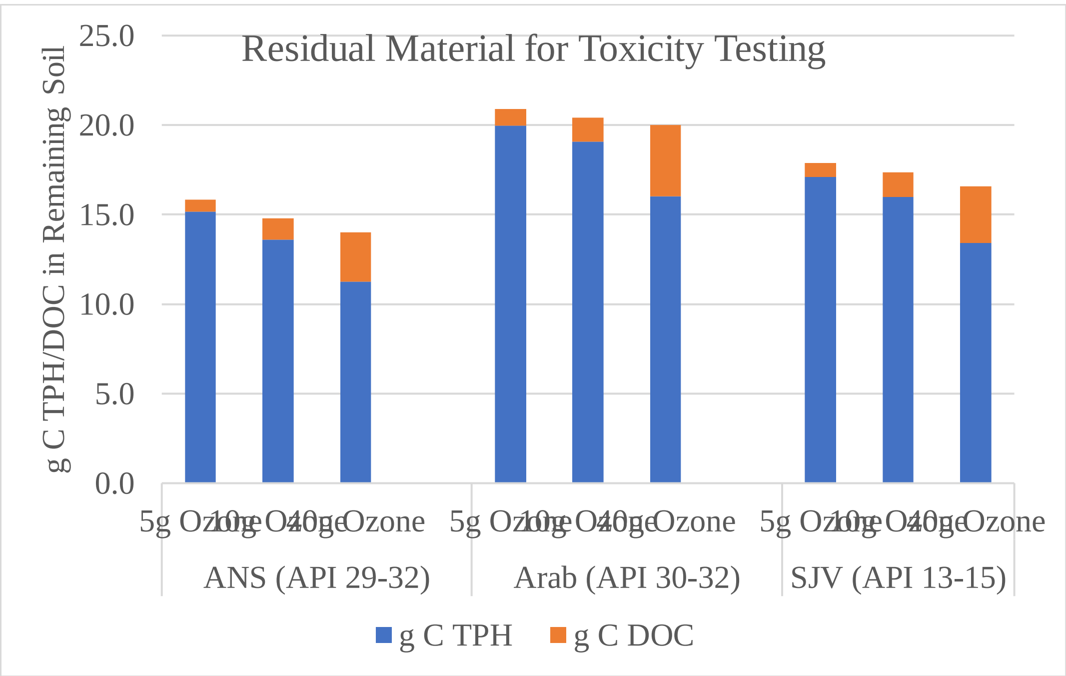

Figure 3.11 The combined concentration of TPH (C9-C40) and DOC in control and ozonated soils. TPH has been normalized to g C for comparison to DOC.

3.3.9 Soil pH, Moisture, and Salinity

The pH of background soil was 7.8 ± 0.25. Treatment with O_3 gas created oxidized residuals, many of which are known to be carboxylic acids.[84,120] Thus, the pH of ozonated soil decreased. Table 3.5 shows the pH of crude oil contaminated soil (TSC) and those treated with O_3 gas at the 5-g, 10-g, and 40pg dose levels (TSOC-5g Ozone, TSCOC-10g Ozone, TSCOC-40g Ozone). The addition of crude oil only (TSC) only slightly lowered pH for all the soils (7.42±0.33). O_3 gas, on the other, hand lowered pH in soils, often significantly. The 5-g dose of O_3 lowered the pH to 7.14±0.15, on average, while the 10-g dose yielded 7.02±0.16. The 40-g dose of O_3 created substantially more acidic conditions, with an average pH of 6.07±0.15. The SJV crude oil appeared somewhat less acidified than either the ANS or the ARAB crude oil.

Table 3.5 Soil pH for crude only contaminated soil (TSC) and crude oil+O3 soils (TSOC) at three different dosages among 3 crude oils.

	SJV	*ANS*	*ARAB*	*Average*	*St dev.*
TSC	7.23	7.15	7.69	7.42	0.33
TSCOC-5g Ozone	7.06	7.02	7.26	7.14	0.15
TSCOC-10g Ozone	6.93	6.94	7.10	7.02	0.16
TSCOC-40g Ozone	6.28	6.15	5.98	6.07	0.15

3.4 Conclusions

This chapter describes the creation and characterization of weathered soils that had been contaminated with three unique crude oil and then dosed with O_3 gas at three levels. The data presented in this chapter do not show great differences in total quantity of oxidized material produced. Furthermore, they do not address whether or not the soils' toxic potentials were affected by the crude oil, the ozone dose, the amount of oxidized material (reported here as DOC), or some combination. I ask in ensuing chapters whether I can detect and quantify the toxicity of oxidized crude oil, whether I can separate that toxicity from that of crude oil alone, whether differences exist for the different crude oils, and whether O_3 dose level change the quantity of oxidized material and the toxic potential of that material. I do this using the techniques of logistic regression in Chapter 4 and Chapter 5.

4 RESEARCH: LETTUCE, GRASS, AND RADISH GERMINATION BY SIMPLE LOGISTIC REGRESSION[z]

4.1 Introduction

Much of the research on weathered petroleum toxicity has followed catastrophic releases, such as the Exxon Valdez or Deepwater Horizon.[39,41,149,165,176] Fish are the most frequent target organisms in these studies because fish populations are key economic and ecological indicators of harm when crude oil is released into a marine environment.[41,142,147,165,177] Abundant evidence indicates that exposures to PAHs and petrogenic mixtures alters normal fish development in multiple mechanisms of toxic action, including severe disruptions in cardiac development and, hence, circulatory function that lead to bradycardia, arrythmia and the interdependent responses of pericardial edema, yolk-sac edema, and mortality.[142,147,149,176,178] Terrestrial examination of crude-oil toxicity is less common, but has focused on the response characteristics of plants like lettuce (*Lactuca sativa*), millet (*Panicum miliaceum*), radish species (*Raphanus*), red clover (*Trifolium pratense*), wheat (*Triticum aestivum*), corn (*Zea mays*), soybean (*Glycine max*), and sunflower (*Helianthus*), as well as animal models like the earthworm (*Eisenia fetidia*).[91,146,151,153,156,179] Lettuce is especially important because it is sensitive to crude oil and is, therefore, used as an indicator species.[91] TPH pollution in the soil has been shown to inhibit seedling emergence, root/shoot biomass, and chlorophyll content. Yields of cereal crops also have been shown to decrease considerably in the presence of crude oil in oil (>0.2 wt%).[79]

[z] This chapter will be combined with the previous chapter into a manuscript for publication.

Oxidation by UV radiation of petrogenic compounds is an important component of natural attenuation of spilled crude oil. Such processes promote oxygenation of the compounds, which can break open otherwise stable ring conformations of saturated and unsaturated ring structures.[64,150,180] As Maki and colleagues have shown, oxidation of biodegraded crude oil by sunlight irradiation decreased the aromatic fraction, with a concomitant increase in asphaltenes and resins, along with an increase in dissolved organic carbon (DOC).[45] The biodegradability of the oil increased with oxygenation. Nevertheless, the chemically transformed water-soluble fraction showed acute toxicity against crustaceans. Similarly, Barron et al. demonstrated photo-enhanced toxicity of weathered Alaska North Slope crude oil (ANS) against the eggs and larvae of Pacific herring (*Clupea pallasi*), as did Incardona *et al.* in a separate study.[48,150]

Attention to the toxicity of oxidized petrogenic compounds also is found in the literature for oil sands process water (OSPW), a type of wastewater produced from the process of hydraulic fracturing (HF), otherwise known as fracking.[181–186] An estimated 3 trillion liters OSPW has resulted from these processes which contain large amounts of salts, mineral particles, metals, radionuclides, and numerous oxidized organic compounds produced in the high-heat/high-pressure operations.[181,182] Particular concerns have been raised about the toxic mixtures of water soluble naphthenic acids (NA) in the process water, thought to be the main toxic factor.[182–185] Analyses by He and colleagues, which separated the organic contaminants from minerals ones, showed that the organic fraction of OSPW significantly increased spinal malformation, pericardial edema, and delayed hatch in exposed zebrafish embryos (*Danio rerio*).[187] The toxicants also altered the expression of a suite of target genes related to biotransformation, oxidative stress, and endocrine-mediation during development.[187] Acids produced from OSPW include alicyclic, aromatic, or naphthenoaromatic species, all of which have been reported from the oxidation of aromatic compounds.[120,185]

O_3 gas has been proposed as an effective tool to oxygenate and sometimes remove residual petrogenic compounds.[84,188] This is particularly true for OSPW, where ozonation (targeted to remove NAs by 90%) has been shown to decrease toxicity of NAs against fish larvae, as noted by He et al.[181,189,190] Nevertheless, most ozonation schemes against high level (>1%) petroleum contamination cannot meet such exhaustive cleanup goals because of practical and chemical limitations.[120,191] The byproducts are most frequently quinones, aldehydes, ketones, alcohols, and, in the presence of excess O_3, carboxylic acids. Thus, in an intact crude oil setting, particularly a terrestrial one where only a moderate level of chemical oxidation by O_3 gas can be achieved, the likelihood of creating byproducts that, though more bioavailable, are also more toxic is high. Therefore, studying the effect of ozonation byproducts on plants and animals in a terrestrial setting is an essential step before ozonation can be recommended as an environmental-remediation tool.

To my knowledge, the effects of ozonated crude oil on plants have not been studied. Moreover, no study has evaluated the effect of three different crude oils simultaneously, nor has any looked at dose effects. Here, I present the result of germination studies of radish (*Raphenus sativus*), grass (*Lagurus ovatus*), and lettuce (*Lactuca sativa*) in 3 crude oils that had been treated at 3 doses of ozone gas that achieved the following final molar ratios[aa]:

- 1.6, 1.2, and 1.4 mol O_3/mol TPH at the low dose (5 g O_3)
- 3.3, 2.4, and 2.8 mol O_3/mol TPH at the medium dose (10 g O_3)
- 13, 9.5, and 11.3 mol O_3/mol TPH at the high dose (40 g O_3)

This study distinguishes whether or not an indicator species can show a dose-response effect to the oxidized residuals of crude oil. I chose radish because of its quick germination and prolific output in good soil conditions, grass as a hardy species, and lettuce because it is an indicator species that shows a statistically sensitive response to petroleum contamination.

4.2 Laboratory Methods

4.2.1 Ozonation of Soils

Chapter 4 describes the methods used to ozonate 600-g batches of soil from 3 distinct crude oils. Briefly, three raw crude oils were obtained from the Chevron Energy Technology Company (ETC): ANS (API gravity 29-32), ARAB (API gravity 30-32), and SJV (API gravity 13-15). Each crude oil was analyzed for gasoline-range (GRO, C5-C12), diesel-range (DRO, C12-C22), and oil-range (ORO, C22-C40) organics, as well as aliphatic and aromatic fractions. A locally sourced topsoil with extremely low organic matter (OM, <2%) content was spiked with each of the three crudes at 10% w/w concentration and attenuated for labile compounds under laboratory conditions. The soils were then ozonated with 5 g, 10 g, and 40 g O_3, with continuous monitoring of effluent

[aa] The differences are based on starting TPH concentrations for ANS, ARAB, and SJV crude oils discussed in Chapter 6.

(unreacted) ozone gas. The control soil and O_3 treated soil were then evaluated for total petroleum hydrocarbon (TPH), dissolved organic carbon (DOC), and pH. The soils were then prepared as described below for toxicity testing. Details of the methods are in Chapter 3.

Each crude oil was used for 5 treatment conditions:

1. untreated Arizona background soil (test soil, TS)
2. soil contaminated with crude oil and synthetically weathered (test soil with crude, TSC)
3. soil contaminated with synthetically weathered crude oil and then treated with 5 g of O_3 gas (test soil with oxidized crude, TSOC-5g)
4. soil contaminated with synthetically weathered crude oil and then treated with 10 g of O_3 gas (test soil with oxidized crude, TSOC-10g)
5. soil contaminated with synthetically weathered crude oil and then treated with 40 g of O_3 gas (test soil with oxidized crude, TSOC-40g)

4.2.2 Water Holding Capacity (WHC)

The water holding capacity (WHC) is the weight percent (w/w) of water that can be stored in a volume of soil. To determine WHC, I saturated 50 g of soil (control, petroleum, and petroleum + ozone) with water and allowed it to drain for one hour. After the excess water had drained from the soil, I measured the weight of the saturated soil to yield "Soil $\text{Mass}_{\text{Saturated}}$" (g). The soil was then dried in an oven (105°C) until constant weight was achieved, and the weight was taken as "Soil Mass_{Dry}" (g). The w/w percent water held by the soil was determined as the difference in saturated weight and the dry weight over saturated weight (multiplied by 100) as follows:

$$WHC = \frac{\text{Soil Mass}_{\text{Saturared}} - \text{Soil Mass}_{\text{Dry}}}{\text{Final Mass}_{\text{Saturated}}} \times 100 \qquad \text{Equation 4.1}$$

All soils were tested for moisture content after ozonation and before the germination studies as described in Section 3.2.5. Depending on moisture content of soils after the ozonation process, between 25 and 100 mL of water was used to bring soils to the 10 w/w (or 50% of total water holding capacity).

4.2.3 pH Adjustment

The pH was measured in 1:2 (w/w) soil/water mixture with a Thermo Scientific Orion 2 Star pH probe (Thermo Fisher Scientific Inc.) and results are described in 3.3.9. Soils in the high-dose group were brought to circumneutral pH with the exceedingly small additions of 50% sodium hydroxide diluted in water (25-50 µL/kg of acidified soil) used to increase hydration. The volumes of NaOH needed (10-50 µL for adjustments of 600-g of soil) did not significantly alter soil conductivity, which remained at 2-4 ds/m.

4.2.4 The Dilution Series, Planted Tray, and Crude-Seed Set

In order to determine the effects of background organic content, test soils were subject to a dilution series using Nature's Care Organic & Natural Potting Mix (Marysville, OH), formulated from 50-60% sphagnum peat moss, processed forest products, coir, perlite, and yucca. The organic matter content was 75.5 ± 2.9% w/w as determined by the loss-on-ignition method (360°C) at University of Connecticut Soil Nutrient Analysis Laboratory (Storrs, CT). It is important to underscore that, with regard to the TSOC group, treatment with O_3 gas preceded dilution with organic background material. This avoided the large O_3 demand from the organic background, which would have obscured the O_3 dose utilization of the weathered crude oil.[192–194]

The basic experimental unit was a 140 × 140 × 22-mm plastic tray (VWR Catalog No. 10770-450) containing 100 g of soil at 70% WHC and planted with 10 seeds, each at a depth of ~2.5-times seed diameter, as recommended by ASTM E1963 − 09.[195] The first planting condition was the full-strength test soil, after which a dilution series was created Like *TS*, *TSC*, and *TSOC*, the potting mix was also moistened to 70% WHC. The dilution series was comprised of 6 trays: The first condition was 0% potting mix (by mass), then 10%, 40%, 80%, 90%, and finally, 100% potting mix (by mass), as shown in Figure 4.1. Because the organic content of the base test soil was 0.5 ± 0.05% w/w, the background organic (*b-ORGANIC*) content was ascribed to the amount added by the potting mix. For the dilution series, *b-ORGANIC* increased with addition of more potting mix, and, thus, germination was expected to increase from left to right in Figure 4.1.

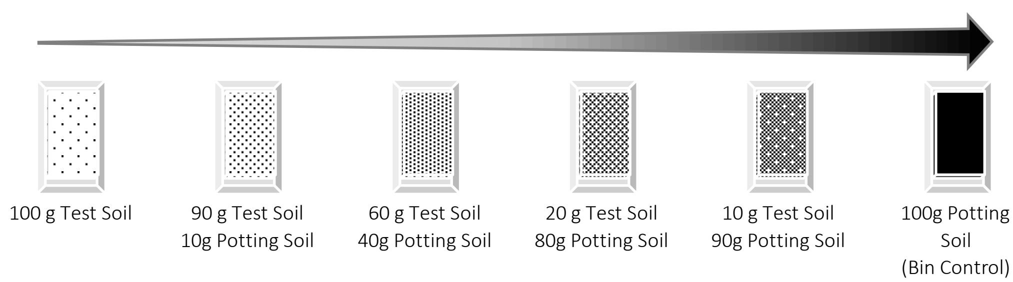

Figure 4.1 Dilution series for a given test condition.

A set of 6 trays in each dilution series were placed together in a larger 28-quart plastic bin. The bottom of the plastic bin was lined with ½-in depth of peat moss moistened to 50% w/w water, and the top of the bin was covered with a transparent plastic film, punctured to allow air exchange. The slow release of moisture from the peat moss and the plastic wrap served to keep ambient growth conditions at ≥80% humidity in accordance with ASTM E1963 − 09.[195] The tray containing 100 g potting mix served as the "bin control" used to determine whether differences in light, temperature, and ambient moisture affected germination between sets of seedlings.

A 6-tray dilution series was created for each of the five experimental categories: TS (control test soil with no crude oil and no ozone), TSC (test soil contaminated with untreated crude oil), and TSOC (test soil contaminated with crude oil and then ozonated). The TSOC group can be further divided into three subgroups based on ozone dose: TSOC-5g, TSOC-10g and TSOC-40g of ozone. Together, the five experimental categories and six trays in each dilution series gave 30 planted trays for each CRUDE OIL—SEED combination, as shown in Figure 4.2. Each CRUDE OIL—SEED set was performed in duplicate, which totaled 60 trays. The trays were placed in a rooftop greenhouse for germination and maintained at 25°C throughout that period. The germination period was set to 14 days, as recommended in ASTM E1963 − 09.[195] Emergent seedlings were counted at 3, 7, 10, and 14 days. After the 14-day period, seedlings were counted and harvested at the base of the hypocotyl, the part of the stem of an embryo plant beneath the stalks of the seed leaves, and directly above the root.

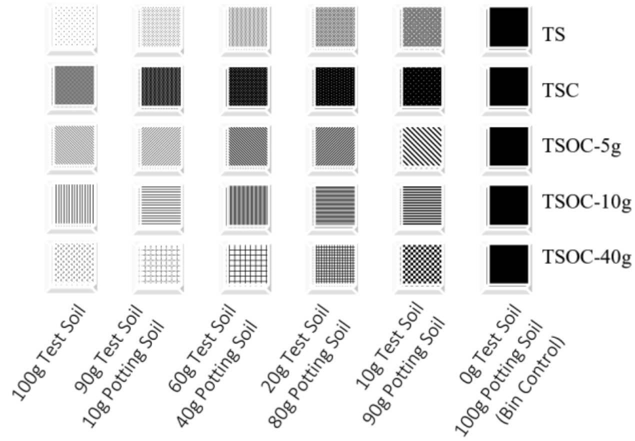

Figure 4.2 Matrix of mixtures of the potting soil and the amounts of each of the test soils.

A complete CRUDE OIL—SEED set was placed in a rooftop greenhouse for germination. Due to limited greenhouse space, one CRUDE OIL—SEED set (60 trays) could be germinated in a given two-week interval. Seeds were germinated between the months of October and February in the following order: ARAB-RADISH, ARAB-LETTUCE, ARAB-GRASS, ANS-RADISH, ANS-LETTUCE, ANS-GRASS, SJV-RADISH, SJV-LETTUCE, SJV-GRASS. In total, this study evaluated 540 trays and counted 5400 seedlings (6 dilutions × 5 groups × 2 duplicates × 3 seeds × 3 crudes x10 seeds). Figure 4.3provides a schematic representation of the test categories and the trays.

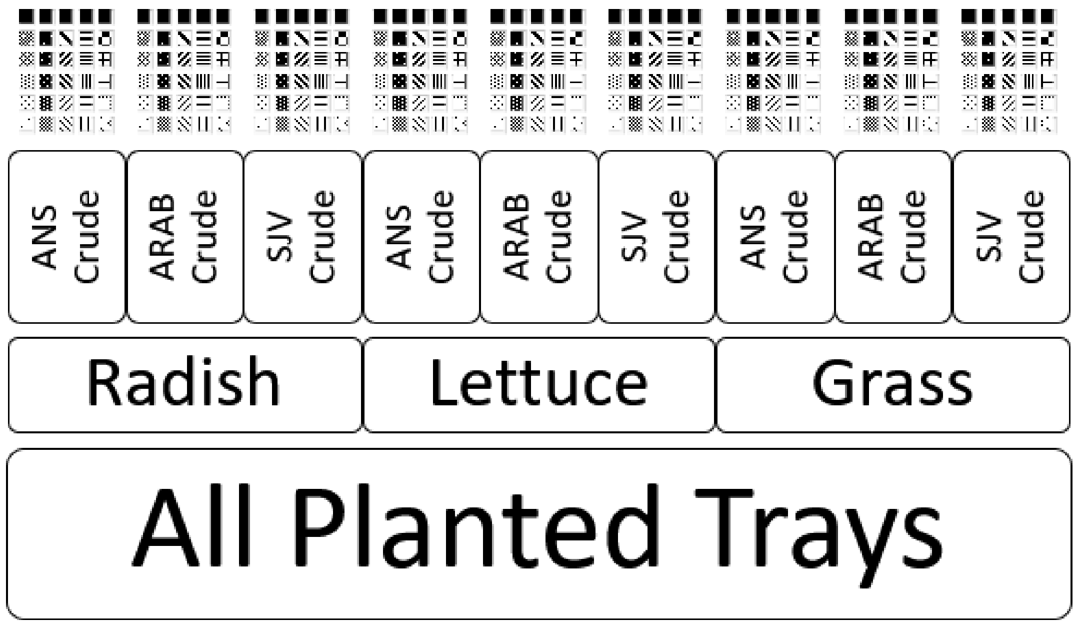

Figure 4.3 Schematic of the study design; the 270 trays above were performed in duplicate for 540 trays total, and 5400 seeds planted.

4.3 Results and Discussion

4.3.1 Water Holding Capacity (WHC)

The 100% WHC values for each of the types of soil are shown in the top row of Table 4.1 as w/w of dry soil. Crude oil contamination increased the total WHC of soils from 17% w/w to approximately 20% w/ for all crude oils. While some test protocols suggest the use of >80% WHC (i.e., 16% w/w soil) for seed planting, the nearly 30% silt/clay content of ASM soils changes soil plasticity at that WHC. Saturation tests showed that soil retained an arable, loamy texture at approximately 70% of the total WHC for all soils (contaminated and clean). This point was 12% w/w moisture for the clean background soil and 14% w/w moisture for crude contaminated soils and. Soils treated with crude oil and ozone gas were kept at the at 14% w/w, the same as the crude-oil-only group.

Table 4.1 Water holding capacity measurements for soils under study.

Soil Type	*Background*	*ANS*	*Arab*	*SJV*
100% WHC (w/w)	**17%**	**20%**	**20%**	**21%**
Ozonation WHC (w/w)	n/a	10%	10%	10%
Ozonation WHC (as % of Total WHC)	n/a	50%	50%	50%
Planting WHC (w/w)	12%	14%	13%	14%
Planting WHC (as % of Total WHC)	70%	70%	68%	68%

4.3.2 Evaluation of the Bin Control for Climate Conditions

The temperature of the greenhouse was maintained by an external system at 25°C throughout that period. The climate and lower latitude of Arizona meant that sunlight was consistent and strong—daylight hours in that period ranged from 10-12 hours (10 h 35 min on average, +/- 32 min). Examination of the 100% potting soil group for each seed (i.e., bin controls) between October and February did not show significant germination differences, demonstrating that the climate conditions were equivalent among germination sequences.

4.3.3 Effects of Treatment Type on Germination

Table C.1 in Appendix C summarizes the statistical differences among treatment groups (TS, TSC, and TSOC) for all crude oils grouped together then evaluated by seed type. Tables C.2-C.4 Appendix C summarize the statistical differences between (i.e., raw) crude oil (TSC) and ozonated crude oil (TSOC) by crude oil type and seed type. Finally, Appendix C, Table C.5 shows differences between dose levels (TSOC-5 g, TSOC-10 g, and TSOC-40 g) for all ozonated soils differentiated by crude oil type and seed type for ozonated soils.

The ”treatment” analysis compares the three broadest categories studies for each individual seed (n = 1800 seeds): TS (n = 360 seeds), TSC (n = 360 seeds), and TSOC (n = 1080 seeds). In this analysis, the ozonation levels (5 g, 10 g, and 40 g) were combined as a single category. Figure 4.4a shows that “treatment” was a predictor of radish germination. Radish in control soil (TS) was 1.6 times more likely to germinate than in soil with crude oil (TSC) ($p = 0.01$). When radish was germinated in the presence of ozonated crude oil (TSOC), the decrease is germination was statistically significant compared to TS ($p = 0.00$) and TSC ($p = 0.00$). The odds of radish germination in the presence of untreated crude oil were nearly 3 times the odds when the same crude was ozonated. The odds of germination in clean background soil were nearly 5 times higher than the odds of germination in the presence of ozonated crude oil.

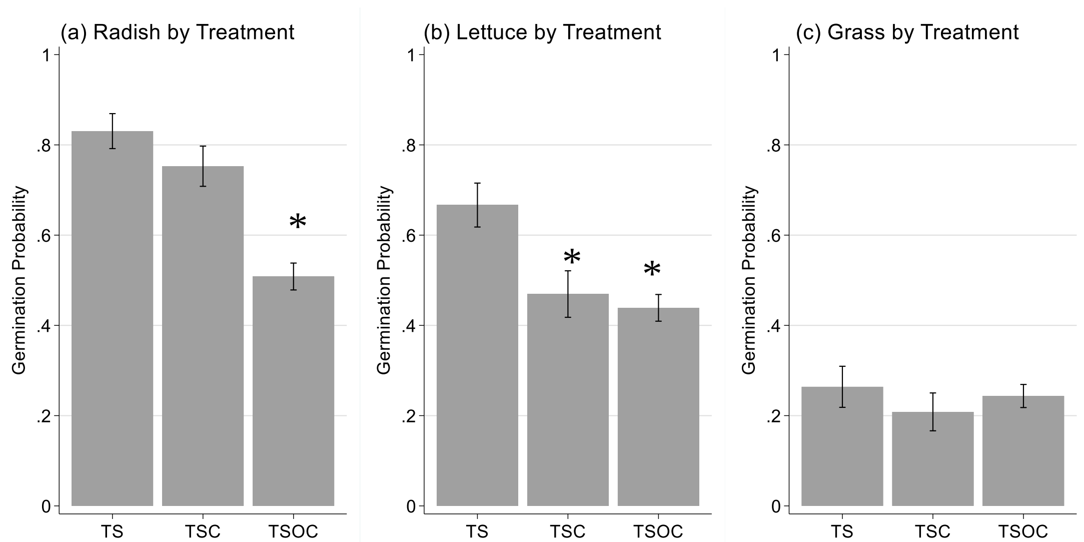

Figure 4.4 Germination of proportions between treatment groups for Radish, Lettuce, and Grass. Statistical differences from TS are noted with an asterisk (*) at p=0.05.

When comparing the treatment groups in lettuce (Figure 4.4b), the presence of untreated crude oil decreased the probability of lettuce germination by approximately 20% ($p = 0.000$). The level did not change when crude oil was ozonated, with TSOC showing a slightly lower, though not statistically different, germination rate than TSC. The odds for lettuce germination in uncontaminated TS was 2.3 times the odds with crude-oil-contaminated soil (p = 0.00, not shown in table) and 2.6 times the odds in soil with oxidized crude (p = 0.00). For grass, Figure 4.4c, the differences between the treatment groups were not statistically significant, although germination was low in all cases.

Radish and lettuce showed statistically significant sensitivity to the presence of crude oil in soil. In both cases, ozonation of petroleum did not attenuate the effects of the crude oil, and, in the case of radish, ozonation decreased germination probability by a significant level. These results show that transforming crude oil into an oxidized intermediate with no additional treatment (e.g., biodegradation) did not attenuate in the toxicity of crude in the short-term, but in fact further decreased germination probability for radish.

4.3.4 Effects of Crude Oil Type on Germination (Both Untreated Crude and Ozonated Crude)

Figure 4.5 shows germination for TS compared to the set of untreated crude oils TSC-ANS, TSC-ARAB, and TSC-SJV, as well as the set of oxidized crudes TSOC-ANS, TSOC-ARAB, and TSOC-SJV for Radish. Although the combined set of TSC germination showed a significant decline as compared to TS, the shift was largely driven by the decrease in radish germination in TSC-SJV (heavy) crude. Taken individually, the TSC-ANS and TSC-ARAB crudes did not show statistically significant differences from TS soil, and, in fact, TSC-ARAB had a slight upward trend. The oxidized counterparts, however, showed statistically significant differences from TS (83%), germinating at 54%, 54%, and 45% for TSOC-ANS, TSOC-ARAB, and TSOC-SJV, respectively.

Each oxidized crude oil also was statistically different from its untreated counterpart for radish, as shown in

Figure 4.6. The ORs of TSC/TSOC were 3.1, 4.6, and 2.1 for pairs of ANS, ARAB, and SJV analyses, respectively. The relative drop in germination from TSC to TSOC were 24%, 30%, and 18% for ANS, ARAB, and SJV crude, respectively. It is also worth noting that TSOC-ANS and TSOC-ARAB also were statistically more likely to germinate than TSOC-SJV (OR = 1.4 and p = 0.026 for both). These results indicate that crude identity made a difference in reaction to the oxidized crude. The general trends, however, remained similar. Radish planted in crude-oil-contaminated soil had less germination when the crude-oil- was ozonated.

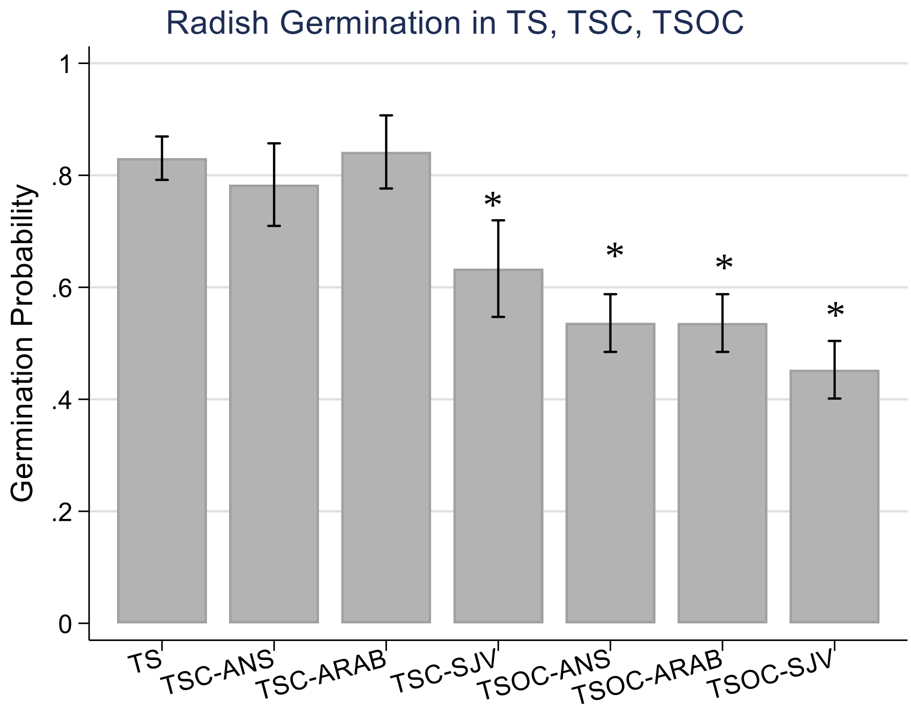

Figure 4.5 Effects of crude oil type on Radish Germination. Statistical differences from TS are noted with an asterisk (*) at p = 0.05.

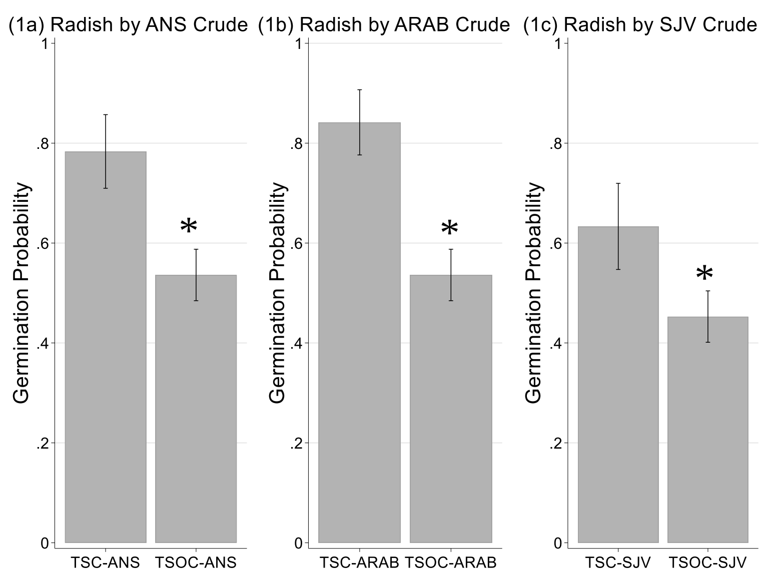

Figure 4.6 Crude/Oxidized Crude comparisons for Radish germination. Statistically significant ORs (TSC/TSOC) noted with an asterisk (*) at p = 0.05.

Analysis according to crude oil did not reveal important differences between untreated and ozonated crude oils for lettuce, as shown in

Figure 4.7 and Figure 4.8, and summarized Table G.2 in Appendix C.

Figure 4.7 shows TS compared to the set of untreated crudes TSC-ANS, TSC-ARAB, and TSC-SJV, as well as the set of oxidized crudes TSOC-ANS, TSOC-ARAB, and TSOC-SJV for lettuce. All crude conditions, whether untreated or oxidized, showed a statistically significant decrease in germination, compared to TS. Like radish, lettuce germination appeared to be lower in the heaviest TCS-SJV, but not a difference of significance as compared to either TCS-ANS or TCS-ARAB ($p = 0.09$ and $p = 0.24$, respectively). Oxidized SJV (TSOC-SJV), on the other hand, was statistically worse than either TSOC-ANS or TSOC-ARAB ($p = 0.01$ and $p = 0.00$, respectively). Figure 4.8 (a-c) shows the comparison between the untreated and oxidized counterparts for each crude. No pair shows statistically significant differences. In other words, the presence of any of the three crude oils decreased lettuce germination, but ozonation did not attenuate the decrease in germination for any crude oil.

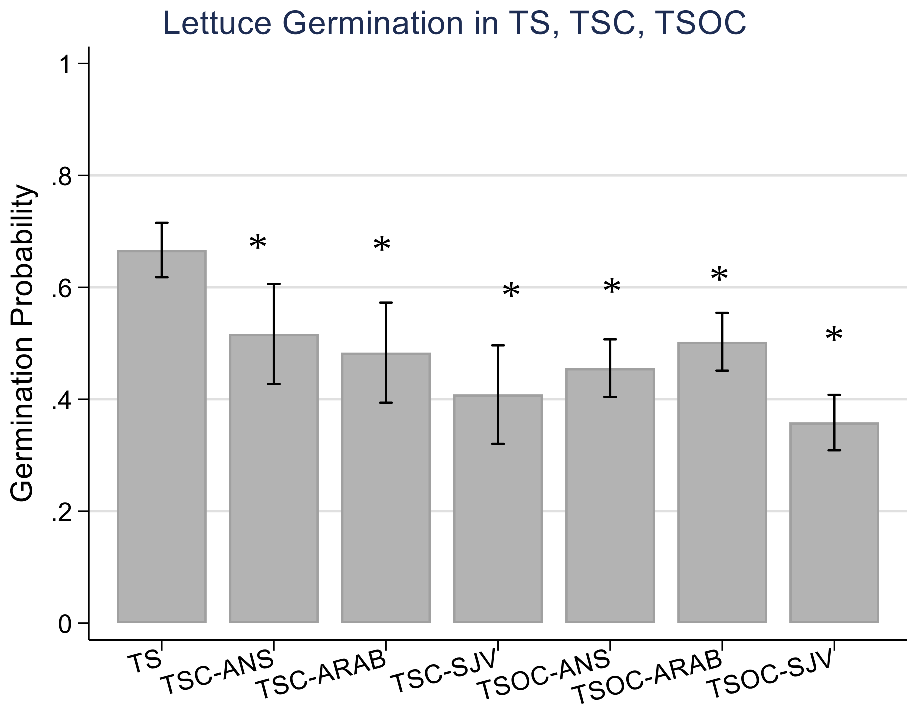

Figure 4.7 Effects of crude oil type on Lettuce Germination. Statistical differences from TS are noted with an asterisk (*) at p = 0.05.

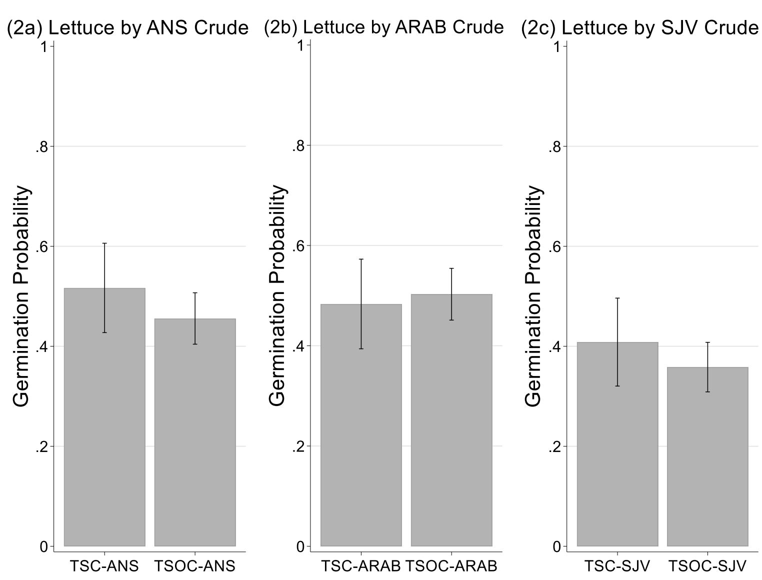

Figure 4.8 Crude/Oxidized Crude comparisons for Lettuce germination. No OR (TSC/TSOC) reaches statistical significance.

Analysis by crude oil reveals that grass germination was worse in TSC-ANS and TSOC-ANS, compared to background TS, as shown in Figure 4.9 and Table G.3 in Appendix C. No other crude-oil condition showed a statistical difference from TS. Figure 4.10 (a-c) shows the comparison between the untreated and oxidized counterparts for each crude oil. The only pair in which a difference existed was ANS (OR = 0.44, p = 0.01), and this was the only instance in which oxidation statistically improved germination for a seed under study. Grass was less than half as likely to germinate in ANS (TSC-ANS) contaminated soil than when some of that crude was oxidized (TSOC-ANS).

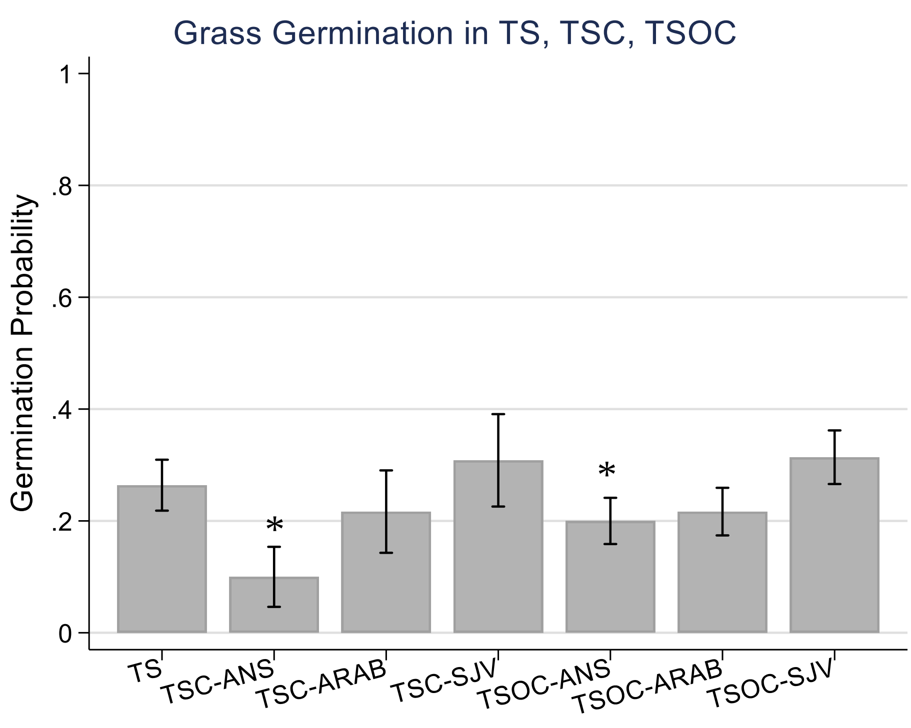

Figure 4.9 Effects of crude oil type on grass germination. Statistical differences from TS are noted with an asterisk (*) at p = 0.05.

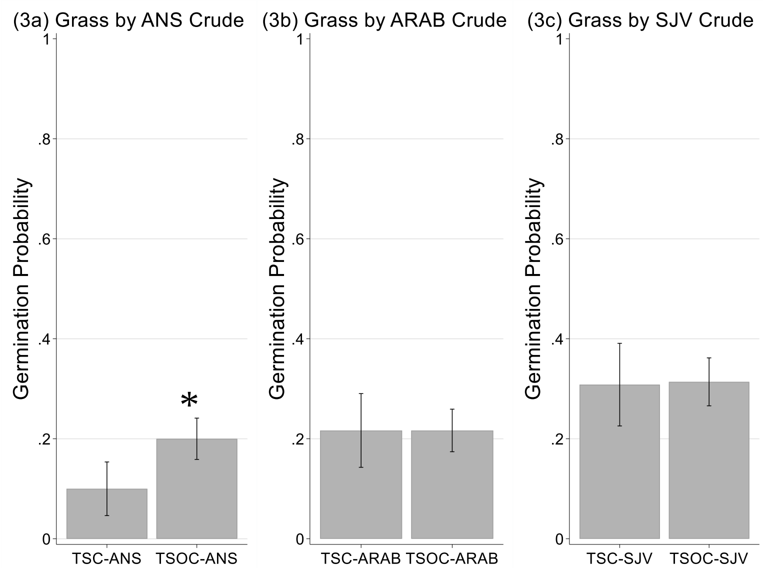

Figure 4.10 Crude/Oxidized Crude comparisons for Grass germination. Statistically significant ORs (TSC/TSOC) noted with an asterisk (*) at p = 0.05.

4.3.5 Effects of Dose on Germination

I showed that radish germination was statistically decreased when any of the three crude oils was ozonated. However, lettuce germination was not more affected by oxidized crude, while grass germination was largely unaffected by either crude or oxidized crude oil (except for the case of ANS). Because crude oil differences largely trended together, I combined crude oils to check for differences among ozone doses. The results are shown in Figure 4.11 and Table H in **Error! Reference source not found.**.

Figure 4.11a showed a downward trend for Radish germination as ozone dose increased from 5 g to 40 g of ozone. The difference between the 5-g dose and the 40-g dose was significance ($p = 0.01$). On the other hand, Lettuce germination at the 10-g showed a statistical improvement over the 5 g dose ($p = 0.00$, not shown in table) and the 40-g dose ($p = 0.03$). Grass germination showed no meaningful differences among dose groups.

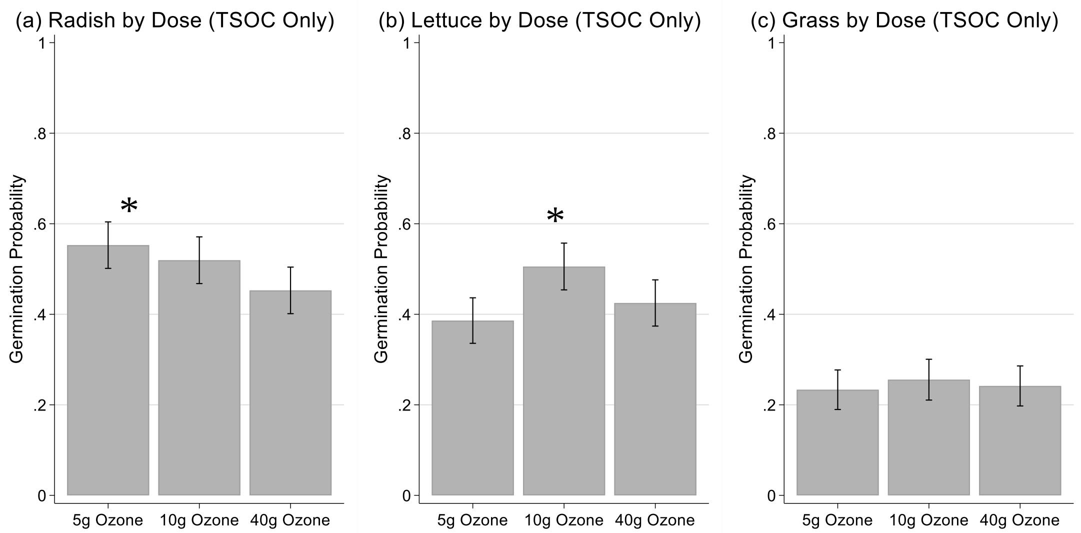

Figure 4.11 Oxidized crude oil comparisons about dose. Statistical differences from the 40-g O_3 dose are denoted with an asterisk (*) at $p = 0.05$.

4.4 Conclusions

This is one of the few studies to look at the terrestrial toxicity of oxidized petroleum crude residuals in plants. To my knowledge, it is the only study to compare multiple crude oils simultaneously and the only study to look at oxidized crude oil residuals by dose. I describe a few key findings:

1. Treatment Effects: Radish germination was slightly reduced by the presence of petroleum crude, and that effect was greatly enhanced when the crude was ozonated. Lettuce germination was greatly reduced by the presence of petroleum crude, but effect was unchanged when the crude was ozonated. Grass germination was unchanged by the presence of petroleum crude, a finding that was unchanged when the crude was ozonated.
2. Crude Oil Effects: Separating treatment effect by crude oil type did not show substantial changes in the treatment effects noted above. The only exception was

the grass species, that showed statistically improved germination in ANS crude after ozonation. This was the only instance where ozonation improved germination outcome.

3. Dose effects: Radish germination was reduced when crude oil was oxidized with 10 g ozone and significantly reduced when the crude oil was oxidized with 40 g ozone, both compared to the 5-g dose. Lettuce germination was significantly improved when crude was oxidized with 10-g ozone, compared to the 5-g and 40-g doses. Grass germination was unchanged by any of the 3 ozone doses.
4. Radish appears to be an important indicator of oxidized crude oil residuals. Radish germination showed a significant decrease in the presence of untreated SJV heavy crude, although the response to untreated crude-oil contamination was not seen with ARAB or ANS crude oils. For all crude oils, the decrease in germination of Radish was amplified by increasing ozonation. This ozone-dose-response effect of Radish should be useful to quantitatively track the response of radish germination to increasing oxidized byproducts, measured as DOC.

In Chapter 5, I use multiple logistic regression to create a multivariable model of radish germination as function of TPH, DOC, crude oil type, and organic background.

5 RESEARCH: USING RADISH (*RAPHANUS LATIVUS* L.) GERMINATION TO ESTABLISH A BENCHMARK DOSE FOR THE TOXICITY OF OZONATED-PETROLEUM BYPRODUCTS IN SOIL

This Chapter is in peer review at *Chemosphere*. The author list is: Yavuz, Burcu; Januszewski, Brielle; Chen, Tengfei; Delgado G., Anca; Westerhoff, Paul; and Rittmann, Bruce.

5.1 Introduction

The accidental release of petroleum into the environment is an inevitable outcome of a global supply chain that moves up to 100 mbd.[4] Such releases, whether on land or sea, are attenuated and transformed by microbial biodegradation, photooxidation, hydrolysis, and evaporation, as well as dispersive and diluting processes of dissolution, spreading, and emulsification.[36,38] Taken together, these collective "weathering" processes enrich recalcitrant components that often are among the most toxic and, via photo-modification, generate oxidized intermediates which have demonstrable acute toxicity to a variety of species.[39–42] Oxidation of petrogenic compounds by UV radiation is an important component of natural weathering of spilled crude oil. It promotes oxygenation that can break open otherwise stable saturated- and unsaturated-ring structures.[64,150,180] Oxidation of weathered crude oil by sunlight decreases the aromatic fraction, with a concomitant increase in asphaltenes and resins, and an increase in dissolved organic carbon (DOC).[45] The increase in aqueous solubility of the oil thereby increases its biodegradability.

The naturally oxidized residuals of crude oil, however, have shown acute ecological toxicity in several settings. Residual DOC has demonstrable toxicity to crustaceans, while the photo-enhanced toxicity of weathered Alaska North Slope crude oil has been proven against the eggs and larvae of Pacific herring (*Clupea pallasi*).[45,48,150] Toxicity of oxidized petrogenic compounds is also found in the literature for oil-sands water produced by hydraulic fracturing (or fracking), with particular concerns about the toxic mixtures of water-soluble naphthenic acids in the process water.[181–186] The organic fraction of oil-sands water significantly increased spinal malformation, pericardial edema, and delayed hatch in exposed zebrafish embryos (*Danio rerio*).[187] The toxicants also altered the expression of a suite of genes related to biotransformation, oxidative stress, and endocrine-mediation during development.[187] Acids produced by fracking include alicyclic, aromatic, and naphthenoaromatic compounds.[120,185]

Ozone (O_3) gas has been proposed as an effective tool to oxygenate and remove residual petrogenic compounds.[84,188] However, most ozonation schemes against high-level (>1% w/w) petroleum contamination cannot meet exhaustive cleanup goals because of practical, chemical, and economic limitations. For direct O_3 attack, the O_3/hydrocarbon mole ratio has been set at 1-to-3, not nearly enough for complete chemical degradation by O_3.[120] The products are most frequently quinones, aldehydes, ketones, alcohols, and, in the presence of excess O_3, carboxylic acids.[83,84,98,101,120] Hence, questions arise as to whether the byproducts of ozonation may demonstrate ecological toxicity as has been observed for the oxidized residuals of UV radiation or those resulting from fracking.

Luster-Teasley *et al*. performed one of the few dose-response studies on the toxicity of ozonation byproducts of a petrogenic compound using chrysene.[139] They found that, at the lowest dose (1.75 mol O_3/mol chrysene), ozonation byproducts of chrysene inhibited *in vitro* gap junctional intercellular communication (GJIC) more than chrysene itself. Only when O_3 was extensively deployed ($\geq$ 3 mol O_3/mol chrysene) did ozonation attenuate the toxicity of chrysene on GJIC. These results indicate that, in a terrestrial setting involving released crude oil where only limited oxidation by O_3 gas can be achieved, the likelihood of creating products that are more toxic than the original contaminants is high. Therefore, studying and understanding the adverse effects of ozonation products of petrogenic compounds on plants and animals in a terrestrial setting is essential before selecting ozonation as a remedial technology for crude oil contamination. Evaluating the differences in toxicity at the dose level is also a salient concern.

Ecological risk assessment is a flexible approach to evaluating data, assumptions, and uncertainties about the likelihood of adverse ecological outcomes of human-related activities or contaminants. Ecological risk assessments often characterize concentration–response (i.e., dose–response relationships) and reference doses, such as the lowest-observed-adverse-effect-level (LOAEL) or the no-observed-adverse-effect-level (NOAEL).[196–198] The LOAEL is the lowest dose at which adverse effects can be detected, while the NOAEL is the highest dose at which no adverse effects can be detected. NOAELs and LOAELs are used to determine a point-of-departure from baseline effects to observable adverse outcomes based on available data.[199,200] In contrast, analysis of a benchmark dose (BMD) can resolve the entire dose–response curve over all available treatment groups.[200] BMD analysis is essentially a "curve-fitting exercise" using a variety of mathematical techniques to find the best-fitting curve to describe the concentration-response relationship in the dataset. Once an appropriate model is identified, the curve can be used to extrapolate a specific effect level (e.g., 10% extra risk in adverse outcomes, described below), called the benchmark response, within the range that the model can statistically predict. The BMD approach is generally used for human-health risk assessments, but it is increasingly used in ecological risk assessments.

In this study, I determined the concentration-response relationship between the adverse germination of radish (*Raphanus. lativus* L.) (i.e., no germination) and oxidized petroleum in soil. I used multiple multivariable logistic regression to perform a BMD analysis of the outcome of adverse radish germination as a function of the continuous variables DOC concentration (*DOC*) and total petroleum hydrocarbon (*TPH*) concentration, along with categorical variables treatment (*TREATMENT*) and background organic (*b-ORGANIC*). Radish was chosen because of its relatively fast and robust germination in good soil conditions, sensitivity to contamination, and bioaccumulating attributes.[30-40] Radish has shown sensitivity to organochlorine insecticides (e.g., hexachlorocyclohexane) and accumulation of a wide range of anthropogenic contaminants including pesticides like diazinon, selenium, boron, bioavailable arsenic and antimony, cadmium, molybdenum, uranium (depending on pH conditions), veterinary antibiotics (e.g., chlortetracycline, enrofloxacin, and sulphathiazole), nanoparticles, and the antimicrobial agents triclosan and triclocarban.[90,201–206] While radish has not been found sensitive to soil contaminated with a high concentration of motor oil (24,000 ppm), some studies have shown that radish accumulates polyaromatic hydrocarbons (PAHs), especially 2- and 3-ring PAHs.[207,208]

5.2 Materials and Methods

5.2.1 Crude Oil and TPH Analyses

Chevron Technical Center (a Chevron U.S.A. Inc. division, Richmond, CA) provided a crude oil known as Alaska North Slope (ANS) having an API gravity of 29-32° and classified as a medium crude oil. Methodology and results for examination of crude oils are listed in 3.2.3 and 3.3.3, respectively.

5.2.2 Characterization of Test Soil (TS)

The base Test Soil (*TS*) used in all experiments was a locally sourced topsoil (All Star Materials, Guadalupe, AZ). Soil preparation and analysis are listed in 3.2.1 and 3.3.1, respectively.

5.2.3 Preparation of Test Soil with Crude Oil (TSC)

Preparation of test soil with crude (TSC) are listed in 3.2.4.

5.2.4 Preparation of Test Soil with Ozonated Crude Oil (TSOC)

A schematic of the experimental system used for ozonation of soil in this study is shown in Figure 3.1. Ozonation followed the procedure described in 3.2.6.

5.2.5 Determination of TPH, DOC, Moisture, pH, and Water-Holding Capacity

The methods for TPH and DOC determination are listed in detail in 3.2.5 and 3.2.7, while water-holding capacity and pH adjustment are noted in 4.2.2 and 4.2.3, respectively.

5.2.6 The Planted Tray and the ORGANIC Series

The methods for the planted tray and the ORGANIC series are noted in 4.2.4 and the figures therein.

5.2.7 The Independent Covariates

I used the multiple logistic regression model to investigate the effects of 4 independent covariates on the probability of adverse effects on radish germination (i.e., no germination): TPH concentration (ppm) by carbon (*TPHc*), DOC concentration (ppm) (*DOC*), the effect of treatment level (categorical at 5 levels) (*TREATMENT*), and background organic content (*b-ORGANIC*). For comparisons of TPH reduction and DOC production, g TPH was converted to g C by multiplying by 85% (according to the approximate mass percentage of C in petroleum hydrocarbons). I used Stata v. 16.1 (College Station, Texas) to find the values for the log-likelihood $L(\boldsymbol{\beta}')$ and the estimated coefficients $\widehat{\boldsymbol{\beta}}'$. The software provides estimates for the standard errors ($\widehat{SE}$) of each coefficient in the model from the matrix of the second partial derivative of the log-likelihood function as well as their respective 95% confidence intervals. Appendix D provides a detailed explanation of the foundation of the simple logistic regression model, the log-likelihood $L(\boldsymbol{\beta}')$, and the formulas used to build a logistic regression model.

5.2.8 Purposeful Selection of Covariates

Appendix D details tables and figures of this section. I treated the germination of each planted seed as an independent observation. *TPHc* and *DOC* are continuous variables, while *TREATMENT* and *b-ORGANIC* are polychotomous independent variables scaled with $k > 2$ possible levels. The method to evaluate such category levels in the logistic regression model is to transform k levels into a set of $k - 1$ design variables. Table J.1 (in *Step 0. The independent covariates* in SI) demonstrates the use of reference cell coding for these variables with further discussion. *TS* served as the control and was the reference cell against which all other levels were compared for the variable *TREATMENT* ($k = 5;\ k - 1 = 4$). The 100% *b-ORGANIC* level (0 g test soil, 100 g potting mix) was the reference cell against which all other levels were compared for the parameter *b-ORGANIC* ($k = 6;\ k - 1 = 5$). The variables and their levels are listed in Table J.2. The equations of the line for each of the individual variables tested are listed in Table J.3.

The logistic regression model was built using the method of "Purposeful Selection of Covariates," as described in Hosmer et al.[209] The first step was to evaluate the importance of each independent variable individually for predicting the germination outcome of radish in a univariable logistic regression model; from this, I obtained estimated coefficients $(\hat{\beta})$, estimated standard errors, and the likelihood ratio test for significance of the coefficient ($G\ statistic$, Equation I.11). Results of Step 1 are listed in Table J.4. The likelihood-ratio statistic (*G*) followed a chi-squared distribution ($df = 1$ for the continuous variables *TPHc* and DOC, $df = 4$ for the *TREATMENT*, and $df = 5$ for *b-ORGANIC*). Each of the covariates were statistically significant ($p < 0.000$) and were included in Step 2.

In step 2, the multivariable model simultaneously fit all independent variables that had significance in Step 1. The importance of each covariate was assessed using the *p*-

value of the Wald Statistic (Equation I.12). The multivariable model simultaneously fit all independent variables and the results, in Table J.5, show that continuous variables *TPHc* and *DOC* had statistically significant positive coefficients, meaning that an increase in the value of either variable increased the likelihood of the outcome (adverse germination), though to differing degrees, as shown by the magnitude of the coefficients (0.00689 for *TPHc* and 1.99 for *DOC*). For the continuous variables, only *DOC* added significant predictive power to the model ($p < 0.000$), and *TPHc* was a candidate for exclusion ($p = 0.784$). For the categorical variables, only the 40-g level of the variable *TREATMENT* was statistically different from the base level. Similarly, the *b-ORGANIC* category was of statistical value when greater than 10% by mass, as compared to the base level.

In step 3, I tested for modifiers (or confounders), a step especially important in this analysis because of the interdependent relationships of soil components.[67,210,211] The equation for delta-beta-hat-percent (Equation I.13) identifies variables that change the magnitude of coefficients of other covariates in the model by more than 20% (our criterion level). The results are listed in Table J.6 (a, b). *TPHc* was a modifier of the *TSC* level of the *TREATMENT* categorical variable and 80% *b-ORGANIC* level. Similarly, *TREATMENT* was a strong modifier of *TPHc* and *DOC*, as well as a modifier of soil *b-ORGANIC* at 40% and 80% levels. Finally, the *b-ORGANIC* covariate was a modifier of *TPHc* and all *TREATMENT* levels. The predictive importance of *DOC* to radish germination is clear. Since *TREATMENT* is a modifier of *DOC*, I kept that variable in the model. As *TPHc* was a modifier of *TREATMENT*, that variable also was held in the model. Similarly, *b-ORGANIC* was a strong modifier of *TREATMENT* at all levels and, therefore, retained.

In step 4, I considered the statistical value of the levels of categorical variables. Compared to the base (100% *b-ORGANIC*), only 0% and 10% *b-ORGANIC* levels presented statistically different conditions based on the Wald p-values (0.000 and 0.0710). That is, all other model inputs being the same, the germination conditions of 0% and 10% organic background were inherently worse. Thus, I condensed the 6-level *b-ORGANIC* covariate to a binary (dichotomous) covariate. Coded at 2 levels, the dichotomous variable was coded as $k = 1$ for conditions when *b-ORGANIC*>10% and $k = 0$ for conditions when *b-ORGANIC*<10%. The new dichotomous covariate was called *b-ORGANIC_2* (coefficients in Table J.7).

The change in covariate levels of *b-ORGANIC* to *b-ORGANIC_2* reduced the difference between *TS* and *TSC* dose levels, as evident in the Wald Statistic ($p = 0.747$). Therefore, I also condensed levels of *TS* and *TSC* to one unified code (TS/TSC) but kept the identification of dose levels TSOC-5 g, TSOC-10 g, and TSOC-40 g of O_3 separate to preserve resolution. The new variable is called *TREATMENT_2* (coefficients in Table J.8) and coded at 4 levels (TS/TSC, TSOC-5 g, TSOC-10 g, TSOC-40 g). All parameters (*TPHc*, *DOC*, *TREATMENT_2*, and *b-ORGANIC_2*) were run through the previous three steps (Table J.9). The covariate *TPHc* was again, a candidate for exclusion (Wald p-value 0.620). However, this time *TPHc* was not found to be a modifier of the condensed variables *TREATMENT_2* and *b-ORGANIC_2* (Table J.10). Hence, *TPHc* was dropped from the model, and the new model contained only three variables (*DOC*, *TREATMENT_*2, and *b-ORGANIC_2*).

In step 5, I checked the assumption that the logit increased or decreased linearly as a function of the covariate for each continuous variable in the model using LOWESS (locally weighted scatterplot smoothing) curves (Figure I.1) and the method of fractional polynomials developed by Royston and Altman (Tables J.10a and J.10b, see sources for further information).[212,213] Both methods supported the assumption that the model was linear in the logit for the continuous variable *DOC*. The model at the end of this step is the main effects model.

In step 6, I added each of the relevant interaction terms— *DOC x TREATMENT_2*, *DOC x b-ORGANIC_2*, *TREATMENT_2 x b-ORGANIC_2*—one at a time, and assessed the statistical significance of the interaction using first the Wald statistic (Equation I.12) and partial likelihood ratio test (Equation I.11) at a significance level of $p \leq 0.01$. These results are in Tables J.11, J.12, and J.13, respectively. No interaction met our criteria for statistical significance cutoff. I therefore excluded interaction terms from this analysis.

The preliminary final model included the relevant main effects: *DOC*, *TREATMENT_2* (coded at 4 levels), and *b-ORGANIC_*2 (coded at 2 levels). In this step, I assessed whether the probabilities predicted by the model accurately reflected the observed data. I used two tests of significance: (1) the receiver operating characteristics (ROC) curve, which is a plot of $sensitivity\ vs. 1 - specificity$ for all possible outcomes of the model and (2) Hosmer-Lemeshow goodness-of-fit tests, which tested the null hypothesis that the estimated output predicted by the model was not different from observed outcomes. The ROC curve is shown in Figure J.2 and provides a measure of the model's ability to discriminate correct outcomes from the data given from the area under the curve (AUC). The AUC (0.902) indicates outstanding discrimination.[209] Furthermore, the Hosmer-Lemeshow goodness-of-fit test (p = 0.0743) indicates that I could not statistically differentiate the observed data from the predicted data. Thus, I conclude that the model fits well and is best represented by the following equation for $\hat{g}(x)$, the estimated logit, which is linear in its parameters:

$$\hat{g}(x) = -0.500 + 1.76x_{DOC} + 0.876x_{TSOC-5g\,O_3} - 0.493x_{TSOC-10g\,O_3} - 1.93x_{TSOC-40g\,O_3} - 2.30x_{HIGH\ ORGANIC}$$

Equation 5.1

The function g(x) represents the log-transformed odds ratio of the conditional mean of an event (Y) under given conditions (x) when the logistic distribution is used. In this case, that event (Y) is the probability of adverse germination, i.e., no germination.

5.3 Results and Discussion

5.3.1 Quantification of TPH Removal (g C from C9 to C36) and DOC Production

Figure 5.1 (A, B, and C) shows our findings with respect to TPH, TPH loss, and DOC gain. Figure 5.1A shows that the changes in TPH concentration (ppm) across C9-C36 by dose were nearly uniform, although the rate of TPH removal was clearly slowing at higher O_3 doses. While O_3 reactivity in the soil column will be a complex mix of reactions including direct attack by the O_3 molecule and indirect attack by radicals formed by the decomposition of O_3, the finding of uniform reactivity across carbon range appears to favor the latter explanation.[101,126,132,192,214] The data for ANS crude indicate a predominately aliphatic character (85%), another point favoring the explanation of indirect O_3 attack via radical oxygen species, since direct attack by the O_3 molecule is usually slow against aliphatic compounds.[101,120] The radical reactions would be facilitated by the reactive metals in the soil (Table 3.1), including iron (13,100 ppm), manganese (250 ppm), copper (16.5 ppm), and nickel (11.0 ppm), all of which decompose O_3 in the gas phase.[192,215,216] For radical-type, ozone-initiated auto-oxidation, the reason for the plateau may be saturation of the metal catalyst surface or that the O_3-induced radical chain process is autoinhibiting.[215,217] For example, a manganese oxide catalyst for O_3 degradation of cyclohexane loses its reactivity after 120 min, and intermediate products can be evolved off the surface as CO_2 upon heating the metal catalyst to 500ºC.[215]

Figure 5.1B shows a direct comparison of loss of TPH (in g C) to gain of DOC (also in g C). The most salient feature is the recovery of 0.745 g C of DOC at the 5 g dose of O_3 gas, a finding that is not recapitulated by TPH measurements, which showed only a loss of 0.165 g C. This indicates the formation of an intermediate set of compounds that could be extracted and detected by TPH and DOC methods, products that were not detectable by DOC methods before ozonation. Intermediate compounds, including 1,2,3- and 1,2,4-trioxolanes, are well-documented for direct O_3 attack double bonds, particularly on µ-conjugated rings, but they are highly unstable and difficult to isolate.[218] Intermediates for radical-type reactions are more elusive, and information is scarce as to the mechanism or intermediate products of such reactions.[120] It also is possible that an initial dose of O_3 reacted first with higher molecular weight asphaltenes and resins, not quantified in the TPH profile.[163,219] Chacon-Patiño found that photo-oxidized lower carbon number asphaltenes with an archipelago (multicore) structural motif exhibited products with a fingerprint typical of dissolved organic matter.[219]

Figure 5.1C shows that measurable TPH loss rates (g Δ C /h) were lowest at the 5-g O_3 dose (-0.330 g C_{TPH}/h), maximized at the 10-g O_3 dose (-1.74 g C_{TPH}/h), and began to plateau at the 40-g dose (-1.02 g C_{TPH} /h). DOC gains, on the other hand, peaked at the 5-g O_3 dose (+1.49 g C_{DOC}/h), slightly decreased at the 10-g O_3 dose (+1.30 g C_{DOC}/h), and then dropped off sharply at the 40-g O_3 dose (+0.780 g C_{DOC}/h). Nonetheless, the peak utilization of O_3 (g O_3/ g Δ C) occurred at the 10-g O_3 dose for TPH (5.76 g O_3/ g Δ C) and DOC (7.67 g O_3/ gΔ C).

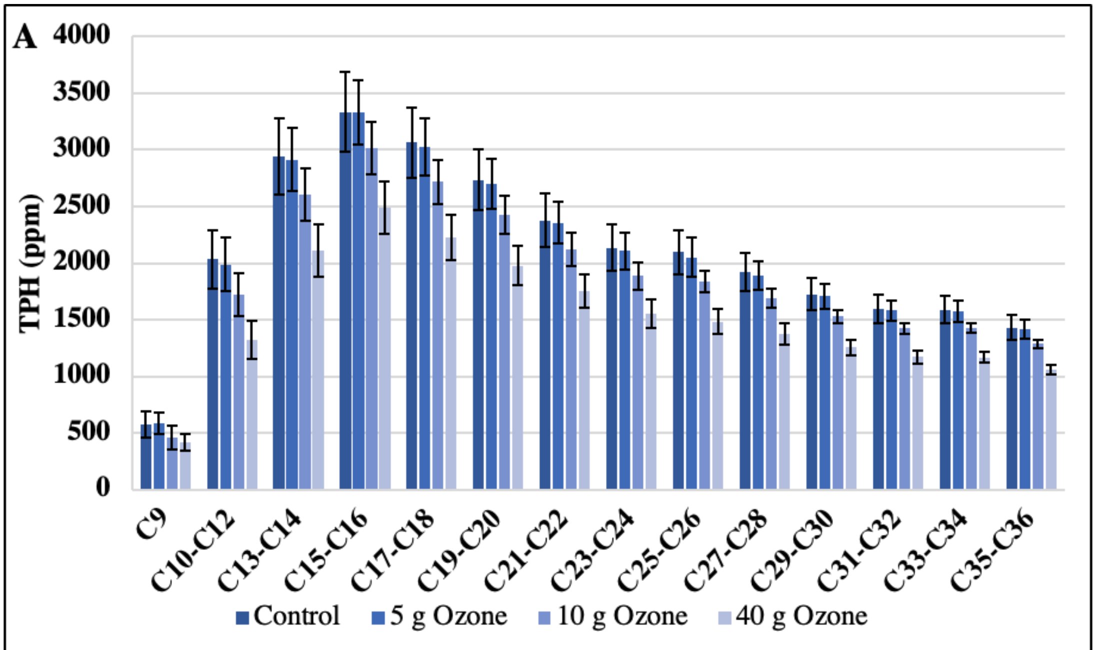

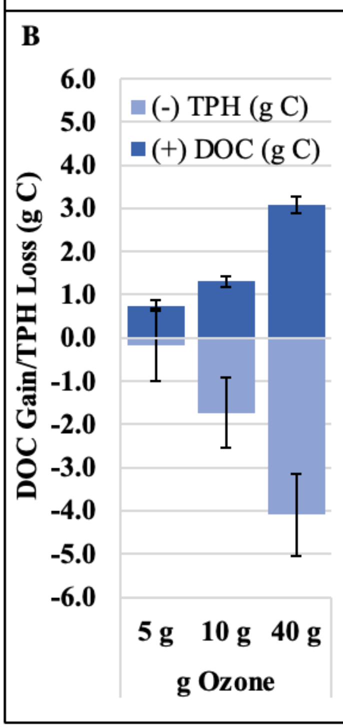

C	Unit	TPH	DOC
Control	**g C**	17.0	0.14
5 g O_3	**g C [%Δ]**	-0.165 [-0.970%]	+0.745 [+532%]
10 g O_3		-1.74 [-10.2%]	+1.30 [+931%]
40 g O_3		-4.10 [-24.1%]	+3.07 [+2200%]
5 g O_3	**g ΔC /h**	-0.330	+1.49
10 g O_3		-1.74	+1.30
40 g O_3		-1.02	+0.768
5 g O_3	**g O_3/g ΔC**	30.3	6.72
10 g O_3		5.76	7.67
40 g O_3		9.77	13.0

Figure 5.1 (A-C). (A) TPH decreases across the carbon range (C9-C36) for ANS crude oil; (B) Direct comparison of TPH loss to DOC gain (both in g C); (C) Comparison of TPH and DOC for absolute change in mass of carbon (g C), mass of carbon change per hour (g Δ C/h), and ozone utilization (g O_3/g Δ C).

5.3.2 NOAEL and LOAEL for TPH and DOC

Figure 5.2 (A-O) summarizes adverse germination rates, TPH, and DOC in the dilution series (*b-ORGANIC*, y-axis) for each treatment group (*TS*, *TSC*, *TSOC-5 g*, *TSOC-10 g*, and *TSOC-40 g*). The baseline adverse germination rate, established by the background control (*TS*) (Figure 5.2A), ranged from 5% to 55%, depending on the amount of *b-ORGANIC*. Adverse germination in the *TSC* (Figure 5.2D) dilution series closely matched that seen in *TS* (control), except at the highest TPH concentration (0 % *b-ORGANIC*), wherein adverse germination was 90%, compared to only 55% in *TS* control. Some regulatory guidelines prescribe a minimum germination rate for the control group: For example, the UN OECD 208 sets minimum germination in the control at 70%.[220] At the highest TPH concentration (0 % *b-ORGANIC*), the 70% criterion was not attained, with only 45% germination; hence, the LOAEL 27,300 ppm for TPH (Figure 5.2E) did not meet the UN OECD criterion.[220]

At up to 10% *b-ORGANIC* (or ~24,500 ppm TPH), the germination rates between *TS* and *TSC* were identical and, thus, 24,600 ppm is the NOAEL TPH (Figure 5.2E). This finding agrees with that of Banks et al., where no statistical evidence of adverse radish germination was observed in soil contaminated with up to 24,000 mg/kg motor oil.[91] The DOC produced from ozonation, on the other hand, had negative impacts on germination at a fraction of the full-strength dose. The NOAEL of *TSOC-5 g* was 150 ppm DOC (Figure 5.2I) and occurred at 10% of the original strength of contamination. The NOAEL of *TSOC-10 g* was 770 ppm (Figure 5.2L) and that of *TSOC-40 g* (Figure 5.2O) was 1730 ppm DOC (both at 20% of the full-strength dose). The LOAEL showed corresponding trends: 480 ppm for the 5-g dose (Figure 5.2I), 1920 ppm for the 10-g dose (Figure 5.2L), and 4320 ppm for the 40-g dose (Figure 5.2O).

TPH (outside the full-strength *TSC*) did not significantly alter germination, as also noted by Banks *et al*.[91] In contrast, DOC produced from ozonation had profoundly negative impacts on radish germination. Moreover, the DOC produced from a 5-g dose was more toxic than from a 10-g or 40-g dose, based on the NOAELs. Potential reasons are discussed more fully in the logistic regression analysis. For *TSOC-5 g*, the NOAEL to LOAEL range was narrow (140 to 480 ppm DOC), while the range for the *TSOC-10 g dose* and *TSOC-40 g* dose levels were broader: 770 to 1920 and 1730 to 4320 ppm DOC, respectively, an artifact of study design.[200] Therefore, I performed a benchmark dose (BMD) analysis using multiple logistic regression to determine a few key benchmark responses for the full set of data and make differentiations based on *TREATMENT_2* and *b-ORGANIC_2* levels.

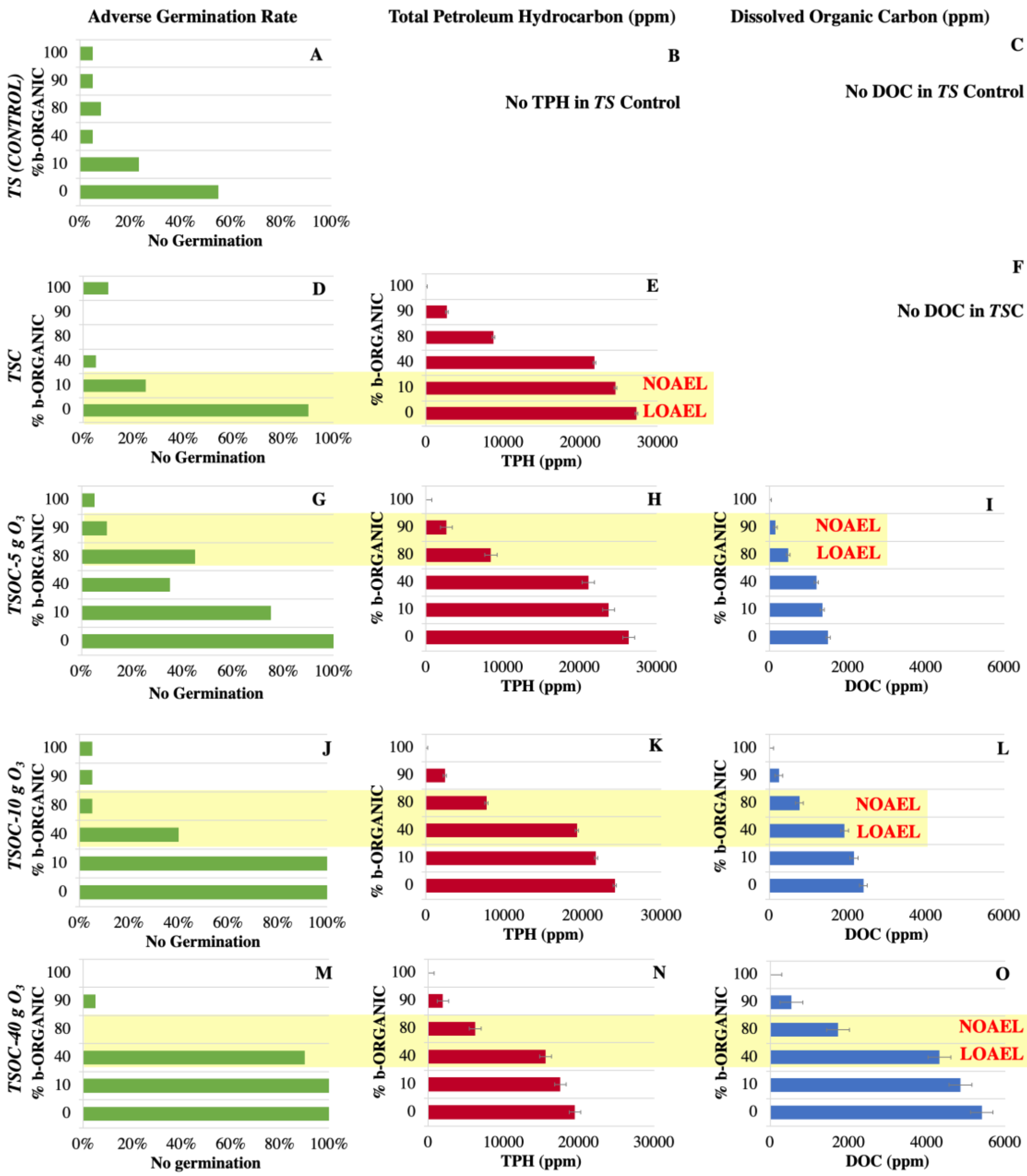

Figure 5.2 (A-O). Comparison of germination rate (%), DOC (ppm), and TPH (ppm), by dilution series (*% b-ORGANIC*) for *TS* (A-C), *TSC* (D-F), *TSOC-5 g O_3* (G-I), *TSOC-10 g O_3* (J-L), and *TSOC-40 g O_3* (M-O). NOAEL and LOAEL are highlighted in yellow and noted in red for TPH (*TSC* only) and DOC (*TSOC* groups only).

5.3.3 Interpretation of Model Results

Examination of the model coefficients (Table 5.1) indicates, first, that the covariate *DOC* had a strong positive slope (1.76), directly indicating the harmful effect of oxidation products on the probability of radish germination. Second, *TPHc* could be excluded from the model, meaning that the presence of background crude oil (as measured by GC-FID) had no predictive bearing on radish germination. Third, dose level had predictive importance: *DOC* produced from a 5-g dose of O_3 gas had meaningfully worse impacts on germination than *DOC* from a 10-g or 40-g dose, implying that the nature of the *DOC* was different. Finally, the presence of *b-ORGANIC* 10% (by mass) strongly attenuated the adverse effects of *DOC*.

Table 5.1. Results of fitting the multivariable logistic regression model with *TPHc*[*] variable removed (n = 840)[†].

Covariate	*Unit/Level*[‡]	*Coef.*	*Std. Err.*	*Wald (z)*	*P*[§]	*95% CI*
DOC	per 1000 ppm	1.76	0.241	7.29	0.0000	(1.29, 2.23)
TREATMENT_2	*TS/TSC*	Base				
	TSOC-5 g	0.876	0.364	2.41	0.0160	(0.163, 1.59)
	TSOC-10 g	-0.493	0.506	-0.970	0.330	(-1.49, 0.499)
	TSOC-40 g	-1.93	0.814	-2.37	0.0180	(-3.53, -0.335)
b-ORGANIC_2	*b-ORG<10%*	Base				
	b-ORG>10%	-2.30	0.268	-8.56	0.0000	(-2.83, -1.77)

*Total petroleum hydrocarbon by carbon (TPHc), approximately 85% of the TPH by mass.
†Intercept-only loglikelihood is -515, the log-likelihood of the model is -278, and G (df = 5) is 474 for the model, statistically significant at $\rho < 0.000$.
‡ *TS*, test soil; *TSC*, test soil contaminated with crude oil; *TSOC*, test soil contaminated with ozonated crude oil.

The categorical variables make it possible to parse the model outcomes based on the effects of organic matter and dose level as shown in Figure 5.3. The results for the full model are shown in Figure 5.3A, in which the probability of adverse effects (i.e., no germination) with 95% confidence intervals (dashed boundaries) are modeled as a function of DOC (ppm); here, *TREATMENT_2* and *b-ORGANIC* are held at mean values. The model parsed by low (< 10% by mass) versus high (> 10% by mass) *b-ORGANIC* is shown in Figure 5.3B, where only *TREATMENT_2* is held in the mean position. The model of low *b-ORGANIC_2* parsed by *TREATMENT_2* is shown in Figure 5.3C, while the high *b-ORGANIC* parsed by *TREATMENT_2* is in Figure 5.3D. The steep slopes of the model at low organic conditions vs. high organic conditions (Figure 5.3B) show that background organic matter strongly attenuated the adverse effects of increasing DOC concentration while Figure 5.3C and Figure 5.3D show the increase in toxic effects of DOC produced from lower doses of O_3.

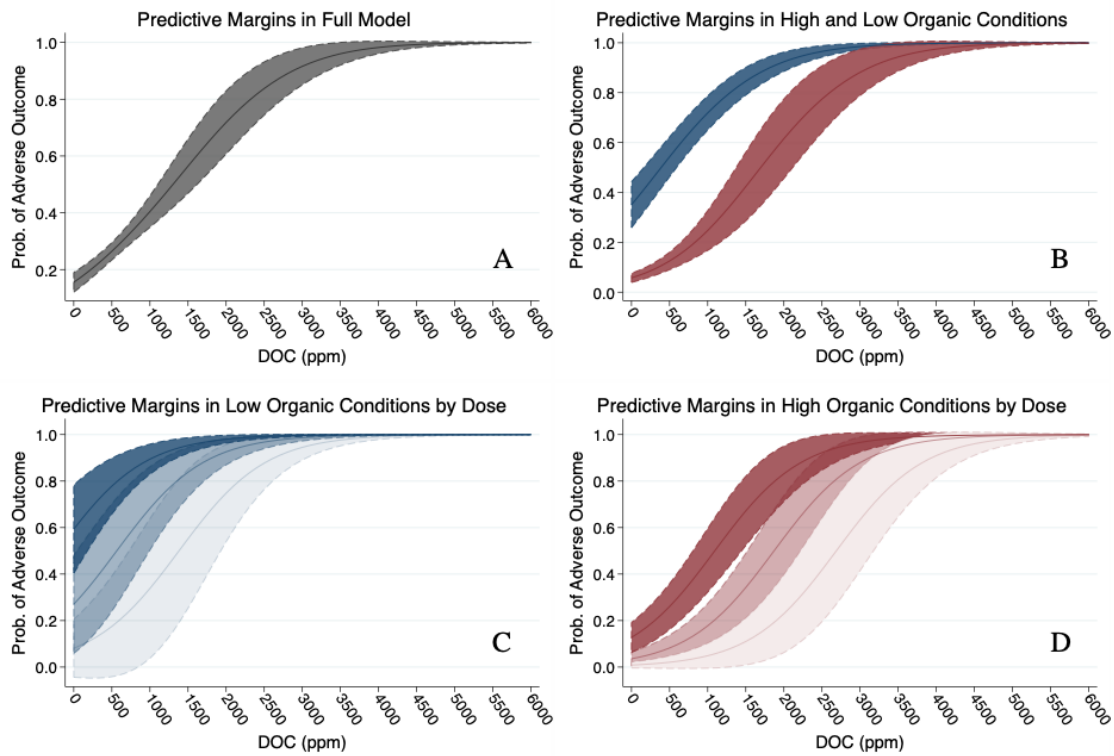

Figure 5.3(A-D). Predictive margins with 95% confidence intervals: (A) the full model; (B) the model parsed by high (navy) and low (maroon) background organic; (C) the model of low background organic parsed by the 5 g (dark navy), 10 g (medium navy), and 40 g (light navy) O_3 dose; (D) the model of high background organic parsed by the 5 g (dark maroon), 10 g (medium maroon), and 40 g (light maroon) O_3 dose.

I used the full model and the parsed models to evaluate the positions of risk of adverse effects. If $p(d)$ is defined as the probability of adverse outcomes (i.e., no germination), and $p(0)$ is defined as the probability at background level, additional risk is defined as:

$$\boldsymbol{y(d) = p(d) - p(0)} \quad \text{Equation 5.2.}[221]$$

Extra risk, y(d), is defined as additional risk of adverse outcomes in the fraction of plants expected to germinate normally:

$$y(d) = \left[\frac{p(d)-p(0)}{1-p(0)}\right] \quad \text{Equation 5.3}$$

When background effects are small (e.g., background organic > 10%), the BMD results are comparable between additional risk and extra risk; when background effects are large, the difference is greater. Thus, extra risk considers background effects.

Table 1.1 lists the 10%, 25%, and 50% extra-risk levels (± std. error) for the full model, the model parsed by *b-ORGANIC_2*, and the model parsed by *b-ORGANIC_2* and *TREATMENT_2*. These values compute the additional risk of adverse germination outcomes given the background risk of adverse germination. Figure 5.4 maps those risk levels along a tree diagram and shows that the mean position of the full model can be subdivided first by background organic and then by dose. For example, at the average position for all criteria, a 10% extra risk of adverse germination is expected at 450 ppm DOC. If I specify *b-ORGANIC_2*<10%, 10% extra risk occurs at 260 ppm DOC, while a *b-ORGANIC_2>10%* tolerates up to 650 ppm DOC (2.5x higher)

Table 5.2 List of the 10%, 25%, and 50% extra-risk margins (± std. error) in ppm of DOC for the full model, the model parsed by high and low organic background, the model of low organic background parsed by dose, and the model of high organic background parsed by dose.

Model	*Extra Risk (10%, 25%, and 50%)*
Full Model	450±15, 900±24, 1550±50
High Organic	250±44, 500±40, 900±36
Low Organic	650±23, 1150±50, 1750±79
Low Organic 5 g Dose	n/a, n/a, 250±79
Low Organic 10 g Dose	450±11, 650±11, 1050±87
Low Organic 40 g Dose	1250±16, 1500±15, 1850±12
High Organic 5 g Dose	150±37, 600±54, 1150±74
High Organic 10 g Dose	900±44, 1400±70, 1950±91
High Organic 40 g Dose	1750±67, 2200±98, 2700±11

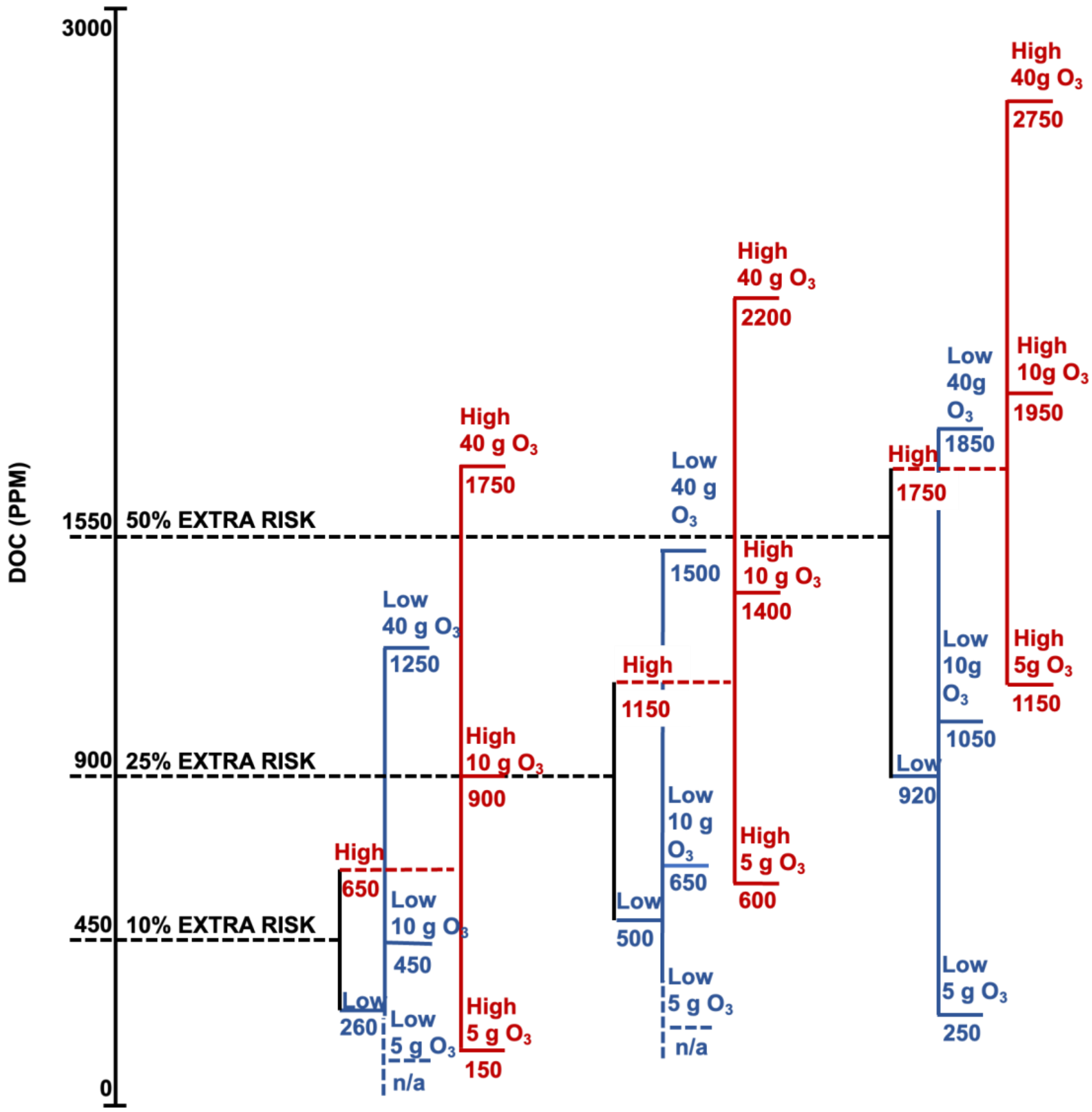

Figure 5.4. The 10%, 25%, and 50% extra-risk margins for the full model (black), the model in *b-ORGANIC_2*<10% (navy), and the *b-ORGANIC_2*> 10% (maroon). At each risk level, risk is delineated first for the full model, then for the *b-ORGANIC_2*, and, finally, for the *TREATMENT_2*.

Low and high *b-ORGANIC* can be further subdivided by dose level. The model could not predict 10% extra risk in *b-ORGANIC_2<10%* because of the steepness of the curve – an area future studies can address. In *b-ORGANIC_2>10%*, the 10% risk at a 5-g dose is drawn at 150 ppm DOC (~3% the full concentration of all the DOC produced at the 40-g dose). Indeed, the first measurable risk level at low *b-ORGANIC* for a 5-g dose of O_3 is the 50% extra-risk level predicted at 250 ppm DOC − in other words, less than 1/5th of the DOC produced by a 5-g dose conferred a nearly 50% increase in adverse germination outcomes. This number is comparable to the LOAEL (480 ppm) (Figure 5.2I). Conversely, the 10% risk level in low *b-ORGANIC* can be resolved for the 10-g O_3 dose (450 ppm) and 40-g O_3 dose (1250 ppm). Increasing dose increased the tolerance to DOC at a given risk level. The same trends are observed with *b-ORGANIC*>10% w/w, where DOC tolerance is even higher.

Our findings are consistent with those of the Luster-Teasely et al., who examined dose levels of 1.75, 3.00, 4.25, and 5.00 mol O_3/mol chrysene and found the lowest dose to be more toxic than chrysene itself.[139] Our dose levels of 5 g, 10 g, and 40 g O_3, expressed as molar ratios, are 1.63, 3.26, and 13.1 mol O_3/mol TPH, respectively. I find that 1.63 mol O_3/mol TPH is considerably more toxic to radish germination than either 3.26 or 13.1 mol O_3/mol TPH. The reaction mechanisms and thermodynamics likely explain these results. First, for ringed structures, the first ozonation step is rate-limiting and has a positive activation energy barrier (e.g., 15.8 kcal/mol in benzene), while the second step is predicted to be faster, more exothermic (−40 to −50 kcal/mol), and with a negative activation energy of −5 kcal/mol. [130,134] Hence, direct O_3 attack may thermodynamically favor the oxidation of a first set of intermediate products over initial products, thereby creating an evolving group of intermediate products that peak in reactivity (and toxicity) after the first ozonation step, where a highly reactive intermediate is created, and then steadily decrease as downstream products become more oxidized. The reaction path for aliphatic compounds involves a complex chain of radical reactions, and is less understood; however, a changing group of intermediates also occurs in such scenarios.[120] The role of background organic matter in quenching the toxicity has been shown for nanoparticles (Zn-O NP), heavy metals (cadmium), and other trace elements by chemisorption or complexation.[222–225] This finding is also true for the more complex molecules like herbicides: For instance, an early study found that five times more herbicide was required at 20% organic matter than at 4% for equal toxicity, regardless of the herbicide.[226] Such results are recapitulated in our study, which shows the ameliorating effects of greater than 10% w/w potting mix (itself containing ~75% organic matter).

5.4 Environmental Implications

Our study highlights that ozonation of weathered-petroleum hydrocarbons in soil is a dynamic process that creates intermediates whose toxicity to radishes depended on the level of ozonation. This finding poses a risk-management paradox. A low dose of O_3 removed less TPH and produced a lower absolute quantity of oxidized byproducts, but that material was more toxic per unit mass. In contrast, a higher dose removed more TPH and produced more DOC, but that DOC was less toxic per unit mass. The tradeoff between toxic potential and absolute quantity of DOC produced must be evaluated with respect to the time it takes to remediate partially oxidized intermediates efficiently, particularly by biodegradation.[83,84,98] Previous findings have indicated that a multicycle treatment process that integrates O_3 doses with periods of bioremediation can reduce contaminant levels to strict regulatory limits of 1% TPH (10,000 mg/kg), remove the residuals created by ozonation treatment, and improve soil quality.[98,79] Until bioremediation of oxidized residuals is complete, ozonation must be coupled with bioremediation, regardless of the dosing regimen.[84,98]

6 RESEARCH: OZONATION OF PETROLEUM HYDROCARBONS IN SOIL COLUMNS: EFFECTS OF OZONE LOADING RATE ALONG THE AXIAL DISTANCE

This chapter is in preparation for publication in the Journal of Hazardous Materials. It is being reviewed within Chevron before submission. The author list is Yavuz, Burcu; Chen, Tengfei; Montoya, Garrett, Januszewski, Brielle; Delgado, Anca; Dahlen, Paul; Westerhoff, Paul; and Rittmann, Bruce.

6.1 Introduction

Aeration-based *in situ* treatment technologies are an established means to remediate petroleum-based contaminants in subsurface source zones and dissolved-contaminant plumes. [59,227,228] For example, *in situ* air sparging injects clean air directly into an aquifer to provide the oxygen (O_2) necessary for aerobic biodegradation. The analogous process for unsaturated soils is bioventing, or the delivery of air to the vadose zone. Air sparging and bioventing are bioremediation tools that promote aerobic biodegradation processes: e.g., mono-oxygenation followed by β-oxidation, tricarboxylic acid cycle, and aerobic respiration.[59]

A non-biological option is *in situ* soil vapor extraction (SVE) for remediating unsaturated soils contaminated with volatile organic chemicals such as chlorinated solvents or petroleum derivatives like the light aromatics benzene, toluene, ethylbenzene, and xylenes (BTEX).[229] An SVE system uses compressors or vacuum pumps to move air through the vadose zone and extract volatile compounds, which are then sent to an above-ground treatment system to condense, adsorb, biodegrade, or incinerate the vapors.[228]

In the case of soil contaminated with unrefined crude oil, these technologies can attenuate some degree of contamination, because raw crude oil contains components with a wide range of water solubility, vapor pressure, and Henry's Law constant.[1] SVE can volatilize lighter fractions, and bioventing or air-sparging can stimulate biodegradation of some n-alkanes (usually C10 to C26), slightly branched alkanes (isoprenoid alkanes), and low-molecular-weight aromatics such as BTEX.[8,37,51] However, SVE, air sparging, and bioventing are not effective for petroleum components that are semi- to non-volatile or recalcitrant to normal oxidative bioremediation. In fact, these technologies enrich the recalcitrant components by removing more labile ones, thus shifting the residual crude oil profile to one with a higher proportion of large aromatic molecules and molecules with greater heteroatom character (i.e., molecules containing nitrogen, sulfur, or oxygen).

Contacting recalcitrant compounds with ozone (O_3) is a means to add oxygen-containing functional groups and overcome the limitations of the conventional *in situ* technologies.[230] The addition of oxygen-containing functional groups to recalcitrant petroleum compounds (e.g., saturated or condensed aromatic rings) often increases solubility and biodegradability.[83,84] Due to the high redox potential of O_3 (2.08 eV) and its primary decomposition product, the hydroxyl radical (•OH) (3.06 eV), O_3 exposure oxidizes a wide range of organic compounds to produce alcohols, aldehydes, ketones, carboxylic acids, and quinones.[97,101,231] Generation of O_3 typically occurs via a high-voltage discharge across an oxygen or air feed-gas; the technology is mature, can be performed on-site, and requires no storage. [86,97,108,192] Hence, *in situ* oxidation with O_3 gas may present a technical avenue to decrease the total time needed for bioremediation and to allow removal of petroleum contamination that is inherently recalcitrant to bioremediation.[232]

How O_3 transports through the soil profile is complex, because O_3 reacts rapidly and non-specifically with many organic and inorganic compounds.[101,193,231,233] Since many factors can promote or impede the ability of O_3 to transport along a soil column, O_3 transport has been the subject of numerous studies.[35,192,193,234–236] Hsu and Masten found O_3 to be an effective oxidant against phenanthrene, with water content and organic matter being factors that impeded O_3 transport in 10-cm and 30-cm columns.[237] Choi et al. examined the effect of soil media, OH-radical scavengers, O_3 dosage, and humic acid for the ozonation of 10 ppm of PAHs (e.g., phenanthrene) in glass beads, sand, and baked sand in a variety of slurry experiments.[236] These authors found that the time needed for O_3 to break-through decreased with greater soil moisture, a result they attributed to decreased pore volume and access to soil organic matter (SOM) and metal oxides. Chen et al. also showed that the reaction of O_3 with petroleum hydrocarbon was impeded by increased soil moisture, even at high concentrations of residual petroleum (18,000 ppm and 33,000 ppm).[99] Most recently, Ying et al., examining the importance of iron-content and soil particle-size distribution, corroborated the impact of SOM in two soil types of an Israeli coastline aquifer.[233]

The prior studies agree that increased water content, SOM, and metal oxides impede O_3 transport, either by blocking gas pores or creating an O_3 demand; the outcome is that the O_3 dose has to be increased to reach a target contaminant. Each of the studies, however, looked at bulk contaminant removal within the column without examining reactivity with axial distance, which affects treatment efficacy for *in situ* applications. Only Zhang *et al.* looked at the degradation of anthracene along 6 points in sand-packed columns, but with a relatively low anthracene concentration, 50 ppm. Moreover, no studies have evaluated treatment regimens with higher than 1 wt% of O_3 gas.

Small-scale O_3 generators can produce between 1-5 wt% O_3 , and high-efficiency O_3 generators can reach concentrations of 15 wt% using an O_2 feed gas, the upper limit for safe-handling.[102] High concentrations deliver treatment mass in a smaller volume of carrier gas (i.e., increased loading of mass O_3/mass soil/time), thereby decreasing treatment time and the volume of the total of gas that must be contacted with soil. On the other hand, increasing the concentration of a reactive gas in complex soil matrix will have non-linear consequences for O_3 half-life, transport distance, and the generation of a hydroxyl radical, a key secondary oxidant that is dependent on available catalytic surfaces.

The spatial reactivity of O_3, the effective O_3 concentration, and the efficiency of a given total dose level are key concerns for *in situ* application of O_3 for soil contaminated with >1 wt% petroleum.[77] Yet little direct evidence demonstrates how O_3 reacts along the gas-flow path using treatment-relevant O_3 concentrations for field-relevant contaminant conditions. This work expands beyond previous work by evaluating O_3 consumption along the axial distance of a 45-cm column using high concentrations of O_3 gas (~2 wt%, ~5 wt%, and ~14 wt %) for soils contaminated with petroleum at 5 wt%, initially by looking at the ability of O_3 to traverse the column (“break-through”) under each condition and secondarily at the removal of total petroleum hydrocarbons (TPH) along axial distance. In addition, the axial length for temperature change, water (H_2O) flux, and total heat evolved based on the specific heat of soil+H_2O, temperature, and ΔH_2O are examined. The results show clear spatial patterns with respect to O_3 transport and utilization efficiency based on a 3x3 array of concentration and total dose, and they reveal key spatial concerns about the balance of heat as the reaction proceeds through a soil column.

6.2 Materials and Methods

6.2.1 Crude Oil Source and Characteristics

Chevron Technical Center (a Chevron U.S.A. Inc. division, Richmond, CA) provided a crude oil known as ARAB having an American Petroleum Institute gravity of 30-32° and classified as a medium crude oil. The crude oil characteristics are described in 3.2.3 and 3.3.3.

6.2.2 Soil Source and Characteristics

Locally sourced topsoil (All Star Materials, Guadalupe, AZ) served as the background soil in all experiments. Soil preparation and classification analyses are described in 3.2.1 and 3.3.1.

6.2.3 Preparation of Petroleum Contaminated Test Soil

A petroleum contaminated test soil using ARAB crude mixed with background soil (initial moisture < 1-2% w/w) at a concentration of 5% w/w was created. The mixture was vigorously mixed with a hand trowel for even consistency, and the soil was transferred to clean, heat-resistant (up to 60°C) 57-L polypropylene containers. Soils were artificially weathered in the lab, in methods described in further detail in 3.2.4.

6.2.4 Soil Column Ozonation Apparatus

The ozonation setup is shown in Figure 6.1. Each experiment was conducted using 600 g of contaminated soil containing 5% w/w crude oil and moistened to 10% w/w moisture. Before ozonation, the experimental soil was loaded to a height of 45 cm into a custom reaction vessel (4.0 cm ID x 60 cm) comprised of two fused chambers: a 700-cm^3 main reaction chamber for soil and a 50-cm^3 antechamber separated by a coarse-grit diffusion plate (ASU Glassblowing Facility, Tempe, AZ). A temperature-indicating label (McMaster-Carr; Aurora, OH) was placed every 5 cm from 0 to 45 cm (inclusive) along the length of the column for a total of 10 measurement points; the labels indicated surface temperature in 5-degree increments from 25°C to 100°C and are rated for accuracy of ±2°C (Figure 6.1, right panel). Ambient laboratory temperature was 24.4°C.

All hosing connections and fittings were made of O_3-compatible polytetrafluoroethylene (PTFE). A tank of ultra-high purity (UHP) compressed O_2 (S.3A) was supplied to a dual-stage pressure regulator (S.3B) and then passed through a flow meter (S.3C) to regulate flow to 2 liters per minute (LPM). The gas then flowed into an Ozonia (Trevose, PA) Triogen LAB2B laboratory O_3 generator (S.3D), which delivered O_3 at a loading rate of ~2 wt% (10,000 ppmv) for the low loading rate and ~5 wt% (30,000 ppmv) for the medium loading rate. For high-loading rate experiments at ~14 wt% (84,000 ppmv), the setup was connected to an Ozonia Model CFS-1 2G O_3 generator.

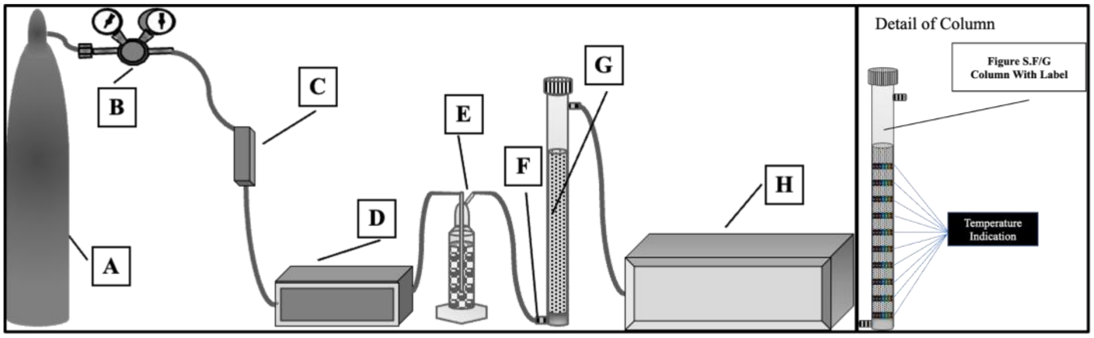

Figure 6.1. Left-panel shows the schematic of the experimental setup for soil ozonation: (A) ultra-high purity (UHP) compressed tank provided O_2 to a (B) dual stage pressure regulator, then to a (C) flowmeter, (D) Ozonia Triogen LAB2B laboratory O_3 generator for low and medium loading rate experiments, or Ozonia Model CFS-1 2G O_3 generator for high loading rate experiments, (E) gas-washing bottle containing 500mL of 18MΩ water for humidification, the (F) ¼"-inlet connection to reaction vessel antechamber, the (G) ¼"-outlet connection, and (H) Model 465M Ozone Monitor. Right-panel shows detail of column (Figure 1. F/G) with temperature indicating labels in position.

The O_3-bearing gas was directed through a gas-washing bottle (S.3E) filled with 500 mL of acidified (pH 2) 18-MΩ deionized water to attenuate stripping of moisture from the soil and then allowed to passively advect in up-flow mode into the first chamber (S.3F), across the diffusion plate, and then into the chamber containing the soil (S.3G). Effluent gas was directed into a Model 465M Ozone Monitor (S.3H) (Teledyne Advanced Pollution Instrumentation, San Diego, CA).

A total of 9 experimental conditions (Table 6.1) were run in duplicate. The O_3 concentration in the effluent gas was recorded every five minutes during an ozonation experiment. Temperature at each of the ten points along the surface of the glass column was also recorded every five minutes. To quantify the spatial differences, the soil in the reaction vessel was removed in 5 discrete sections (as demonstrated in Figure E, Appendix E) and analyzed in triplicate for TPH and moisture. An O_2-only control column was run for 240 minutes to determine moisture stripping effects of gas-flow along the five column sections.

Table 6.1. Summary of the 9 ozonation experiments, each using 600 g of TSC.

Ozone Gas *Loading* Rate (mg_{ozone}/ g_{soil}/ h**)**	**Conditions to Achieve Targeted Ozone Dose For a Gas flow rate of 2 LPM for different times and Ozone Gas Phase Concentrations**		
	5 g Ozone Dose	**10 g Ozone Dose**	**40 g Ozone Dose**
4	120 min of 10,000 ppmv [O_3]	240 min of 10,000 ppmv [O_3]	480 min of 10,000 ppmv [O_3]
12	40 min of 30,000 ppmv [O_3]	80 min of 30,000 ppmv [O_3]	160 min of 30,000 ppmv [O_3]
36	15 min of 84,000 ppmv [O_3]	30 min of 84,000 ppmv [O_3]	60 min of 84,000 ppmv [O_3]

6.2.5 Quantification for TPH and Moisture

Extraction and quantitation of TPH (C9-C36) closely followed the methods described in 3.2.7.

6.3 Results and Discussion

6.3.1 Extractable TPH Prior to Ozonation of Soil Columns

Figure 6.2 compares TPH concentrations (C9-C36) between raw and weathered crude oil. The initial pre-weathering concentration was ~23,600±700 ppm TPH (coefficient of variation [CV] = 3%). After weathering, the TPH concentration was on average 20,000 ± 1,200 ppm TPH (CV = 6%). DCM-extractable carbon accounted for ~40% of available hydrocarbons, since asphaltenes and resins were not quantified in the analysis.[83] The synthetic weathering process removed 86% of hydrocarbons from C9 to C12, 26% from C12 to C13, and ~15% of overall TPH.

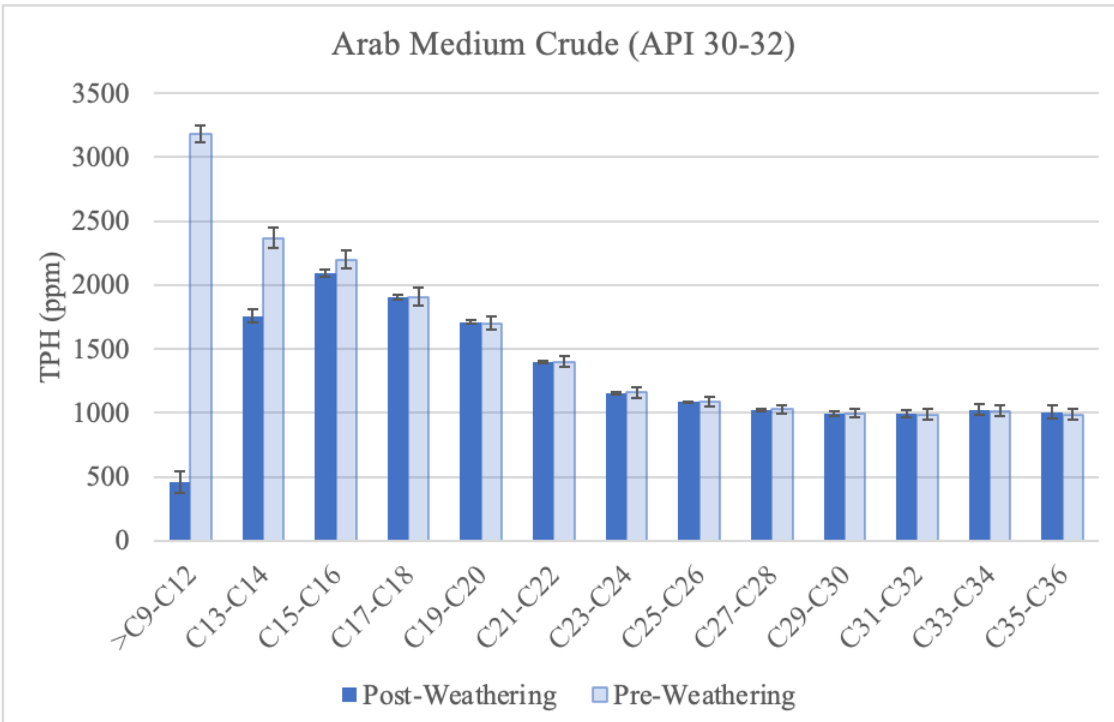

Figure 6.2 Arab medium crude oil before and after laboratory weathering processes.

6.3.2 Effluent Ozone Profiles ("Break-through") over Time

Effluent O_3 is defined as the concentration of O_3 in the gas exiting during the ozonation experiments. Integrated over time, I measured how much for the supplied dose exited the column unreacted. Gas flowrates influenced the change in measured gas phase ozone concentrations across the lengths of the soil column. For experiments at the low-gas loading rate, 2-3% of the supplied O_3 dose exited as effluent at the 5 g total dose, 7% at the 10 g total dose, and 32% at the 20 g total dose. Thus, O_3 traveled the length of the column and broke through for the low O_3-loading rate. At the medium loading rate, the O_3 concentration in the effluent was negligible at the 5 g and 10 g total dose, and it was 2% at the 20 g dose. No effluent O_3 was detected at any total dose level for highest gas loading rate.

6.3.3 Bulk TPH Removal and O_3-utilization Efficiency

TPH results for the matrix of O_3 loading rates and total O_3 doses are summarized in Table 6.2. TPH loss rates (g Δ C /h) increased with increasing O_3 loading rate: from 0.44 g ΔC/hr for the lowest O_3-loading rate to 2.3 g ΔC/hr for the highest rate. This trend is expected, given that organic oxidations involving O_3 are commonly bimolecular, i.e., first-order with respect to each reactant.[101,238,239] In contrast, the efficiency of the reaction between O_3 and TPH was greatest at the lowest O_3 loading rate at every total dose, as evidenced by the O_3 utilization ratios, which were highest for the lowest loading rate.

A possible reason for decreased O_3 utilization with increased loading rate is that the higher gas loading rates of ozone led to more direct attacks by molecular O_3 and fewer radical reactions. The generation of hydroxyl radicals is a dominant reaction when O_3 is deployed in a complex matrix like soil, where metals in soil mineral backbone (Table 3.1) catalyze the formation of hydroxyl radicals.[214–216,240] Catalytic ozonation has been found to be almost 3-fold more efficient than ozonation alone for the oxidation of hydrocarbons.[241] The major catalytic mechanisms depend on surface absorption such that either (1) the O_3 decomposes to free radicals by metal ions which react with hydrocarbons or (2) the complexation between organic molecule and the catalyst and subsequent oxidation of the complex.[242–246] With a high ozone loading rate, radical-generating sites may have become saturated, thereby increasing the proportion of molecular O_3 present.[236,247] Direct attack by the O_3 molecule is more selective and slower than radical attack and may favor larger, more complex hydrocarbons.[101,237]

Table 6.2. TPH Summary of average TPH values for 9 ozonation experiments are noted below. Ozonation-utilization was tabulated from grams of carbon removed (85% of TPH).

Total O_3 Applied		***5 g O_3***	***10 g O_3***	***20 g O_3***
Low Loading rate 4 $mg_{ozone}/ g_{soil}/ h$	Start TPH	21,000	19,000	21,000
	End TPH	18,000	15,000	15,000
	% TPH Reduction	13%	20%	30%
	g TPH removed	1.4	2.0	3.0
	Utilization ratio, g O_3/g C	4.1	5.8	7.9
Medium Loading rate 12 $mg_{ozone}/ g_{soil}/ h$	Start TPH	18,000	19,000	20,000
	End TPH	17,000	16,000	15,000
	% TPH Reduction	9%	17%	24%
	g TPH removed	0.84	1.8	2.4
	Utilization ratio, g O_3/g C	7.0	6.5	9.9
High Loading rate 36 $mg_{ozone}/ g_{soil}/ h$	Start TPH	21,000	20,000	22,000
	End TPH	19,000	17,000	18,000
	% TPH Reduction	8%	10%	18%
	g TPH removed	0.90	1.1	2.2
	Utilization ratio, g O_3/g C	6.5	11	11

6.3.4 TPH Removal by Distance Through the Length of the Soil Column

The removal of TPH along the column is presented in Figure 6.3. The horizontal axis is the TPH concentration normalized to the respective control, while the vertical axis represents axial distance along the column. The top row of Figure 6.3 (A-C) shows the low loading rate (4 mg_{ozone}/ g_{soil}/ h), the middle row (D-F) shows the medium loading rate (12 mg_{ozone}/ g_{soil}/ h), and the bottom row (G-I) shows the high loading rate (36 mg_{ozone}/ g_{soil}/ h).

Because O_3 gas reacts with the first available hydrocarbons along the transport path, the inlet end always had a more pronounced TPH removal than the outlet end. This TPH pattern was also shown for the degradation of phenanthrene.[35] The degree of asymmetry between the ends of the column increased sharply with increasing O_3 loading rate. At the low loading rate, TPH removal began to equalize as the dose time moved from 120 to 480 min (top row). TPH removal for medium loading rate, however, retained a pronounced difference between the two ends, and the difference was more extreme at high O_3 loading rate, where TPH removal stalled at the 20-cm mark, even at the highest dose (20 g O_3). A trade-off was that the high loading rate conferred a significant improvement in TPH reduction at a short distance (0-10 cm) compared to the medium and low loading rates: 62%, 56%, and 48%, for high, medium, and low loading rate, respectively. This feature, combined with the lack of effluent O_3 observed for high loading rate experiments, may be an advantage to the high-loading rate regimen for contamination scenarios that have a shallow depth.

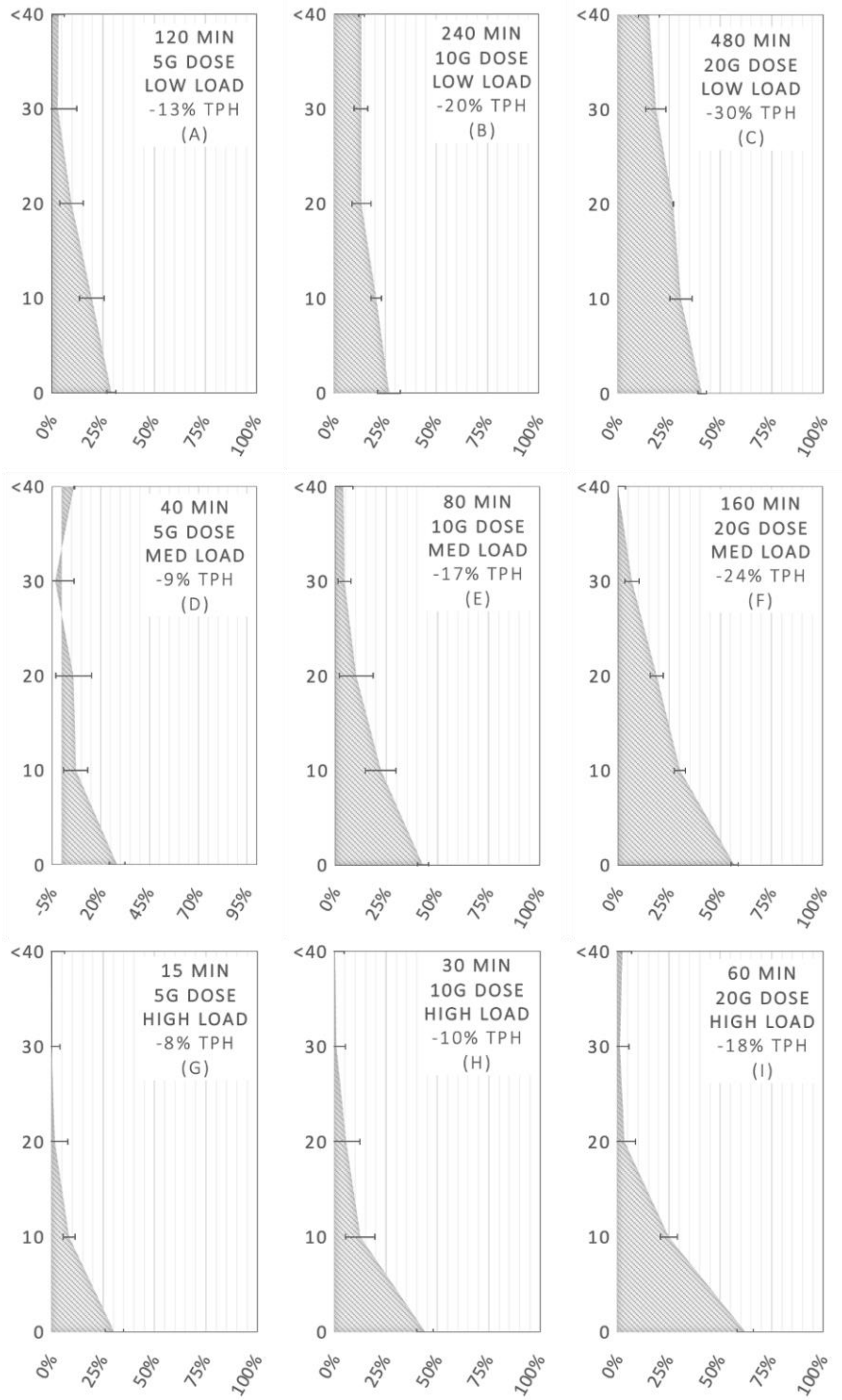

Figure 6.3 (A-I). The vertical axis represents distance (cm) from the inlet end, and the horizontal axis represents % TPH removal normalized to respective control experiments. The axes correspond to a column's orientation, i.e., upright (Figure 6.1).

6.3.5 Temperature at Input, Mid-Point, and Outlet End of the Soil Columns

Temperature measurements made at 10 points along the axial length every five minutes enabled the monitoring of a "heat front" that began at the inlet end and moved along the soil column in each of the 9 experimental conditions. Figure 6.4 (A-I) shows the temperature profile (y-axis) as a function of experimental duration (x-axis) at the inlet (5 cm), mid-point (10-20 cm), and outlet (>40cm) ends of the column. For the low O_3-loading rate (Figure 6.4 (A-C)), the heat front emerged within 1-2 minutes, traversed >40 cm in 60±20 min, and then dissipated, although the column did not completely cool to the ambient temperature, ~24°C. Peak temperature, which was 35°C at each total-dose level of low loading, was observed only between 10 and 20 cm and only in the first 60 minutes. After 60 minutes of ozonation, the heat front reached >40 cm, but the column temperature did not continue to increase along the length, and remained at 27±2°C for the duration of the experiment, even though TPH removal continued from 120 to 480 minutes (Figure 6.3B and 1C). The temperature results show that the initial reactions were strongly exothermic, while later reactions were less so.[231,248] The stable temperatures indicate that the energy emission from the oxidation reactions was balanced by heat loss due to the advection of warm gas, latent heat of evaporation, and losses to the surroundings.

The heat front generated by the medium O_3-loading rate (Figure 6.4 (D-F)) shows that tripling the O_3-loading rate increased the reaction rate and, thus, shortened the time for a temperature increase to reach >40cm from 60±20 min to 36±20 minutes. Heat accumulated more quickly, as evidenced by the increase in peak temperature, to 40-45°C recorded at 10-20 cm along the column. Since O_3 lost in the effluent was significantly decreased (<2%), the higher temperature may have increased O_3 reaction kinetics, which decreased its half-life.[109,249] The increase in O_3 consumption was not matched by more removal of TPH, as shown in Figure 6.3 (D-F); instead, O_3 may have been oxidizing asphaltenes and resins, which were not measured. Similar to the low O_3 loading, medium loading showed no further increases in temperature >60 min, but converged to ~35±4°C for the remainder of the experiment at the highest total dose (20 g).

The trends intensified at the highest loading rate (Figure 6.4 (G-I)), which had an additional tripling of the O_3 loading rate to 36 mg_{ozone}/ g_{soil}/ h. Temperature increases occurred at >40cm after only 18±5 min, and peak temperatures at 10-20 cm were higher than for lower O_3 loading rates: 55°C for the total dose of 5 g O_3, 60°C for 10 g O_3, 65°C for 20 g O_3. The 20-g total dose yielded a second heat front after 55-60 minutes at the O_3 inlet (0-5cm): There, the temperatures spiked to >100°C. The temperature spike was exacerbated by the substantial loss of water from the inlet end of the column (discussed below). Schubert et al. noted that 100°C is approximately the lower limit wherein alkanes can be induced into slow combustion in the presence of O_2 and O_3. The combustion reactions increase temperature still further, which vaporizes more moisture and further propagates the reaction,[250,251] a smoldering phenomenon that was noted by Chen et al.[99]

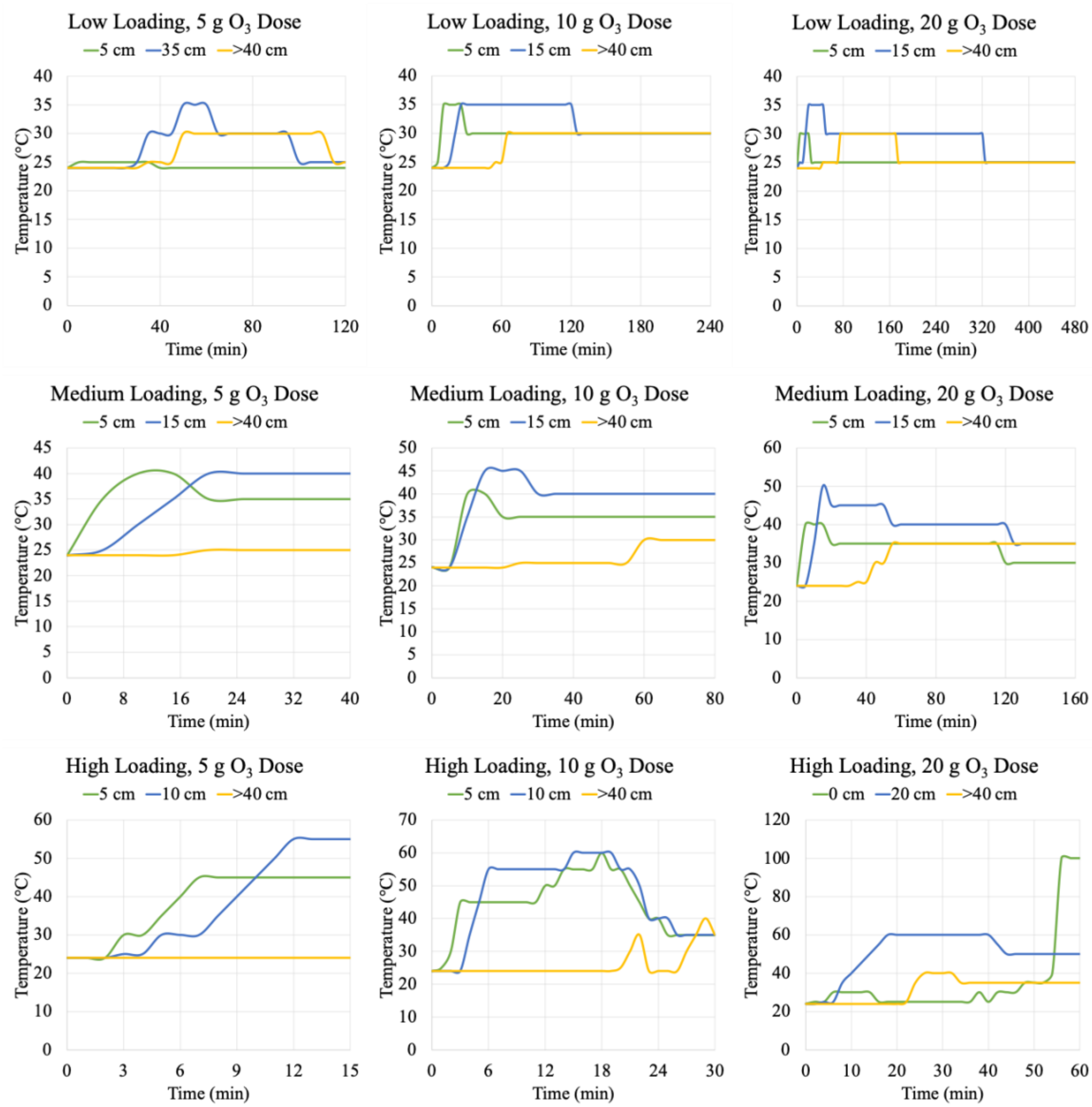

Figure 6.4 (A-I). The vertical axis represents distance (cm) from the inlet end, and the horizontal axis represents time (min) of each experimental condition. For each condition, temperature is monitored at the inlet (green), mid-point (blue), and outlet (yellow) to O_3 distribution.

6.3.6 Movement of Moisture Across the Column

Precise moisture measurements taken across the column for each of the 9 experimental conditions allowed us to evaluate the mass of water gained or lost (compared to the starting level) along the axial direction; the moisture results are shown in Figure 6.5 (A-I). These data provide a “snapshot” of the moisture profile at each dose level (i.e., each time point) and demonstrate that a moisture “front” moved along the reaction path, creating a non-uniform moisture pattern; water loss near the column’s inlet and gain near the column’s outlet. For total doses >5 g O_3, experiments indicated a net loss of moisture. The low loading rate experiments (Figure 6.5 A-C) delivered volumetrically more gas than those for higher loading rates; hence, the moisture-stripping effect was more pronounced. At the highest total O_3 dose, the low loading rate experiment yielded a net loss of 9 g H_2O from the column over 480 minutes, with the inlet and outlet ends showing approximately -8 g H_2O and +3 g H_2O, respectively. The medium loading rate experiments (Figure 6.5 D-F) showed a greater degree of imbalance between moisture at inlet and outlet ends for the highest dose: approximately -9 g and +7 g H_2O, respectively. This pattern was heightened at the highest O_3-loading rate (Figure 6.5 G-I): approximately -12 g and +7 g H_2O, respectively.

The flux of water along the axial distance was reinforced by the balance point (net zero ΔH_2O). At low loading, the axial position for the balance point of water increased from ~15 to 30 cm as the reaction time increased, showing that moisture moved up and out of the column (as evidenced by the 9 g net loss of water from the entire column at the 20 g total dose). The balance point for medium loading also advanced, but at a lower final position (~25 cm). The balance point of high loading, on the other hand, stalled at ~15 cm, even while the temperature increased still further at the inlet end to 100°C due to both a decrease in water content near the diffusion plate and stalled evaporative cooling. Moreover, the accumulation of water at the outlet end had a detrimental effect on O_3 reactivity at >20cm.[99,192] The finding that moisture impedes ozonation by blocking catalytic surfaces and access to the contaminant target has been shown to be one of the chief hindrances to O_3 transport in the soil column, which was recapitulated here at high loading.[99,192]

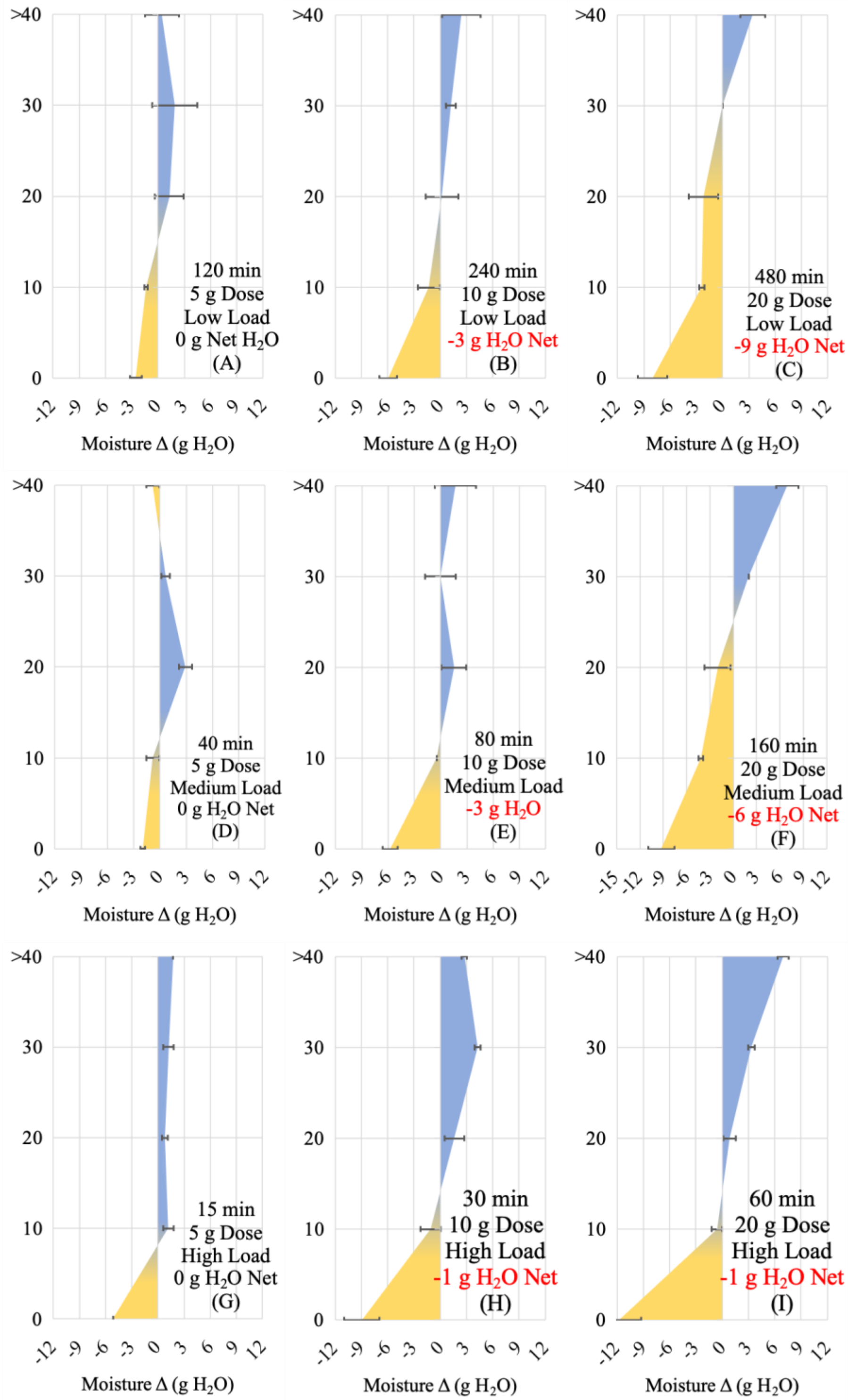

Figure 6.5 (A-I). The vertical axis represents distance (cm) from the inlet end, and the horizontal axis represents g of moisture (lost is in orange and gained is in blue). The axes correspond to a column's orientation, i.e., upright (Figure 6.1).

6.3.7 Heat Gain and Loss Along the Column

The continuous temperature measurements (Figure 6.4) and changes in moisture content (Figure 6.5) make it possible to compute the net heat generated or lost by a change in temperature (specific heat) and by the latent heat of evaporation or condensation (latent heat) by location and time. The specific heat (kJ) was computed from:

$$\boldsymbol{Q_{spec} = \Delta T\left[\left(M_{dry\,soil} C_{dry\,soil}\right) + \left(M_{water}\, C_{water}\right)\right]} \qquad \text{Equation 6.1}$$

The latent heat (kJ) was:

$$\boldsymbol{Q_{lat} = M_{water\,(loss/gain)} L_{water}} \qquad \text{Equation 6.2}$$

The net heat (kJ) was calculated from:

$$\boldsymbol{Q_{net} = \Delta T\left[\left(M_{dry\,soil} C_{dry\,soil}\right) + \left(M_{water}\, C_{water}\right)\right] + M_{water\,(loss/gain)} L_{water}} \qquad \text{Equation 6.3}$$

where ΔT is the temperature change for a given time interval (°C), $M_{dry\ soil}$ is the mass (g) of dry soil, $C_{dry\ soil}$ is the specific heat capacity of the dry soil (0.837 J/g/°C), M_{water} is the mass of water in the fraction, C_{water} is the specific heat capacity of the water (4.186 J/g/°C), L_{water} is the latent heat of vaporization for water (2,260 J/g), and $M_{water\ (loss/gain)}$ is the net change in water for a given time interval at a given position. Latent heat measurements were corrected for moisture losses due to the movement of O_2 gas only, as described in the Appendix F with Figure F and Table F. The moisture adjustment preserved all original trends such that the final reported values for Q_{lat} are conservative.

Figure 6.6 (A-I), which presents Q_{spec}, Q_{lat}, Q_{net}, and the sum of Q_{net} along the column, identifies three key trends. First, Q_{net} was positive for all experiments and increased with loading rate and dose, such that the highest total heat production occurred at the 20 g dose of high loading (bottom-right panel). Second, increasing the loading rate at each dose level increased the Q_{net} sum, even though TPH reduction was not increased, as evidenced in Figure 6.3 (A-I). Hence, heat generation likely was the result of O_3 oxidation of hydrocarbons outside the C9-C36 TPH range, particularly with aromatics.[101,120,237] Third, Q_{net} (Figure 6.6, grey lines) was nearly always net negative at >20cm on the columns in every experiment, indicating that the heat measured at the outlet end was overwhelmingly due to the condensation of heat removed from the inlet end. Heat deposition was primarily due to heat released from condensation, and Q_{net} closely tracks latent heat throughout the column. Thus, moisture changes along the reaction path were key to controlling temperature. For example, heat release from the reaction with the low loading rate could be balanced by evaporating moisture such that the inlet, midpoint, and outlet points of the column converged to ~27°C (Figure 6.4 B, C). In contrast, overall heat production for the highest loading rate was great enough that the evaporation could not moderate the temperature rise, particularly in the middle of the column (Figure 6.4 G, H, and I). The high rate of moisture loss at the inlet end was matched by high condensation at the outlet end, effectively blocking evaporative cooling such that high loading became self-limiting with respect to axial transport but self-propagating with respect to heating at the inlet end. This created a risk for smoldering near the diffusion plate which has been observed previously.[99]

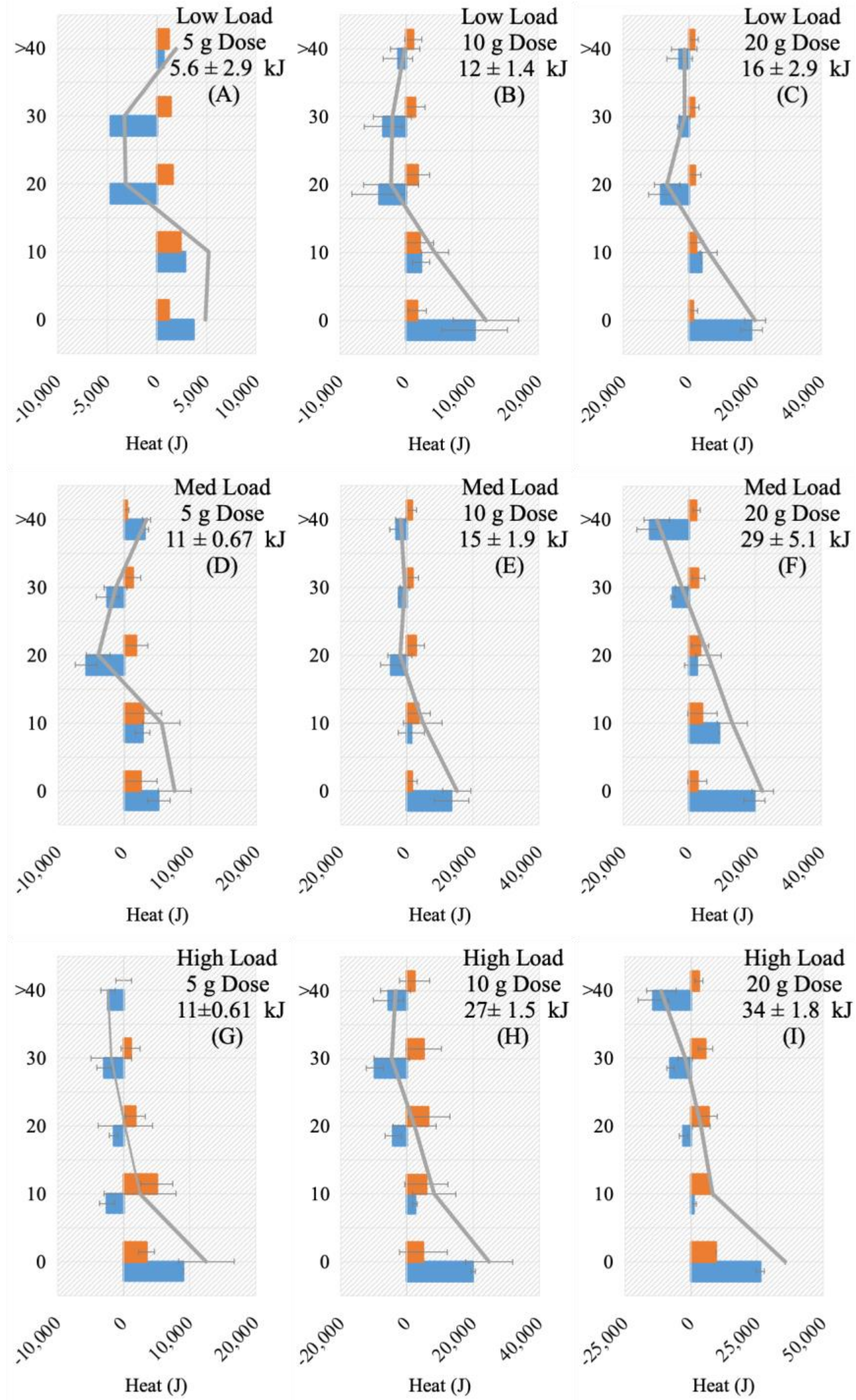

Figure 6.6 (A-I). Spatial distribution of specific heat and latent released or gained along the column in the same orientation as the experimental design, i.e., upright (Figure 6.1). The vertical axis represents distance (cm) from the inlet, and the horizontal axis represents heat released (+) or lost (-) (J). Q_{lat} is in blue bars, Q_{spec} is in red bars, and Q_{net} is in the grey line. The sum of Q_{net} for the entire column is listed in kJ.

6.4 Summary and Conclusion

The results have immediate applicability to the *in situ* use of O_3 to accelerate the bioremediation of soils contaminated with crude oil. The O_3 reaction in the soil column was made more uniform by using a low O_3 concentration and gas phase loading rate. A more uniform reaction improved the O_3-utilization efficiency for removing TPH in the C9-C36 range. It also lowered the net heat generation, making the temperature more even along the axial direction of the column and minimizing the disparity of moisture content from the inlet to the outlet. Evaporation and condensation of water were crucial to determining the heat balance and temperature as the reaction moved forward. The rate of TPH oxidation, causing heat release, could be well-balanced at the low loading rate, and the temperature did not increase to >35°C. Evaporative heat losses were less able to moderate the temperature for the high loading rate, and a heat pocket with a possible ignition risk occurred, especially near the O_3 inlet, where moisture losses were greatest. Overall, it is clear that O_3 deployment has great potential for i*n situ* oxidation, but concentration, total dose, and moisture dynamics must be balanced to maintain a reaction that reaches the intended treatment zone.

7 SUMMARY AND FUTURE WORK

7.1 Summary and Implications

The remediation of petroleum hydrocarbons will remain a global concern even as crude oil is displaced in the energy mix by renewables like solar, wind, and hydro-electric.[1-5] Site closure will entail investigation of petroleum contamination and remediation of contaminated soil stockpiles. Oxidation with O_3 is a valuable component of the technology toolbox needed to remediate residuals left from decades of crude oil handling.

I experimentally evaluated a wide range of ozonation conditions for the loss of TPH, utilization of O_3, and formation of DOC.

Table 7.1 lists the experimental conditions evaluated in Chapters 3 and Chapter 6. In aggregate, O_3 gas was capable of removing 18%-30% of TPH hydrocarbon at single high dose. Chapter 3 demonstrated that increasing the crude oil's API led to improved ozonation efficiency: 5.6, 4.8, and 4.9 g O_3/gTPHc removed for SJV (API 13-15), ARAB (API 30-32), and ANS (API 29-32), respectively. However, Chapter 6 demonstrated that O_3 concentration was a stronger governing factor over O_3 utilization, as illustrated by the differences at a 20-g dose among low, medium, and high loadings (i.e., via the input O_3 concentration). The over-arching conclusion is that O_3 could remove close to 25% of TPH, regardless of crude API, with dosing strategy being more important than crude oil type.

Table 7.1 Summary of the impacts of O_3 dosage among the three crude oils, O_3 dosages, O_3 concentrations

Crude oil	API gravity	[O_3] (ppmv)	Flow (LPM)	O_3 (g)	Start TPH	End TPH	% TPH Removal	gO_3/gTPHc Removed
ARAB	30-32	17,000	5	5	45,000	44,000	4%	5.0
ARAB	30-32	17,000	5	10	45,000	42,000	8%	4.8
ARAB	30-32	17,000	5	40	45,000	35,000	23%	7.1
ANS	29-32	17,000	5	5	33,000	33,000	1%	25.7
ANS	29-32	17,000	5	10	33,000	30,000	11%	4.9
ANS	29-32	17,000	5	40	33,000	25,000	27%	8.8
SJV	13-15	17,000	5	5	38,000	37,000	2%	10.9
SJV	13-15	17,000	5	10	38,000	35,000	9%	5.6
SJV	13-15	17,000	5	40	38,000	29,000	23%	7.9
ARAB	30-32	10,000	2	5	21,000	18,000	13%	4.1
ARAB	30-32	10,000	2	10	19,000	15,000	20%	5.8
ARAB	30-32	10,000	2	20	21,000	15,000	30%	7.9
ARAB	30-32	30,000	2	5	18,000	17,000	9%	7.0
ARAB	30-32	30,000	2	10	19,000	16,000	17%	6.5
ARAB	30-32	30,000	2	20	20,000	15,000	24%	9.9
ARAB	30-32	84,000	2	5	21,000	19,000	8%	6.5
ARAB	30-32	84,000	2	10	20,000	17,000	10%	11
ARAB	30-32	84,000	2	20	22,000	18,000	18%	11

A key focus of this dissertation is to determine whether ozonation byproducts have toxic effects on seedling germination, since the utility of applying O_3 for large stockpiles of soil is necessarily linked to toxicity of remaining residuals as soils wait for or undergo bioremediation treatment. Chapter 4 focused on screening of three distinct ozonated crude oils (ANS, ARAB, and SJV) for the germination of three seeds (Grass, Lettuce, and Radish). The key finding from Chapter 5 was that radish (*Raphanus lativus* L.) germination was demonstrably affected by the presence of DOC, but not by the presence of remaining petroleum as TPH. These findings were critical in the identification of radish as an indicator species of oxidized petroleum residuals, a result that is greatly relevant to eco-toxicity assessments after petroleum clean-up. Moreover, the differences in radish germination among the oxidized residuals of three distinct crude oils (Chapter 5) were minimal, with only a slight increase in adverse germination effects of oxidized heavy crude oil, SJV. This is an important finding, since it shows that toxicity thresholds maybe broadly applicable among different crude oils when using radish as an indicator species.

The continuous measurements and the categorical variables allowed me to build a multiple logistic regression model of radish germination (in Chapter 5) to assess the relative toxicity of ozonation byproducts (measured as DOC), while controlling for variables like TPH concentration, crude oil type, organic background, and O_3 dose-level. The final model showed that, while absolute concentration of DOC could be used to draw boundaries for risk to germination, lower overall doses of O_3 yielded products that had greater effective toxicity. These results are corroborated by other studies that have shown toxic effect of ozonation of hydrocarbons increasing before they decrease with further oxidation.[139] Organic background content was important to attenuating toxic effects, while petroleum could be excluded from the model entirely. Establishing benchmark doses for adverse effects of oxidized petroleum hydrocarbon is a key step to field deployment of O_3 gas.

Another field concern addressed by this dissertation is O_3 transport within the soil column. For a static contacting scenario in which ozone is being pumped through a given volume of soil, the utilization of O_3 greatly depends on distance, especially at higher concentrations of O_3 as demonstrated in low, medium, and high loading rate experiments in Chapter 6. The use of three distinct doses for each of the three loading rates provided a timeline of O_3 reactivity across the column length. By looking at the spatial orientation of the reaction, I provided a visualization of reaction position with time. I demonstrated that a lower loading rate improved the efficiency of O_3 utilization and increased O_3-transport distance. These trends suggest that a lower loading rate favored oxidation reactions with TPH over secondary reactions with already oxidized intermediates. Alternatively, a higher loading rate increased oxidation reactions with organics outside the TPH range.

The low loading rate ([O_3] at 10,000 ppmv) was self-propagating in that heat was evolved from the reaction path and transported out of the column (~45cm); in other words, those columns experienced net cooling. Alternatively, the high loading experiments ([O_3] at 84,000 ppmv) were self-limiting as demonstrated by net heating. These studies demonstrate that maintaining a heat balance by taking advantage of the high latent heat of water can ensure that the reaction is maintained at a safe temperature (e.g., 35°C in low loading). The alternative is to risk a reaction, particularly at the distribution point, that undergoes a runaway heat spike. These results are relevant to scenarios in which O_3 may be deployed either to treat large batches of soil (e.g., 1000 m^3) in which gas would have to be contacted with bulk soil volumes or to amend already existing gas-based technologies for *in situ* soil treatment.

In conclusion, ozonation has the potential to be an important technology for remediating soils contaminated with residual crude oil, since O_3 is effective for removing substantial percentages petroleum hydrocarbon. However, the byproducts of ozonation pose ecological toxicity, and radish emerges as an important indicator species that is sensitive to oxidized byproducts but not sensitive to untreated petroleum. The risk of ecological toxicity underscores that importance of coupling ozonation with bioremediation, as the soluble products of ozonation are biodegradable.[83,84,98] The column studies show that O_3-transport distance, O_3-utilization efficiency, and heat/moisture balancing can be enhanced by using lower O_3-loading rates. This is particularly important to bioremediation settings when large volumes of soil must be contacted with O_3 gas over extended periods.

7.2 Potential for Field Deployment

This research lays the foundation for a practical means to optimize field deployment of O_3+bioremediation. The fundamental concept driving a field-practicable application is one in which ozone is delivered intermittently in a series of discrete applications that reduce TPH hydrophobicity and increase its biodegradability. Chen *et al.* showed how a multi-cycle approach can remove TPH and other organic carbon using sequence of biodegradation and ozonation.[98] In this treatment regimen, DOC becomes the dominant substrate for microbial consumption as the concentration of readily biodegradable TPH decreases. While O_3 treatment does not directly enhance the biodegradation rate of the residual TPH after ozonation, the conversion of TPH into DOC makes it possible to utilize microbial activity for greater overall TPH reductions.

One example of a treatment regimen is one in which O_3 generation takes advantage of a pulsed-injection technology applicable for *in-situ* and *ex-situ* applications. For example, pulsed-injection technology was initially developed by

Arizona State University as a low-cost, low-Operations and Maintenance (O&M) method for the treatment of dissolved-phase hydrocarbons in groundwater.[252,253] Pulsed injection enabled effective treatment and minimized infrastructure investment to successfully remediate hydrocarbon-contaminated groundwater in a large-scale (500-ft long, 250-injection well) biobarrier application in Port Hueneme, CA.[252] Translating the pulsed-injection technology into a treatment mechanism for soil containing residual weathered petroleum in the soil has great potential. The resulting technology could be utilized *in-situ* for large-scale treatment areas or *ex-situ* as a method to more quickly and more effectively treat stockpiled soils with weathered-petroleum residuals.

My research evaluates key concerns of field-scale deployment, such as a pulsed injection sequence. First, I show important advantages and disadvantages for using a high ozone loading rate versus a low loading rate. The application of a maximum O_3 concentration (10% v/v) over a short treatment time (i.e., a high loading rate) yielded the greatest reductions in TPH for points physically closest to the ozone distribution point. In contrast, applying the same dose of ozone using a lower concentration and longer reaction time (i.e., a low loading rate) enhanced the overall efficiency of O_3 utilization and distributed the reaction over a greater treatment volume. As such, a pulsed-injection scenario utilizing O_3 at the highest concentration (i.e., taking advantage of the maximum generator capacity) will require closely spaced injection points; on the other hand, delivery of O_3 at a lower concentration will improve spatial reach and utilization efficiency requiring fewer wells and treating larger soil volumes.

For *ex situ* settings like land farms or biopiles, the pulsed injection approach may be coupled to gas-extraction wells to aid in containing and distributing O_3 gas, as well as improving timeframes for bioremediation post-contact with O_3. Soil-gas extraction has been in use for decades as a cost-effective and relatively low-tech strategy for the removal of volatile or semi-volatile contaminants from the vadose zone, where it is termed soil vapor extraction (SVE).[229,254,255] In attempting to remediate heavy weathered crude oil, which is low in volatile elements, SVE is not utilized as a remediation tool. Instead, gas-extraction wells can be used to create a closed injection loop through the subsurface without the need for full containment infrastructure, thereby eliminating the possibility of escaping O_3. This may be especially useful in low-loading rate scenarios which have proven effluent discharge. Extracted gas can also be monitored for effluent O_3 creating an effective and simple way to determine that O_3 consumption is nearing completion for a given dosing sequence. After a pulse of O_3 is passed through the treatment radius, the pulsed-injection system can be used to introduce air into the treatment zone to meet the minimum needs of aerobic biodegradation *in situ*, or can take the place of tilling in an *ex situ* land-farming scenario.[83,84,98]

My research provides a picture of the trends in the reaction profile in the direction of gas flow in soil columns. It also outlines a risk management strategy for periods between ozonation and biodegradation. Here, I show minimum distances for treatment, the profile of TPH reduction along the O_3 reaction path, the transfer of heat and the movement of water in the direction of gas flow, all as functions of loading rate and dose. I also demonstrate that, if biodegradation is not completed, the ecological risk of oxidized residuals may be monitored by the impacts on radish germination. Taken together, my loading-rate experiments help determine the O_3-application strategy, and my risk-assessment model can be utilized to manage risks associated with the generation of oxidized petroleum byproducts.

7.3 Future Research

The plateau of O_3 utilization during petroleum treatment must be better understood, especially for *in situ* scenarios. At the molecular scale, this may be understood as a function of the molecular scale transport and reactivity of O_3 at the soil-petroleum interface. While some authors describe agglomerated petroleum particles, it is more likely that petroleum spreads and coats soil surfaces, creating non-aqueous phase liquid (NAPL) on a microscopic scale.[256,257] Asphaltenes and resins stack toward to soil minerals.[160,258] A molecular simulation by Wu et al. showed that the most likely oil distribution on quartz surface was a complex of asphaltenes surrounded by resins, into and out which transported aromatics and saturates. [160] If O_3 transport is limited by the diffusion across a NAPL layer, advanced imaging technologies -- like scanning electron microscopy, spectroscopy of sorbed O_3, or molecular simulations -- may be helpful to determine the nature of the layer.[256,259,260]

Studies of O_3 reactivity would be greatly aided by measuring hydroxyl radical production directly. The quantitation of radical activity is particularly important for detecting a shift in chemistry from hydroxyl radical attack to direct O_3 attack. While heat measurements showed an increase in absolute heat production in high loading experiments, this finding was not directly linked to a relative decrease in radical activity in favor of direct O_3 attack. The production of hydroxyl radicals can be tested indirectly by measuring the production of hydroxyl-radical adducts to petroleum hydrocarbons through the use of chemical derivatization and then measurement with high-performance liquid chromatography linked mass spectrometry.[132,248,261,262] Other techniques include direct measurement using liquid chromatography with electrochemical detection and mass spectrometry, gas chromatography with mass spectrometry, capillary electrophoresis, electron spin resonance and chemiluminescence.[263]

Advanced methods for total hydrocarbon characterization are necessary to go beyond the analysis of saturates, aromatics, resins, and asphaltenes (SARA). The fractions of crude oil that may be reacting O_3 may change significantly based on overall composition and dynamically as the reaction of O_3 oxygenates larger molecular groups.[258] Physical approaches take advantage of dominating affects like solubility in solvents of differing polarity. Dichloromethane was used in this dissertation, but this solvent did not capture the initial or changing composition of asphaltenes and resins. For instance, thin layer chromatography with flame ionization detector (TLC/FID) has been shown to be a sensitive indicator of compositional changes of coal derived liquids and may be applicable to the changing composition of petroleum contamination after contacting with O_3 gas.[29]

Once the characteristics of O_3 diffusion at the NAPL surface and the reaction of O_3 with the complete crude oil matrix are better characterized, experimental and theoretical analysis of O_3 transport in the soil column will be much better understood. While this dissertation explored greater distances than reported elsewhere, it did not ascertain a fundamental limit for O_3 transport and reactivity along the macroscopic scale. Typical soil vapor extraction (SVE) technologies, for instance, can operate from 15 to 100 feet between injection wells.[228,265] At the lower limit, this is 10 times the distance explored here. Hence, building a theoretical and empirical knowledge base of O_3 transport will be key before the technology could be recommended on a large scale. Detailed techno-economic analysis would also be of high value as a means to integrate advancements on the molecular scale and the industrial scale.

BIBLIOGRAPHY

(1) Barret, C.; Bosoni, T.; Garcimartin, M.; Kloss, A.; Lejuene, O.; Mackey, P.; Petrosyan, K.; Yarita, M. *Oil 2020 Analysis and Forecast to 2025*; International Energy Agency / OECD: 75739 Paris Cedex 15 France, 2020.

(2) Robin, R.; Thomson, L.; De Luca, F. *Oil Information Statistics 2017*; 2017 Edition; International Energy Agency / OECD: 75739 Paris Cedex 15, France.

(3) BP. *Statistical Review of World Energy 2020*; 69th Edition; London, United Kingdom.

(4) Venosa, A. D.; Campo, P.; Suidan, M. T. Biodegradability of Lingering Crude Oil 19 Years after the Exxon Valdez Oil Spill. *Environ. Sci. Technol.* **2010**, *44* (19), 7613–7621. https://doi.org/10.1021/es101042h.

(5) Incardona, J. P.; Swarts, T. L.; Edmunds, R. C.; Linbo, T. L.; Aquilina-Beck, A.; Sloan, C. A.; Gardner, L. D.; Block, B. A.; Scholz, N. L. Exxon Valdez to Deepwater Horizon: Comparable Toxicity of Both Crude Oils to Fish Early Life Stages. *Aquatic Toxicology* **2013**, *142–143*, 303–316. https://doi.org/10.1016/j.aquatox.2013.08.011.

(6) Granitz, E.; Klein, B. Monopolization by "Raising Rivals' Costs": The Standard Oil Case. *The Journal of Law and Economics* **1996**, *39* (1), 1–47. https://doi.org/10.1086/467342.

(7) Marshall, A. G.; Rodgers, R. P. Petroleomics: Chemistry of the Underworld. *PNAS* **2008**, *105* (47), 18090–18095. https://doi.org/10.1073/pnas.0805069105.

(8) Tissot, B. P.; Welte, D. H. *Petroleum Formation and Occurrence*; Springer Science & Business Media, 2013.

(9) Marshall, A. G.; Rodgers, R. P. Petroleomics: The Next Grand Challenge for Chemical Analysis. *Acc. Chem. Res.* **2004**, *37* (1), 53–59. https://doi.org/10.1021/ar020177t.

(10) Gaweł, B.; Eftekhardadkhah, M.; Øye, G. Elemental Composition and Fourier Transform Infrared Spectroscopy Analysis of Crude Oils and Their Fractions. *Energy Fuels* **2014**, *28* (2), 997–1003. https://doi.org/10.1021/ef402286y.

(11) Fahim, M. A.; Alsahhaf, T. A.; Elkilani, A. Chapter 2 - Refinery Feedstocks and Products. In *Fundamentals of Petroleum Refining*; Fahim, M. A., Alsahhaf, T. A., Elkilani, A., Eds.; Elsevier: Amsterdam, 2010; pp 11–31. https://doi.org/10.1016/B978-0-444-52785-1.00002-4.

(12) Wentzel, A.; Ellingsen, T. E.; Kotlar, H.-K.; Zotchev, S. B.; Throne-Holst, M. Bacterial Metabolism of Long-Chain n-Alkanes. *Appl Microbiol Biotechnol* **2007**, *76* (6), 1209–1221. https://doi.org/10.1007/s00253-007-1119-1.

(13) Sanfilippo, D.; Miracca, I.; Di Girolamo, M. Engineering Alkanes to Olefins and Higher Value Chemicals. In *Sustainable Strategies for the Upgrading of Natural Gas: Fundamentals, Challenges, and Opportunities*; Derouane, E. G., Parmon, V., Lemos, F., Ramôa Ribeiro, F., Eds.; NATO Science Series II: Mathematics, Physics and Chemistry; Springer Netherlands: Dordrecht, 2005; pp 217–247. https://doi.org/10.1007/1-4020-3310-9_11.

(14) Bixon, M.; Lifson, S. Potential Functions and Conformations in Cycloalkanes. *Tetrahedron* **1967**, *23* (2), 769–784. https://doi.org/10.1016/0040-4020(67)85023-3.

(15) Rücker, G.; Rücker, C. On Topological Indices, Boiling Points, and Cycloalkanes. *J. Chem. Inf. Comput. Sci.* **1999**, *39* (5), 788–802. https://doi.org/10.1021/ci9900175.

(16) Seifert, W. K.; Michael Moldowan, J. Applications of Steranes, Terpanes and Monoaromatics to the Maturation, Migration and Source of Crude Oils. *Geochimica et Cosmochimica Acta* **1978**, *42* (1), 77–95. https://doi.org/10.1016/0016-7037(78)90219-3.

(17) Venosa, A. D.; Suidan, M. T.; King, D.; Wrenn, B. A. Use of Hopane as a Conservative Biomarker for Monitoring the Bioremediation Effectiveness of Crude Oil Contaminating a Sandy Beach. *J Ind Microbiol Biotech* **1997**, *18* (2–3), 131–139. https://doi.org/10.1038/sj.jim.2900304.

(18) Yin, F.; John, G. F.; Hayworth, J. S.; Clement, T. P. Long-Term Monitoring Data to Describe the Fate of Polycyclic Aromatic Hydrocarbons in Deepwater Horizon Oil Submerged off Alabama's Beaches. *Science of The Total Environment* **2015**, *508*, 46–56. https://doi.org/10.1016/j.scitotenv.2014.10.105.

(19) Reed, W. Molecular Compositions of Weathered Petroleum and Comparison with Its Possible Source. *Geochimica et Cosmochimica Acta* **1977**, *41* (2), 237–247. https://doi.org/10.1016/0016-7037(77)90231-9.

(20) Sadeghbeigi, R. Chapter 3 - FCC Feed Characterization. In *Fluid Catalytic Cracking Handbook (Third Edition)*; Sadeghbeigi, R., Ed.; Butterworth-Heinemann: Oxford, 2012; pp 51–86. https://doi.org/10.1016/B978-0-12-386965-4.00003-3.

(21) McNaught, A. D.; Wilkinson, A. *Compendium of Chemical Terminology*, 2nd edition.; Wiley: Oxford England ; Malden, MA, USA, 1997.

(22) Kissin, Y. V. Catagenesis and Composition of Petroleum: Origin of n-Alkanes and Isoalkanes in Petroleum Crudes. *Geochimica et Cosmochimica Acta* **1987**, *51* (9), 2445–2457. https://doi.org/10.1016/0016-7037(87)90296-1.

(23) Zhang, L.; Xu, Z.; Shi, Q.; Sun, X.; Zhang, N.; Zhang, Y.; Chung, K. H.; Xu, C.; Zhao, S. Molecular Characterization of Polar Heteroatom Species in Venezuela Orinoco Petroleum Vacuum Residue and Its Supercritical Fluid Extraction Subfractions. *Energy Fuels* **2012**, *26* (9), 5795–5803. https://doi.org/10.1021/ef3009663.

(24) Shi, Q.; Hou, D.; Chung, K. H.; Xu, C.; Zhao, S.; Zhang, Y. Characterization of Heteroatom Compounds in a Crude Oil and Its Saturates, Aromatics, Resins, and Asphaltenes (SARA) and Non-Basic Nitrogen Fractions Analyzed by Negative-Ion Electrospray Ionization Fourier Transform Ion Cyclotron Resonance Mass Spectrometry. *Energy Fuels* **2010**, *24* (4), 2545–2553. https://doi.org/10.1021/ef901564e.

(25) Mullins, O. Rebuttal to Comment by Professors Herod, Kandiyoti, and Bartle on “Molecular Size and Weight of Asphaltene and Asphaltene Solubility Fractions from Coals, Crude Oils and Bitumen.” *Fuel* **2007**, *86*, 309–312. https://doi.org/10.1016/j.fuel.2006.05.030.

(26) Badre, S.; Carla Goncalves, C.; Norinaga, K.; Gustavson, G.; Mullins, Oliver. C. Molecular Size and Weight of Asphaltene and Asphaltene Solubility Fractions from Coals, Crude Oils and Bitumen. *Fuel* **2006**, *85* (1), 1–11. https://doi.org/10.1016/j.fuel.2005.05.021.

(27) Groenzin, H.; Mullins, O. C. Molecular Size and Structure of Asphaltenes from Various Sources. *Energy Fuels* **2000**, *14* (3), 677–684. https://doi.org/10.1021/ef990225z.

(28) Elkahky, S.; Lagat, C.; Sarmadivaleh, M.; Barifcani, A. A Comparative Study of Density Estimation of Asphaltene Structures Using Group Contribution Methods and Molecular Dynamic Simulations for an Australian Oil Field. *J Petrol Explor Prod Technol* **2019**, *9* (4), 2699–2708. https://doi.org/10.1007/s13202-019-0641-x.

(29) K. D. Mannistu; H. W. Yarranton, and; Masliyah*, J. H. *Solubility Modeling of Asphaltenes in Organic Solvents*. http://pubs.acs.org/doi/abs/10.1021/ef9601879 (accessed 2020-11-11). https://doi.org/10.1021/ef9601879.

(30) Aguiar, J. I. S.; Neto, J. S. G.; Almeida, S. M.; Mansur, C. R. E. Evaluation of the Influence of Polyoxide-Based Surfactants on the Separation Process of Model Emulsions of Asphaltenes Using the FTIR-ATR Technique. *Journal of Applied Polymer Science* **2013**, *128* (3), 1390–1397. https://doi.org/10.1002/app.38292.

(31) Sharma, B.; Sharma, C.; Tyagi, O. S.; Bhagat, D.; Erhan, S. Structural Characterization of Asphaltenes and Ethyl Acetate Insoluble Fractions of Petroleum Vacuum Residues. *Petroleum Science and Technology* **2007**, *25*. https://doi.org/10.1080/10916460601054263.

(32) Klein, G. C.; Angström, A.; Rodgers, R. P.; Marshall, A. G. Use of Saturates/Aromatics/Resins/Asphaltenes (SARA) Fractionation to Determine Matrix Effects in Crude Oil Analysis by Electrospray Ionization Fourier Transform Ion Cyclotron Resonance Mass Spectrometry. *Energy Fuels* **2006**, *20* (2), 668–672. https://doi.org/10.1021/ef050353p.

(33) Fernandez-Lima, F. A.; Becker, C.; McKenna, A. M.; Rodgers, R. P.; Marshall, A. G.; Russell, D. H. Petroleum Crude Oil Characterization by IMS-MS and FTICR MS. *Anal. Chem.* **2009**, *81* (24), 9941–9947. https://doi.org/10.1021/ac901594f.

(34) Cui, D.; Wang, Q.; Wang, Z. C.; Liu, Q.; Pan, S.; Bai, J.; Liu, B. Compositional Analysis of Heteroatom Compounds in Huadian Shale Oil Using Various Analytical Techniques. *Energy & Fuels* **2019**. https://doi.org/10.1021/acs.energyfuels.8b03889.

(35) Zhang, H.; Ji, L.; Wu, F.; Tan, J. In Situ Ozonation of Anthracene in Unsaturated Porous Media. *Journal of Hazardous Materials* **2005**, *120* (1), 143–148. https://doi.org/10.1016/j.jhazmat.2004.12.019.

(36) Fingas, M. Oil and Petroleum Evaporation. In *Handbook of Oil Spill Science and Technology*; John Wiley & Sons, Ltd, 2014; pp 205–223. https://doi.org/10.1002/9781118989982.ch7.

(37) Studies on the Evaporation of Crude Oil and Petroleum Products: I. the Relationship between Evaporation Rate and Time. *Journal of Hazardous Materials* **1997**, *56* (3), 227–236. https://doi.org/10.1016/S0304-3894(97)00050-2.

(38) Yim, U. H.; Ha, S. Y.; An, J. G.; Won, J. H.; Han, G. M.; Hong, S. H.; Kim, M.; Jung, J.-H.; Shim, W. J. Fingerprint and Weathering Characteristics of Stranded Oils after the Hebei Spirit Oil Spill. *Journal of Hazardous Materials* **2011**, *197*, 60–69. https://doi.org/10.1016/j.jhazmat.2011.09.055.

(39) Marty, G. D.; Hose, J. E.; McGurk, M.; Brown, E.; Hinton, D. Histopathology and Cytogenetic Evaluation of Pacific Herring Larvae Exposed to Petroleum Hydrocarbons in the Laboratory or in Prince William Sound, Alaska, after the Exxon Valdez Oil Spill. *Canadian Journal of Fisheries and Aquatic Sciences* **2011**, *54*, 1846–1857. https://doi.org/10.1139/cjfas-54-8-1846.

(40) Marty, G. D.; Hinton, D. E.; Short, J. W.; Heintz, R. A.; Rice, S. D.; Dambach, D. M.; Willits, N. H.; Stegeman, J. J. Ascites, Premature Emergence, Increased Gonadal Cell Apoptosis, and Cytochrome P4501A Induction in Pink Salmon Larvae Continuously Exposed to Oil-Contaminated Gravel during Development. *Can. J. Zool.* **1997**, *75* (6), 989–1007. https://doi.org/10.1139/z97-120.

(41) Carls, M. G.; Rice, S. D.; Hose, J. E. Sensitivity of Fish Embryos to Weathered Crude Oil: Part I. Low-Level Exposure during Incubation Causes Malformations, Genetic Damage, and Mortality in Larval Pacific Herring (Clupea Pallasi). *Environmental Toxicology and Chemistry* **1999**, *18* (3), 481–493. https://doi.org/10.1002/etc.5620180317.

(42) Incardona, J. P.; Collier, T. K.; Scholz, N. L. Defects in Cardiac Function Precede Morphological Abnormalities in Fish Embryos Exposed to Polycyclic Aromatic Hydrocarbons. *Toxicol. Appl. Pharmacol.* **2004**, *196* (2), 191–205. https://doi.org/10.1016/j.taap.2003.11.026.

(43) Bobra, M. *A Study of the Evaporation of Petroleum Oils*; K1N 8E3; Environment Canada: Ottawa, Ontario, 1992.

(44) Studies on the Evaporation of Crude Oil and Petroleum Products II. Boundary Layer Regulation. *Journal of Hazardous Materials* **1998**, *57* (1–3), 41–58. https://doi.org/10.1016/S0304-3894(97)00051-4.

(45) Maki, H.; Sasaki, T.; Harayama, S. Photo-Oxidation of Biodegraded Crude Oil and Toxicity of the Photo-Oxidized Products. *Chemosphere* **2001**, *44* (5), 1145–1151. https://doi.org/10.1016/S0045-6535(00)00292-7.

(46) Yu, H.; Xia, Q.; Yan, J.; Herreno-Saenz, D.; Wu, Y.-S.; Tang, I.-W.; Fu, P. P. Photoirradiation of Polycyclic Aromatic Hydrocarbons with UVA Light – A Pathway Leading to the Generation of Reactive Oxygen Species, Lipid Peroxidation, and DNA Damage. *Int J Environ Res Public Health* **2006**, *3* (4), 348–354.

(47) Barron, M. G. Photoenhanced Toxicity of Petroleum to Aquatic Invertebrates and Fish. *Arch Environ Contam Toxicol* **2017**, *73* (1), 40–46. https://doi.org/10.1007/s00244-016-0360-y.

(48) Barron, M. G.; Carls, M. G.; Short, J. W.; Rice, S. D. Photoenhanced Toxicity of Aqueous Phase and Chemically Dispersed Weathered Alaska North Slope Crude Oil to Pacific Herring Eggs and Larvae. *Environ. Toxicol. Chem.* **2003**, *22* (3), 650–660.

(49) Yu, D.-Y.; Kang, N.; Bae, W.; Banks, M. K. Characteristics in Oxidative Degradation by Ozone for Saturated Hydrocarbons in Soil Contaminated with

Diesel Fuel. *Chemosphere* **2007**, *66* (5), 799–807. https://doi.org/10.1016/j.chemosphere.2006.06.053.

(50) Styler, S. A.; Loiseaux, M.-E.; Donaldson, D. J. Substrate Effects in the Photoenhanced Ozonation of Pyrene. *Atmospheric Chemistry and Physics* **2011**, *11* (3), 1243–1253. https://doi.org/10.5194/acp-11-1243-2011.

(51) Petroleum Biodegradation and Oil Spill Bioremediation. *Marine Pollution Bulletin* **1995**, *31* (4–12), 178–182. https://doi.org/10.1016/0025-326X(95)00113-2.

(52) Fingas, M. Chapter 15 - Deepwater Horizon Well Blowout Mass Balance. In *Oil Spill Science and Technology (Second Edition)*; Fingas, M., Ed.; Gulf Professional Publishing: Boston, 2017; pp 805–849. https://doi.org/10.1016/B978-0-12-809413-6.00015-1.

(53) Prince, R. C.; Garrett, R. M.; Bare, R. E.; Grossman, M. J.; Townsend, T.; Suflita, J. M.; Lee, K.; Owens, E. H.; Sergy, G. A.; Braddock, J. F.; Lindstrom, J. E.; Lessard, R. R. The Roles of Photooxidation and Biodegradation in Long-Term Weathering of Crude and Heavy Fuel Oils. *Spill Science & Technology Bulletin* **2003**, *8* (2), 145–156. https://doi.org/10.1016/S1353-2561(03)00017-3.

(54) Leahy, J. G.; Colwell, R. R. Microbial Degradation of Hydrocarbons in the Environment. *Microbiol. Rev.* **1990**, *54* (3), 305–315.

(55) Atlas, R. M. Microbial Degradation of Petroleum Hydrocarbons: An Environmental Perspective. *Microbiol Rev* **1981**, *45* (1), 180–209.

(56) Caldwell, M. E.; Garrett, R. M.; Prince, R. C.; Suflita, J. M. Anaerobic Biodegradation of Long-Chain n-Alkanes under Sulfate-Reducing Conditions. *Environ. Sci. Technol.* **1998**, *32* (14), 2191–2195. https://doi.org/10.1021/es9801083.

(57) Atlas, R. M. Petroleum Microbiology. **1984**.

(58) Pritchard, P. H. Bioremediation of Oil Contaminated Beach Material in Prince William Sound, Alaska. *American Chemical Society, Division of Environmental Chemistry, Preprints; (USA)* **1990**, *30:1*.

(59) Hinchee, R. E.; Leeson, A. *Soil Bioventing: Principles and Practice*; CRC Press, 1996.

(60) U.S. Environmental Protection Agency. *Groundwater Issue: Light Nonaqueous Phase Liquids*; Groundwater Forum; EPA/540/S-95/500; Superfund Technology Support Center for Ground Water: Ada, Oklahoma, 1995.

(61) Mayer, A. *Soil and Groundwater Contamination: Nonaqueous Phase Liquids, Principles and Observations*; American Geophysical Union, 2005.

(62) Yao, Y.; Wu, Y.; Wang, Y.; Verginelli, I.; Zeng, T.; Suuberg, E. M.; Jiang, L.; Wen, Y.; Ma, J. A Petroleum Vapor Intrusion Model Involving Upward Advective Soil Gas Flow Due to Methane Generation. *Environ. Sci. Technol.* **2015**, *49* (19), 11577–11585. https://doi.org/10.1021/acs.est.5b01314.

(63) Curtis, F.; Lammey, J. Intrinsic Remediation of a Diesel Fuel Plume in Goose Bay, Labrador, Canada. *Environmental Pollution* **1998**, *103* (2–3), 203–210. https://doi.org/10.1016/S0269-7491(98)00126-2.

(64) Farwell, C.; Reddy, C. M.; Peacock, E.; Nelson, R. K.; Washburn, L.; Valentine, D. L. Weathering and the Fallout Plume of Heavy Oil from Strong Petroleum Seeps Near Coal Oil Point, CA. *Environ. Sci. Technol.* **2009**, *43* (10), 3542–3548. https://doi.org/10.1021/es802586g.

(65) Hernández-Espriú, A.; Martínez-Santos, P.; Sánchez-León, E.; Marín, L. E. Free-Product Plume Distribution and Recovery Modeling Prediction in a Diesel-Contaminated Volcanic Aquifer. *Physics and Chemistry of the Earth, Parts A/B/C* **2012**, *37–39*, 43–51. https://doi.org/10.1016/j.pce.2010.12.007.

(66) Sposito, G. Green Water and Global Food Security. *Vadose Zone Journal* **2013**, *12* (4), vzj2013.02.0041. https://doi.org/10.2136/vzj2013.02.0041.

(67) Sposito, G. *The Chemistry of Soils*; Oxford University Press, Inc.: New Yok, NY, 2008.

(68) Mekonnen, M. M.; Hoekstra, A. Y. The Green, Blue and Grey Water Footprint of Crops and Derived Crop Products. *ResearchGate* **2011**, *15* (5). https://doi.org/10.5194/hess-15-1577-2011.

(69) Milà i Canals, L.; Romanyà, J.; Cowell, S. J. Method for Assessing Impacts on Life Support Functions (LSF) Related to the Use of 'Fertile Land' in Life Cycle Assessment (LCA). *Journal of Cleaner Production* **2007**, *15* (15), 1426–1440. https://doi.org/10.1016/j.jclepro.2006.05.005.

(70) Koellner, T.; Baan, L.; Beck, T.; Brandão, M.; Civit, B.; Margni, M.; Canals, L. M.; Saad, R.; Souza, D. M.; Müller-Wenk, R. UNEP-SETAC Guideline on Global Land Use Impact Assessment on Biodiversity and Ecosystem Services in LCA. *Int J Life Cycle Assess* **2013**, *18* (6), 1188–1202. https://doi.org/10.1007/s11367-013-0579-z.

(71) Abdel-Shafy, H. I.; Mansour, M. S. M. A Review on Polycyclic Aromatic Hydrocarbons: Source, Environmental Impact, Effect on Human Health and

Remediation. *Egyptian Journal of Petroleum* **2016**, *25* (1), 107–123. https://doi.org/10.1016/j.ejpe.2015.03.011.

(72) Brewer, R.; Nagashima, J.; Kelley, M.; Heskett, M.; Rigby, M. Risk-Based Evaluation of Total Petroleum Hydrocarbons in Vapor Intrusion Studies. *International Journal of Environmental Research and Public Health* **2013**, *10* (6), 2441–2467. https://doi.org/10.3390/ijerph10062441.

(73) Incardona, J. P.; Carls, M. G.; Teraoka, H.; Sloan, C. A.; Collier, T. K.; Scholz, N. L. Aryl Hydrocarbon Receptor-Independent Toxicity of Weathered Crude Oil during Fish Development. *Environ. Health Perspect.* **2005**, *113* (12), 1755–1762. https://doi.org/10.1289/ehp.8230.

(74) Di Toro, D. M.; McGrath, J. A.; Stubblefield, W. A. Predicting the Toxicity of Neat and Weathered Crude Oil: Toxic Potential and the Toxicity of Saturated Mixtures. *Environ. Toxicol. Chem.* **2007**, *26* (1), 24–36. https://doi.org/10.1897/06174r.1.

(75) Williams, S. D.; Ladd, D. E.; Farmer, J. *Fate and Transport of Petroleum Hydrocarbons in Soil and Ground Water at Big South Fork National River and Recreation Area, Tennessee and Kentucky, 2002-2003*; Scientific Investigations Report; USGS Numbered Series 2005–5104; 2006; Vol. 2005–5104, p 34. https://doi.org/10.3133/sir20055104.

(76) Michel, J.; Owens, E. H.; Zengel, S.; Graham, A.; Nixon, Z.; Allard, T.; Holton, W.; Reimer, P. D.; Lamarche, A.; White, M.; Rutherford, N.; Childs, C.; Mauseth, G.; Challenger, G.; Taylor, E. Extent and Degree of Shoreline Oiling: Deepwater Horizon Oil Spill, Gulf of Mexico, USA. *PLOS ONE* **2013**, *8* (6), e65087. https://doi.org/10.1371/journal.pone.0065087.

(77) Burgherr, P. In-Depth Analysis of Accidental Oil Spills from Tankers in the Context of Global Spill Trends from All Sources. *Journal of Hazardous Materials* **2007**, *140* (1), 245–256. https://doi.org/10.1016/j.jhazmat.2006.07.030.

(78) Braddock, J. F.; Lindstrom, J. E.; Prince, R. C. Weathering of a Subarctic Oil Spill over 25 Years: The Caribou-Poker Creeks Research Watershed Experiment. *Cold Regions Science and Technology* **2003**, *36* (1–3), 11–23. https://doi.org/10.1016/S0165-232X(02)00076-9.

(79) de Jong, E. The Effect of a Crude Oil Spill on Cereals. *Environmental Pollution Series A, Ecological and Biological* **1980**, *22* (3), 187–196. https://doi.org/10.1016/0143-1471(80)90013-6.

(80) Barron, M. G.; Vivian, D. N.; Heintz, R. A.; Yim, U. H. Long-Term Ecological Impacts from Oil Spills: Comparison of Exxon Valdez, Hebei Spirit, and

Deepwater Horizon. *Environ. Sci. Technol.* **2020**, *54* (11), 6456–6467. https://doi.org/10.1021/acs.est.9b05020.

(81) Loehr, R. C.; Webster, M. T.; Smith, J. R. Fate of Treated and Weathered Hydrocarbons in Soil—Long-Term Changes. *Practice Periodical of Hazardous, Toxic, and Radioactive Waste Management* **2000**, *4* (2), 53–59. https://doi.org/10.1061/(ASCE)1090-025X(2000)4:2(53).

(82) Jolliet, O.; Margni, M.; Charles, R.; Humbert, S.; Payet, J.; Rebitzer, G.; Rosenbaum, R. IMPACT 2002+: A New Life Cycle Impact Assessment Methodology. *Int J LCA* **2003**, *8* (6), 324. https://doi.org/10.1007/BF02978505.

(83) Chen, T.; Delgado, A. G.; Yavuz, B. M.; Proctor, A. J.; Maldonado, J.; Zuo, Y.; Westerhoff, P.; Krajmalnik-Brown, R.; Rittmann, B. E. Ozone Enhances Biodegradability of Heavy Hydrocarbons in Soil. *J. Environ. Eng. Sci.* **2016**, *11* (1), 7–17. https://doi.org/10.1680/jenes.16.00002.

(84) Chen, T.; Delgado, A. G.; Yavuz, B. M.; Maldonado, J.; Zuo, Y.; Kamath, R.; Westerhoff, P.; Krajmalnik-Brown, R.; Rittmann, B. E. Interpreting Interactions between Ozone and Residual Petroleum Hydrocarbons in Soil. *Environ. Sci. Technol.* **2017**, *51* (1), 506–513. https://doi.org/10.1021/acs.est.6b04534.

(85) Cheng, M.; Zeng, G.; Huang, D.; Lai, C.; Xu, P.; Zhang, C.; Liu, Y. Hydroxyl Radicals Based Advanced Oxidation Processes (AOPs) for Remediation of Soils Contaminated with Organic Compounds: A Review. *Chemical Engineering Journal* **2016**, *284*, 582–598. https://doi.org/10.1016/j.cej.2015.09.001.

(86) Brown, R. A.; Hinchee, R. E.; Norris, R. D.; Wilson, J. T. Bioremediation of Petroleum Hydrocarbons: A Flexible, Variable Speed Technology. *Remediation Journal* **1996**, *6* (3), 95–109. https://doi.org/10.1002/rem.3440060308.

(87) Danh, L. T.; Truong, P.; Mammucari, R.; Tran, T.; Foster, N. Vetiver Grass, Vetiveria Zizanioides: A Choice Plant for Phytoremediation of Heavy Metals and Organic Wastes. *Int J Phytoremediation* **2009**, *11* (8), 664–691. https://doi.org/10.1080/15226510902787302.

(88) Merkl, N.; Schultze-Kraft, R.; Infante, C. Assessment Of Tropical Grasses And Legumes For Phytoremediation Of Petroleum-Contaminated Soils. *Water Air Soil Pollut* **2005**, *165* (1–4), 195–209. https://doi.org/10.1007/s11270-005-4979-y.

(89) Davies, B. E. Radish as an Indicator Plant for Derelict Land: Uptake of Zinc at Toxic Concentrations. *Communications in Soil Science and Plant Analysis* **1993**, *24* (15–16), 1883–1895. https://doi.org/10.1080/00103629309368925.

(90) Chung, H. S.; Lee, Y.-J.; Rahman, Md. M.; Abd El-Aty, A. M.; Lee, H. S.; Kabir, Md. H.; Kim, S. W.; Park, B.-J.; Kim, J.-E.; Hacımüftüoğlu, F.; Nahar, N.; Shin,

H.-C.; Shim, J.-H. Uptake of the Veterinary Antibiotics Chlortetracycline, Enrofloxacin, and Sulphathiazole from Soil by Radish. *Sci. Total Environ.* **2017**, *605–606*, 322–331. https://doi.org/10.1016/j.scitotenv.2017.06.231.

(91) Banks, M. K.; Schultz, K. E. Comparison of Plants for Germination Toxicity Tests in Petroleum-Contaminated Soils. *Water Air Soil Pollut.* **2005**, *167* (1–4), 211–219. https://doi.org/10.1007/s11270-005-8553-4.

(92) Angiolini, C.; Bonari, G.; Landi, M. Focal Plant Species and Soil Factors in Mediterranean Coastal Dunes: An Undisclosed Liaison? *Estuarine, Coastal and Shelf Science* **2018**, *211*, 248–258. https://doi.org/10.1016/j.ecss.2017.06.001.

(93) Sarma, H.; Islam, N. F.; Prasad, M. N. V. Plant-Microbial Association in Petroleum and Gas Exploration Sites in the State of Assam, North-East India—Significance for Bioremediation. *Environ Sci Pollut Res* **2017**, *24* (9), 8744–8758. https://doi.org/10.1007/s11356-017-8485-8.

(94) Tissot, B. P.; Welte, D. H. Composition of Crude Oils. In *Petroleum Formation and Occurrence: A New Approach to Oil and Gas Exploration*; Tissot, B. P., Welte, D. H., Eds.; Springer: Berlin, Heidelberg, 1978; pp 333–368. https://doi.org/10.1007/978-3-642-96446-6_19.

(95) Maila, M. P.; Cloete, T. E. Bioremediation of Petroleum Hydrocarbons through Landfarming: Are Simplicity and Cost-Effectiveness the Only Advantages? *Rev Environ Sci Biotechnol* **2004**, *3* (4), 349–360. https://doi.org/10.1007/s11157-004-6653-z.

(96) Walworth, J. L.; Reynolds, M. C.; Rutter, A.; Snape, I. Landfarming. In *Bioremediation of Petroleum Hydrocarbons in Cold Regions*; Cambridge University Press, 2008; Vol. 9780521869706, pp 170–189. https://doi.org/10.1017/CBO9780511535956.010.

(97) Batakliev, T.; Georgiev, V.; Anachkov, M.; Rakovsky, S.; Zaikov, G. E. Ozone Decomposition. *Interdiscip Toxicol* **2014**, *7* (2), 47–59. https://doi.org/10.2478/intox-2014-0008.

(98) Chen, T.; Yavuz, B. M.; Delgado, A. G.; Januszewski, B.; Zuo, Y.; Westerhoff, P.; Krajmalnik-Brown, R.; Rittmann, B. E. Multicycle Ozonation+Bioremediation for Soils Containing Residual Petroleum. *Environmental Engineering Science* **2019**, *36* (12), 1443–1451. https://doi.org/10.1089/ees.2019.0195.

(99) Chen, T.; Yavuz, B. M.; Delgado, A. G.; Montoya, G.; Winkle, D. V.; Zuo, Y.; Kamath, R.; Westerhoff, P.; Krajmalnik-Brown, R.; Rittmann, B. E. Impacts of Moisture Content during Ozonation of Soils Containing Residual Petroleum.

Journal of Hazardous Materials **2018**, *344*, 1101–1108. https://doi.org/10.1016/j.jhazmat.2017.11.060.

(100) Rubin, M. B. The History of Ozone Part I: The Schönbein Period, 1839-1868. *Bull. Hist. Chem.* **2001**, *26* (1), 17.

(101) Razumovskii, S. D.; Zaikov, G. E. *Ozone and Its Reactions with Organic Compounds*; Elsevier Science Publishers B.V.: Amsterdam, 1984.

(102) Loeb, B. L.; Thompson, C. M.; Drago, J.; Takahara, H.; Baig, S. Worldwide Ozone Capacity for Treatment of Drinking Water and Wastewater: A Review. *Ozone: Science & Engineering* **2012**, *34* (1), 64–77. https://doi.org/10.1080/01919512.2012.640251.

(103) Luo, X.; Wang, R.; Wang, L.; Li, Y.; Bian, Y.; Chen, Z. Effect of Ozone Treatment on Aflatoxin B1 and Safety Evaluation of Ozonized Corn. *Food Control* **2014**, *37*, 171–176. https://doi.org/10.1016/j.foodcont.2013.09.043.

(104) Steenstrup, L. D.; Floros, J. D. Inactivation of E. Coli 0157:H7 in Apple Cider by Ozone at Various Temperatures and Concentrations. *Journal of Food Processing and Preservation* **2004**, *28* (2), 103–116. https://doi.org/10.1111/j.1745-4549.2004.tb00814.x.

(105) Rubin, M. B. The History of Ozone Part III: C. D. Harries and the Introduction of Ozone into Organic Chemistry. *Helvetica Chimica Acta* **2003**, *86* (4), 930–940. https://doi.org/10.1002/hlca.200390111.

(106) Brown, C.; Franson, K. D. Manometric Determination of the Density of Liquid Ozone. *J. Chem. Phys.* **1953**, *21* (5), 917–919. https://doi.org/10.1063/1.1699060.

(107) Brown, C.; Berger, A. W.; Hersh, C. K. Solid Ozone. *J. Chem. Phys.* **1954**, *22* (6), 1151–1152. https://doi.org/10.1063/1.1740311.

(108) Itoh, H.; Taguchi, M.; Suzuki, S. Thermal Decomposition of Ozone at High Temperature Leading to Ozone Zero Phenomena. *J. Phys. D: Appl. Phys.* **2020**, *53* (18), 185206. https://doi.org/10.1088/1361-6463/ab71a9.

(109) Suzuki, S.; Mitkov Rusinov, I.; Teranishi, K.; Shimomura, N.; Itoh, H. Re-Evaluation of Rate Coefficients for Ozone Decomposition by Oxygen in Wide Range of Gas Pressures (20-1000 Torr) and Temperatures (293-423 K). *Journal of Physics D Applied Physics* **2018**, *51*, 305201. https://doi.org/10.1088/1361-6463/aacd61.

(110) Koike, K.; Nifuku, M.; Izumi, K.; Nakamura, S.; Fujiwara, S.; Horiguchi, S. Explosion Properties of Highly Concentrated Ozone Gas. *Journal of Loss*

Prevention in the Process Industries **2005**, *18* (4), 465–468. https://doi.org/10.1016/j.jlp.2005.07.020.

(111) Rubin, M. The History of Ozone Part VI: Ozone on Silica Gel ("Dry Ozone"). *undefined* **2008**.

(112) Criegee, R. Mechanism of Ozonolysis. *Angewandte Chemie International Edition in English* **1975**, *14* (11), 745–752. https://doi.org/10.1002/anie.197507451.

(113) Hoops, M. D.; Ault, B. S. Matrix Isolation Study of the Early Intermediates in the Ozonolysis of Cyclopentene and Cyclopentadiene: Observation of Two Criegee Intermediates. *J. Am. Chem. Soc.* **2009**, *131* (8), 2853–2863. https://doi.org/10.1021/ja8065286.

(114) Bentley, K. W.; Kirby, G. W. *Elucidation of Organic Structures by Physical and Chemical Methods*; 1972.

(115) Deb, D. K.; Sarkar, B. Formation of Criegee Intermediates and Peroxy Acids: A Computational Study of Gas-Phase 1,3-Cycloaddition of Ozone with Catechol. *Phys. Chem. Chem. Phys.* **2019**, *21* (27), 14589–14597. https://doi.org/10.1039/C9CP01312A.

(116) A. Taatjes, C.; Welz, O.; J. Eskola, A.; D. Savee, J.; L. Osborn, D.; F. Lee, E. P.; M. Dyke, J.; K. Mok, D. W.; E. Shallcross, D.; J. Percival, C. Direct Measurement of Criegee Intermediate (CH 2 OO) Reactions with Acetone , Acetaldehyde , and Hexafluoroacetone. *Physical Chemistry Chemical Physics* **2012**, *14* (30), 10391–10400. https://doi.org/10.1039/C2CP40294G.

(117) Osborn, D. L.; Taatjes, C. A. The Physical Chemistry of Criegee Intermediates in the Gas Phase. *International Reviews in Physical Chemistry* **2015**, *34* (3), 309–360. https://doi.org/10.1080/0144235X.2015.1055676.

(118) Berndt, T.; Jokinen, T.; Mauldin, R. L.; Petäjä, T.; Herrmann, H.; Junninen, H.; Paasonen, P.; Worsnop, D. R.; Sipilä, M. Gas-Phase Ozonolysis of Selected Olefins: The Yield of Stabilized Criegee Intermediate and the Reactivity toward SO2. *J. Phys. Chem. Lett.* **2012**, *3* (19), 2892–2896. https://doi.org/10.1021/jz301158u.

(119) Feixas, F.; Matito, E.; Poater, J.; Solà, M. Understanding Conjugation and Hyperconjugation from Electronic Delocalization Measures. *J. Phys. Chem. A* **2011**, *115* (45), 13104–13113. https://doi.org/10.1021/jp205152n.

(120) Bailey, P. S. *Ozonation in Organic Chemistry, Volume II: Nonolefinic Compounds*; Academic Press: New York, NY, 1982.

(121) Kameda, T.; Asano, K.; Bandow, H.; Hayakawa, K. Estimation of Rate Constants for Gas-Phase Reactions of Chrysene, Benz[a]Anthracene, and Benzanthrone with OH and NO3 Radicals via a Relative Rate Method in CCl4 Liquid Phase-System. *Polycyclic Aromatic Compounds* **2017**, *37* (2–3), 101–105. https://doi.org/10.1080/10406638.2016.1159583.

(122) Alkorta, I.; Elguero, J. The Carbon–Carbon Bond Dissociation Energy as a Function of the Chain Length. *Chemical Physics Letters* **2006**, *425* (4), 221–224. https://doi.org/10.1016/j.cplett.2006.05.050.

(123) Wodrich, M. D.; McKee, W. C.; Schleyer, P. von R. On the Advantages of Hydrocarbon Radical Stabilization Energies Based on R−H Bond Dissociation Energies. *J. Org. Chem.* **2011**, *76* (8), 2439–2447. https://doi.org/10.1021/jo101661c.

(124) Pitt, C. G. Hyperconjugation and Its Role in Group IV Chemistry. *Journal of Organometallic Chemistry* **1973**, *61*, 49–70. https://doi.org/10.1016/S0022-328X(00)86535-3.

(125) Ingold, K. U.; DiLabio, G. A. Bond Strengths: The Importance of Hyperconjugation. *Org. Lett.* **2006**, *8* (26), 5923–5925. https://doi.org/10.1021/ol062293s.

(126) Paltenghi, R.; Ogryzlo, E. A.; Bayes, K. D. Rates of Reaction of Alkyl Radicals with Ozone. *J. Phys. Chem.* **1984**, *88* (12), 2595–2599. https://doi.org/10.1021/j150656a034.

(127) Kerr, J. A. Bond Dissociation Energies by Kinetic Methods. *Chem. Rev.* **1966**, *66* (5), 465–500. https://doi.org/10.1021/cr60243a001.

(128) Cataldo, F.; Rosati, A.; Lilla, E.; Ursini, O. On the Action of Ozone at High Concentration on Various Grades of Polyethylene and Certain Straight Chain Paraffins. *Polymer degradation and stability* **2011**.

(129) Kwok, E. S. C.; Atkinson, R.; Arey, J. Kinetics of the Gas-Phase Reactions of Indan, Indene, Fluorene, and 9,10-Dihydroanthracene with OH Radicals, NO3 Radicals, and O3. *International Journal of Chemical Kinetics* **1997**, *29* (4), 299–309. https://doi.org/10.1002/(SICI)1097-4601(1997)29:4<299::AID-KIN9>3.0.CO;2-P.

(130) Hendrickx, M. F. A.; Vinckier, C. 1,3-Cycloaddition of Ozone to Ethylene, Benzene, and Phenol: A Comparative Ab Initio Study. *J. Phys. Chem. A* **2003**, *107* (38), 7574–7580. https://doi.org/10.1021/jp034541x.

(131) Mbouombouo Ndassa, I.; Silvi, B.; Volatron, F. Understanding Reaction Mechanisms in Organic Chemistry from Catastrophe Theory: Ozone Addition on

Benzene. *J. Phys. Chem. A* **2010**, *114* (49), 12900–12906. https://doi.org/10.1021/jp105874j.

(132) Atkinson, Roger.; Aschmann, S. M.; Pitts, J. N. Kinetics of the Reactions of Naphthalene and Biphenyl with Hydroxyl Radicals and with Ozone at 294 .+-. 1 K. *Environ. Sci. Technol.* **1984**, *18* (2), 110–113. https://doi.org/10.1021/es00120a012.

(133) Atkinson R; Arey J. Atmospheric Chemistry of Gas-Phase Polycyclic Aromatic Hydrocarbons: Formation of Atmospheric Mutagens. *Environmental Health Perspectives* **1994**, *102* (suppl 4), 117–126. https://doi.org/10.1289/ehp.94102s4117.

(134) Wen, Z.; Wang, Z.; Zhou, J.; Cen, K. A Theoretical Study on the Mechanism and Kinetic of the Reaction between Ozone and Benzene. *Ozone: Sci. Eng.* **2009**, *31* (5), 393–401. https://doi.org/10.1080/01919510903157879.

(135) Aihara, J. Why Are Some Polycyclic Aromatic Hydrocarbons Extremely Reactive? *Physical Chemistry Chemical Physics* **1999**, *1* (14), 3193–3197. https://doi.org/10.1039/A902032B.

(136) Kampschmidt, L. W. F.; Wibaut, J. P. On the Ozonization and the Ozonolysis of Naphthalene, 2,3-Dimethylnaphthalene, and 1,4-Dimethylnaphthalene in Connection with the Reactivity of the Ring System. *Recueil des Travaux Chimiques des Pays-Bas* **1954**, *73* (6), 431–454. https://doi.org/10.1002/recl.19540730602.

(137) Rindone, B.; Saliu, F.; Suarez-Bertoa, R. The Synthesis of Phthalic Anhydride via Ozonation of Naphthalene. *Ozone: Science & Engineering* **2010**, *32* (3), 161–165. https://doi.org/10.1080/01919511003788001.

(138) Stehr, J.; Müller, T.; Svensson, K.; Kamnerdpetch, C.; Scheper, T. Basic Examinations on Chemical Pre-Oxidation by Ozone for Enhancing Bioremediation of Phenanthrene Contaminated Soils. *Appl Microbiol Biotechnol* **2001**, *57* (5), 803–809. https://doi.org/10.1007/s00253-001-0840-4.

(139) Luster-Teasley, S. L.; Yao, J. J.; Herner, H. H.; Trosko, J. E.; Masten, S. J. Ozonation of Chrysene: Evaluation of Byproduct Mixtures and Identification of Toxic Constituent. *Environ. Sci. Technol.* **2002**, *36* (5), 869–876. https://doi.org/10.1021/es011090q.

(140) Brassington, K. J.; Hough, R. L.; Paton, G. I.; Semple, K. T.; Risdon, G. C.; Crossley, J.; Hay, I.; Askari, K.; Pollard, S. J. T. Weathered Hydrocarbon Wastes: A Risk Management Primer. *Critical Reviews in Environmental Science and Technology* **2007**, *37* (3), 199–232. https://doi.org/10.1080/10643380600819625.

(141) Balseiro-romero, M.; Monterroso, C.; Casares, J. J. Environmental Fate of Petroleum Hydrocarbons in Soil: Review of Multiphase Transport, Mass Transfer, and Natural Attenuation Processes. *Pedosphere* **2018**, *28* (6), 833–847. https://doi.org/10.1016/S1002-0160(18)60046-3.

(142) Barron, M.; Carls, M.; Heintz, R.; Rice, S. Evaluation of Fish Early Life-Stage Toxicity Models of Chronic Embryonic Exposures to Complex Polycyclic Aromatic Hydrocarbon Mixtures. *Toxicological sciences : an official journal of the Society of Toxicology* **2004**, *78*, 60–67. https://doi.org/10.1093/toxsci/kfh051.

(143) Billiard, S. M.; Querbach, K.; Hodson, P. V. Toxicity of Retene to Early Life Stages of Two Freshwater Fish Species. *Environmental Toxicology and Chemistry* **1999**, *18* (9), 2070–2077. https://doi.org/10.1002/etc.5620180927.

(144) Chaîneau, C. H.; Yepremian, C.; Vidalie, J. F.; Ducreux, J.; Ballerini, D. Bioremediation of a Crude Oil-Polluted Soil: Biodegradation, Leaching and Toxicity Assessments. *Water, Air, & Soil Pollution* **2003**, *144* (1–4), 419–440. https://doi.org/10.1023/A:1022935600698.

(145) Salanitro, J. P.; Dorn, P. B.; Huesemann, M. H.; Moore, K. O.; Rhodes, I. A.; Rice Jackson, L. M.; Vipond, T. E.; Western, M. M.; Wisniewski, H. L. Crude Oil Hydrocarbon Bioremediation and Soil Ecotoxicity Assessment. *Environ. Sci. Technol.* **1997**, *31* (6), 1769–1776. https://doi.org/10.1021/es960793i.

(146) Tang, J.; Wang, M.; Wang, F.; Sun, Q.; Zhou, Q. Eco-Toxicity of Petroleum Hydrocarbon Contaminated Soil. *J Environ Sci (China)* **2011**, *23* (5), 845–851. https://doi.org/10.1016/s1001-0742(10)60517-7.

(147) Brette, F.; Machado, B.; Cros, C.; Incardona, J. P.; Scholz, N. L.; Block, B. A. Crude Oil Impairs Cardiac Excitation-Contraction Coupling in Fish. *Science* **2014**, *343* (6172), 772–776. https://doi.org/10.1126/science.1242747.

(148) Han, Y.; Nambi, I. M.; Prabhakar Clement, T. Environmental Impacts of the Chennai Oil Spill Accident – A Case Study. *Science of The Total Environment* **2018**, *626*, 795–806. https://doi.org/10.1016/j.scitotenv.2018.01.128.

(149) Klinger, D. H.; Dale, J. J.; Machado, B. E.; Incardona, J. P.; Farwell, C. J.; Block, B. A. Exposure to Deepwater Horizon Weathered Crude Oil Increases Routine Metabolic Demand in Chub Mackerel, Scomber Japonicus. *Marine Pollution Bulletin* **2015**, *98* (1), 259–266. https://doi.org/10.1016/j.marpolbul.2015.06.039.

(150) Incardona, J. P.; Vines, C. A.; Linbo, T. L.; Myers, M. S.; Sloan, C. A.; Anulacion, B. F.; Boyd, D.; Collier, T. K.; Morgan, S.; Cherr, G. N.; Scholz, N. L. Potent Phototoxicity of Marine Bunker Oil to Translucent Herring Embryos after Prolonged Weathering. *PLOS ONE* **2012**, *7* (2), e30116. https://doi.org/10.1371/journal.pone.0030116.

(151) Zhu, Y.; Song, Z.; Chen, J.; Li, C.; Xiao, B.; Wang, Q. Effects of Oil-Contaminated Soil on the Seed Germination and Seedling Growth of Selected Crops. In *World Automation Congress 2012*; 2012; pp 1–4.

(152) Shin Kyung-Hee; Jung Haeryong; Chang Peichun; Choi Heechul; Kim Kyoung-Woong. Earthworm Toxicity during Chemical Oxidation of Diesel-contaminated Sand. *Environmental Toxicology and Chemistry* **2009**, *24* (8), 1924–1929. https://doi.org/10.1897/04-442R.1.

(153) Bona, C.; Rezende, I. M. de; Santos, G. de O.; Souza, L. A. de. Effect of Soil Contaminated by Diesel Oil on the Germination of Seeds and the Growth of Schinus Terebinthifolius Raddi (Anacardiaceae) Seedlings. *Braz. arch. biol. technol.* **2011**, *54*, 1379–1387. https://doi.org/10.1590/S1516-89132011000600025.

(154) Sanches, I. D.; Souza Filho, C. R.; Magalhães, L. A.; Quitério, G. C. M.; Alves, M. N.; Oliveira, W. J. Assessing the Impact of Hydrocarbon Leakages on Vegetation Using Reflectance Spectroscopy. *ISPRS Journal of Photogrammetry and Remote Sensing* **2013**, *78*, 85–101. https://doi.org/10.1016/j.isprsjprs.2013.01.007.

(155) Hussain, I.; Puschenreiter, M.; Gerhard, S.; Sani, S. G. A. S.; Khan, W.; Reichenauer, T. G. Differentiation between Physical and Chemical Effects of Oil Presence in Freshly Spiked Soil during Rhizoremediation Trial. *Environ Sci Pollut Res Int* **2019**, *26* (18), 18451–18464. https://doi.org/10.1007/s11356-019-04819-6.

(156) Ogboghodo, I. A.; Iruaga, E. K.; Osemwota, I. O.; Chokor, J. U. An Assessment of the Effects of Crude Oil Pollution on Soil Properties, Germination and Growth of Maize (Zea Mays) Using Two Crude Types – Forcados Light and Escravos Light. *Environ Monit Assess* **2004**, *96* (1), 143–152. https://doi.org/10.1023/B:EMAS.0000031723.62736.24.

(157) Zhang, Y.; Ran, Y.; Mao, J. Role of Extractable and Residual Organic Matter Fractions on Sorption of Phenanthrene in Sediments. *Chemosphere* **2013**, *90* (6), 1973–1979. https://doi.org/10.1016/j.chemosphere.2012.10.064.

(158) Fingas, M. A Literature Review of the Physics and Predictive Modelling of Oil Spill Evaporation. *Journal of Hazardous Materials* **1995**, *42* (2), 157–175. https://doi.org/10.1016/0304-3894(95)00013-K.

(159) Mackay, D.; Shiu, W. Y.; Maijanen, A.; Feenstra, S. Dissolution of Non-Aqueous Phase Liquids in Groundwater. *Journal of Contaminant Hydrology* **1991**, *8* (1), 23–42. https://doi.org/10.1016/0169-7722(91)90007-N.

(160) Wu, G.; He, L.; Chen, D. Sorption and Distribution of Asphaltene, Resin, Aromatic and Saturate Fractions of Heavy Crude Oil on Quartz Surface: Molecular Dynamic Simulation. *Chemosphere* **2013**, *92* (11), 1465–1471. https://doi.org/10.1016/j.chemosphere.2013.03.057.

(161) Council, N. R. *Polycyclic Aromatic Hydrocarbons: Evaluation of Sources and Effects*; 1983. https://doi.org/10.17226/738.

(162) Wess, J. A.; Olsen, L. D.; Sweeney, M. H. *Asphalt (Bitumen)*; Concise international chemical assessment document; World Health Organization: Geneva, 2004.

(163) Fakher, S.; Ahdaya, M.; Elturki, M.; Imqam, A. Critical Review of Asphaltene Properties and Factors Impacting Its Stability in Crude Oil. *J. Pet. Explor. Prod. Technol.* **2020**, *10* (3), 1183–1200. https://doi.org/10.1007/s13202-019-00811-5.

(164) Farwell, A. J.; Nero, V.; Croft, M.; Rhodes, S.; Dixon, D. G. Phototoxicity of Oil Sands–Derived Polycyclic Aromatic Compounds to Japanese Medaka (Oryzias Latipes) Embryos. *Environmental Toxicology and Chemistry* **2006**, *25* (12), 3266–3274. https://doi.org/10.1897/05-637R1.1.

(165) Heintz, R. A.; Short, J. W.; Rice, S. D. Sensitivity of Fish Embryos to Weathered Crude Oil: Part II. Increased Mortality of Pink Salmon (Oncorhynchus Gorbuscha) Embryos Incubating Downstream from Weathered Exxon Valdez Crude Oil. *Environmental Toxicology and Chemistry* **1999**, *18* (3), 494–503. https://doi.org/10.1002/etc.5620180318.

(166) Lee, R. Photo-Oxidation and Photo-Toxicity of Crude and Refined Oil Spills. *Spill Science & Technology Bulletin* **2003**, *8*, 157–162. https://doi.org/10.1016/S1353-2561(03)00015-X.

(167) ASTM International. *Standard Test Methods for Particle-Size Distribution (Gradation) of Soils Using Sieve Analysis*; ASTM D6913/D6913M-17: West Conshohocken, PA, 2021.

(168) ASTM International. *Standard Test Methods for Liquid Limit, Plastic Limit, and Plasticity Index of Soils*; ASTM D4318-00: West Conshohocken, PA, 2017.

(169) ASTM International. *Standard Practice for Classification of Soils for Engineering Purposes (Unified Soil Classification System)*; ASTM D2487-17e1: West Conshohocken, PA, 2022.

(170) Sparks, D. L.; Page, A. L.; Helmke, P. A.; Loeppert, R. H. *Methods of Soil Analysis, Part 3: Chemical Methods*; John Wiley & Sons, 2020.

(171) Davies, B. E. Loss-on-Ignition as an Estimate of Soil Organic Matter. *Soil Science Society of America Journal* **1974**, *38* (1), 150–151. https://doi.org/10.2136/sssaj1974.03615995003800010046x.

(172) United States Environmental Protection Agency (US EPA). *U.S. EPA Method 3051A: Microwave Assisted Acid Digestion of Sediments, Sludges, and Oils*; U.S. EPA Method 3051A, 2019.

(173) United States Environmental Protection Agency (US EPA). *Semivolatile Organic Compounds by Gas Chromatography/Mass Spectrometry (GC-MS)*; EPA Method 8270E (SW-846): Washington, D.C., 2014.

(174) Massachusetts Department of Environmental Protection. *Method for the Determination of Total Extractable Petroleum Hydocarbons (EPH)*; Revision 2.1: Boston, MA, 2019.

(175) Buol, S. W.; Southard, R. J.; Graham, R. C.; McDaniel, P. A. *Soil Genesis and Classification*, Sixth Edition.; Wiley-Blackwell: Chichester, West Sussex; Ames, Iowa, 2011.

(176) Incardona, J. P.; Gardner, L. D.; Linbo, T. L.; Brown, T. L.; Esbaugh, A. J.; Mager, E. M.; Stieglitz, J. D.; French, B. L.; Labenia, J. S.; Laetz, C. A.; Tagal, M.; Sloan, C. A.; Elizur, A.; Benetti, D. D.; Grosell, M.; Block, B. A.; Scholz, N. L. Deepwater Horizon Crude Oil Impacts the Developing Hearts of Large Predatory Pelagic Fish. *PNAS* **2014**, *111* (15), E1510–E1518. https://doi.org/10.1073/pnas.1320950111.

(177) Carls, M. G.; Meador, J. P. A Perspective on the Toxicity of Petrogenic PAHs to Developing Fish Embryos Related to Environmental Chemistry. *Human and Ecological Risk Assessment: An International Journal* **2009**, *15* (6), 1084–1098. https://doi.org/10.1080/10807030903304708.

(178) Hicken, C. E.; Linbo, T. L.; Baldwin, D. H.; Willis, M. L.; Myers, M. S.; Holland, L.; Larsen, M.; Stekoll, M. S.; Rice, S. D.; Collier, T. K.; Scholz, N. L.; Incardona, J. P. Sublethal Exposure to Crude Oil during Embryonic Development Alters Cardiac Morphology and Reduces Aerobic Capacity in Adult Fish. *PNAS* **2011**, *108* (17), 7086–7090. https://doi.org/10.1073/pnas.1019031108.

(179) Besalatpour, A. A.; Khoshgoftarmanesh, A.; Hajabbasi, M.; Majid, A. Germination and Growth of Selected Plants in a Petroleum Contaminated Calcareous Soil. *Soil and Sediment Contamination* **2008**, *17*, 665–676. https://doi.org/10.1080/15320380802425113.

(180) Jonker, M. T. O.; Brils, J. M.; Sinke, A. J. C.; Murk, A. J.; Koelmans, A. A. Weathering and Toxicity of Marine Sediments Contaminated with Oils and

Polycyclic Aromatic Hydrocarbons. *Environ. Toxicol. Chem.* **2006**, *25* (5), 1345–1353. https://doi.org/10.1897/05-296r.1.

(181) He, Y.; Patterson, S.; Wang, N.; Hecker, M.; Martin, J. W.; El-Din, M. G.; Giesy, J. P.; Wiseman, S. B. Toxicity of Untreated and Ozone-Treated Oil Sands Process-Affected Water (OSPW) to Early Life Stages of the Fathead Minnow (Pimephales Promelas). *Water Research* **2012**, *46* (19), 6359–6368. https://doi.org/10.1016/j.watres.2012.09.004.

(182) Rowland, S. J.; Scarlett, A. G.; Jones, D.; West, C. E.; Frank, R. A. Diamonds in the Rough: Identification of Individual Naphthenic Acids in Oil Sands Process Water. *Environ. Sci. Technol.* **2011**, *45* (7), 3154–3159. https://doi.org/10.1021/es103721b.

(183) Clemente, J. S.; Fedorak, P. M. A Review of the Occurrence, Analyses, Toxicity, and Biodegradation of Naphthenic Acids. *Chemosphere* **2005**, *60* (5), 585–600. https://doi.org/10.1016/j.chemosphere.2005.02.065.

(184) Scarlett, A. G.; West, C. E.; Jones, D.; Galloway, T. S.; Rowland, S. J. Predicted Toxicity of Naphthenic Acids Present in Oil Sands Process-Affected Waters to a Range of Environmental and Human Endpoints. *Sci. Total Environ.* **2012**, *425*, 119–127. https://doi.org/10.1016/j.scitotenv.2012.02.064.

(185) Jones, D.; West, C. E.; Scarlett, A. G.; Frank, R. A.; Rowland, S. J. Isolation and Estimation of the “Aromatic” Naphthenic Acid Content of an Oil Sands Process-Affected Water Extract. *J. Chromatogr. A* **2012**, *1247*, 171–175. https://doi.org/10.1016/j.chroma.2012.05.073.

(186) Headley, J. V.; McMartin, D. W. A Review of the Occurrence and Fate of Naphthenic Acids in Aquatic Environments. *J. Environ. Sci. Health - Toxic/Hazard. Subst. Environ. Eng.* **2004**, *39* (8), 1989–2010. https://doi.org/10.1081/ese-120039370.

(187) He, Y.; Sun, C.; Zhang, Y.; Folkerts, E. J.; Martin, J. W.; Goss, G. G. Developmental Toxicity of the Organic Fraction from Hydraulic Fracturing Flowback and Produced Waters to Early Life Stages of Zebrafish (Danio Rerio). *Environ. Sci. Technol.* **2018**, *52* (6), 3820–3830. https://doi.org/10.1021/acs.est.7b06557.

(188) Ji, H.; Gong, Y.; Duan, J.; Zhao, D.; Liu, W. Degradation of Petroleum Hydrocarbons in Seawater by Simulated Surface-Level Atmospheric Ozone: Reaction Kinetics and Effect of Oil Dispersant. *Mar. Pollut. Bull.* **2018**, *135*, 427–440. https://doi.org/10.1016/j.marpolbul.2018.07.047.

(189) Li, C.; Fu, L.; Stafford, J.; Belosevic, M.; Gamal El-Din, M. The Toxicity of Oil Sands Process-Affected Water (OSPW): A Critical Review. *Science of The Total*

Environment **2017**, *601–602*, 1785–1802. https://doi.org/10.1016/j.scitotenv.2017.06.024.

(190) Scott, A. C.; Zubot, W.; MacKinnon, M. D.; Smith, D. W.; Fedorak, P. M. Ozonation of Oil Sands Process Water Removes Naphthenic Acids and Toxicity. *Chemosphere* **2008**, *71* (1), 156–160. https://doi.org/10.1016/j.chemosphere.2007.10.051.

(191) Kahan, T. F.; Kwamena, N.-O. A.; Donaldson, D. J. Heterogeneous Ozonation Kinetics of Polycyclic Aromatic Hydrocarbons on Organic Films. *Atmospheric Environment* **2006**, *40* (19), 3448–3459. https://doi.org/10.1016/j.atmosenv.2006.02.004.

(192) Choi, H.; Lim, H.-N.; Kim, J.; Hwang, T.-M.; Kang, J.-W. Transport Characteristics of Gas Phase Ozone in Unsaturated Porous Media for In-Situ Chemical Oxidation. *J. Contam. Hydrol.* **2002**, *57* (1–2), 81–98.

(193) Hsu I-yuang; Masten Susan J. Modeling Transport of Gaseous Ozone in Unsaturated Soils. *Journal of Environmental Engineering* **2001**, *127* (6), 546–554. https://doi.org/10.1061/(ASCE)0733-9372(2001)127:6(546).

(194) Jung, H.; Choi, H. Effects of In Situ Ozonation on Structural Change of Soil Organic Matter. *Environmental Engineering Science* **2003**, *20* (4), 289–299. https://doi.org/10.1089/109287503322148564.

(195) ASTM International. *Standard Guide for Conducting Terrestrial Plant Toxicity Tests*; ASTM E1963-09: West Conshohocken, PA, 2014.

(196) Barnthouse, L. ES&T Series: Case Studies in Ecological Risk Assessment. *Environ. Sci. Technol.* **1992**, *26* (2), 230–231. https://doi.org/10.1021/es00026a608.

(197) Hanson, M. L.; Solomon, K. R. New Technique for Estimating Thresholds of Toxicity in Ecological Risk Assessment. *Environ. Sci. Technol.* **2002**, *36* (15), 3257–3264. https://doi.org/10.1021/es011490d.

(198) Hope, B. K. An Examination of Ecological Risk Assessment and Management Practices. *Environ Int* **2006**, *32* (8), 983–995. https://doi.org/10.1016/j.envint.2006.06.005.

(199) United States Environmental Protection Agency (US EPA). *Benchmark Dose Technical Guidance*; EPA/100/R-12/001: Washington, D.C, 2012.

(200) Mayfield, D. B.; Skall, D. G. Benchmark Dose Analysis Framework for Developing Wildlife Toxicity Reference Values. *Environ. Toxicol. Chem.* **2018**, *37* (5), 1496–1508. https://doi.org/10.1002/etc.4082.

(201) Bidlan, R.; Afsar, M.; Manonmani, H. K. Bioremediation of HCH-Contaminated Soil: Elimination of Inhibitory Effects of the Insecticide on Radish and Green Gram Seed Germination. *Chemosphere* **2004**, *56* (8), 803–811. https://doi.org/10.1016/j.chemosphere.2004.01.015.

(202) Modlitbová, P.; Hlaváček, A.; Švestková, T.; Pořízka, P.; Šimoníková, L.; Novotný, K.; Kaiser, J. The Effects of Photon-Upconversion Nanoparticles on the Growth of Radish and Duckweed: Bioaccumulation, Imaging, and Spectroscopic Studies. *Chemosphere* **2019**, *225*, 723–734. https://doi.org/10.1016/j.chemosphere.2019.03.074.

(203) Ngo, L. K.; Pinch, B. M.; Bennett, W. W.; Teasdale, P. R.; Jolley, D. F. Assessing the Uptake of Arsenic and Antimony from Contaminated Soil by Radish (Raphanus Sativus) Using DGT and Selective Extractions. *Environ. Pollut.* **2016**, *216*, 104–114. https://doi.org/10.1016/j.envpol.2016.05.027.

(204) Shimazu, H. Absorption and Bioaccumulation in the Garden Radish (Raphanus Raphanistrum Ssp. Sativus). *Int. J. GEOMATE* **2019**, *17*. https://doi.org/10.21660/2019.62.50812.

(205) Ogra, Y.; Kitaguchi, T.; Ishiwata, K.; Suzuki, N.; Iwashita, Y.; T. Suzuki, K. Identification of Selenohomolanthionine in Selenium-Enriched Japanese Pungent Radish. *J. Anal. At. Spectrom.* **2007**, *22* (11), 1390–1396. https://doi.org/10.1039/B707348H.

(206) Prosser, R. S.; Lissemore, L.; Topp, E.; Sibley, P. K. Bioaccumulation of Triclosan and Triclocarban in Plants Grown in Soils Amended with Municipal Dewatered Biosolids. *Environ. Toxicol. Chem.* **2014**, *33* (5), 975–984. https://doi.org/10.1002/etc.2505.

(207) Guo, J.; Chai, C.; Ge, W.; Zeng, L.; Wu, J.; Xiang, D.; Zhang, X. Accumulation and Health Risk Assessment of PAHs in Radish. *Pol. J. Environ. Stud.* **2018**, *27* (6), 2529–2539. https://doi.org/10.15244/pjoes/81087.

(208) Wang, Y.-C.; Qiao, M.; Liu, Y.-X.; H. Arp, H. P.; Zhu, Y.-G. Comparison of Polycyclic Aromatic Hydrocarbon Uptake Pathways and Risk Assessment of Vegetables from Waste- Water Irrigated Areas in Northern China. *J.of Environ. Monit.* **2011**, *13* (2), 433–439. https://doi.org/10.1039/C0EM00098A.

(209) Hosmer, D. W.; Lemeshow, S.; Sturdivant, R. X. *Applied Logistic Regression*, Third.; John Wiley & Sons: Hoboken, New Jersey, 2013.

(210) Palm, C.; Sanchez, P.; Ahamed, S.; Awiti, A. Soils: A Contemporary Perspective. *Annu. Rev. Environ. Resour.* **2007**, *32* (1), 99–129. https://doi.org/10.1146/annurev.energy.31.020105.100307.

(211) Jenny, H. *Factors of Soil Formation: A System of Quantitative Pedology*; Dover Publications: New York, 2011.

(212) Royston, P.; Altman, D. G. Regression Using Fractional Polynomials of Continuous Covariates: Parsimonious Parametric Modelling. *Journal of the Royal Statistical Society. Series C (Applied Statistics)* **1994**, *43* (3), 429–467. https://doi.org/10.2307/2986270.

(213) Royston, P.; Sauerbrei, W. *Multivariable Model - Building: A Pragmatic Approach to Regression Analysis Based on Fractional Polynomials for Modelling Continuous Variables*, First Edition.; Wiley: Chichester, England; Hoboken, NJ, 2008.

(214) Hoigné, J.; Bader, H.; Haag, W. R.; Staehelin, J. Rate Constants of Reactions of Ozone with Organic and Inorganic Compounds in Water—III. Inorganic Compounds and Radicals. *Water Research* **1985**, *19* (8), 993–1004. https://doi.org/10.1016/0043-1354(85)90368-9.

(215) Einaga, H.; Futamura, S. Comparative Study on the Catalytic Activities of Alumina-Supported Metal Oxides for Oxidation of Benzene and Cyclohexane with Ozone. *React. Kinet. Catal. Lett.* **2004**, *81* (1), 121–128. https://doi.org/10.1023/B:REAC.0000016525.91158.c5.

(216) Heisig, C.; Zhang, W.; Oyama, S. T. Decomposition of Ozone Using Carbon-Supported Metal Oxide Catalysts. *Appl. Catal. B: Environ.* **1997**, *14* (1), 117–129. https://doi.org/10.1016/S0926-3373(97)00017-9.

(217) Martinez, R.; Herron, J. Stopped-flow Study of the Gas-phase Reaction of Ozone with Organic Sulfides: Dimethyl Sulfide. *Int. J. Chem. Kinet.* **1978**. https://doi.org/10.1002/KIN.550100503.

(218) Yoshioka, S.; Inokuma, Y.; Duplan, V.; Dubey, R.; Fujita, M. X-Ray Structure Analysis of Ozonides by the Crystalline Sponge Method. *J. Am. Chem. Soc.* **2016**, *138* (32), 10140–10142. https://doi.org/10.1021/jacs.6b05817.

(219) Chacón-Patiño, M. L.; Niles, S. F.; Marshall, A. G.; Hendrickson, C. L.; Rodgers, R. P. Role of Molecular Structure in the Production of Water-Soluble Species by Photo-Oxidation of Petroleum. *Environ. Sci. Technol.* **2020**, *54* (16), 9968–9979. https://doi.org/10.1021/acs.est.0c01158.

(220) OECD (2006). Test No. 208: Terrestrial Plant Test: Seedling Emergence and Seedling Growth Test, OECD Guidelines for the Testing of Chemicals, Section 2. *OECD Publishing, Paris* **2006**.

(221) Haber, L. T.; Dourson, M. L.; Allen, B. C.; Hertzberg, R. C.; Parker, A.; Vincent, M. J.; Maier, A.; Boobis, A. R. Benchmark Dose (BMD) Modeling: Current

Practice, Issues, and Challenges. *Crit. Rev. Toxicol.* **2018**, *48* (5), 387–415. https://doi.org/10.1080/10408444.2018.1430121.

(222) Fageria, N. K. Role of Soil Organic Matter in Maintaining Sustainability of Cropping Systems. *Commun. in Soil Sci. Plant Anal.* **2012**, *43* (16), 2063–2113. https://doi.org/10.1080/00103624.2012.697234.

(223) Oudeh, M.; Khan, M.; Scullion, J. Plant Accumulation of Potentially Toxic Elements in Sewage Sludge as Affected by Soil Organic Matter Level and Mycorrhizal Fungi. *Environ. Pollut.* **2002**, *116* (2), 293–300. https://doi.org/10.1016/S0269-7491(01)00128-2.

(224) Ondrasek, G.; Rengel, Z. The Role of Soil Organic Matter in Trace Element Bioavailability and Toxicity. In *Abiotic Stress Responses in Plants: Metabolism, Productivity and Sustainability*; Ahmad, P., Prasad, M. N. V., Eds.; Springer: New York, NY, 2012; pp 403–423. https://doi.org/10.1007/978-1-4614-0634-1_22.

(225) Haynes, R.; Mokolobate, M. S. Amelioration of Al Toxicity and P Deficiency in Acid Soils by Additions of Organic Residues: A Critical Review of the Phenomenon and the Mechanisms Involved. *Nutr. Cycl. Agroecosystems* **2001**, *59*, 47–63. https://doi.org/10.1023/A:1009823600950.

(226) Upchurch, R. P.; Mason, D. D. The Influence of Soil Organic Matter on the Phytotoxicity of Herbicides. *Weeds* **1962**, *10* (1), 9–14. https://doi.org/10.2307/4040550.

(227) Johnson, P. C. Assessment of the Contributions of Volatilization and Biodegradation to in Situ Air Sparging Performance. *Environ. Sci. Technol.* **1998**, *32* (2), 276–281. https://doi.org/10.1021/es9704850.

(228) Johnson, P. C. In-Situ Soil Heating Press/Vapor Extraction System. US5244310 A, September 14, 1993.

(229) Johnson, P.; Stanley, C. C.; Kemblowski, M. W.; Byers, D. L.; Colthart, J. D. A Practical Approach to the Design, Operation, and Monitoring of In Situ Soil-Venting Systems. *Ground Water Monitoring & Remediation* **1990**, *10*, 159–178. https://doi.org/10.1111/j.1745-6592.1990.tb00347.x.

(230) Huling, S. G.; Pivetz, B. E. *In-Situ Chemical Oxidation*; ENVIRONMENTAL PROTECTION AGENCY WASHINGTON DC OFFICE OF WATER, 2006.

(231) Bailey, P. S. The Reactions Of Ozone With Organic Compounds. *Chem. Rev.* **1958**, *58* (5), 925–1010. https://doi.org/10.1021/cr50023a005.

(232) Derudi, M.; Gianluca, V. Biodegradation Combined with Ozone for the Remediation of Contaminated Soils. *European Journal of Soil Biology - EUR J SOIL BIOL* **2007**, *43* (5), 297–303. https://doi.org/10.1016/j.ejsobi.2007.03.001.

(233) Ying, Z.; Yecheskel, Y.; Huo, M.; Hübner, U.; Zucker, I. Ozone Consumption by Soils: A Critical Factor in In Situ Ozonation Processes. *ACS EST Water* **2021**, *1* (11), 2403–2411. https://doi.org/10.1021/acsestwater.1c00236.

(234) Kim, J.; Choi, H. Modeling in Situ Ozonation for the Remediation of Nonvolatile PAH-Contaminated Unsaturated Soils. *Journal of Contaminant Hydrology* **2002**, *55* (3), 261–285. https://doi.org/10.1016/S0169-7722(01)00196-6.

(235) Jung Haeryong; Kim Jeongkon; Choi Heechul. Reaction Kinetics of Ozone in Variably Saturated Porous Media. *Journal of Environmental Engineering* **2004**, *130* (4), 432–441. https://doi.org/10.1061/(ASCE)0733-9372(2004)130:4(432).

(236) Choi, H.; Kim, Y. Y.; Lim, H.; Cho, J.; Kang, J. W.; Kim, K. S. Oxidation of Polycyclic Aromatic Hydrocarbons by Ozone in the Presence of Sand. *Water Sci. Technol.* **2001**, *43* (5), 349–356.

(237) Hsu, M. I. Y.; Masten, S. J. The Kinetics of the Reaction of Ozone with Phenanthrene in Unsaturated Soils. *Environmental Engineering Science* **1997**, *14* (4), 207–218.

(238) Bufalini, J. J.; Altshuller, A. P. KINETICS OF VAPOR-PHASE HYDROCARBON–OZONE REACTIONS. *Canadian Journal of Chemistry* **2011**. https://doi.org/10.1139/v65-302.

(239) Hayashi, J.; Ikeda, J.; Kusakabe, K.; Morooka, S. Decomposition Rate of Volatile Organochlorines by Ozone and Utilization Efficiency of Ozone with Ultraviolet Radiation in a Bubble-Column Contactor. *Water Research* **1993**, *27* (6), 1091–1097. https://doi.org/10.1016/0043-1354(93)90074-R.

(240) Sun, W.; Gao, X.; Wu, B.; Ombrello, T. The Effect of Ozone Addition on Combustion: Kinetics and Dynamics. *Progress in Energy and Combustion Science* **2019**, *73*, 1–25. https://doi.org/10.1016/j.pecs.2019.02.002.

(241) Zhang, T.; Ma, J. Catalytic Ozonation of Trace Nitrobenzene in Water with Synthetic Goethite. *Journal of Molecular Catalysis A: Chemical* **2008**, *279* (1), 82–89. https://doi.org/10.1016/j.molcata.2007.09.030.

(242) Gracia, R.; Aragües, J. L.; Ovelleiro, J. L. Study of the Catalytic Ozonation of Humic Substances in Water and Their Ozonation Byproducts. *Ozone: Science & Engineering* **1996**, *18* (3), 195–208. https://doi.org/10.1080/01919519608547326.

(243) Piera, E.; Calpe, J. C.; Brillas, E.; Domènech, X.; Peral, J. 2,4-Dichlorophenoxyacetic Acid Degradation by Catalyzed Ozonation: TiO2/UVA/O3 and FE(II)/UVA/O3 Systems. **2000**, *27* (3), 169–177. https://doi.org/10.1016/S0926-3373(00)00149-1.

(244) Sauleda, R.; Brillas, E. Mineralization of Aniline and 4-Chlorophenol in Acidic Solution by Ozonation Catalyzed with Fe2+ and UVA Light. *Applied Catalysis B: Environmental* **2001**, *29* (2), 135–145. https://doi.org/10.1016/S0926-3373(00)00197-1.

(245) Beltrán, F. J.; Rivas, F. J.; Montero-de-Espinosa, R. Ozone-Enhanced Oxidation of Oxalic Acid in Water with Cobalt Catalysts. 1. Homogeneous Catalytic Ozonation. *Ind. Eng. Chem. Res.* **2003**, *42* (14), 3210–3217. https://doi.org/10.1021/ie0209982.

(246) Nawrocki, J.; Kasprzyk-Hordern, B. The Efficiency and Mechanisms of Catalytic Ozonation. *Applied Catalysis B: Environmental* **2010**, *99* (1–2), 27–42. https://doi.org/10.1016/j.apcatb.2010.06.033.

(247) Dhandapani, B.; Oyama, S. T. Gas Phase Ozone Decomposition Catalysts. *Applied Catalysis B: Environmental* **1997**, *11* (2), 129–166. https://doi.org/10.1016/S0926-3373(96)00044-6.

(248) Cerkovnik, J.; Erzen, E.; Koller, J.; Plesnicar, B. Evidence for HOOO Radicals in the Formation of Alkyl Hydrotrioxides (ROOOH) and Hydrogen Trioxide (HOOOH) in the Ozonation of C-H Bonds in Hydrocarbons. *J Am Chem Soc* **2002**, *124* (3), 404–409. https://doi.org/10.1021/ja017320i.

(249) McClurkin, J. D.; Maier, D. E.; Ileleji, K. E. Half-Life Time of Ozone as a Function of Air Movement and Conditions in a Sealed Container. *Journal of Stored Products Research* **2013**, *55*, 41–47. https://doi.org/10.1016/j.jspr.2013.07.006.

(250) Schubert, C. C.; Schubert, S. J.; Pease, R. N. The Oxidation of Lower Paraffin Hydrocarbons. I. Room Temperature Reaction of Methane, Propane, n-Butane and Isobutane with Ozonized Oxygen1. *J. Am. Chem. Soc.* **1956**, *78* (10), 2044–2048. https://doi.org/10.1021/ja01591a006.

(251) Schubert, C. C.; Schubert, S. J.; Pease, R. N. The Oxidation of Lower Paraffin Hydrocarbons. II. Observations on the Role of Ozone in the Slow Combustion of Isobutane1. *J. Am. Chem. Soc.* **1956**, *78* (21), 5553–5556. https://doi.org/10.1021/ja01602a024.

(252) Johnson, P. C.; Bruce, C. L.; Miller, K. D. A Practical Approach to the Design, Monitoring, and Optimization of In Situ MTBE Aerobic Biobarriers. *Ground*

Water Monitoring & Remediation **2010**, *30* (1), 58–66. https://doi.org/10.1111/j.1745-6592.2009.01254.x.

(253) Salanitro, J. P.; Johnson, P. C.; Stearns, S. M.; Maner, P. M.; Miller, J. H.; Spinnler, G. E. Situ Method and Apparatus for Biodegradation of Alkyl Ethers and Tertiary Butyl Alcohol. US6503395 B1, January 7, 2003.

(254) Johnson, P. C.; Ettinger, R. A. Considerations for the Design of In Situ Vapor Extraction Systems: Radius of Influence vs. Zone of Remediation. *Groundwater Monitoring & Remediation* **1994**, *14* (3), 123–128. https://doi.org/10.1111/j.1745-6592.1994.tb00473.x.

(255) Johnson, P. C.; Kemblowski, M. W.; Colthart, J. D. Quantitative Analysis for the Cleanup of Hydrocarbon-Contaminated Soils by In-Situ Soil Venting. *Ground Water* **1990**, *28* (3), 413–429. https://doi.org/10.1111/j.1745-6584.1990.tb02271.x.

(256) Chakraborty, S.; Mukherji, S.; Mukherji, S. Surface Hydrophobicity of Petroleum Hydrocarbon Degrading Burkholderia Strains and Their Interactions with NAPLs and Surfaces. *Colloids and Surfaces B: Biointerfaces* **2010**, *78* (1), 101–108. https://doi.org/10.1016/j.colsurfb.2010.02.019.

(257) Non-Aqueous Phase Liquid (NAPL) Cleanup Alliance. Understanding the Behavior of Light Non-Aqueous Phase Liquids (LNAPLs) in the Subsurface, 2005.

(258) Aguilera-Mercado, B.; Herdes, C.; Murgich, J.; Müller, E. A. Mesoscopic Simulation of Aggregation of Asphaltene and Resin Molecules in Crude Oils. *Energy Fuels* **2006**, *20* (1), 327–338. https://doi.org/10.1021/ef050272t.

(259) McLachlan, M. S.; Czub, G.; Wania, F. The Influence of Vertical Sorbed Phase Transport on the Fate of Organic Chemicals in Surface Soils. *Environ. Sci. Technol.* **2002**, *36* (22), 4860–4867.

(260) IR Spectra of Adsorbed Ozone. *Colloids and Surfaces A: Physicochemical and Engineering Aspects* **1995**, *101* (2–3), 153–158. https://doi.org/10.1016/0927-7757(95)03130-6.

(261) Donaldson, K.; Brown, D. M.; Mitchell, C.; Dineva, M.; Beswick, P. H.; Gilmour, P.; MacNee, W. Free Radical Activity of PM10: Iron-Mediated Generation of Hydroxyl Radicals. *Environmental Health Perspectives* **1997**, *105* (suppl 5), 1285–1289. https://doi.org/10.1289/ehp.97105s51285.

(262) Byvoet, P.; Balis, J. U.; Shelley, S. A.; Montgomery, M. R.; Barber, M. J. Detection of Hydroxyl Radicals upon Interaction of Ozone with Aqueous Media

or Extracellular Surfactant: The Role of Trace Iron. *Archives of Biochemistry and Biophysics* **1995**, *319* (2), 464–469. https://doi.org/10.1006/abbi.1995.1318.

(263) Cheng, F.-C.; Jen, J.-F.; Tsai, T.-H. Hydroxyl Radical in Living Systems and Its Separation Methods. *Journal of Chromatography B* **2002**, *781* (1), 481–496. https://doi.org/10.1016/S1570-0232(02)00620-7.

(264) Selucky, M. L.; Hafermann, P.; lacchelli, A.; Manske, T. Thin-Layer Chromatography as an Alternative to Sara Analysis of Coal Derived Liquids. *Liquid Fuels Technology* **1985**, *3* (1), 15–54. https://doi.org/10.1080/07377268508915370.

(265) Agency, U. S. E. P. *Remediation Case Studies Soil Vapor Extraction*; BiblioBazaar, 2013.

APPENDIX A

SOIL PHYSICAL AND CHEMICAL DATA

Table A.1 Sieve analysis to determine particle size distribution of TS.

Sieve (Particle Diameter)	Particle Diameter (mm, µM)	Classification	Size Terms (Wentworth, 1922)	% Mass Retained on Sieve	Cumulative % Passing
All particles	All Sizes		--		
3/8 in	>9.5 mm	Pebbles	Medium Pebbles and above	0.00%	0.00%
No. 4	9.5 mm – 4.75 mm		Medium and Fine Pebbles	0.00%	
No. 10	4.75 mm – 2 mm		Very fine pebbles	0.00%	
No. 20	2 mm – 850 µM	Sand	Very course/Course Sand	6.25%	71.3%
No. 40	850 µM – 425 µM		Course and Medium Sand	21.30%	
No. 60	425 µM – 250 µM		Medium Sand	14.91%	
No. 140	250 µM – 106 µM		Fine and Very fine Sand	20.22%	
No. 200	106 µM – 75 µM		Very fine Sand	8.64%	
Pan	<75 µM	Silt & Clay	Very fine sand, All Silt, All Clay	28.68%	28.7%
All particles	All Sizes			100.00%	100.00%

=

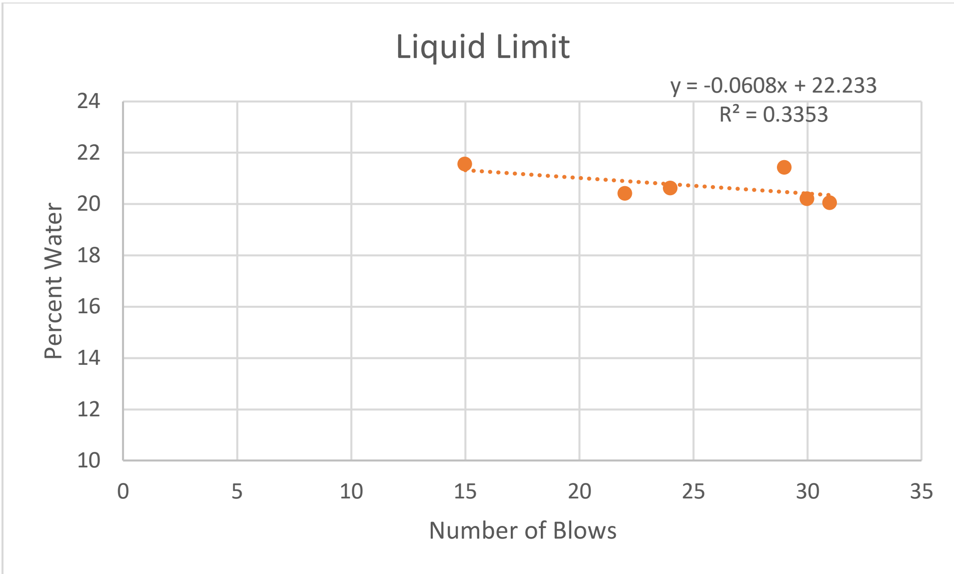

Figure A.1 Liquid limit of the test soil (TS).

Table A.2 Plastic limit results of the test soil (TS).

Trial	*Cup (g)*	*Cup+Soil+Water (g)*	*Cup+Soil (g)*	*Soil+Water Only (g)*	*Water (g)*	*% Water*
1	14.10	15.95	15.64	1.85	0.31	16.76
2	14.02	18.85	18.07	4.83	0.78	16.15
3	14.19	17.54	17.01	3.35	0.53	15.82

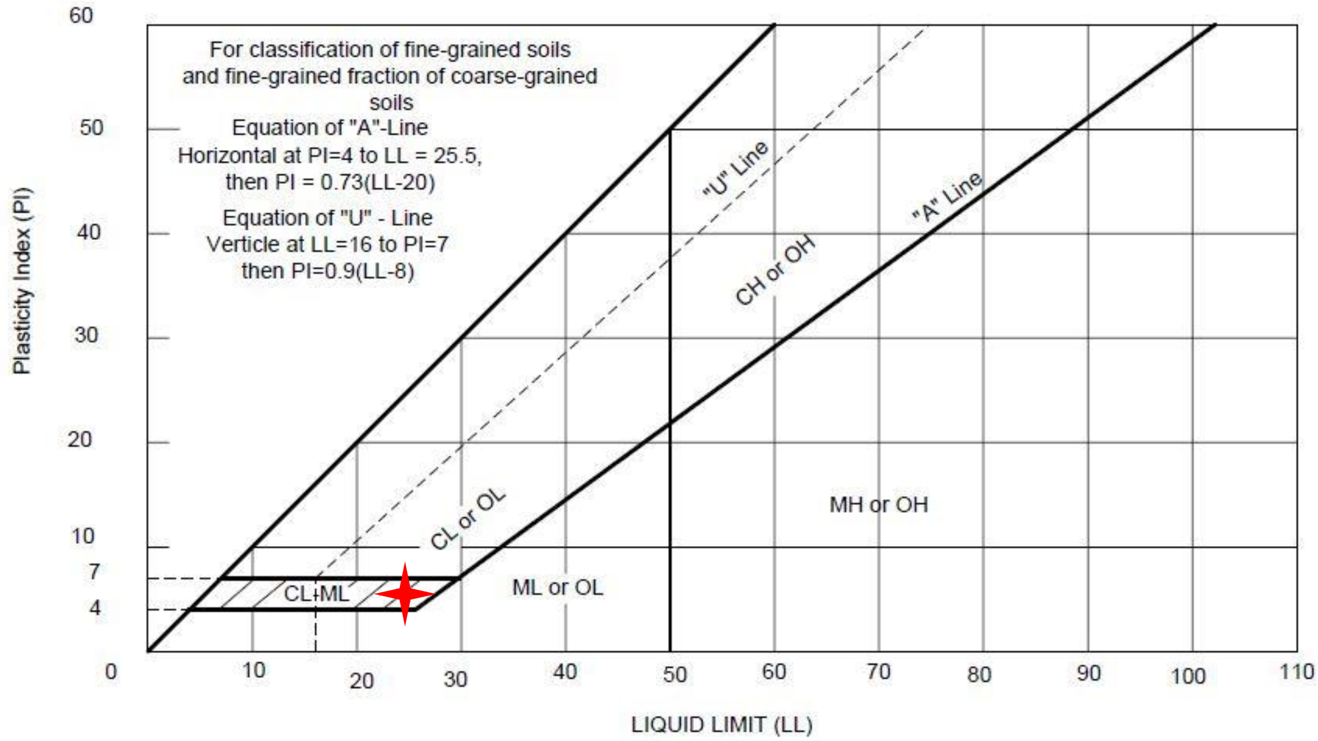

Figure A.2. Soil classification using liquid limit and plastic limit. The red star indicates position for TS, which is classified as a silty-clayey sand (SC-SM), or a "course-grained soil with fines.

APPENDIX B

TPH CONCENTRATIONS OF RAW/WEATHERED CRUDE OILS

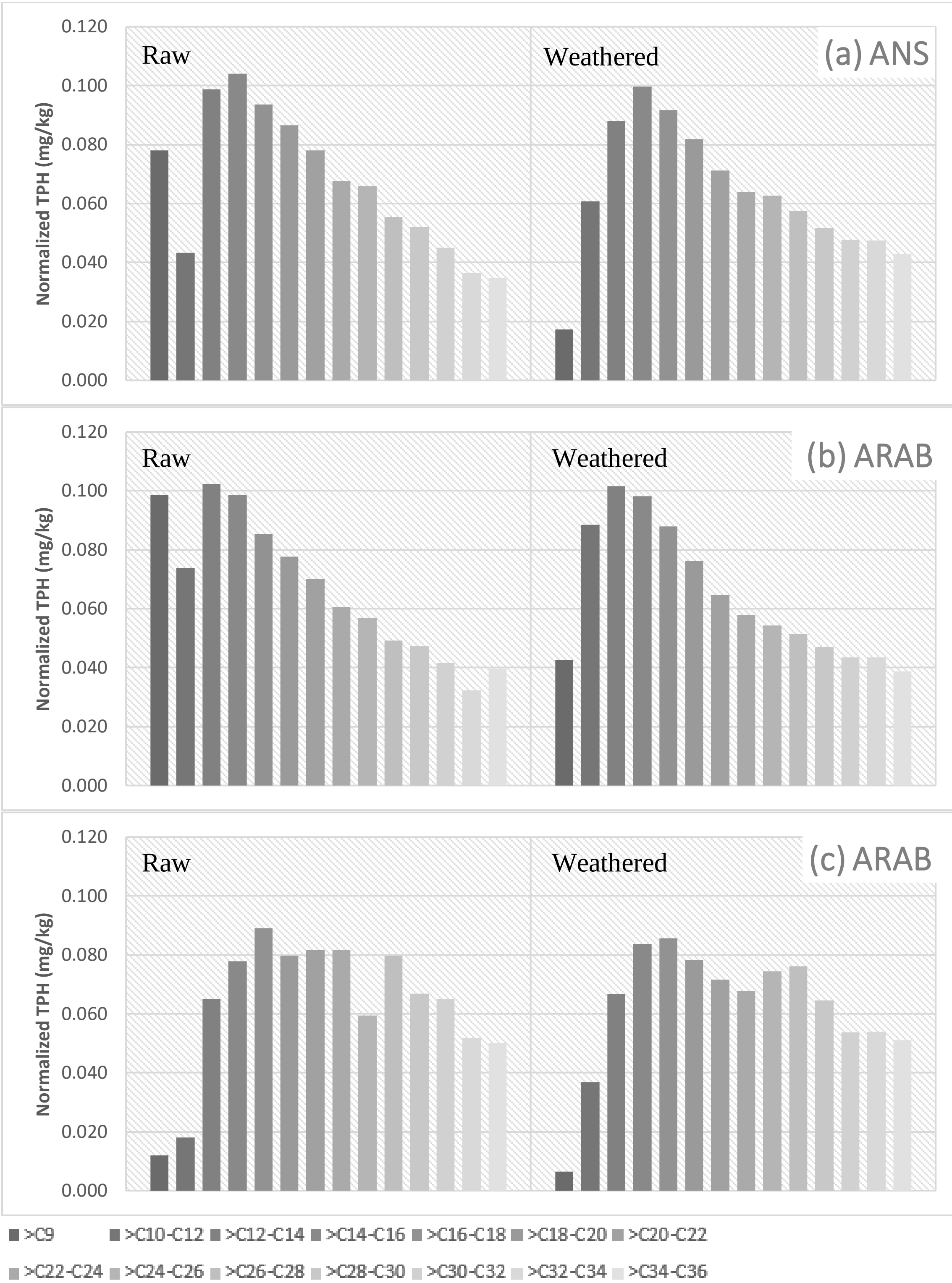

Figure B. Normalized TPH concentrations for raw (left panels) and weathered (right panels) for (a) ANS, (b) ARAB, and (c) SJV crude oils.

APPENDIX C

SUPPLEMENTARY DATA FOR LOGISTIC REGRESSION

Binary Codes

Treatment, *Dose*, and *Crude* are polychotomous independent variables scaled with $k > 2$ possible levels. The k levels are categories without numeric significance. The method to evaluate such category levels in the logistic regression model is to transform k levels into a set of $k - 1$ design variables. Coded as either 0 or 1, $k - 1$ design variables can accommodate k levels when all design variables are set to zero for the reference cell. Table (a-c) demonstrates the use of reference cell coding for this study. In the logistic regression model, the slope of the logit assessed when a categorical variable is in effect (i.e., when k=1). Although the use of any reference cell yields mathematically equivalent relative comparisons, I selected the category with the lowest probability germination (where possible) as the reference cell to yield whole number odds ratios.

Table C.1. Reference-cell coding for scaled variables Treatment, Dose, and Crude

Treatment (Code)	*BS*	*BSC*
Background soil only	1	0
Background soil with crude	0	1
Background soil with oxidized crude	0	0

Dose (Code)	*BS*	*BSC*	*BSOC-5g*	*BSOC-10g*
Background soil only	1	0	0	0
Background soil with crude	0	1	0	0
Background soil with oxidized crude, 5g	0	0	1	0
Background soil with oxidized crude, 10g	0	0	0	1
Background soil with oxidized crude, 40g	0	0	0	0

Crude (Code)	*BS*	*BSC-ANS*	*BSC-ARAB*
Background soil only	1	0	0
Background soil with untreated ANS crude	0	1	0
Background soil with untreated ARAB crude	0	0	1
Background soil with untreated SJV crude	0	0	0

Statistical Differences Between Treatment Groups by Seed

Table C.2. Probabilities, Odds, and Odds Ratios (OR) between treatment groups for Radish, Lettuce, and Grass.

	Treatment	*No*	*Yes*	*Total*	*Prob.*	*Odds*	*OR*	*P*	*95% CI*
Radish	TS	61	299	360	0.83	4.90	4.74	0.00	(3.51, 6.40)
	TSC	89	271	360	0.75	3.04	2.95	0.00	(2.25, 3.84)
	TSOC	531	549	1080	0.51	1.03	Base		
Lettuce	TS	120	240	360	0.67	2.00	2.56	0.00	(1.99, 3.28)
	TSC	191	169	360	0.47	0.88	1.13	0.31	(0.89, 1.43)
	TSOC	606	474	1080	0.44	0.78	Base		
Grass	TS	265	95	360	0.26	0.36	1.11	0.44	(0.84, 1.46)
	TSC	285	75	360	0.21	0.26	0.82	0.17	(0.61, 1.09)
	TSOC	817	263	1080	0.24	0.32	Base		

Statistical Differences Between Raw and Ozonated Crude by Seed

Table C.3. Probability, Odds, and OR for Radish germination by crude/oxidized crude.

	Treatment	*No*	*Yes*	*Total*	*Prob.*	*Odds*	*OR*	*P*	*95% CI*
Radish	TSC-ANS	26	94	120	0.78	3.62	3.13	0 .00	(1.93, 5.06)
	TSOC-ANS	167	193	360	0.54	1.16	Base		
	TSC-ARAB	19	101	120	0.84	5.32	4.60	0.00	(2.70, 7.83)
	TSOC-ARAB	167	193	360	0.54	1.16	Base		
	TSC-SJV	44	76	120	0.63	1.73	2.09	0.00	(1.36, 3.19)
	TSOC-SJV	197	163	360	0.45	0.83	Base		

Table C.4. Probability, Odds, and OR for Lettuce germination by crude/oxidized crude.

	Treatment	*No*	*Yes*	*Total*	*Prob.*	*Odds*	*OR*	*P*	*95% CI*
Lettuce	TSC-ANS	58	62	120	0.52	1.07	1.28	0.25	(0.84, 1.93)
	TSOC-ANS	196	164	360	0.46	0.84	Base		
	TSC-ARAB	62	58	120	0.48	0.94	0.93	0.71	(0.61, 1.39)
	TSOC-ARAB	179	181	360	0.50	1.01	Base		
	TSC-SJV	71	49	120	0.41	0.69	1.24	0.33	(0.80, 1.88)
	TSOC-SJV	231	129	360	0.36	0.56	Base		

Table C.5. Probability, Odds, and OR for Grass germination by crude/oxidized crude.

	Treatment	*No*	*Yes*	*Total*	*Prob.*	*Odds*	*OR*	*P*	*95% CI*
Grass	**TSC-ANS**	**108**	**12**	**120**	**0.10**	**0.11**	**0.44**	**0.01**	**(0.23, 0.85)**
	TSOC-ANS	288	72	360	0.20	0.25	Base		
	TSC-ARAB	94	26	120	0.22	0.28	1.00	1.00	(0.60, 1.65)
	TSOC-ARAB	282	78	360	0.22	0.28	Base		
	TSC-SJV	83	37	120	0.31	0.45	0.97	0.91	(0.62, 1.52)
	TSOC-SJV	247	113	360	0.31	0.46	Base		

Statistical Differences Between Ozonated Group by Dose and Seed

Table C.6 Probability, Odds, and OR for germination by TSOC dose. Highest dose is the base for all seeds.

	Dose	*No*	*Yes*	*Total*	*Prob.*	*Odds*	*OR*	*P*	*95% CI*
Radish	**5g Ozone**	**161**	**199**	**360**	**0.55**	**1.24**	**1.49**	**0.01**	**(1.11, 2.00)**
	10g Ozone	173	187	360	0.52	1.08	1.31	0.07	(0.97, 1.75)
	40g Ozone	197	163	360	0.45	0.83	Base		
Lettuce	5g Ozone	221	139	360	0.39	0.63	0.85	0.29	(0.63, 1.14)
	10g Ozone	**178**	**182**	**360**	**0.51**	**1.02**	**1.38**	**0.03**	**(1.03, 1.85)**
	40g Ozone	207	153	360	0.43	0.74	Base		
Grass	5g Ozone	276	84	360	0.23	0.30	0.96	0.79	(0.67, 1.34)
	10g Ozone	268	92	360	0.26	0.34	1.08	0.67	(0.76, 1.51)
	40g Ozone	273	87	360	0.24	0.32	Base		

APPENDIX D

THE LOGISTIC REGRESSION METHOD

The Simple Logistic Regression Model

Linear regression determines the mean value of an outcome variable Y given a specific value for the independent variable x. This "expected value of Y given x" is a conditional mean and can be expressed as $E(Y|x)$. An example of the equation of the line with an intercept β_0 and a single independent variable β_1 in the linear regression model is:

$$E(Y|x) = \beta_0 + \beta_1 x \qquad \text{Equation D.1}$$

Equation I.1 implies that (1) as x varies from $-\infty$ to $+\infty$, so does Y and (2) that the equation is linear in x. I compare this to a logistic-regression scenario, in which the outcome Y is coded as either 1 or 0. Here, the scatterplot of Y by x falls along two lines: a set of values for the independent variable x when the outcome is present ($Y = 1$) and another set of x values when the outcome is absent ($Y = 0$). If x is a good predictor of Y, those two scatterplots will have greater separation along x.

To achieve some of the useful properties of the linear-regression method, the first step of logistic regression is to reframe the dichotomous Y values as a set of numbers that can vary along a single line. This is achieved if Y is expressed as the cumulative probability of the positive outcome ($Y = 1$) along x. In other words, the expression $E(Y = 1|x)$ must denote the "conditional probability that the outcome is present given x". In simpler notation, $E(Y = 1|x)$ is represented by $\pi(x)$.

This transformation has limitations, however. For the plot of $\pi(x)$ along x, the continuous predictor x can vary from $-\infty$ to $+\infty$, but the conditional probability $\pi(x)$ can only vary between 0 to 1 (i.e., $0 \leq \pi(x) \leq 1$). Moreover, as $\pi(x)$ approaches its lower and upper boundaries, the change in the conditional probability per unit change in

x becomes smaller, yielding a more gradual slope. Instead of a line, the plot of $\pi(x)$ by x resembles an S-shaped curve. The functional form of that curve is one derived from the logistic distribution:

$$\pi(x) = \frac{e^{\beta_0+\beta_1 x}}{1+e^{\beta_0+\beta_1 x}} \quad \text{Equation D.2}$$

To regain some of the useful attributes of a linear model, the logistic regression method uses another transformation called the "logit transformation," one that is central to the procedure. This transformation, in terms of $\pi(x)$, is:

$$g(x) = \ln\left(\frac{\pi(x)}{1-\pi(x)}\right) = \beta_0 + \beta_1 x \quad \text{Equation D.3}$$

By this transformation, the logit, $g(x)$, becomes linear in its parameters, can be continuous, and can range from $-\infty$ to $+\infty$; it can also adhere to some of the principles that guide linear regression. If I denote the probability of the positive outcome as $Pr(Y = 1|x) = \pi(x)$, the multiple logistic-regression model (with p independent variables) is given by:

$$g(x) = \ln\left(\frac{\pi(x)}{1-\pi(x)}\right) = \beta_0 + \beta_1 x_1 + \beta_2 x_2 + \cdots + \beta_p x_p \quad \text{Equation D.4}$$

where $\pi(x) = \frac{e^{g(x)}}{1+e^{g(x)}}$. If the collection of p independent variables (also called "covariates") in a multivariable model can be denoted by the following vector:

$$\mathrm{x}' = (x_1, x_2, \ldots, x_p) \quad \text{Equation D.5}$$

then the collection of coefficients (also called "parameters") of those variables can be denoted by:

$$\beta' = (\beta_0, \beta_1, \beta_2, \ldots \beta_{\mathrm{p}}) \quad \text{Equation D.6}$$

The goal of logistic-regression modeling is to find the best collection of independent variables x' to predict $g(x)$ and to find the best estimates for the coefficients of those variables in the set β'.

The log-likelihood

Linear regression uses the least squares function to find the unknown parameters that minimize the sum-of-squared deviations of the observed values from predicted values for a given model. The least-squares function is derived from a general method of estimation called *maximum likelihood;* this general method is also used to estimate values of predictive parameters in logistic regression.

In the context of logistic regression, the method of *maximum likelihood* yields a likelihood function, called $l(\beta')$, that expresses the probability of the observed data as a function of the set of unknown parameters β'. The objective is to find the set of values of β' that maximize $l(\beta')$. In practice, this is done by taking the log of the likelihood function $l(\beta')$, denoted $L(\beta')$ and differentiating $L(\beta')$ with respect to the unknown parameters (e.g., $\beta_0, \beta_1, \beta_2, \ldots \beta_p$). The resulting equations (one for each parameter) are set to zero and solved for a set of *maximum likelihood estimators* called $\hat{\beta}'$. This process is iterative and requires statistical software.

I used Stata v. 16.1 (College Station, Texas) to find the values for the log-likelihood $L(\beta')$ and the estimated coefficients $\hat{\beta}'$. The software provides estimates for the standard errors ($\widehat{SE}$) of each coefficient in the model from the matrix of second partial derivative of the log-likelihood function as well as their respective 95% confidence intervals:

$$\hat{\beta} \pm z_{1-\alpha/2}\widehat{SE}(\hat{\beta}) \qquad \text{Equation D.7}$$

where $z_{1-\alpha/2}$ is the upper $100(1-\alpha/2)\%$ point from the standard normal distribution (i.e., 1.96). The value of the log-likelihood $L(\beta')$ reflects the probability that the data would give the estimated parameters. A theoretically perfect (or saturated) model has a log-likelihood of zero $(L(\beta')=0)$. Thus, the closer the value of log-likelihood is to 0, the better is the model.

Building the logistic regression model

When log-likelihood is multiplied by -2, it yields a statistic called the deviance (D), which follows a chi-square distribution with p degrees of freedom (equal to the number of variables in the model, not including the constant β_0). The deviance D and the set of estimates $\hat{\beta}'$ are the foundation of model building in logistic regression by a simple test called the *likelihood ratio*. The *likelihood ratio* produces the statistic G, which is chi-square distributed with degrees of freedom equal to the *difference* in the number of independent variables between the two models being compared:

$$G = D(model\ without\ the\ variable) - D(model\ with\ the\ variable)$$ [bb]

Equation D.8

I used the statistic G in two important ways. First, I tested the importance of each independent variable of interest by subtracting the deviance of the univariable fitted model from the deviance of the intercept-only model:

$$G = Deviance_{g(x)=\beta_0} - Deviance_{g(x)=\beta_0+\beta_1 x}$$ Equation D.9

[bb] The likelihood ratio test gets its name from the following expression for G:

$$G = -2\ln\left[\frac{\text{(likelihood of model without the variable)}}{\text{(likelihood of model with the variable)}}\right]$$

In this case of simple logistic regression, I test the null hypothesis that $\beta_1 = 0$ against the alternative hypothesis that $\beta_1 \neq 0$; the statistic G follows the chi-square distribution with 1 degree of freedom.

The likelihood ratio also allowed us to test whether any single coefficient in the set p coefficients for a multivariable model was equal to zero:

$$G = \; Deviance_{g(x) = \; \beta_0} - Deviance_{g(x) = \; \beta_0 + \beta_1 x_1 + \beta_2 x_2 + \cdots + \beta_p x_p}$$

Equation D.10

Here, I tested the null hypothesis that all p coefficients are equal to zero against the alternative hypothesis that at least one coefficient is not equal to zero; the statistic G follows the chi-square distribution with p degrees of freedom.

The likelihood ratio allowed us to systematically build a logistic regression model by adding and removing coefficients and testing the significance of G using the *partial likelihood ratio test*:

$$G = \; Deviance_{g(x) = \; \beta_0 + \beta_1 x_1} - Deviance_{g(x) = \; \beta_0 + \beta_1 x_1 + \beta_2 x_2 + \beta_3 x_3}$$

Equation D.11

In the above case, I tested the null hypothesis that either β_2 or β_3 is equal to zero, against the alternative hypothesis that at least one of the added variables did not equal zero; the statistic G follows the chi-square distribution with 2 degrees of freedom. The *likelihood ratio (LLR) test* determined the overall significance of p coefficients in each model.

In summary, these tests (Equations I.9 to I.11), used in conjunction with the Chi-squared table, tested the null hypothesis that any additional coefficients beyond that represented by the base model equal zero. The alternative hypothesis was that at least one of the added covariates had a coefficient that did not equal zero.

The univariable Wald test statistic (z) tested each individual variable for significance:

$$W_j = \frac{\hat{\beta}}{\widehat{SE}_{\hat{\beta}}} \qquad \text{Equation D.12}$$

The Wald test examined the null hypothesis that a given coefficient was zero and followed the standard normal distribution. It was used to evaluate each covariate in a multi-variable model.

Finally, the degree of statistical adjustment (i.e., *controlling for confounding*) was determined by looking at the relative change in the value of a coefficient between models. This occurred when a model contained a covariate, "d", that was important to the overall log-likelihood, and another covariate, "a," the adjustment covariate, that was not important to the predictive value of the model overall but affected the value of the coefficient "d". The coefficient of "d" in a model without the adjustment variate "a" was $\hat{\theta}_1$, while the coefficient of "d" in a model that contained the adjustment variate "a" was $\hat{\beta}_1$. The degree to which the presence of the covariate "a" in a model changed the value of the coefficient of "d" is known as delta-beta-hat-percent and was determined from:

$$\Delta\hat{\beta}\% = 100\left(\frac{\hat{\theta}_1 - \hat{\beta}_1}{\hat{\beta}_1}\right) \qquad \text{Equation D.13}$$

If the presence of "a" in the model changed the coefficient of "d" by more than some set minimum, then the covariate "a" was used to adjust the value of "d." The minimum % change was set to 20%.

Preliminaries

Step 0. The independent covariates

Table J.1 demonstrates the use of reference cell coding for these variables. Any reference level yields mathematically equivalent relative comparisons; reference levels are noted in the table below. The blank test soil (*TS*) served as the control and was the reference cell against which all other levels were compared for the variable *TREATMENT* ($k = 5;\ k - 1 = 4$). The 0% Test soil (i.e., 100% potting mix) was the reference cell against which all other levels were compared for the parameter *b-ORGANIC* ($k = 6;\ k - 1 = 5$). The variables and their levels are listed in Table J.2. The equations of the line for each of the individual variables tested are listed in Table J.3.

Table D.1. Reference-cell coding for scaled variables *TREATMENT* and *b-ORGANIC*

(a) TREATMENT (Code)	*BSC*	*BSOC-5g*	*BSOC-10g*	*BSOC-40g*
Background soil only (Base)	0	0	0	0
Background soil with crude	1	0	0	0
Background soil with oxidized crude, 5g	0	1	0	0
Background soil with oxidized crude, 10g	0	0	1	0
Background soil with oxidized crude, 40g	0	0	0	1

(b) b- ORGANIC (Code)	*10%*	*20%*	*60%*	*90%*	*100%*
0% Test / 100% Organic (base)	0	0	0	0	0
10% Test / 900% Organic	1	0	0	0	0
20% Test / 80% Organic	0	1	0	0	0
60% Test / 40% Organic	0	0	1	0	0
90% Test / 10% Organic	0	0	0	1	0
100% Test / 0% Organic	0	0	0	0	1

Table D.2. Individual variables tested in the multiple logistic regression model

Covariate	*Type*	*Increment*
TPHc	Continuous	per 1000 ppm C
DOC	Continuous	per 1000 ppm C
TREATMENT	Categorical ($k-1=4\ levels$)	TS (base)
		TSC
		TSOC+5 g Ozone
		TSOC+10 g Ozone
		TSOC+40 g Ozone
b-ORGANIC	Categorical ($k-1=5\ levels$)	0% Test / 100% Organic (base)
		10% Test / 90% Organic
		20% Test / 80% Organic
		60% Test / 40% Organic
		90% Test / 10% Organic
		100% Test / 0% Organic

Table D.3. Equations of the line for each of individual variable tests

Covariate	Univariable Model
TPHc	$\hat{g}(x) = \hat{\beta}_0 + \hat{\beta}_{TPHc} x_{TPHc}$
DOC	$\hat{g}(x) = \hat{\beta}_0 + \hat{\beta}_{DOC} x_{DOC}$
TREATMENT*	$\hat{g}(x) = \hat{\beta}_0 + \hat{\beta}_{TSC} x_{TSC} + \widehat{\beta}_{TSOC-5g\,O_3} x_{TSOC-5g\,O_3} + \widehat{\beta}_{TSOC-10g\,O_3} x_{TSOC-10g\,O_3} + \widehat{\beta}_{TSOC-40g\,O_3} x_{TSOC-40g\,O_3}$ **
b-ORGANIC*	$\hat{g}(x) = \hat{\beta}_0 + \hat{\beta}_{10\%} x_{10\%} + \hat{\beta}_{20\%} x_{20\%} + \hat{\beta}_{60\%} x_{60\%} + \hat{\beta}_{90\%} x_{90\%} + \hat{\beta}_{100\%} x_{100\%}$ ***

**TS* is base of categorical comparisons. When all other variables are 0, the intercept-only represents *TS*.

***0% Test Soil/100% Potting Soil* is base of categorical comparisons. When all other variables are 0, the intercept-only represents *0% Test Soil/100% Potting Soil*.

Model Construction

Step 1. Univariable analysis of each independent variable

Table D.4. Results of fitting the univariable logistic regression model (n = 840) [*]

Covariate	*Units*	*Coeff*	*Std. Err.*	*G (df)*	*p*[***]
TPHc[**]	per 1000 ppm	0.125	0.00877	266 (1)	<0.000
DOC	per 1000 ppm	1.49	0.131	305 (1)	<0.000
TREATMENT	TS	Base		80.6 (4)	<0.000
	TSC	0.304	0.262		
	TSOC-5g	1.49	0.231		
	TSOC-10g	1.29	0.232		
	TSOC-40g	1.56	0.230		
b-ORGANIC	100%	Base		308 (5)	<0.000
	90%	-0.379	0.508		
	80%	0.445	0.427		
	40%	1.54	0.380		
	10%	2.68	0.369		
	0%	3.91	0.389		

[*]Intercept-Only Loglikelihood is -515 for all variables.

[**]TPH is input into the model as mass of carbon in the TPH (TPHc), or approximately 85% of the TPH by mass.

[***]Stata does show more than 3 decimal places for the p-value

Step 2. The multivariable model

Table D.5. Results of fitting the multivariable logistic regression model (n = 840)*

	Units	*Coeff*	*Std. Err.*	*Wald (z)*	*P****	*95% CI*
*TPHc***	per 1000 ppm	0.00689	0.0251	0.270	0.784	(-0.0423, 0.0562)
DOC	**per 1000 ppm**	**1.99**	**0.355**	**5.60**	**0.000**	**(1.29, 2.68)**
TREATMENT	TS	Base				
	TSC	0.122	0.588	0.210	0.835	(-1.03, 1.27)
	TSOC-5g	0.865	0.474	1.82	0.0680	(-0.0640, 1.79)
	TSOC-10g	-0.572	0.565	-1.01	0.312	(-1.68, 0.536)
	TSOC-40g	**-2.34**	**0.952**	**-2.46**	**0.0140**	**(-4.20, -0.474)**
b-ORGANIC	100%	Base				
	90%	-0.605	0.516	-1.17	0.241	(-1.62, 0.405)
	80%	-0.0462	0.444	-0.100	0.917	(-0.917, 0.824)
	40%	-0.710	0.540	-1.31	0.189	(-1.77, 0.348)
	10%	0.933	0.517	1.80	0.0710	(-0.0803, 1.95)
	0%	**2.84**	**0.492**	**5.77**	**0.000**	**(1.87, 3.80)**

*Intercept-only loglikelihood is -514, the log-likelihood of the model is -260, and G ($df = 11$) is 510 for the model, statistically significant at ρ<0.000.

**TPH is input into the model as mass of carbon in the TPH (TPHc), approximately 85% of the TPH by mass.

***Stata does show more than 3 decimal places for the p-value

Step 3. Evaluation for Confounding (Delta-Beta-Hat%)

Table D.6a Delta-beta-hat-percent

	Category	*Full Model*	*Reduced Model*	$\Delta\hat{\beta}$	*Comment*
TPHc	**Dropped**				
DOC	Continuous	1.99	2.03	-2.07%	
TREATMENT	TS	Base			
	TSC	0.122	0.256	**-110%**	TPHc2 is a modifier
	TSOC-5g	0.865	0.941	-8.74%	
	TSOC-10g	-0.572	-0.526	7.96%	
	TSOC-40g	-2.34	-2.37	-1.19%	
b-ORGANIC	100%	Base			
	90%	-0.605	-0.597	1.22%	
	80%	-0.0462	-0.0278	**39.8%**	TPHc2 is modifier
	40%	-0.710	-0.665	6.35%	
	10%	0.933	0.998	-7.03%	
	0%	2.84	2.90	-2.13%	

Table D.6b Delta-beta-hat-percent (continued)

	Category	*Full Model*	*Reduced Model*	$\Delta\hat{\beta}$	*Comment*
TPHc	Continuous	0.00689	0.0354	**-414%**	DOSE is a modifier
DOC	Continuous	1.99	1.26	**36.7%**	DOSE is a modifier
TREATMENT		**Dropped**			
b-ORGANIC	100%	Base			
	90%	-0.605	-0.672	-11.2%	
	80%	-0.0462	-0.200	-334%	DOSE is modifier
	40%	-0.710	-0.379	46.6%	DOSE is modifier
	10%	0.933	1.03	-10.6%	
	0%	2.84	2.81	0.875%	
TPHc	Continuous	0.00689	0.0839	-1120%	ORGANIC is a modifier
DOC	Continuous	1.99	1.60	19.3%	
TREATMENT	TS	Base			
	TSC	0.122	-1.32	1190%	ORGANIC is a modifier
	TSOC-5g	0.865	-0.894	203%	ORGANIC is a modifier
	TSOC-10g	-0.572	-2.17	-279%	ORGANIC is a modifier
	TSOC-40g	-2.34	-3.41	-45.6%	ORGANIC is a modifier
b-ORGANIC		**Dropped**			

Step 4. Establishing the preliminary main-effects model

Table D.7. Results of fitting the multivariable logistic regression model with *b-ORGANIC* variable condensed to *b-ORGANIC_2* (n=840)*

Covariate	*Unit*	*Coef.*	*Std. Err.*	*Wald (z)*	*p*	*95% CI*
TPHc	per 1000 ppm	0.00131	0.0234	0.0600	0.955	(-0.0444, 0.047)
DOC	per 1000 ppm	1.73	0.305	5.68	0.000	(1.14, 2.33)
TREATMENT	TS	Base				
	TSC	0.184	0.569	0.320	0.747	(-0.932, 1.30)
	TSOC-5g	0.929	0.452	2.06	0.0400	(0.0433, 1.82)
	TSOC-10g	-0.424	0.534	-0.790	0.427	(-1.47, 0.623)
	TSOC-40g	-1.83	0.834	-2.19	0.0280	(-3.46, -0.193)
b-ORGANIC_2	Organic<10%	Base				
	Organic>10%	-2.30	0.301	-7.64	0.000	(-2.89, -1.71)

*Intercept-only loglikelihood is -515, the log-likelihood of the model is -278, and G(df=7) is 474 for the model, statistically significant at ρ<0.000.

**TPH is input into the model as mass of carbon in the TPH (TPHc), approximately 85% of the TPH by mass.

***Stata does show more than 3 decimal places for the p-value.

Table D.8. Results of fitting the multivariable logistic regression model with *TREATMENT* variable condensed to *TREATMENT_2* (n = 840)*

Covariate	*Unit*	*Coef.*	*Std. Err.*	*Wald (z)*	*P****	*95% CI*
*TPHc***	per 1000 ppm	0.00771	0.0123	0.620	0.532	(-0.0165, 0.0319)
DOC	per 1000 ppm	1.69	0.264	6.39	0.000	(1.17, 2.20)
TREATMENT_2	TS/TSC	Base				
	TSOC-5g	0.846	0.368	2.30	0.022	(0.124, 1.57)
	TSOC-10g	-0.479	0.503	-0.950	0.341	(-1.47, 0.507)
	TSOC-40g	-1.80	0.821	-2.20	0.028	(-3.41, -0.196)
b-ORGANIC_2	Organic<10%	Base				
	Organic>10%	-2.26	0.275	-8.22	0.000	(-2.80, -1.72)

*Intercept-only loglikelihood is -515, the log-likelihood of the model is -279, and G(df=6) is 474 for the model, statistically significant at ρ<0.000.

**TPH is input into the model as mass of carbon in the TPH (TPHc), approximately 85% of the TPH by mass.

***Stata does show more than 3 decimal places for the p-value

Table D.9. Delta-beta-hat-percent for *TPHc* removal.

Covariate	*Units*	*Full*	*Reduced*	*Delta-Beta-Hat-Percent*
TPHc	*per 1000 ppm*	*0.0077109*	*Dropped*	*n/a*
DOC	per 1000 ppm	1.69	1.76	4.14%
TREATMENT_2	TS/TSC	Base		
	TSOC-5g	0.846	0.876	3.51%
	TSOC-10g	-0.479	-0.493	2.89%
	TSOC-40g	-1.80	-1.93	6.52%
b-ORGANIC_2	Organic<10%	Base		
	Organic>10%	-2.26	-2.30	1.64%

Step 5. Linearity of the logit for continuous variables/the main effects model.

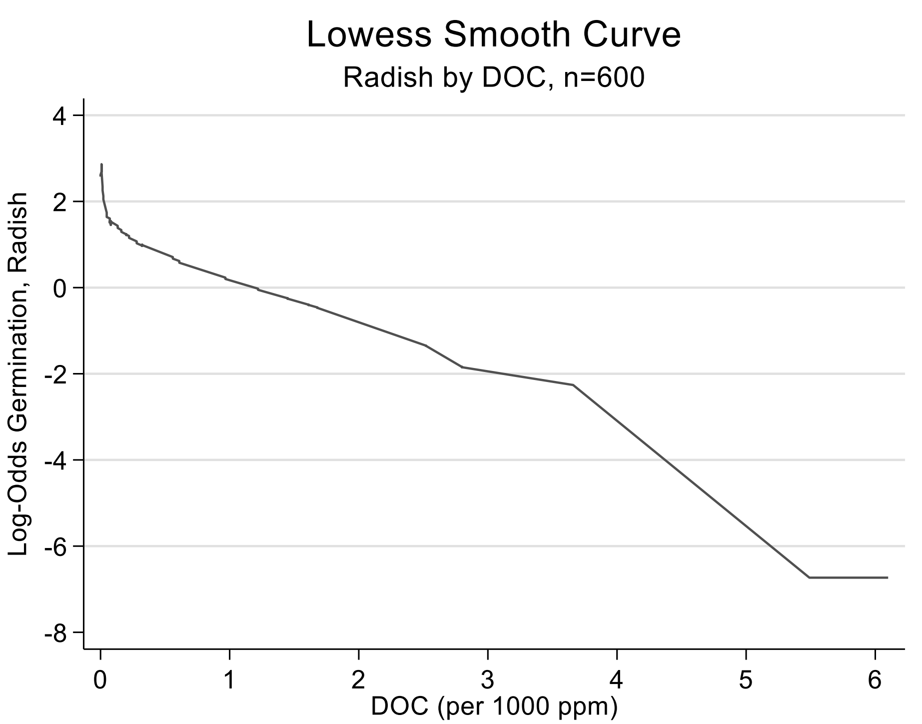

Figure D.1. Lowess smooth on the log-odds scale of the outcome, radish germination, versus DOC (per 1000 ppm), n = 600.

Table D.10a. Fractional polynomial analysis of linearity of DOC in the logit.

	df	*Deviance*	*diff.*	*p*	*Powers*	
omitted	4	556	4.98	0.290		
linear	4	556	4.98	**0.290**	1	
m = 1	2	552	0.979	0.613	3	
m = 2	0	551	0	--	0.5	2

Table D.10b Fractional polynomial analysis of linearity of DOC in the logit

Covariate	*Units*	*Coef.*	*Std. Err.*	*Wald (z)*	*p*	*95% CI*
DOC	per 1000 ppm	-1.15	1.76	-0.660	0.512	(-4.60, 2.29)
TREATMENT_2	TS/TSC	Base				
	TSOC-5g	1.14	0.421	2.71	0.007	(0.316, 1.96)
	TSOC-10g	-0.0517	0.559	-0.0900	0.926	(-1.15, 1.04)
	TSOC-40g	-2.63	1.24	-2.12	0.0340	(-5.05, -0.202)
b-ORGANIC_2	Organic<10%	Base				
	Organic>10%	-2.26	0.303	-7.44	0.000	(-2.85, -1.66)
DOC	m=1	2.06	1.84	1.12	0.264	(-1.55, 5.68)
DOC	m=2	0.625	0.320	1.95	0.051	(-0.00276, 1.25)

*Intercept-only loglikelihood is -515, the log-likelihood of the model is -276, and G(df=5) is 479 for the model, statistically significant at ρ<0.000.

**TPH is input into the model as mass of carbon in the TPH (TPHc), approximately 85% of the TPH by mass.

Step 6. Interactions between terms are systemically checked/preliminary final model.

Table D.11 Results of fitting the multivariable model with interaction term *DOC x TREATMENT_2*

	Category	*Coeff*	*Std. Err.*	*Wald (z)*	*p*	*95% CI*
DOC	per 1000 ppm	5.70	2.47	2.31	0.021	(0.859, 10.5)
TREATMENT _2	TS/TSOC	Base				
	TSOC-5g	1.75	0.445	3.92	0.000	(0.872, 2.62)
	TSOC-10g	-0.688	0.800	-0.86	0.390	(-2.26, 0.879)
	TSOC-40g	-2.67	1.35	-1.98	0.048	(-5.32, -0.0293)
b-ORGANIC_2	Organic<10%	Base				
	Organic>10%	-2.18	0.325	-6.70	0.000	(-2.82, -1.54)
Interaction	DOC x TS/TSC	Base				
	DOC x TSOC-5g	-4.91	2.41	-2.03	0.042	(-9.63, -0.178)
	DOC x TSOC-10g	-3.59	2.48	-1.45	0.148	(-8.45, 1.28)
	DOC x TSOC-40g	-3.55	2.51	-1.42	0.156	(-8.47, 1.36)
	LL Interactions	-273		G	-0.17	
	LL Model	-278		**p-value**	**0.0196**	

Table D.12. Results of fitting the multivariable model with interaction term *DOC x b-ORGANIC_2*.

	Category	*Coeff*	*Std. Err.*	*Wald*	*p*	*95% CI*
DOC	per 1000 ppm	1.68	0.347	4.83	0.000	(0.997, 2.36)
TREATMENT_2	TS/TSOC	Base				
	TSOC-5g	0.893	0.369	2.42	0.015	(0.170, 1.62)
	TSOC-10g	-0.487	0.509	-0.96	0.339	(-1.49, 0.511)
	TSOC-40g	-1.99	0.852	-2.34	0.019	(-3.66, -0.323)
b-ORGANIC_2	Organic<10%	Base				
	Organic>10%	-2.34	0.299	-7.82	0.000	(-2.93, -1.75)
Interaction	DOC x Organic<10%	Base				
	DOC x Organic>10%	0.117	0.367	0.32	0.751	(-0.603, 0.836)
	LL Interactions	-278		G	-0.64	
	LL Model	-278		p-value	0.755	

Table D.13. Results of fitting the multivariable model with interaction term *TREATMENT x b-ORGANIC_2*.

	Category	*Coeff*	*Std. Err.*	*Wald*	*p*	*95% CI*
DOC	per 1000 ppm	1.88	0.280	6.72	0.000	(1.33, 2.43)
TREATMENT	TS/TSOC	Base				
	TSOC-5g	-0.470	0.641	-0.73	0.464	(-1.73, 0.786)
	TSOC-10g	-0.633	0.548	-1.15	0.249	(-1.71, 0.442)
	TSOC-40g	-2.12	0.903	-2.34	0.019	(-3.89, -0.347)
b-ORGANIC_2	Organic<10%	Base				
	Organic>10%	-2.47	0.297	-8.33	0.000	(-3.06, -1.89)
Inter.	TS/TSC x Org<10%	Base				
	TS/TSC x Org >10%	Base				
	TSOC-5g x Org <10%	Base				
	TSOC-5g x Org >10%	1.65	0.680	2.43	0.015	(0.320, 2.99)
	TSOC-10g x Org <10%	Empty				
	TSOC-10g x Org >10%	Omitted				
	TSOC-40g x Org <10%	Empty				
	TSOC-40g x Org >10%	Omitted				
	LL Interactions	-274	G	Obs differ: 760 vs. 840		
	LL Model	-278	p-value	n/a		

Step 7. Goodness-of-fit testing

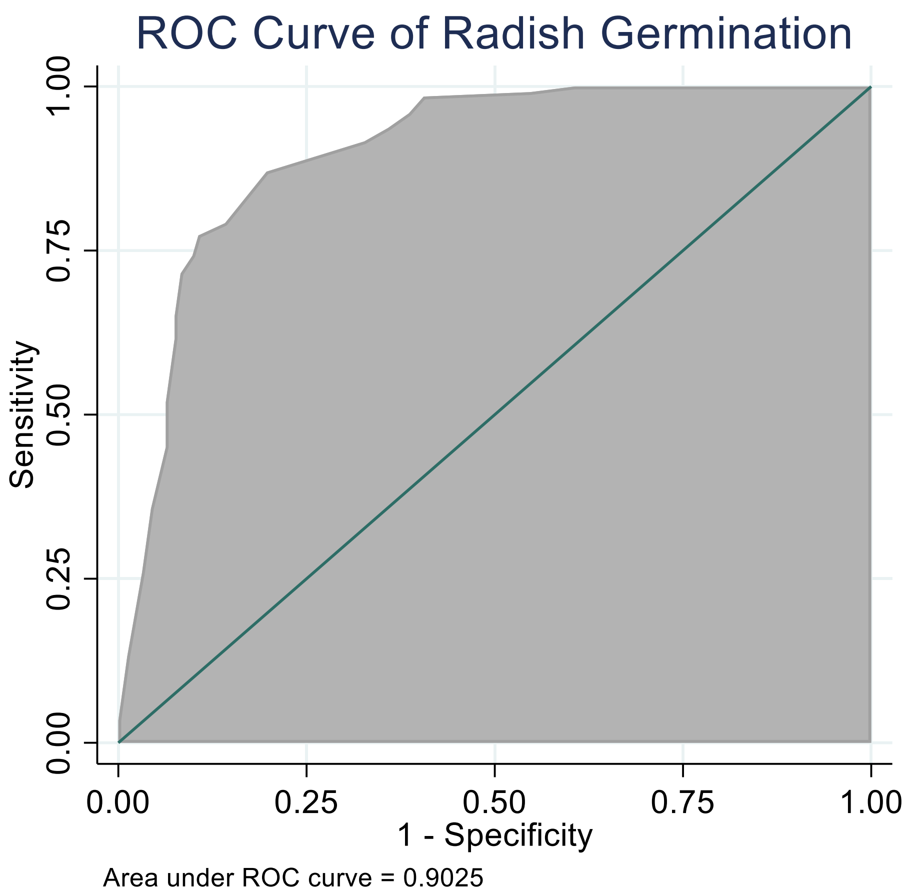

Figure D.2. Receiver operating characteristic (ROC) curve of Radish germination by the model.

APPENDIX E
COLUMN AND COLUMN BREAKDOWN

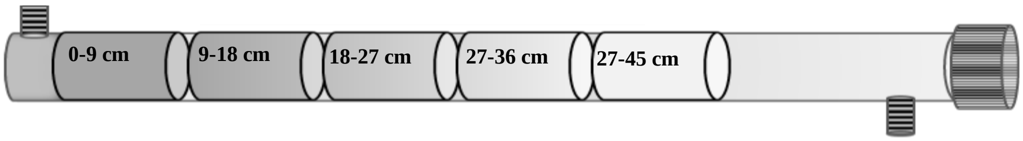

Figure E. The soil column after during ozonation experiments, including the five sections sampled at the end of the experiment.

APPENDIX F

LATENT HEAT ADJUSTMENT FOR MOISTURE LOSS

Prediction of Moisture Flux

An oxygen (O_2) only control column was run for 240 minutes to evaluate the effect of gas-flow on moisture changes across the column, without the element of heating. The column was evaluated in 5 segments for the change in moisture and the normalized results are graphed in Figure L to evaluate the slope changes.

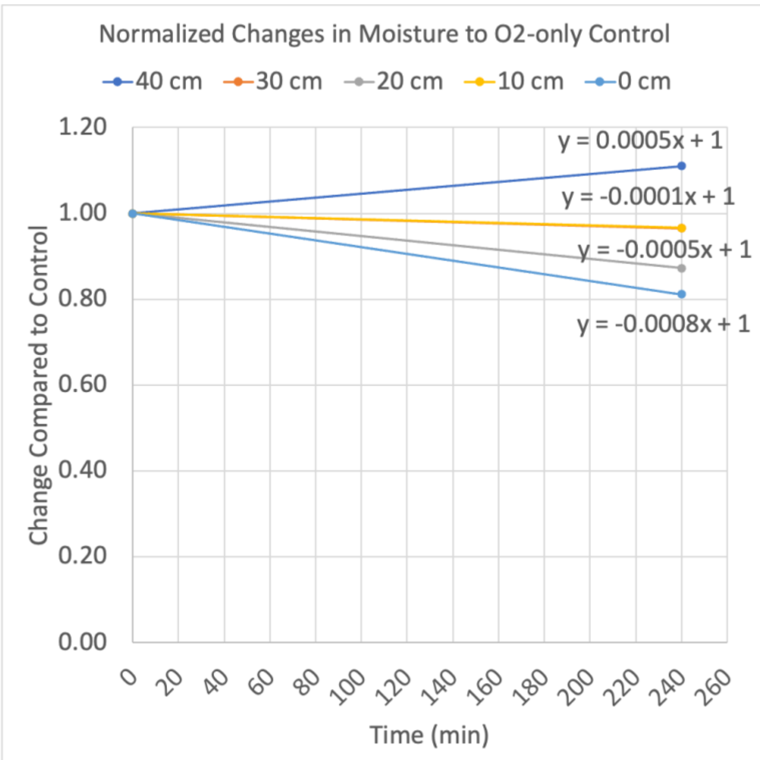

Figure F. Normalized changes in column moisture over time for each column segment. Equations of the lines predict moisture (y) at given time (x) for 40 cm (y = 0.0005x + 1), 30 cm (y = -0.0001x + 1), 20 cm (y = -0.0001x + 1), 10 cm (y = -0.0005x + 1), and 0 cm (y = -0.0008x + 1).

The equation for the trendline shown in Figure L at each column segment was used to predict changes in moisture due to the flow of O_2 gas-only as a function of time. Table L shows the changes in absolute mass of H_2O (from starting mass of ~6 g), expected for a given loading rate, time (i.e., total dose), and column position. Predictably, changes are most significant at low loading, where gas-flow is the longest duration. The final total moisture values in each experiment were adjusted by the amount of H_2O lost/gained due to gas flow of gas-only such that latent heat calculations for evaporation/condensation increased from 0-30cm and decreased at >40 cm. These moisture adjustments do not change trends and, in fact, decrease the degree of difference observed between experimental groups. Hence, reported values for Q_{lat} are conservative.

Table F. Mass of H_2O (g) change due to the flow of O_2 gas-only. The negative (-) values of moisture noted below are added back in to final moisture such that 0-30 cm is increased by the moisture lost and >40 cm is decreased by the water gained through the flow of gas-only.

	Time (min)	*0 cm*	*10 cm*	*20 cm*	*30 cm*	*>40 cm*
Low Loading	120 (5 g O_3)	-0.58	-0.36	-0.07	-0.07	0.36
	240 (10 g O_3)	-1.15	-0.72	-0.14	-0.14	0.72
	480 (20 g O_3)	-2.30	-1.44	-0.29	-0.29	1.44
Medium Loading	40 (5 g O_3)	-0.19	-0.12	-0.02	-0.02	0.12
	80 (10 g O_3)	-0.38	-0.24	-0.05	-0.05	0.24
	160 (20 g O_3)	-0.77	-0.48	-0.10	-0.10	0.18
High Loading	15 (5 g O_3)	-0.07	-0.04	-0.01	-0.01	0.04
	30 (10 g O_3)	-0.14	-0.09	-0.02	-0.02	0.09
	60 (20 g O_3)	-0.29	-0.18	-0.04	-0.04	0.18